

Multiscale modeling of drug-induced toxicity in humans

Von der Fakultät für Mathematik, Informatik, und Naturwissenschaften der RWTH Aachen University zur
Erlangung des akademischen Grades eines Doktors der Naturwissenschaften genehmigte Dissertation

vorgelegt von

Master of Science
Christoph Thiel

aus
Saarbrücken, Deutschland

Berichter

Univ.-Prof. Dr.-Ing. Lars M. Blank
Univ.-Prof. Dr.-Ing. Julio Saez-Rodriguez

Tag der mündlichen Prüfung: 26.09.2017

Statement

I hereby confirm that this PhD thesis is my own work and that I have documented all sources used.

Cologne, 5th October 2017

Christoph Thiel

Acknowledgments

I want to express my special thanks to Dr. Lars Küpfer for his great support. I also want to thank Professor Lars Blank for giving me the opportunity to write my PhD thesis at the Institute of Applied Microbiology. Furthermore, I own gratitude to all my colleagues and particularly to my family.

Cologne,
5th October 2017

Christoph Thiel

Abstract

Drug toxicity poses a crucial problem in drug development and particularly in clinical care and in public health. Although in vitro experiments can obtain valuable information of the mechanisms underlying drug-induced toxicity, there is still a clear lack of approaches translating such in vitro findings into a patient situation. In this thesis, a novel translational approach is presented and is successfully applied in three different studies to investigate the onset of adverse drug events at patient level. Here, multiscale modeling enables the coupling of in vitro concentration-response relationships, at the cellular level, with drug concentration-time profiles, at the organism level, to predict cellular responses following drug administration of different doses in vivo. The application of the developed translational approach allowed studying drug-induced toxicity in humans (i) for acute and chronic administration of azathioprine in a proof-of-concept study, (ii) for fifteen hepatotoxic drugs in a comparative manner focusing on drug administration of therapeutic and toxic doses, and (iii) for a drug combination therapy of acetaminophen and caffeine. The presented translational approach may lead to useful knowledge for clinical application gained from in vitro experiments thereby contributing to the ongoing discussion of the predictive value of preclinical research. Overall, the results shown here provide novel insights into drug-induced toxicity within a patient context and, thus, may improve patient safety in drug development.

Zusammenfassung

Medikamententoxizität stellt ein schwerwiegendes Problem in der Medikamentenentwicklung und insbesondere in der klinischen Versorgung und im Gesundheitswesen dar. Obwohl in vitro-Experimente nützliche Informationen über die zugrundeliegenden Mechanismen der Medikamenten-induzierten Toxizität liefern können, so fehlt es immer noch an Ansätzen, die solche in vitro-Erkenntnisse in eine Patientensituation übertragen. In dieser Arbeit wird ein neuer translationaler Ansatz präsentiert und in drei verschiedenen Studien erfolgreich angewendet, um den Beginn von unerwünschten Arzneimittelnebenwirkungen auf Patientenebene zu untersuchen. Die Multiskalenmodellierung ermöglicht dabei die Kopplung von in vitro-Konzentrations-Wirkungs-Beziehungen auf zellulärer Ebene mit zeitaufgelösten Medikamentenkonzentrationen auf Organismusebene, um zelluläre Antworten als Folge von der Medikamentengabe verschiedener in vivo-Dosen vorherzusagen. Durch die Anwendung des entwickelten translationalen Ansatzes konnte Medikamenten-induzierte Toxizität in Menschen in drei Studien untersucht werden: (i) im Zuge einer Machbarkeitsstudie für akute und chronische Medikamentengabe von Azathioprin, (ii) in einer vergleichenden Analyse für fünfzehn hepatotoxische Substanzen mit Fokus auf der Medikamentengabe von therapeutischen und toxischen Dosen und (iii) für eine Kombinationstherapie bestehend aus Acetaminophen und Koffein. Der präsentierte translationale Ansatz kann zu nützlichem Wissen für die klinische Anwendung führen, welches aus in vitro-Experimenten gewonnen wurde, und dadurch zu der andauernden Diskussion des prädiktiven Wertes von präklinischer Forschung beitragen. Insgesamt liefern die hier gezeigten Ergebnisse neue Einblicke in Medikamenten-induzierte Toxizität in einem Patientenkontext, wodurch die Patientensicherheit während der Arzneimittelentwicklung verbessert werden kann.

Contents

General introduction	17
-----------------------------------	----

Part I Background

1 Drug toxicity	23
1.1 Drug-induced hepatotoxicity	25
1.2 Modeling drug-induced toxicity with systems biology models	28
2 Pharmacokinetics and pharmacodynamics	31
2.1 Pharmacokinetics	31
2.1.1 Absorption	32
2.1.2 Distribution	33
2.1.3 Metabolism	34
2.1.4 Elimination	35
2.2 Pharmacodynamics	36
3 Physiologically-based pharmacokinetic modeling	39
3.1 Applications	40
3.2 Model development and validation	41
3.3 Model parameters	41
3.4 Differentiation from conventional pharmacokinetic modeling	44
3.5 Physiologically-based pharmacokinetic/pharmacodynamic modeling	44
3.6 Modeling software	46
4 Drug-drug interactions	47
4.1 Pharmacokinetic drug interactions	48
4.2 Pharmacodynamic drug interactions	49
5 Toxicogenomics	51
5.1 Transcriptomics	52
5.1.1 Workflow of a microarray experiment	52
5.1.2 Analysis of microarray data	53
6 Biomarkers	55
6.1 Transcriptional biomarkers	55
6.2 Biomarkers for drug-induced hepatotoxicity	56

Part II Results

7	Model-based contextualization of in vitro toxicity data quantitatively predicts in vivo drug response in patients	61
7.1	Introduction	62
7.2	Materials and methods	64
7.2.1	Analysis of in vitro toxicity data	64
7.2.2	Physiologically-based pharmacokinetic model development	64
7.2.3	Prediction of in vivo drug responses in humans and rats	65
7.2.4	Validation of predicted in vivo drug responses in rats	66
7.2.5	Clinical cases of acute toxicity after single dosing of azathioprine	66
7.3	Results	67
7.3.1	PBPK-based in vivo contextualization of in vitro toxicity data (PICD)	67
7.3.2	Use of PICD for individual patients	67
7.3.3	Organism level: Physiologically-based pharmacokinetic models	69
7.3.4	Cellular Level: In vitro toxicity data	72
7.3.5	Validation of PICD in rats	73
7.3.6	Application of PICD in humans	75
7.3.7	Acute toxicity after single dosing of azathioprine: Patient cohort study	77
7.3.8	Acute toxicity after single dosing of azathioprine: Patient case study 1	78
7.3.9	Acute toxicity after multiple dosing of azathioprine: Patient case study 2	80
7.4	Discussion	82
8	A comparative analysis of drug-induced hepatotoxicity in clinically relevant situations	87
8.1	Introduction	88
8.2	Materials and methods	89
8.2.1	Set of drugs	89
8.2.2	Key cellular processes	91
8.2.3	Therapeutic and toxic dose levels	91
8.2.4	In vitro toxicity data	93
8.2.5	Identification of significantly perturbed key cellular processes	93
8.2.6	Development of whole-body physiologically-based pharmacokinetic models	94
8.2.7	Prediction and validation of in vivo drug responses	97
8.2.8	Calculation of toxic changes	97
8.2.9	Prediction of molecular biomarkers and potential drug interactions	98
8.3	Results	98
8.3.1	Whole-body physiologically-based pharmacokinetic models	98
8.3.2	Integrating in vitro toxicity data into physiologically-based pharmacokinetic models	101
8.3.3	Validation of predicted in vivo drug responses in rats	101
8.3.4	Comparative toxicity analysis	102
8.4	Discussion	110

9	Multiscale modeling reveals inhibitory and stimulatory effects of caffeine on acetaminophen-induced toxicity in humans	115
9.1	Introduction	116
9.2	Materials and methods	118
9.2.1	Physiologically-based pharmacokinetic model development	118
9.2.2	Analysis of in vitro toxicity data	118
9.2.3	Predicting the pharmacodynamic responses of acetaminophen and caffeine	119
9.2.4	Modeling the pharmacodynamic response of acetaminophen co-administered with caffeine	121
9.2.5	Other systems biology models for acetaminophen	122
9.3	Results	122
9.3.1	Physiologically-based pharmacokinetic models of acetaminophen and caffeine	122
9.3.2	Analyzing pharmacodynamic responses of acetaminophen and caffeine	125
9.3.3	Dose escalation study – Transition from therapeutic to toxic conditions	129
9.3.4	Investigating the effect of caffeine on the analgesic action of acetaminophen	130
9.4	Discussion	131
	General conclusions and outlook	135
	References	139
<hr/>		
	Part III Appendix	
<hr/>		
A	General supplementary information to Part II	161
A.1	Toxicogenomics database	161
A.2	Software	161
B	Supplementary information to Chapter 7	162
B.1	Supplementary materials	162
B.1.1	Filtering of gene ontology terms	162
B.2	Supplementary tables	163
B.2.1	Analysis of in vitro toxicity data	163
B.2.2	Assessment of predicted in vivo drug responses in rats	177
B.2.3	Genes and pathways	178
C	Supplementary information to Chapter 8	185
C.1	Supplementary tables	185
C.1.1	Key cellular processes	185
C.1.2	Analysis of in vitro toxicity data	187
C.1.3	Physiologically-based pharmacokinetic model development	197
C.1.4	Prediction of molecular biomarkers and potential drug interactions	199
D	Supplementary information to Chapter 9	203
D.1	Supplementary tables	203
D.1.1	Physiologically-based pharmacokinetic model development and validation	203
D.1.2	System biology models of acetaminophen	205
E	Curriculum vitae	207

List of Tables

7.1	Dose identification.	65
7.2	Clinical cases of acute azathioprine overdose.	66
7.3	PBPK model parameters.	71
7.4	Experimental conditions.	71
8.1	Drug-specific annotations.	91
8.2	Experimental conditions.	92
8.3	Toxic dose levels.	93
8.4	Physicochemical drug properties used in the PBPK models.	94
8.5	Active drug transport and metabolic processes.	95
8.6	Renal and biliary clearance processes.	96
8.7	Common molecular biomarkers.	110
9.1	Physicochemical properties used in the developed PBPK models.	120
9.2	Active drug transport and metabolic reactions.	120
9.3	Elimination processes.	120
9.4	Experimental conditions.	121
B.1	Enriched terms and pathways.	163
B.2	Deleted gene ontology terms.	169
B.3	Correlation results for significantly regulated pathways and cellular processes in rats.	177
B.4	Toxicity-related biological pathways.	178
B.5	Genes involved in the DNA damage & repair pathway.	181
B.6	Interaction network.	182
B.7	Genes related to jaundice.	183
C.1	Toxicity lists.	185
C.2	Over-representation analysis for humans.	187
C.3	Over-representation analysis for rats.	193
C.4	Intestinal permeabilities.	197
C.5	Calculation methods for partition coefficients and cellular permeabilities.	198
C.6	Bioavailability values.	198
C.7	Molecular biomarkers.	199
C.8	Drug-drug interactions.	201
D.1	Relative expression values of relevant enzymes and transporters.	203
D.2	Comparison between observed and predicted pharmacokinetic parameters.	204
D.3	Other system biology models for acetaminophen and their application.	206

List of Figures

1.1	Schematic representation of the drug development process.....	23
1.2	Attrition and success rates in drug development.	25
1.3	Three-step working model of drug-induced hepatotoxicity.	27
2.1	Pharmacokinetics.	31
2.2	Passive and active drug transport mechanisms.	32
2.3	Capillary structure.	33
2.4	Influence of plasma protein binding.	33
2.5	Drug metabolism.	34
2.6	Major renal processes.....	35
2.7	Drug concentration-response relationships.	37
3.1	Schematic representation of a multiscale whole-body PBPK model.	39
3.2	Applications of PBPK modeling.	40
3.3	Drug-related biological processes for pravastatin.	41
3.4	Workflow of PBPK model development and validation.	42
3.5	Conventional pharmacokinetic modeling.	45
3.6	Basic concept of PBPK/PD modeling.	45
4.1	Different effects caused by co-administration of multiple drugs.	47
4.2	Pharmacokinetic drug interactions.	48
5.1	Toxicogenomics study.	51
5.2	Simple workflow of a microarray experiment.....	52
5.3	Volcano plot.	53
6.1	Simple workflow for the identification of transcriptional biomarkers.....	56
7.1	Overview of the use of PICD.	63
7.2	Workflow of PICD.	68
7.3	Use of PICD for individual patients.	69
7.4	PBPK model development and validation.	70
7.5	PBPK model assessment.....	70
7.6	Cross-species extrapolation.....	71
7.7	Azathioprine-induced gene expression data.	72
7.8	Correlation of predicted drug response profiles with in vivo measurements in rats.	73
7.9	Correlation between observed in vivo, in vitro and predicted in vivo drug responses.	74
7.10	Application of PICD on the hepatotoxicant azathioprine in humans.	75
7.11	Predicted in vivo drug responses in humans.	76

7.12	Predicted in vivo drug responses for DNA replication.	77
7.13	Application of PICD on eight clinical cases of acute azathioprine overdose.	78
7.14	Acute liver toxicity after single dosing of azathioprine.	79
7.15	Acute liver failure after multiple dosing of azathioprine.	81
7.16	Predicted in vivo cytotoxicity over time.	82
8.1	PBPK-based in vivo contextualization of in vitro toxicity data.	89
8.2	General workflow.	90
8.3	Human PBPK models.	99
8.4	PBPK model assessment.	100
8.5	Therapeutic and toxic pharmacokinetic profiles.	102
8.6	Validation of predicted drug response with in vivo measurements in rats.	103
8.7	Comparative toxicity analysis of key cellular processes.	104
8.8	Principal component analysis.	105
8.9	Toxic changes predicted for functional classes of genes involved in key cellular processes. .	106
8.10	Comparison of toxic changes between azathioprine and valproic acid in cell cycle checkpoint regulation.	108
8.11	Potential drug interactions between the high-responsive drugs.	111
9.1	Overview of the use of PICD.	117
9.2	Workflow of PBPK model development and validation.	119
9.3	Reaction diagram of biochemical processes implemented in the PBPK models of acetaminophen and caffeine	122
9.4	PBPK models of acetaminophen and caffeine.	123
9.5	PBPK model assessment.	124
9.6	Simulated plasma concentrations for single administration of acetaminophen and co-administration of caffeine.	125
9.7	Pharmacodynamic response of key cellular processes.	126
9.8	Pharmacodynamic response of individual genes.	127
9.9	Pharmacodynamic response of additional individual genes.	128
9.10	Dose escalation study.	129
9.11	Pharmacodynamic response of genes associated to pain.	130
B.1	Filtering gene ontology terms.	162

List of Abbreviations

13U	1,3-Dimethyluric acid
1X	1-Methylxanthine
7X	7-Methylxanthine
6-MP	6-Mercaptopurine
ABC	ATP-binding cassette
ADME	Absorption, distribution, metabolism, and elimination
AD	Amiodarone
AhR	Aryl hydrocarbon receptor
ALB	Albumin
ANOVA	Analysis of variance
ALT	Alanine transaminase
AST	Aspartate transaminase
apaf-1	Apoptotic protease-activating factor 1
APAP	Acetaminophen
APAPC	Acetaminophen cysteine
APAPG	Acetaminophen glucuronide
APAPS	Acetaminophen sulfate
ATC	Anatomical Therapeutic Chemical
ATP	Adenosine triphosphate
AUC	Area under the curve
AZA	Azathioprine
BCS	Biopharmaceutics Classification System
Bid	BH3 interacting-domain death agonist
BP	Biological processes
CAF	Caffeine
CAR	Constitute androstane receptor
CC	Cellular component
cDNA	complementary deoxyribonucleic acid
CENP-A	Centromere protein A
CES	Carboxylesterase
CI	Confidence interval
cMax	Maximal concentration
CPA	Cyclophosphamide
CSA	Cyclosporine A
CYP	Cytochrome P450
DEGs	Differentially expressed genes
DDI	Drug-drug interaction
DFN	Diclofenac

DILI	Drug-induced liver injury
DISC	Death-inducing signaling complex
DNA	Deoxyribonucleic acid
ER	Endoplasmatic reticulum
ERY	Erythromycin
ERY-PED	Erythromycin ethylsuccinate
FADD	Fas ligand-associated death domain protein
FasL	Fas ligand
FDA	Food and Drug Administration
FT	Flutamide
F _u	Fraction unbound
FXR	Farnesoid X receptor
GC-RMA	GC Robust Multi-array Average
GDH	Glutamate dehydrogenase
GSH	Glutathione
GO	Gene ontology
GGT	Gamma-glutamyltransferase
GST	Glutathione S-transferase
HPL	Haloperidol
IL-1	Interleukine-1
INH	Isoniazid
IV	Intravenous
IVIVE	In vitro-to-in vivo extrapolation
JNK	C-jun N-terminal kinase
KEGG	Kyoto Encyclopedia of Genes and Genomes
K _m	Michaelis-Menten constant
K _d	Dissociation constant
LDH	Lactate dehydrogenase
Limma	Linear models for microarray data
logP	Octanol/water partition coefficient
LPS	Lipopolysaccharide
LXR	Liver X receptor
MCM	Minichromosome maintenance
MDR2	Multidrug-resistant protein 2
MED	Minimum effective dose
MF	Molecular function
MTP	Mitochondrial permeability transition
MTD	Maximum tolerated dose
MW	Molecular weight
NAAA	N-acylethanolamine acid amidase
NAC	N-acetyl cysteine
NAPQI	N-acetyl-p-benzoquinone imine
NAT	N-acetyltransferase
NF-κB	Nuclear factor kappa B
Nrf2	Nuclear factor erythroid-derived 2-like 2
OATP	Organic anion transporter pump
PBPK	Physiologically-based pharmacokinetic

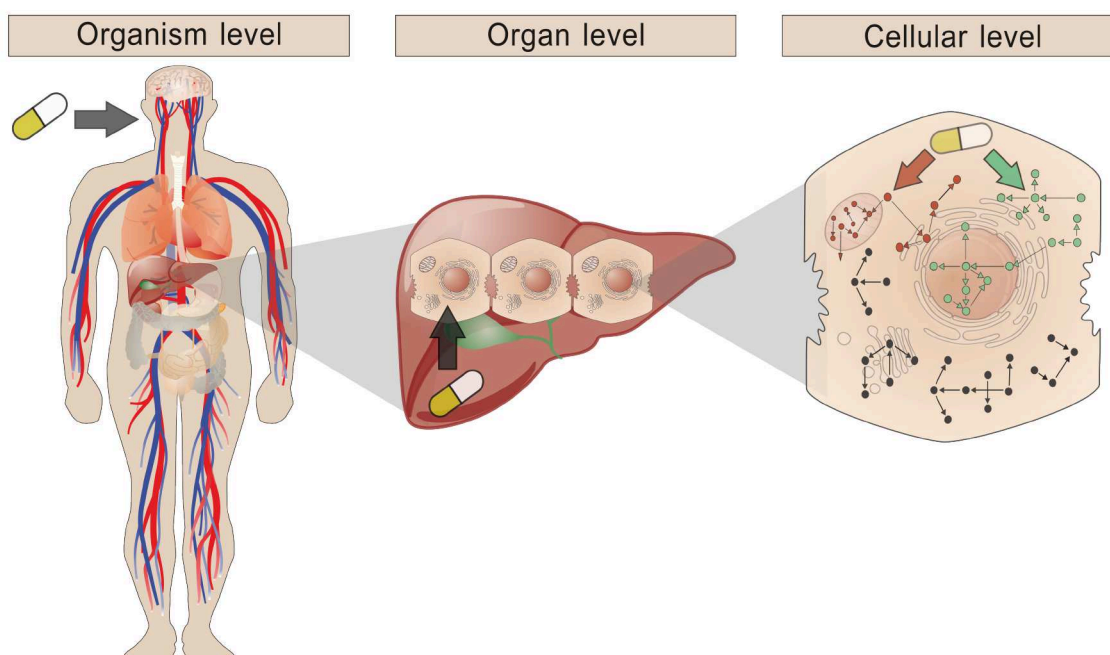
PD	Pharmacodynamic(s)
PB	Phenobarbital
P-gp	P-glycoprotein
PHE	Phenytoin
PICD	PBPK-based in vivo contextualization of in vitro toxicity data
PK	Pharmacokinetic(s)
pKa	Acid dissociation constant
PO	Per os
PPAR α	peroxisome proliferator-activated receptor α
PSS	Poisoning Severity Scores
PX	Paraxanthine
PXR	Pregnane X receptor
R ²	Coefficient of determination
RIF	Rifampicin
RMSD	Root-mean-square deviation
RNA	Ribonucleic acid
RXR	Retinoid X receptor
SST	Simvastatin
SULT	Sulfotransferase
TB	Theobromine
TCDD	2,3,7,8-tetrachloro-dibenzo-p-dioxin
TGF- β	Transforming growth factor- β
TG-GATEs	Toxicogenomics Project-Genomics Assisted Toxicity Evaluation System
TNF- α	Tumor necrosis factor α
TRADD	TNF- α receptor-associated death domain protein
TP	Theophylline
TR	Thyroid receptor
UGT	Uridine 5'-diphospho-glucuronosyltransferase
VDR	Vitamin D receptor
VPA	Valproic acid
v _{max}	Maximum velocity
XO	Xanthine oxidase

General introduction

Drug-induced toxicity is an important issue in drug development and patient safety with hepatotoxicity being one of the most common problems [Schuster et al., 2005; Takikawa et al., 2009; Andrade et al., 2005; Kaplowitz, 2004]. Extensive drug abuse, whether intentionally or inadvertently, may cause toxic effects in humans that, at worst, can be fatal. The prediction of drug-induced adverse events at an early stage in drug development is thus of key relevance. In this respect, clinical biomarkers may help to facilitate an early diagnosis of such toxic events. Drug combination therapies, which are often applied in clinical practice, may even aggravate adverse drug reactions through interactions between the applied drugs as reported, for instance, for co-administration of acetaminophen and caffeine in rats, as well as in several other studies [Askgaard et al., 1995; Deray et al., 1987; Chen and Raymond, 2006; Sato et al., 1985]. Since the molecular mechanisms underlying drug-induced toxicity are rather unclear, a mechanistic understanding of these mechanisms has great significance with particular emphasis on cellular processes occurring during the transition from desired drug effects to unwanted adverse events following therapeutic and toxic doses, respectively.

Besides the pharmaceutical phase comprising the disintegration of the dosage form and the dissolution of the drug substance, the efficiency of a drug can be described by two phases: a pharmacokinetic phase determining the amount of drug at the target site, and a pharmacodynamic phase including the pharmacological activity of the drug at the site of action. To simulate drug concentration-time profiles in different tissues or organs, physiologically-based pharmacokinetic (PBPK) modeling is nowadays routinely applied during drug development [Jones et al., 2006]. PBPK modeling aims for a mechanistic representation of absorption, distribution, metabolism, and elimination (ADME) processes governing the fate of a drug within the human body. Whole-body PBPK models are explicitly representing important tissues and organs that are connected by blood flow. Since the parametrization of PBPK models is based on the physiology and anatomy of the organism as well as on drug-specific parameters, these models contain a large amount of mechanistic information [Kuepfer et al., 2016]. Notably, PBPK models are well suited for specific extrapolation scenarios such as cross-species extrapolation [Thiel et al., 2015]. Moreover, these models allow the consideration of pharmacokinetic drug interactions affecting their concentration-time courses within the body.

Several drugs initiate their pharmacological effect through the interaction with specific targets (e.g., receptors). This may provoke a cascade of reactions and finally lead to temporal changes of genes, proteins, and metabolites within the cell. Cellular alterations can nowadays be measured at different biological levels by omics technologies such as transcriptomics, proteomics, or metabolomics. Analyzing omics measurements of cells exposed to toxic drug concentrations can ultimately provide novel insights into central mechanisms involved in drug-induced toxicity and, furthermore, could facilitate a better characterization of adverse drug events. [Waters and Fostel, 2004; Heijne et al., 2005; Chen et al., 2012]. These findings, however, are based on in vitro assays, which often presents a severe drawback in terms of translatability to patients in actual clinical practice. The lack of in vivo context may be overcome with approaches that somehow contextualize the observed in vitro findings into an in vivo situation. For instance, steady state



Introductory Figure: Schematic representation of an integrative multiscale approach. Multiscale approaches allow a detailed representation of biological processes by integrating different levels of biological organization following drug administration within humans. After medication treatment, a drug is transported via the organism and organ level to the cellular level where its pharmacological action may occur finally leading to therapeutic effects (green) or adverse events (red).

blood concentrations were identified by use of reverse toxicokinetics to correlate *in vivo* equivalent doses with *in vitro* bioactivity data [Dix et al., 2007; Judson et al., 2011; Wetmore et al., 2013; Judson et al., 2014]. Another study used physiologically-based kinetic models of different glycol ethers to obtain dose-response relationships in rats and humans [Louisse et al., 2010]. However, a systematic consideration of *in vitro* toxicity data into an *in vivo* context thereby reflecting cellular changes over time induced by *in vivo* drug administration of clinically-relevant doses remains still challenging.

Integrative multiscale approaches strive for a detailed representation of cellular processes after drug administration in humans by integrating different levels of biological organization (Introductory Figure). Therapeutic or toxic effects at the cellular level could be ultimately explored following drug-related ADME processes from the organism level via the organ level to the cellular level (Introductory Figure). The use of such multiscale approaches in the context of systems toxicology might allow, at best, the elucidation of molecular mechanisms underlying drug-induced toxicity in patients. A systematic application on a large number of drugs that are known to be toxic in some circumstances could further help to identify similarities in adverse reactions for specific sets of drugs. In this regard, robust clinical biomarkers could be discovered for different modes of toxicity. Identified biomarkers could be further analyzed in a systematic way to predict potential drug interactions by assuming a high probability of interaction between two drugs that similarly alter respective biomarkers. Moreover, the integration of different levels of biological organization such as the organism and cellular level might allow the consideration of pharmacokinetic and pharmacodynamic drug interactions in humans. Drugs that are known to affect the pharmacokinetic or pharmacodynamic behavior of co-administered agents *in vitro* or in animals can be thereby studied within a whole-body context.

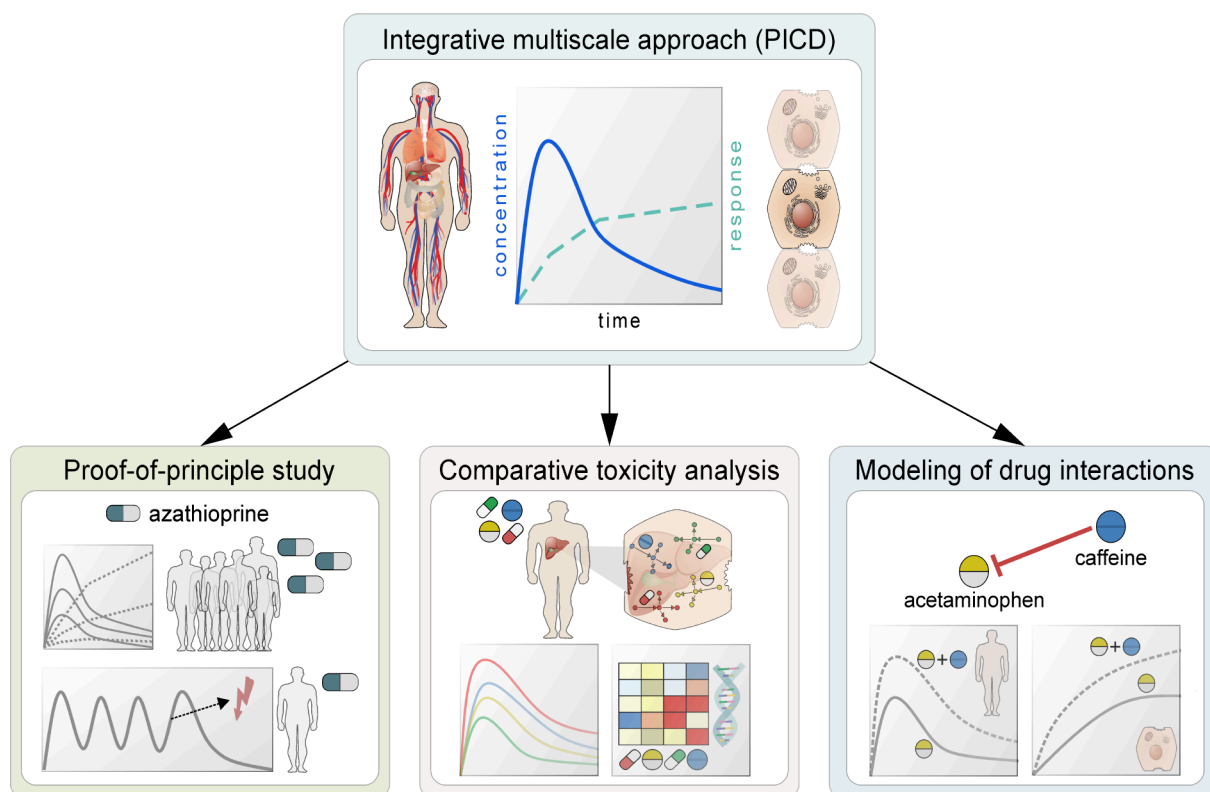
In this thesis, an integrative multiscale approach is presented for significantly supporting the translation of *in vitro* findings into an *in vivo* situation by the coupling of drug-specific whole-body PBPK models, at the organism level, with *in vitro* toxicity data obtained in a toxicogenomics study, at the cellular level

[Thiel et al., 2016]. The developed approach 'PBPK-based in vivo contextualization of in vitro toxicity data' (PICD) is further used in three different cases of drug-induced toxicity (Overview Figure):

In the first case, PICD is exemplarily applied for the hepatotoxicant azathioprine in a proof-of-principle study for rats and humans (Overview Figure) [Thiel et al., 2016]. To this end, the explicit incorporation of patient physiology in individualized PBPK models enables quantitative dose-response relationships in a patient-specific manner. Molecular mechanisms underlying acute toxicity following various dosage regimens could be thereby explored. In particular, this first application of PICD shows its potential use in clinical practice for potential risk assessment of individual patients during drug development.

Secondly, a comparative study of drug-induced hepatotoxicity is presented in the face of therapeutic and toxic drug doses (Overview Figure) [Thiel et al., 2017a]. PICD is therefore systematically applied on a set of fifteen known hepatotoxic drugs. Quantitatively analyzing the transition from therapeutic to toxic drug responses at the functional- and gene-level with particular focus on biological processes having toxicological relevance finally allows discovering molecular biomarkers and potential drug interactions.

The last case presents multiscale modeling of drug interactions at patient level (Overview Figure). The objective of this study is the investigation of the effects of caffeine on toxic events induced by acetaminophen during co-administration in humans [Thiel et al., 2017b]. In this last application, PICD is used to simulate pharmacodynamic responses of both drugs either administered individually or concomitantly. The consideration of pharmacokinetic and pharmacodynamic drug interactions at the organism and cellular level, respectively, finally reveals inhibitory and stimulatory effects of caffeine during co-medication with acetaminophen. This last analysis shows the opportunity for safety assessment of drug combination therapies by use of PICD, which eventually might play a significant role in improving patient safety in clinical care.



Overview Figure: Applications of the developed integrative multiscale approach. The developed integrative multiscale approach 'PICD' is applied in three different studies at patient level: (i) a proof-of-principle study for the hepatotoxicant azathioprine; (ii) a comparative toxicity analysis for fifteen hepatotoxic drugs; (iii) a multiscale modeling study of drug interactions between acetaminophen and caffeine. PICD, PBPK-based in vivo contextualization of in vitro toxicity data.

Besides this general introduction and a general conclusions and outlook section presented at the end, the thesis overall contains three different parts: an introductory part (Part I), a results part (Part II) containing three research chapters (Chapter 7, 8, and 9), and an appendix part (Part III). Each research chapter is structured as journal article and is composed of an abstract, an introduction, a materials and methods as well as a result and a discussion section.

In Part I, the basic knowledge underlying Part II is presented. Chapter 1 gives a brief introduction into drug toxicity emphasizing its important role in specific phases in pharmaceutical research and development. Drug-induced hepatotoxicity is thereby highlighted since drugs causing adverse effects in the liver are of great interest and are investigated in the research chapters (Chapters 7, 8, and 9). The fundamental concepts of pharmacokinetics and pharmacodynamics (Chapter 2), as well as PBPK modeling (Chapter 3) are subsequently explained. Chapter 4 deals with pharmacokinetic drug interactions and, to a minor degree, with pharmacodynamic drug interactions. General information about toxicogenomics and in particular the application of transcriptomics in a standard toxicogenomics approach is outlined in Chapter 5. At last fundamental knowledge about biomarkers, which are a key outcome of a toxicogenomics study, is given in Chapter 6. The different steps in the identification process of transcriptional biomarkers is exemplarily described in this chapter. Moreover, biomarkers for drug-induced hepatotoxicity are presented in more detail.

In the first research chapter (Chapter 7) of Part II, the development of the integrative multiscale approach PICD is presented and eventually applied in a proof-of-concept study to explore azathioprine-induced hepatotoxicity at patient level. Chapter 7 is published as original article in *Archives of Toxicology* [Thiel et al., 2016].

The second research chapter (Chapter 8) is focusing on a systematic application of PICD on fifteen known hepatotoxic drugs to perform a comparative toxicity analysis in clinically relevant situations. To this end, cellular perturbations induced by therapeutic and toxic doses are evaluated at different levels to finally predict molecular biomarkers and potential drug interactions. Chapter 8 is published as research article in *PLoS Computational Biology* [Thiel et al., 2017a].

In the third research chapter (Chapter 9), multiscale modeling is used to investigate the effect of caffeine on acetaminophen-induced toxicity during co-medication by considering pharmacokinetic and pharmacodynamic interactions between both drugs in humans. Chapter 9 is published as original article in *CPT: Pharmacometrics & Systems Pharmacology* [Thiel et al., 2017b].

Part III contains general supplementary information for Part II (Appendix A), as well as specific supplementary information for each research chapter individually (Appendix B, C, and D).

Background

Drug toxicity

Drug toxicity may simply be defined as detrimental consequence of drug intake in animals or humans. Such undesired toxic events may either occur by acute drug overdoses exceeding recommended dose levels or by chronic drug treatment of therapeutic doses over a long period of time. To detect drug-induced adverse events at an early stage during drug development (Figure 1.1), biomarkers are of utmost importance (see more in Chapter 6).

Acute overdosing may be accidental or intentional, for instance, by misuse of prescription or in case of suicidal intent. Clinical symptoms of acute drug overdoses generally arise quite short after drug administration. According to a grading system of acute poisoning [Persson et al., 1998], the degree of severity of clinical symptoms may be classified into four groups: none (0), minor (1), moderate (2), severe (3), or fatal (4). In non-fatal cases, terminating drug administration often leads to a relatively fast disappearance of the symptoms, which can be expedited by initiating countermeasures such as the application of activated charcoal that binds the drug and prevents the penetration into the bloodstream. Whether and to what extent acute overdoses may produce unwanted side effects is strongly dependent on the therapeutic window. The therapeutic window is defined as the range between the pharmacological responses induced by the minimum effective dose (MED) and the maximum tolerated dose (MTD). The narrower the therapeutic window the higher the risk for adverse drug effects. This is in particular of high relevance when inter-individual variability substantially affects important ADME processes that may result in elevated drug-concentrations at the target site and ultimately to possible toxic reactions.

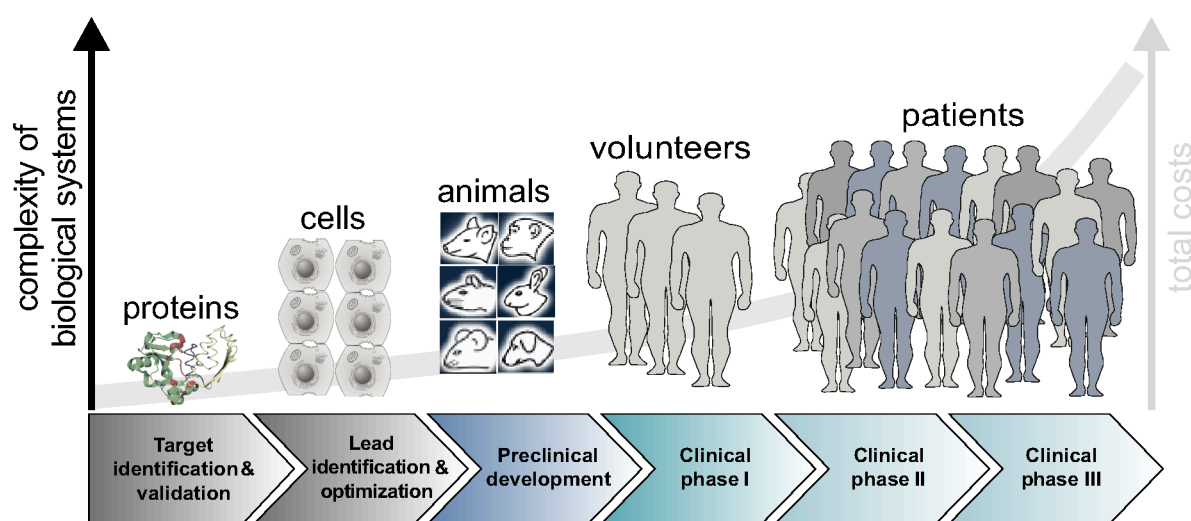


Figure 1.1: Schematic representation of the drug development process. In drug development, the total costs increase more or less exponentially over time. (adapted from [Kuepfer et al., 2012])

Chronic toxicity may be caused by a long-term drug exposure (normally more than several months) to therapeutic dose levels. In contrast to acute poisoning, chronic toxicity is more challenging to handle with respect to the early detection of adverse events and the introduction of potential countermeasures. Termination of the therapy and re-application with other pharmacologically similar agents may often help to control or even to stop such adverse drug events. However, in some cases, the manifestation of the processes underlying drug-induced toxicity might lead to persistent symptoms lasting for several months or years.

The causes of drug-induced toxicity can be separated into on-target and off-target toxicity, immune hypersensitivity, bioactivation, and, rarely, idiosyncratic response [Guengerich, 2011]. On-target and off-target toxicity is due to the interaction of the drug to its intended and alternative target, respectively. Immune-mediated drug-toxicity may be caused by the covalent binding of the drug or its metabolites to specific proteins initiating antibody production [Guengerich, 2011]. In the context of bioactivation, drugs are converted to reactive metabolites that might be accumulated in cells or tissues because of inefficient conversion and clearance processes within the body provoked by extensive drug metabolism after acute overdoses. The accumulated reactive metabolites may then interact with cellular proteins that finally may trigger toxic effects. Drug toxicity induced by idiosyncratic response is a quite rare event with a low incidence rate (one out of 1,000 or 10,000) but though quite problematic. Idiosyncratic cases are hardly predictable in first-in-human trials or clinical phase I studies. This might become a serious problem in follow-up clinical studies and in postmarketing surveillance with significantly increased numbers of patients (Figure 1.1), which, in the worst case, may end up with several clinical cases of toxicity and a market withdrawal of the considered drug.

Analyzing the attrition rates of approved drugs and drug candidates revealed that drug toxicity is one of the major causes for market withdrawals and drug attrition in pharmaceutical research and development (Figure 1.2). Based on results provided by ten big pharmaceutical companies in the US and Europe, pharmacokinetics and bioavailability were the main reasons for drug attrition in 1991 (~40 % of all attrition) [Kola and Landis, 2004] (Figure 1.2A). In 2000, this dramatically changed with a lack of clinical efficacy and safety being the primary reasons accounting for more than 50 % of all attrition [Kola and Landis, 2004]. Great advances in the area of pharmacokinetic modeling were a key factor for this shift. An overall success rate from first-in-human trials to registration of 11 % was observed on the same dataset with high variations in therapeutic indication of the compounds especially for cardiovascular and oncology drugs (difference in success rate ~15 %) (Figure 1.2B).

Similar results were presented in a study of about 800 small molecule development compounds (Figure 1.2D) [Waring et al., 2015]. Causes of failure during drug development were analyzed separately and were compared between preclinical, phase I and phase II development [Waring et al., 2015]. While non-clinical toxicology is by far the main cause of failure in the candidate nomination accounting for more than 60 % of all attrition, clinical safety (~30 %) and drug efficacy (~35 %) are the prime reasons in phase I and phase II, respectively (Figure 1.2D).

Another study about seventeen approved drugs, which were removed from Western market between 1992 and 2006, also showed that drug toxicity is substantially responsible for their market withdrawals accounting for more than 90 %, of which cardiovascular toxicity (38 %) and hepatotoxicity (31 %) were the major causes (Figure 1.2C) [Schuster et al., 2005]. Famous cases are the market withdrawals of fenfluramine, amineptine, cerivastatin, rofecoxib, and ximelagatran in 1997, 2000, 2001, 2004, and 2006, respectively. For instance, rofecoxib (Vioxx®) was launched as cyclooxygenase (COX)-2 inhibitor in 1999. It was shown that rofecoxib had a lower susceptibility to gastrointestinal toxicity than other nonsteroidal anti-inflammatory drugs (NSAIDs) such as ibuprofen or diclofenac. Five years later, the pharmaceutical company Merck withdrew rofecoxib due to an elevated risk of cardiovascular diseases like heart attack or stroke [Schuster et al., 2005].

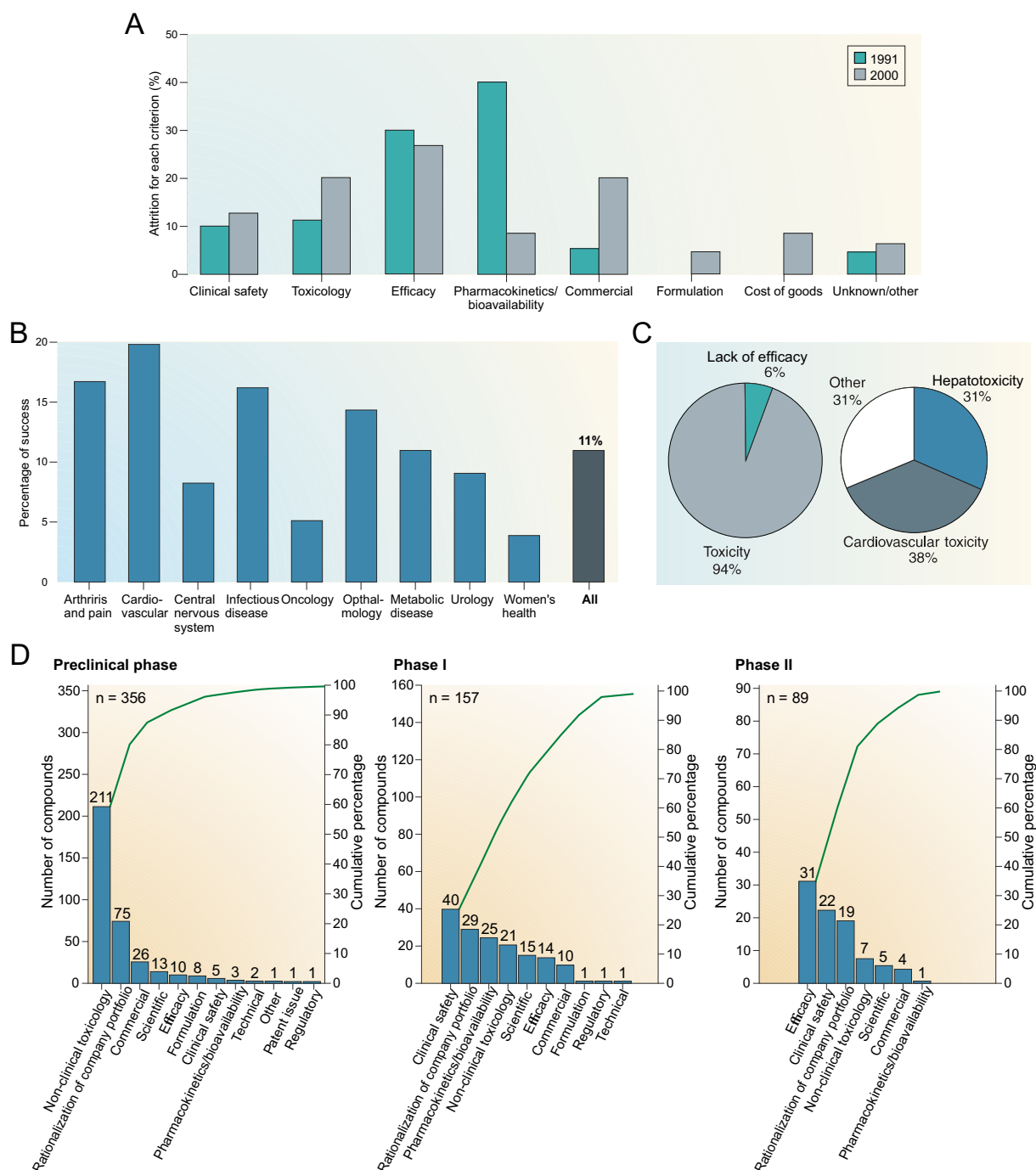


Figure 1.2: Drug attrition and success rates in drug development. (A) Reasons for attrition between 1991-2000. (adapted from [Kola and Landis, 2004]) (B) Success rates from first-in-man trials to registration between 1991-2000 based on therapeutic indication. (adapted from [Kola and Landis, 2004]) (C) Reasons for market withdrawal of seventeen drugs and corresponding toxicity profile of the withdrawn drugs. (adapted from [Schuster et al., 2005]) (D) Differences in the cause of failure for terminated compounds in preclinical, phase I and phase II development between 2000-2010. (taken from [Waring et al., 2015])

1.1 Drug-induced hepatotoxicity

Drug-induced hepatotoxicity is the leading cause of acute liver failure in the US and Western Europe [Russmann et al., 2009; Wang et al., 2013]. The liver is the most important metabolic organ with multiple key functions such as the metabolism of carbohydrates, lipids, or proteins, as well as drug detoxification. Due to its primary role in metabolizing drugs, the liver is a particular target for drug-induced toxicity.

Although the incidences of idiosyncratic drug-induced liver injury (DILI) are rare (less than one per 10,000 exposed patients) [Russmann et al., 2009], liver disorders may have severe consequences emphasized by a strikingly high mortality rate [Bernal et al., 2010]. The detection of liver failure induced by drug treatment is a very challenging task and hardly foreseeable [Kaplowitz, 2004]. Newly investigated DILI biomarkers with both a high sensitivity and specificity are hence indispensable to predict such toxic events causing hepatic insufficiency (see more in section 6.2).

DILI events can be classified as predictable (also direct or intrinsic), or unpredictable (also indirect or extrinsic) often termed as idiosyncratic [Russmann et al., 2009; Kaplowitz, 2004; Wang et al., 2013]. Predictable DILI events are mostly dose-dependent with a high incidence, whereas unpredictable DILI events primarily occur with a low incidence and without an obvious dose-dependency [Kaplowitz, 2004]. Intrinsic hepatotoxicity usually includes direct cell stress provoked by the drug or its metabolites, while the pathogenesis of idiosyncratic DILI is usually immune-mediated involving innate or adaptive immune responses. However, the question how the activated immune system cause DILI remains rather unclear [Wang et al., 2013]. Prominent examples of drugs causing predictable and unpredictable hepatotoxicity are acetaminophen with a short latency (few days), as well as phenytoin and isoniazid with intermediate (one to eight weeks) and long (about one year) latency, respectively [Kaplowitz, 2004]. Predictable DILI events are often associated with hepatitis, for instance, induced by amiodarone or acetaminophen. In the case of acetaminophen overdose, a depletion of glutathione leaves the reactive intermediate N-Acetyl-p-benzoquinone imine (NAPQI) free to interact with critical proteins within the cell eventually causing drug-induced adverse events [Jaw and Jeffery, 1993].

A classification system based on FDA-approved drug labeling was proposed to assess the DILI potential for several drugs [Chen et al., 2011]. The provided benchmark dataset contains 287 drugs that covers a wide range of therapeutic categories. The systematic classification scheme includes severity scores between one (mild symptoms e.g., steatosis) to eight (fatal symptoms) [Chen et al., 2011].

The majority of drug-induced liver diseases can be grouped into three patterns: (i) hepatocellular (acute hepatitis), (ii) cholestatic (acute cholestasis), (iii) and mixed (hepatocellular/cholestatic) [Kaplowitz, 2004]. These patterns are defined by typical clinical signatures including affected laboratory values such as alanine transaminase and alkaline phosphatase [Kaplowitz, 2004]. In addition, there are several other liver pathologies such as liver fibrosis or steatohepatitis playing a minor role [Wang et al., 2013]. In a study about 446 DILI cases observed between 1994-2004 in Spain, the distribution of hepatitis, cholestasis and the mixed presentation was 58 %, 20 % and 22 %, respectively [Andrade et al., 2005]. The most responsible drug treatment causing liver failure in 13 % of all cases was the concomitant administration of amoxicillin and clavulanate (37 % hepatocellular, 27 % cholestatic, and 36 % mixed, $n = 59$). A similar incidence of the three major patterns was shown in another study about 1674 DILI cases reported in Japan between 1997-2006 (59 % hepatocellular, 21 % cholestatic, and 20 % mixed) [Takikawa et al., 2009]. Frequent symptoms noticed at diagnosis were jaundice, anorexia, nausea/vomiting, fever, pruritus, and skin rash [Takikawa et al., 2009].

The accepted definitions of the three most severe manifestations of DILI (hepatitis, cholestasis, and the combination of both) are helpful in clinical practice since they are based on observed elevations of clinically-measured enzyme levels. However, this classification system is rather descriptive. Because understanding the mechanisms underlying drug-induced hepatotoxicity is very crucial in order to develop strategies to predict and prevent DILI events, a three-step working model of DILI was proposed taking into account mechanistic concepts of hepatotoxicity (Figure 1.3) [Russmann et al., 2009].

In a first step, reactive metabolites or to a lesser extent the parent drug lead to an initial injury either by inducing direct cell stress (intrinsic pathway), specific immune reactions (extrinsic pathway), or direct mitochondrial inhibition (Figure 1.3). Direct cell stress may be exerted through drug metabolites, which can be reactive radicals promoting or undergoing reactions such as glutathione depletion or covalent

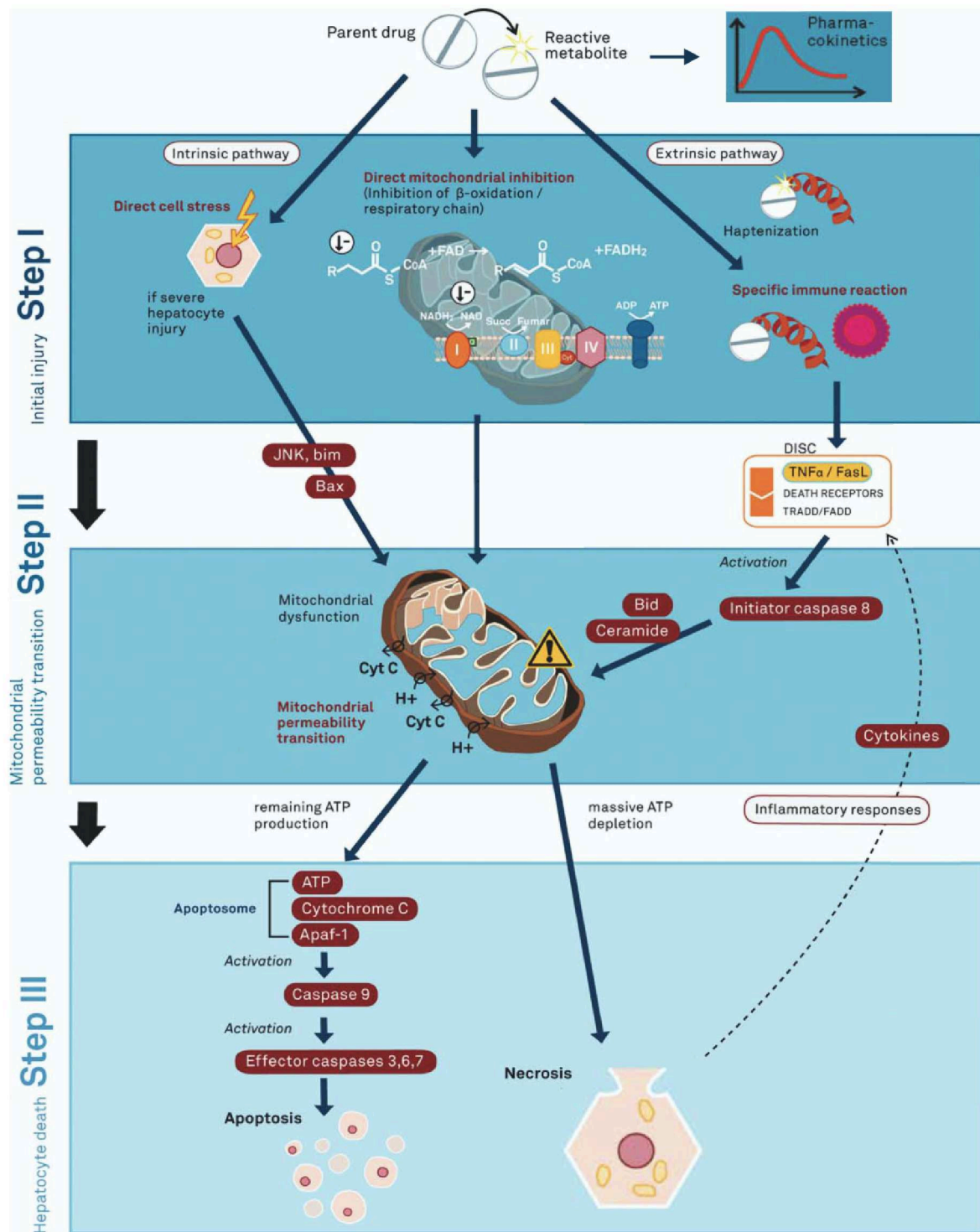


Figure 1.3: Three-step working model of drug-induced hepatotoxicity. An initial injury caused by a specific immune reaction, direct mitochondrial inhibition or cell stress leads to a mitochondrial dysfunction and finally to hepatocyte death by necrosis or apoptosis. (adapted from [Russmann et al., 2010])

binding to enzymes, proteins, or nucleic acids. They also may regulate key hepatocellular functions such as the bile salt efflux pump by activating or inhibiting signal kinases or transcription factors [Russmann et al., 2009; Kaplowitz, 2004]. The direct mitochondrial inhibition mainly includes the inhibition or uncoupling of the β -oxidation or the respiratory chain leading to ATP depletion and increased reactive oxygen species. The covalent binding of reactive metabolites to proteins forming neo-antigens (hapteneization) may result in antibody formation, which eventually stimulates specific immune responses (Figure 1.3).

In case that mitochondrial permeability transition (MPT) did not occur through direct impairment of mitochondrial functions, the initial injury may evoke an opening of the MPT pore by regulation of pro- and anti-apoptotic factors. This may subsequently enable a tremendous influx of protons and in turn a release of cytochrome c into the cytosol. In the intrinsic pathway, pro- and anti-apoptotic proteins such as Bax and bim might be activated and inhibited, respectively, by c-jun N-terminal kinase (JNK). In the extrinsic pathway, the release of tumor necrosis factor α (TNF α) and Fas ligand (FasL) is increased by specific immune reactions. The death-inducing signaling complex (DISC) involving TNF α -receptor and FasL-associated death domain proteins (TRADD/FADD) stimulates initiator caspase 8, which activates other pro-apoptotic proteins (e.g., BH3 interacting-domain death agonist [Bid]) and signaling lipids like ceramide (Figure 1.3) [Russmann et al., 2009].

Finally, the mitochondrial dysfunction lead to apoptosis or necrosis dependent on the availability of ATP (Figure 1.3). A massive ATP depletion initiates necrosis characterized by cell swelling and lysis. Cell lysis may trigger the release of cytokines through inflammatory responses, which may amplify the initial injury by sensitizing other hepatocytes [Russmann et al., 2009]. In case of a remaining ATP production by still intact mitochondria, the programmed apoptotic cell death is provoked under energy consumption by the apoptosome. The apoptosome consisting of cytochrome c, apoptotic protease-activating factor 1 (apaf-1) and ATP thereby activates caspase 9, which further activates effector caspases ultimately ending up in hepatocyte death (Figure 1.3).

Several environmental and genetic risk factors influence the susceptibility of severe DILI events in individual patients and, thus, complicate to make predictions with a high confidence. Drug interactions or genetic variations in ADME-related enzymes and transporters may alter the drug concentration-time course at the target site and may finally increase the risk for hepatotoxic events [Russmann et al., 2010]. Furthermore, pre-existing liver diseases (e.g., hepatitis B or C) in patients are supposed to play a major role in the development of acute or chronic liver failure [Kaplowitz, 2004].

1.2 Modeling drug-induced toxicity with systems biology models

One key goal of using systems biology models in clinical toxicology is to quantitatively investigate dose-response behavior of various small molecules or biologics in humans for studying drug-induced adverse events at the cellular scale. Different concepts of modeling drug-induced toxicity, in particular hepatotoxicity, are exemplarily discussed in the following, which utilize (i) computational systems biology pathway models, (ii) agent-based models, or (iii) ordinary differential equation (ODE)-based multiscale mechanistic models.

Bhattacharya et al. proposed an approach of causal network mapping that can be applied, for instance, on nuclear receptor (NR) pathways such as the peroxisome proliferator-activated receptor α (PPAR α) pathway, to analyze NR-mediated transcriptional regulation [Bhattacharya et al., 2012]. After heterodimerization with retinoid X receptor (RXR), PPAR α plays a central role in fatty acid metabolism in the liver. The use of dynamic gene expression signatures in combination with in vitro binding data thereby allows the discrimination of regulatory hubs according to concentration- or time-dependent effects. Moreover, the latter approach coupled with simulated in vivo concentrations of various drugs would clearly enhance the understanding of drug-induced transcriptional changes at patient level [Thiel et al., 2016].

In agent-based modeling approaches, 'agents' such as molecules or cells are modeled as discrete entities. Well-stirred compartments as assumed by several ODE-based modeling approaches are hence not required. Such spatial modeling concepts may be used to represent multicellular in vivo environments of specific organs (so called 'virtual tissues') by partitioning in individual cells, which extend conventional compartmental models [Shah and Wambaugh, 2010]. Agent-based spatial modeling of the liver lobule can

be realized, for instance, by utilizing the NetLogo software framework [Chiacchio et al., 2014]. The toxicant 2,3,7,8-tetrachloro-dibenzo-p-dioxin (TCDD) acts through binding to the aryl hydrocarbon receptor (AhR). To study spatio-temporal cellular effects of TCDD and subsequently liver damage, an agent-based model of the liver lobule can be linked to a mechanistic model representing the AhR toxicity pathway in liver cells. The accumulation of TCDD in the liver can be realized by a correspondent PBPK model of TCDD that allows the simulation of tissue concentrations over time for different doses [Bhattacharya et al., 2012].

Hamon et al. incorporated in vitro pharmacokinetics of cyclosporine A as well as correspondent transcriptomic, proteomic, and metabolomic data into a systems biology model of the nuclear factor erythroid-derived 2-like 2 (Nrf2) pathway. Time- and dose-dependent cellular response of cyclosporine A to oxidative stress could be successfully reflected by the coupled pharmacokinetic-systems biology model [Hamon et al., 2015].

The DILIsymTM model is a multiscale mechanistic model that represents physiological processes involved in drug-induced hepatotoxicity [Woodhead et al., 2012; Howell et al., 2012]. The development of this model was made possible by the DILI-sim Initiative guided by the Hamner Institutes for Health Sciences. Since DILIsymTM is divided into submodels including, inter alia, PBPK dynamics, glutathione (GSH) depletion, and clinical biomarkers, the model is particularly well suited to analyze hepatotoxic events induced by reactive metabolites, as is the case with NAPQI during acute acetaminophen overdose. The application of DILIsymTM, moreover, allowed the evaluation of N-acetyl cysteine (NAC) treatment protocols with respect to intervention strategies for acute liver failure caused by acetaminophen overdose.

Pharmacokinetics and pharmacodynamics

The efficiency of a drug within the body is basically determined by two major aspects: (i) the amount of drug that reaches the target site (e.g., a specific organ); (ii) the pharmacological action of the drug at the target site (e.g., drug binding to a specific receptor). The underlying processes are studied by pharmacokinetics and pharmacodynamics, respectively.

2.1 Pharmacokinetics

Pharmacokinetics (PK) studies the rate and extent of processes that determine the amount of drug over time after administration to a living organism (Figure 2.1A). These processes include drug absorption, distribution, metabolism, and elimination (ADME) (Figure 2.1B). In the course of this, the living organism is regarded as an open system and the applied substance as perturbation of the steady-state. Pharmacokinetics comprise all processes trying to restore the dynamic equilibrium after drug exposure. These processes are influenced by drug-specific properties such as the molecular weight or the lipophilicity, as well as by individual-related factors, for instance, the age, the gender, or renal and hepatic failure.

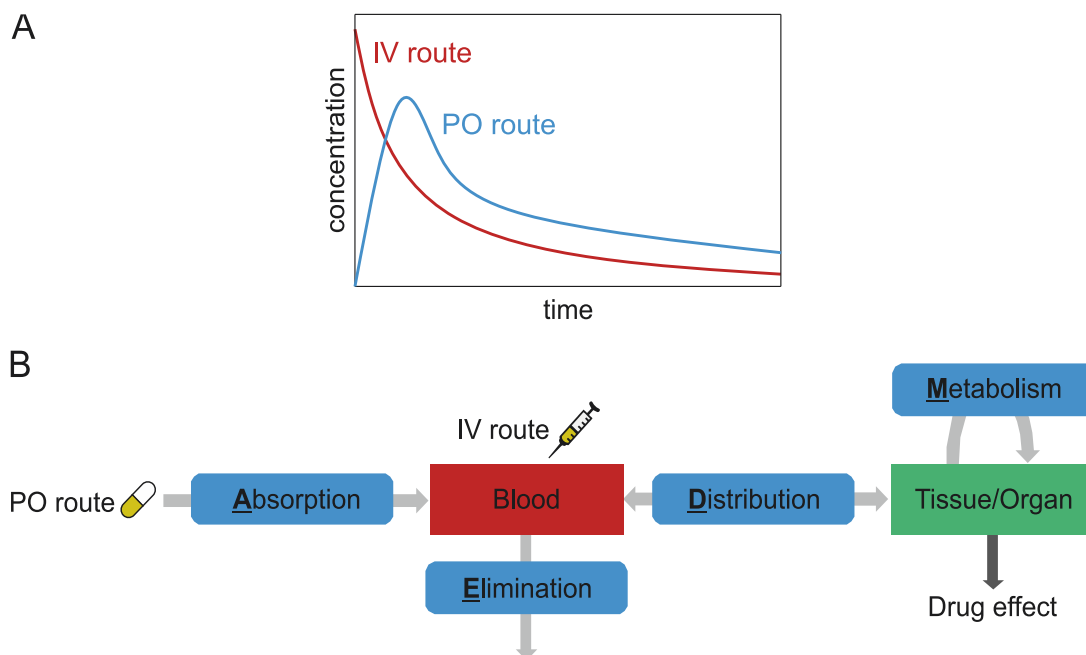


Figure 2.1: Pharmacokinetics. (A) Typical pharmacokinetic profile showing drug concentrations over time in blood plasma following an oral (PO) (blue) and an intravenous (IV) (red) administration. (B) Schematic representation of pharmacokinetic processes including absorption, distribution, metabolism, and elimination. The entry points of the IV and the PO administration routes are additionally illustrated.

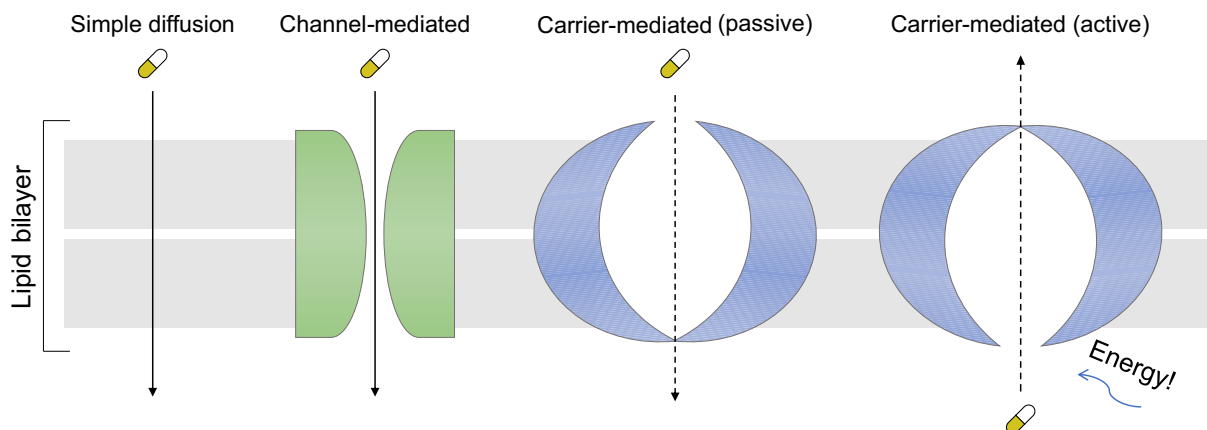


Figure 2.2: Passive and active drug transport mechanisms. Passive and active drug transport mechanisms comprise simple diffusion, channel-mediated and carrier-mediated (passive, active) transport. In the case of active transport, the drug is transported under the consumption of energy. (adapted from www.fwcdscience.wikispaces.com/)

2.1.1 Absorption

Absorption describes the route on which a drug enters the blood circulation. The administration route determines to what extent absorption occurs. In case of intravenous (IV) administration, the drug is directly entering the blood circulation, while after oral (PO) drug administration the blood circulation is reached via the gastro-intestinal tract by passing the intestinal wall. The barrier between the gastric mucosa and the blood circulation is formed by the surface membrane of the cells. There are both passive and active transport mechanisms to pass this semipermeable membrane (Figure 2.2).

In case of passive lipid diffusion, the partition coefficient between lipids and water is often considered to quantify the extent of drug absorption. In that respect, the logarithm of the octanol/water partition coefficient ($\log P$) is mostly used. Drugs with high $\log P$ values such as diclofenac or amiodarone generally show a higher absorption contrarily to drugs with low $\log P$ values (e.g., isoniazid). Moreover, the acid dissociation constant (pK_a) of a drug represents also a key parameter for drug absorption since the ionization of a drug may influence its absorption characteristics. In this regard, simple diffusion is favored for drugs that are present in its unionized state.

In contrast to passive diffusion, drugs may also be transferred across the membrane by channel- or carrier-mediated transport processes whereby active carrier-mediated transport occurs under the consumption of energy (Figure 2.2). P-glycoprotein (P-gp) is a protein of the cell membrane that is found to be an important transporter for several drugs [Brown and Tomlin, 2010]. Since P-gp is not only expressed in the GI-tract but also in the liver or kidney, for instance, P-gp-mediated transport also plays an essential role in drug distribution and elimination.

Apart from these mechanisms, physiological factors like gastric emptying or blood flow rates, as well as dietary intake and other physicochemical properties of the drug may have a decisive influence on the amount of drug that is entering the systemic circulation.

The bioavailability is a measure to denote the absorbed fraction of the drug entering the systemic circulation after oral administration. By definition, the bioavailability after intravenous drug administration is 100 %. Besides the influencing variables mentioned above, the bioavailability is heavily altered due to the extent of the first-pass effect, which describes the 'first-pass' of the drug through the liver after the absorption phase. Since a certain amount of drug at the site of action is required to exert its therapeutic effect, the bioavailability should be as high as possible for orally administered pharmaceuticals.

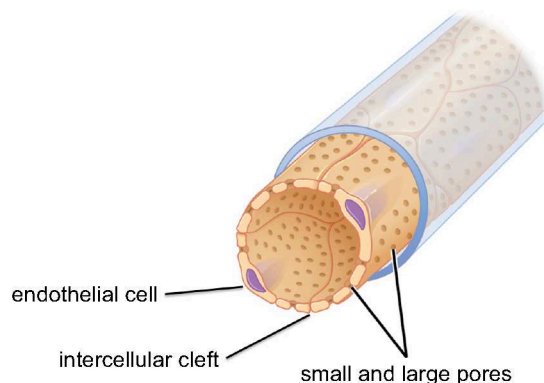


Figure 2.3: Capillary structure. A simplified capillary structure including the endothelial cells, intercellular clefts, as well as small and large pores. (adapted from cnx.org/content/m46597/latest/).

2.1.2 Distribution

Distribution describes the reversible drug exchange between the blood and the tissues and organs. After having passed the gastric mucosa, the drug is distributed from the bloodstream through capillaries to the site of action due to a concentration gradient from the blood to the tissues and organs until the partition equilibrium is reached. The initial rate of distribution is strongly influenced by blood flow.

To exert their pharmacological action in the target organ, drugs often reach their site of action through extracellular fluids by passing through the endothelial wall. Small and large pores as well as intercellular clefts between adjacent vascular endothelial cells thereby allow a permeation through the endothelial membrane (Figure 2.3) [Palade et al., 1979]. The relative contribution of this process to drug disposition depends on the molecular weight. Macromolecular pharmaceuticals benefit more from a higher number of these pores than small molecules, since the intercellular cleft mainly allows the exchange of substances with a low molecular weight. Likewise in the absorption phase, logP values also play an important role for distribution processes because of lipid diffusion.

Beside passive and active transport mechanisms across the endothelial membrane, reversible binding to plasma proteins, in particular to albumins and α_1 -acid glycoproteins, significantly prolong the residence time of a drug in capillaries [Jusko and Gretch, 1976]. Protein binding prevents the drug from penetration into the tissues since the formed drug-protein complex is too large to reach the interstitial tissue fluid (Figure 2.4). As a consequence, only the unbound fraction (F_u) of the drug is available at the site of action, which may be indispensable for drug efficacy.

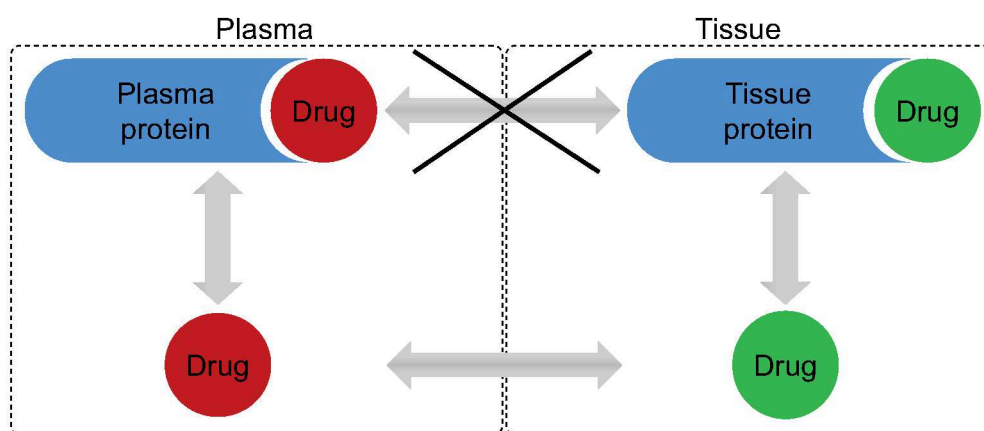


Figure 2.4: Influence of plasma protein binding. Drug transport between the blood plasma and certain tissues only occurs if the drug is not bound to plasma proteins. (adapted from [Mutschler et al., 2001])

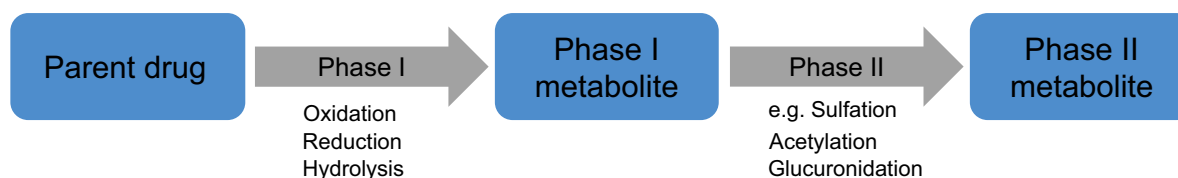


Figure 2.5: Drug metabolism. The two phases of drug metabolism leading to phase I and phase II metabolites. In phase I, oxidation, reduction, and hydrolysis reactions predominantly occur. In phase II, phase I metabolites are mostly conjugated with groups such as acetyl, sulfate, or glucuronic acid. (adapted from [Mutschler et al., 2001])

2.1.3 Metabolism

Drug metabolism comprises biotransformation processes from parent compounds into corresponding metabolites. These chemical changes of xenobiotics lead to detoxification and improve the conditions for excretion. For instance, the renal elimination of highly lipophilic compounds is clearly retarded in contrast to more polar substances [Reynolds and Knott, 1989]. Thus, lipid-soluble drugs were chemically modified to become more water-soluble. Moreover, in the metabolism phase some inactive prodrugs were transformed into its active form. Azathioprine, for instance, is catalyzed into 6-mercaptopurine by glutathione transferase thereby making the prodrug pharmacologically active. However, it may also happen that reactive intermediates are formed, for instance, due to saturation of enzymatic pathways or impaired capacity of transport processes, which eventually may induce adverse drug effects. One prominent example is the increased conversion of acetaminophen to its reactive metabolite NAPQI due to a depletion of glutathione, which allows NAPQI to more frequently interact with macromolecules within the cell [Jaw and Jeffery, 1993].

Drug metabolism can be divided into two phases (Figure 2.5). In the first phase, parent drugs are transformed to phase I metabolites predominantly by oxidation, hydrolysis or reduction. Cytochrome P450 (CYP) monooxygenase enzymes are of utmost importance for oxidative reactions. They differ in the amount in various organs due to tissue-specific protein abundance that often reaches the highest level in the liver [Wrighton and Stevens, 1992]. Enzymes of the cytochrome P450 family catalyze a wide range of drugs because of their low substrate specificity. For instance, CYP2C19 chemically modifies warfarin as well as diazepam to their corresponding phase I metabolites [Scordo et al., 2004]. The CYP enzymes CYP3A4, CYP2D6, CYP1A2, CYP2C9, and CYP2C19 account for about 90 % of phase I metabolism with a minor contribution of CYP2A6, CYP2B6, CYP2C8, and CYP2E1 [Brown and Tomlin, 2010].

Phase II consists of conjugation reactions with endogenous substances that often result in an inactivation of the parent drug and in a decrease in lipid solubility. Acidic groups are generally added here. In this way, hydrophilicity is increased and facilitates elimination mechanisms to easier pass into urine. The transfer of glucuronic acid is an important example of such modifications [Brodie et al., 1958]. To add groups such as sulfate, acetyl, or glucuronic acid, a prerequisite is the attachment of an adequately labile group to the drug, mostly a hydroxyl or thiol group, that is fulfilled during phase I metabolism [Brown and Tomlin, 2010].

Since genetic polymorphism as well as anatomical and physiological characteristics may alter the expression of metabolizing enzymes, inter-individual variability can have a significant influence on drug concentrations in plasma and at the target site. This may, in turn, lead to different dose levels that are required to attain the same therapeutic effect. For instance, acetylation is an important step in the metabolism of isoniazid. In therapeutic indication, individuals classified as slow acetylators, thus, need higher doses than individuals identified as fast acetylators [Cordes et al., 2016].

The most dominant organ for drug metabolism is the liver, even though other organs are considerably involved such as the kidney or the gastro-intestinal tract. The latter plays a crucial role particularly

after oral drug administration, since several ADME enzymes and transporters are also expressed in the intestine and the stomach. Hence, these enzymes may metabolize drugs during the absorption phase and thus may significantly reduce their bioavailability. Consequently, the orally administered dose of drugs with a low bioavailability need to be increased compared to intravenous administration in order to reach the same therapeutic efficiency.

Dietary intake may also have a substantial impact on drug metabolism. For instance, the intake of grapefruit juice can considerably inhibit the expression of CYP3A4. In this way, the concentration-time profile of drugs extensively metabolized by CYP3A4 (e.g., felodipine or cyclosporine A) can be significantly changed [Bailey et al., 1998].

2.1.4 Elimination

The excretion of a parent drug and their metabolic products from the body is referred to as elimination. The two most prominent ways to remove exogenous substances from the body are the renal excretion via the kidney into urine, as well as the biliary excretion via the gallbladder into the intestine and finally into feces. Which way is used is mainly driven by compound-specific properties such as the molecular weight and the lipophilicity [Rollins and Klaassen, 1979].

In case of renal elimination, two prominent mechanisms occur (Figure 2.6): (i) the glomerular filtration, (ii) and the tubular secretion. Glomerular filtration is a passive diffusion process where the unbound drug or metabolite is filtered from renal glomerular capillaries into urine. Drug-protein and metabolite-protein complexes with a high molecular weight are not filtered by this passive process since the complexes are too large to pass through the capillary system.

The tubular secretion, on the other hand, is an active mechanism that describes a carrier-mediated excretion. Acidic and basic compounds are thereby transported by two non-selective carrier systems located in the proximal tubule [Brown and Tomlin, 2010]. The major benefit of this clearance mechanism

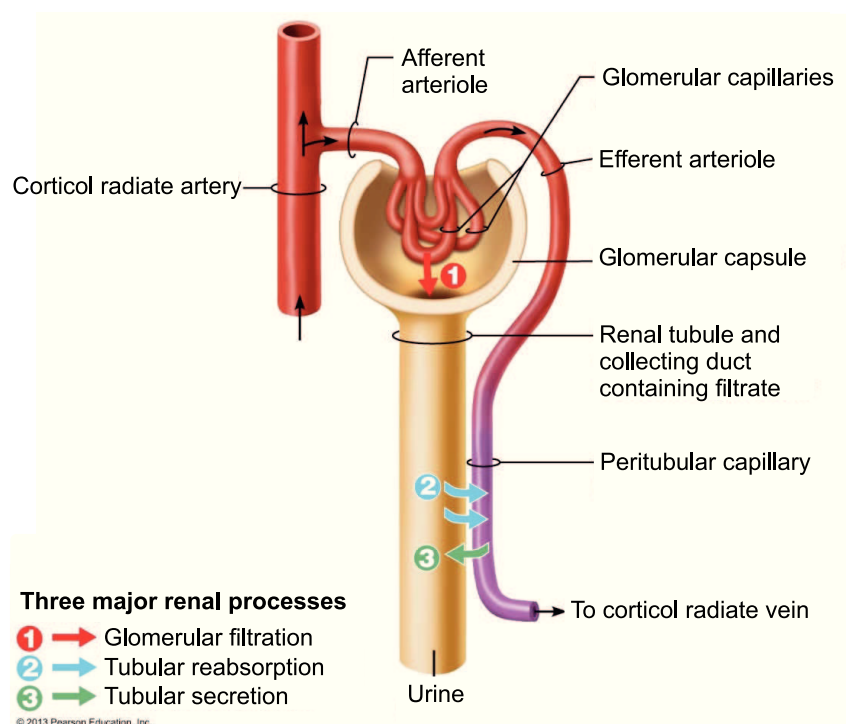


Figure 2.6: Major renal processes. There are three major renal processes occurring in the kidney: Glomerular filtration (passive), tubular secretion (active), and tubular reabsorption (mostly passive). (taken from http://classes.midlandstech.edu/carterp/Courses/bio211/chap25/figure_25_09_labeled.jpg)

compared to glomerular filtration is the facilitated dissociation of the drug or the metabolite from plasma proteins, which allows an enhanced renal excretion even for high plasma protein binding rates. Once the compound reached the tubular fluid, either by glomerular filtration or tubular secretion, a tubular reabsorption may subsequently occur (Figure 2.6). In this mainly passively driven process, the drug or the metabolite is reabsorbed by diffusion from the tubular fluid into the blood. The extent of reabsorption of the compound is dependent on its lipid solubility and its pKa value. Highly lipophilic and weak acidic compounds are more prone for tubular reabsorption than hydrophilic and more alkaline compounds assuming a slightly acidic pH of the urine [Brater, 2002]. Elimination can further be increased by specific active transport processes mostly mediated by apical ATP-binding cassette (ABC)-transporters like the multi-drug-resistant protein 2 (MDR2) [Nies and Keppler, 2007].

Patients with renal insufficiency may have a reduced drug clearance via the kidney and, thus, an increased systemic exposure. A consequence might be drug toxicity in particular if the drug and its metabolites are predominantly excreted in urine, such as acetaminophen [Wishart et al., 2006]. To decrease the high systemic drug exposure and finally to avoid such adverse events, dose adjustments may be suggested as in the case of cyclophosphamide treatment [Haubitz et al., 2002].

In the case of biliary excretion, the parent drug and its metabolites can be transported from the liver via the bile into the intestine and subsequently into feces. In this regard, enterohepatic circulation may occur, especially for drugs and metabolites with high lipophilicity because of a reabsorption from the intestine. This enterohepatic circulation can significantly prolong the half-life of applied drugs and eventually the desired drug effects [Brown and Tomlin, 2010].

2.2 Pharmacodynamics

In contrast to pharmacokinetics, which study ADME processes leading to the specific concentration-time course of a drug within the body, pharmacodynamics (PD) investigate the effect of a drug at the target site. This contains the study of the mechanism of action and the side of action of the drug, as well as drug efficacy and drug potency [Mutschler et al., 2001]. The latter two describe the maximal response that is achievable from the drug (efficacy) and the concentration that is needed to cause a specific intensity of this response (potency). Drug potency and efficacy are key determinants to characterize concentration-response profiles for specific drugs. An example of concentration-response relationships for two arbitrary drugs differing in drug efficacy and potency is illustrated in Figure 2.7.

Most of the clinically approved drugs are initiating their desired activity by specific interactions with targets associated with the disease to be treated, such as receptors, key enzymes, transporters, and, to a lesser extent, DNA, RNA, and lipids. A recent study about more than 800 small molecule compounds revealed a distribution of the five most popular target classes containing G-protein-coupled receptors (34 %), enzymes (20 %), kinases (15 %), nuclear hormone receptors (11 %), and ion channels (8 %) [Waring et al., 2015]. The mechanisms of action for a wide range of drugs involve (i) a specific binding to membrane-bound or intracellularly located receptors to attain a stimulation or perturbation of signal cascades and a down- or up- regulation of transcription regulation, respectively, (ii) the activation or inhibition of key metabolic reactions or active transport processes mediated by target enzymes or transporters, and (iii) the specific opening or closing of ion channels [Mutschler et al., 2001].

The most common drug mechanisms of action are receptor-mediated by the formation of a drug(D)-receptor(R)-complex (DR):



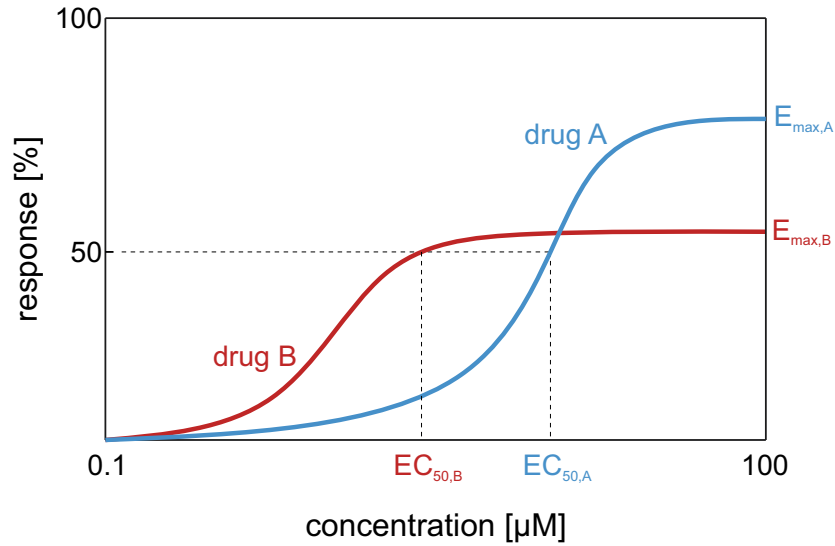


Figure 2.7: Drug concentration-response relationship. Drug concentration-response profiles are presented for two arbitrary drugs differing in their efficacy and potency. Drug A (blue) shows a higher efficacy than drug B (red) ($E_{\max,A} > E_{\max,B}$). In contrast, drug B is more potent than drug A, referring to a half maximal response ($EC_{50,B} < EC_{50,A}$). E_{\max} , maximal possible response; EC_{50} , half maximal effective concentration.

Whether and to what extent this complex is formed is determined by the dissociation constant K_d , which is defined as follows:

$$K_d = \frac{[D][R]}{[DR]} \quad (2.2)$$

where $[D]$, $[R]$, and $[DR]$ are the concentrations of the drug, the receptor, and the drug-receptor complex, respectively. In this context, drugs can either stimulate or inhibit the receptor-mediated response (i.e., act as agonist or antagonist). A further distinction is often made between pure and partial agonists, as well as competitive, non-competitive and uncompetitive antagonists. These terms describe the magnitude of stimulation of the mediated response and the type of inhibition, respectively.

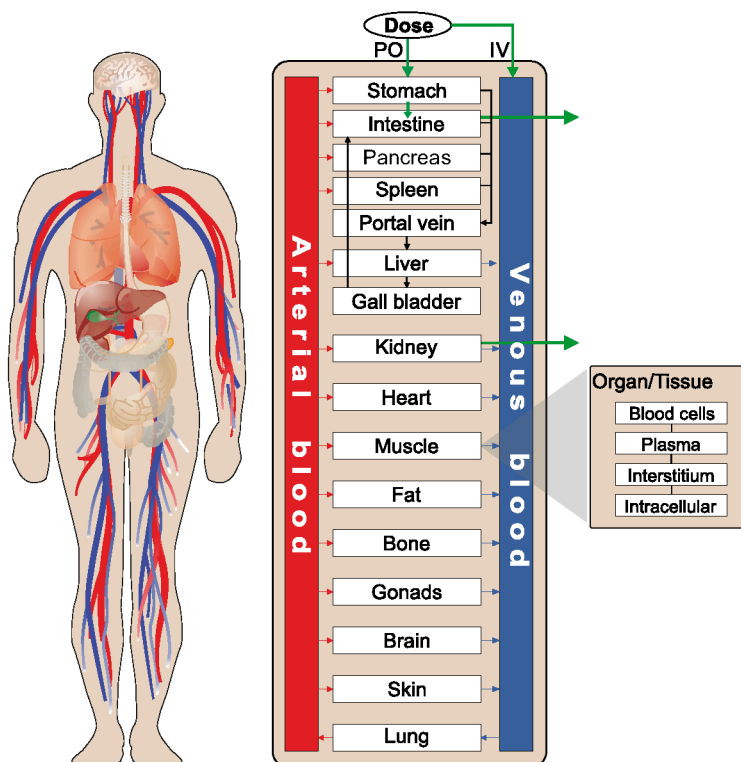
Physiologically-based pharmacokinetic modeling

The goal of pharmacokinetic modeling is to explore quantitative relationships between the fate of administered drugs in a living organism with drug concentration-time profiles obtained in preclinical animal tests and clinical trials. A widely-used concept to model pharmacokinetics is PBPK modeling [Barron et al., 1990].

The basic idea behind the concept of PBPK modeling is the description of the human body with compartments representing real tissues and organs [Jones et al., 2009]. These compartments are connected by the blood circulation and can be further subdivided into blood cells and plasma, as well as the interstitial and the intracellular space (Figure 3.1). Distribution models can describe mass transfer based on physicochemical drug properties in order to determine partition coefficients between the compartments [Rodgers and Rowland, 2006; Rodgers et al., 2005; Schmitt, 2008; Willmann et al., 2005].

PBPK models are mechanistic models that describe pharmacokinetics based on drug-specific properties as well as on prior knowledge about the physiology and anatomy of the organism. Physiological processes can be thus represented at a very high level of detail. The mechanistic understanding allows the prediction of drug concentration-time profiles not only in the plasma but also at the site of action, which is of high relevance in pharmaceutical research and development [Kuepfer et al., 2016].

Figure 3.1: Schematic representation of a multiscale whole-body PBPK model. The presented multiscale whole-body PBPK model includes fifteen different tissues and organs that are connected by blood flow. Subcompartmentalization into blood cells, blood plasma, interstitial and intracellular space is exemplarily presented for a default compartment.



3.1 Applications

The applications of PBPK modeling in pharmaceutical research and development are diverse ranging from the use of PBPK models in preclinical drug development towards translational modeling approaches in humans (Figure 3.2).

Since PBPK modeling aims for a mechanistic understanding of physiological processes describing drug-related ADME processes within the body, PBPK models are well-suited for different extrapolations scenarios (Figure 3.2): (i) cross-species extrapolations, e.g., to extrapolate the PK profile of a drug from mice to humans; (ii) dose extrapolations, e.g., to simulate drug concentration-time profiles for toxic doses observed in humans based on PBPK models validated for therapeutic indication; (iii) extrapolations to different patient subgroups, to infants or elderly people, for whom specific administration protocols are hard to apply due to safety concerns regarding potential adverse drug reactions. Moreover, multiscale modeling approaches, which couple PBPK models and *in vitro* drug response data at the organism and cellular level, respectively, may help to identify clinical biomarkers and drug interactions (Figure 3.2). The mechanisms underlying drug-induced toxicity may also be investigated by such approaches.

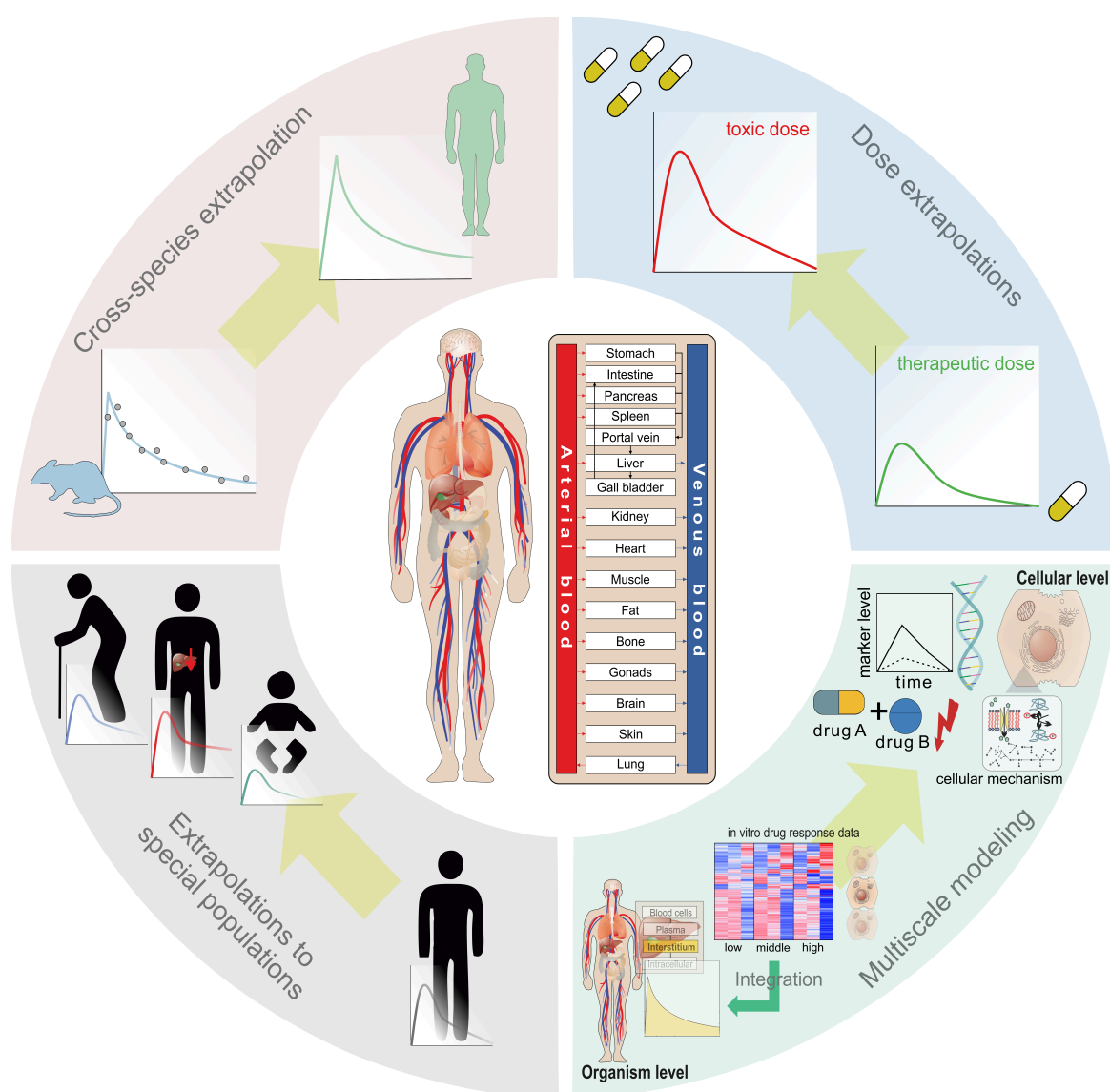


Figure 3.2: Applications of PBPK modeling. Schematic representation of important applications of PBPK modeling. (adapted from [Kuepfer et al., 2016])

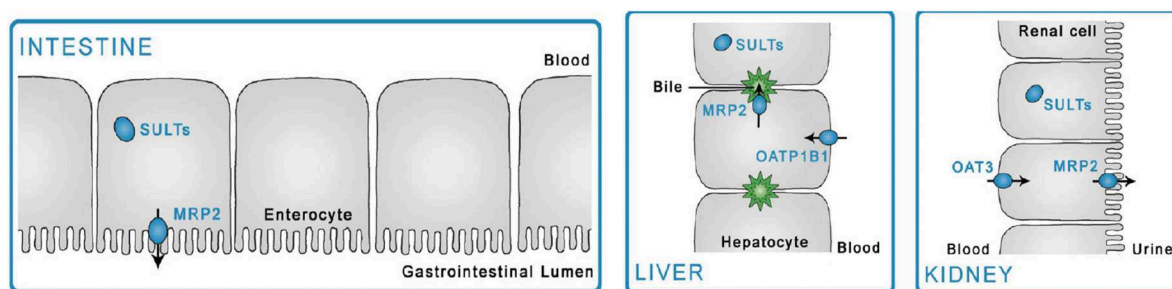


Figure 3.3: Drug-related biological processes for pravastatin. Enzymes and transporters involved in drug metabolism and distribution of pravastatin. (taken from [Meyer et al., 2012])

3.2 Model development and validation

Besides the administration protocol specifying the dose level and the route of administration, a PBPK model generally consists of two major components: a drug and an individual (Figure 3.4). The drug is defined by specific physicochemical properties, such as the molecular weight or the lipophilicity, as well as by drug-specific biochemical reactions describing drug metabolism and excretion. The individual consists of organism-specific parameters characterizing the anatomy and physiology, such as organ volumes or blood flow rates. Since protein-mediated processes in drug metabolism and elimination occur simultaneously in various tissues and organs, tissue-specific gene expression profiles can be used to estimate the abundances of involved enzymes and transporters in specific compartments within the PBPK model [Meyer et al., 2012]. In this regard, several enzymes and transporters are involved in the metabolism and distribution of the drug pravastatin such as the apical multi-drug-resistant protein 2 (MRP2), which is responsible for drug transport in the intestine, the liver, and the kidney (Figure 3.3).

To create a PBPK model both components, the individual and the drug, are merged thereby linking enzyme and transporter abundances in specific compartments of the organism to initial drug-specific kinetic parameters (Figure 3.4). In this way, biological processes are considered that represent ADME processes of the considered drug in the specific individual.

The next step in PBPK model development is model identification and parameter optimization by comparing simulated concentration-time profiles with measured clinical PK data in order to establish a reference PBPK model (Figure 3.4). Once a sufficient model accuracy is reached, quantified in general by visual inspection, model validity can be confirmed by extrapolating the initial reference PBPK model to different dosage regimens or different patient populations. Note that all model parameters of the reference PBPK model are left unchanged for the validation step, except anthropometric parameters characterizing the specific patient subgroup.

3.3 Model parameters

Apart from information specifying the administration protocol, PBPK model parameters can be separated into drug-specific and organism-specific parameters that are linked to represent drug-related biological processes of the considered drug in the specific individual (Figure 3.4) [Kuepfer et al., 2016].

Drug-specific parameters

In a PBPK model, the physicochemistry of a drug and its metabolites are mostly described by parameters specifying the molecular weight, the lipophilicity, the plasma protein binding, the strength of acidic and basic groups, and the solubility. These physicochemical properties may have a significant influence on

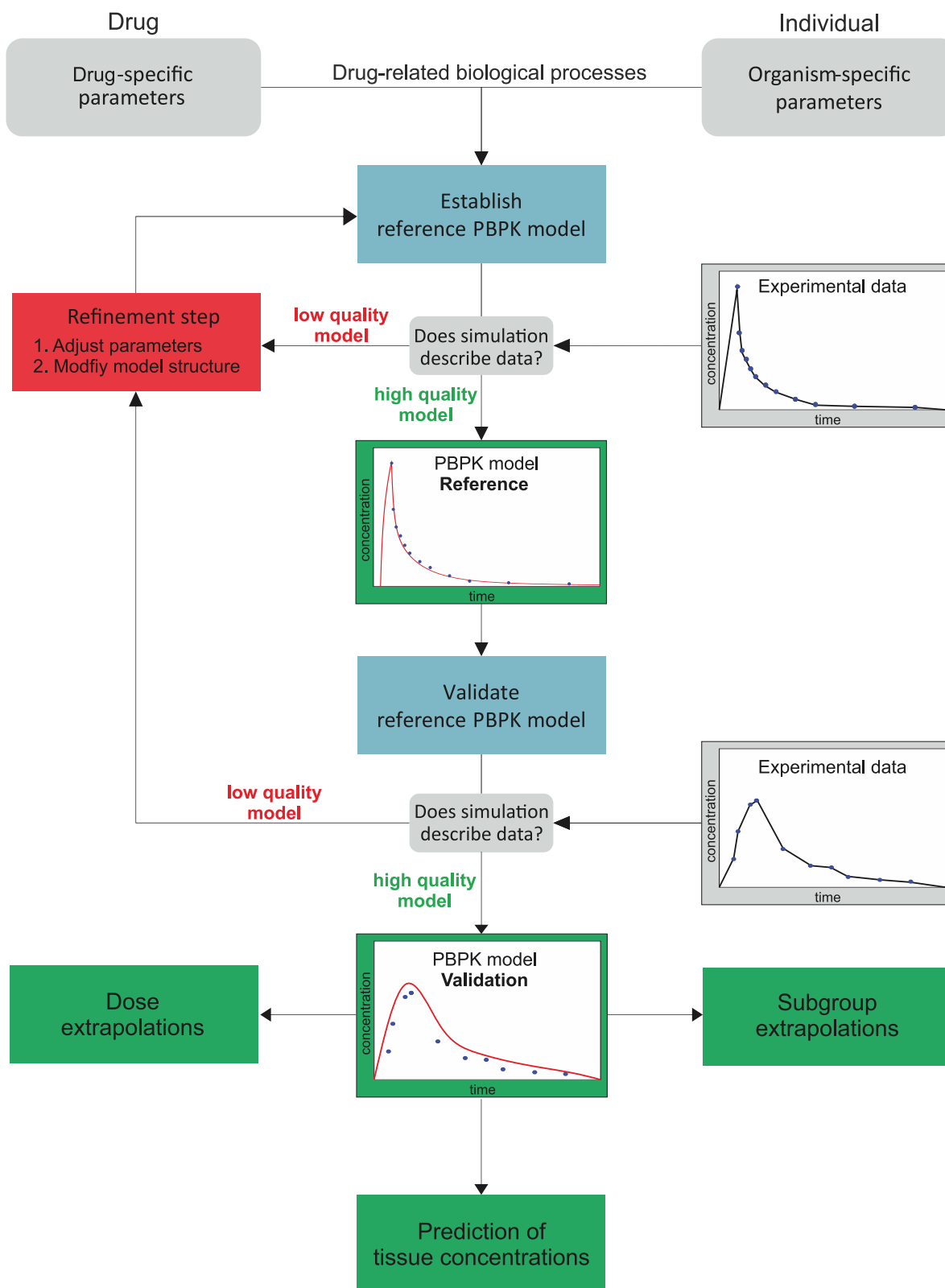


Figure 3.4: Workflow of PBPK model development and validation. After parametrizing drug-specific properties and organism-specific parameters in the reference PBPK model, the model quality is evaluated by comparing simulated drug concentrations with experimental data from literature. If a sufficient model accuracy has been reached, a subsequent validation step enables reliable model extrapolations. Amongst others, this validation step ensures accurate predictions of concentration-time profiles in various compartments. Otherwise, the PBPK model is revised in a refinement step thereby adjusting key model parameters or adding more active transport processes or metabolizing reactions to improve the description of physiological processes governing the fate of the considered drug within the body.

ADME processes leading to the specific concentration-time course of a drug and its metabolites after oral or intravenous drug administration.

The plasma protein binding may be generally considered as compound-specific characteristic. Various physicochemical properties such as the lipophilicity or the acid dissociation constant may lead to different protein binding affinities [Obach et al., 2008]. However, organism-specific parameters may also have an impact on the fraction of the drug that is not bound to plasma proteins. For instance, the F_u of a drug is increased by a shift of the plasma/tissue protein ratio in species to the tissue.

Organism-specific parameters

Organism-specific parameters are describing the anatomy and physiology of a specific species. Most of the PBPK modeling software environments provide these parameters once the biometric input (age, body weight, ethnicity, and gender) was selected. In general, the anatomical and physiological parameters were carefully collected from the literature or estimated from validated formulas.

The anatomy comprises parameters for gastrointestinal-dimensions, organ volumes, as well as surface areas between different subcompartments like interstitial and intracellular space. To represent the physiology, blood flow rates and organ compositions, as well as pH values of interstitial and intracellular space are used. In addition, the set of physiological parameters is extended by parameters specifying the vascular system, the tissue and body fluids, as well as the gastro-intestinal tract.

Overall, hundreds of parameters are defining the physiology and the anatomy of a specific organism. Amongst others, the pharmacokinetic behavior of a given drug in different compartments and subcompartments is influenced by these parameters.

Drug-related biological processes

In the PBPK model structure, biological processes are presenting drug-specific metabolizing reactions and active drug transport processes in a specific organism. The maximal velocity (v_{max}) and the Michaelis-Menten constant (K_m) may be used to reflect reaction equations for these crucial biological processes occurring in drug metabolism and excretion. V_{max} is defined as the maximal rate that can be attained when the enzyme or the transporter is completely saturated. K_m denotes the substrate concentration that yields the half-maximal reaction rate [Michaelis et al., 2011]. Assuming that enzymes or transporters follow the Michaelis-Menten kinetic, the rate constant k_{cat} is calculated by normalizing the specific v_{max} to the respective enzyme or transporter concentration. The calculation of a reaction rate v in a compartment i (v_i) is described as follows:

$$v_i = \frac{E_i \times k_{cat} \times V_i \times S_i \times K_{wc}}{(K_m + S_i \times K_{wc})} \quad (3.1)$$

E_i and S_i denote the concentration of the enzyme or the substrate and V_i represents the volume of the correspondent compartment. K_{wc} [-] indicates the water/cell partition coefficient of a given substrate. Note that $v_{max,i} = k_{cat} \times E_i$ (3.1). Reaction rates for active transport processes are computed in a similar way.

The quantitative description of protein-mediated processes occurring in drug disposition is difficult since there is a limited experimental accessibility of tissue-specific protein activity in vivo. To overcome this issue, tissue-specific mRNA expression is used to estimate protein concentrations in different tissues and organs [Meyer et al., 2012]. The idea of using tissue-specific expression data is based on the definition of the maximum velocity v_{max} [$\frac{mol}{l \times min}$], which is calculated according to Equation (3.2) and derived from the Michaelis-Menten kinetic.

$$v_{max} = k_{cat} \times E_{total} \quad (3.2)$$

In equation (3.2), $k_{cat} [\frac{1}{min}]$ is the catalytic rate constant that indicates how much substrate molecules are catalyzed per minute. $E_{total} [\frac{mol}{l}]$ refers to the total amount of enzyme or transporter concentration. Under the assumption that the catalytic rate constant is not affected by in vivo factors such as posttranslational modifications, the maximum velocity for organ i ($v_{max,i}$) is defined by:

$$v_{max,i} = k_{cat} \times E_{total,i} \quad (3.3)$$

In equation (3.4), the total protein concentration E_{total} is replaced by the product of the relative expression in organ i ($e_{rel,i}$) and a scaling factor $SF [\frac{mol}{l}]$ that corrects for the absolute in vivo protein concentration.

$$v_{max,i} = k_{cat} \times SF \times e_{rel,i} \quad (3.4)$$

In this way, relative expression values obtained from in vitro experiments serve as a surrogate for protein abundance in different organs [Meyer et al., 2012]. In contrast, k_{cat} is a global parameter, which quantifies the rate of the corresponding active process. Coupling estimated protein abundances of relevant enzymes and transporters in the organism with kinetic rate constants identified for relevant enzymatic and transport reactions, thus, allows the representation of drug-related biological processes in a specific individual.

3.4 Differentiation from conventional pharmacokinetic modeling

Conventional pharmacokinetic modeling establishes simple kinetic models by fitting PK parameters to experimental data. The identified parameters are then used to characterize the behavior of a given substance. Since the model structure is defined by the data, conventional pharmacokinetic modeling is a rather data-driven approach with a limited potential of extrapolations, for example, to different patient subgroups or even to different regimens of administration. A one-compartment and a two-compartment model are exemplarily illustrated in Figure 3.5.

In contrast to the phenomenological models obtained by classical pharmacokinetic modeling, PBPK modeling aims for a mechanistic description of physiological processes by integrating drug-specific properties and prior knowledge about the physiology and the anatomy of the specific organism. Physiological processes of the organism can be thus represented at a higher level of detail, which allows more rationale extrapolations to novel clinical situations.

3.5 Physiologically-based pharmacokinetic/pharmacodynamic modeling

Since a pharmacological activity of a drug within the body is dependent on both, the drug concentration at the target site (PK) and the efficacy of this concentration (PD), the integration of PD response data and PK profiles is of high relevance concerning clinical drug development and patient safety. The application of PBPK modeling here allows the simulation of drug concentrations over time at the site of action for different administration regimens.

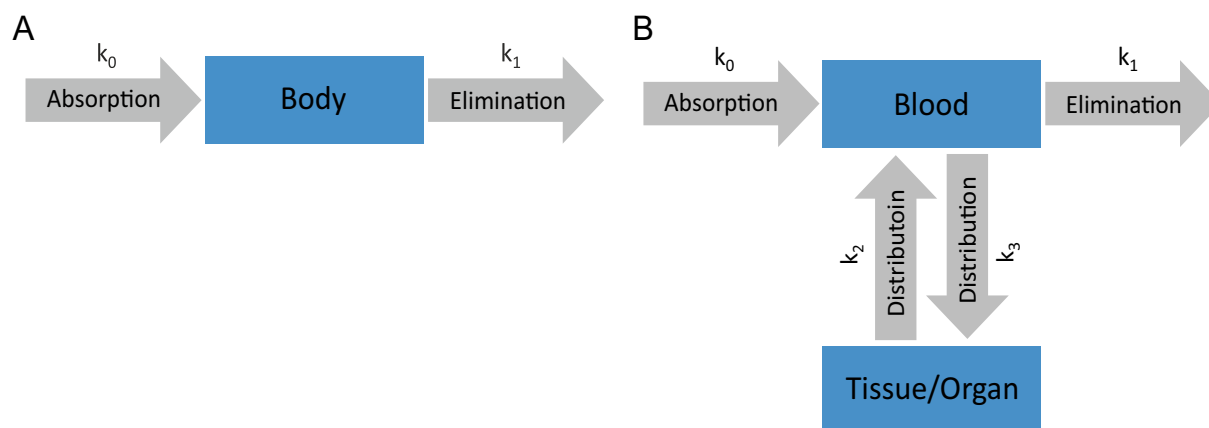


Figure 3.5: Conventional pharmacokinetic modeling. (A) Simple representation of a one-compartment model including absorption and elimination, and their rate constants k_0 and k_1 . (B) Simple representation of a two-compartment model including absorption, distribution, and elimination, and their rate constants k_0 , k_1 , k_2 , and k_3 .

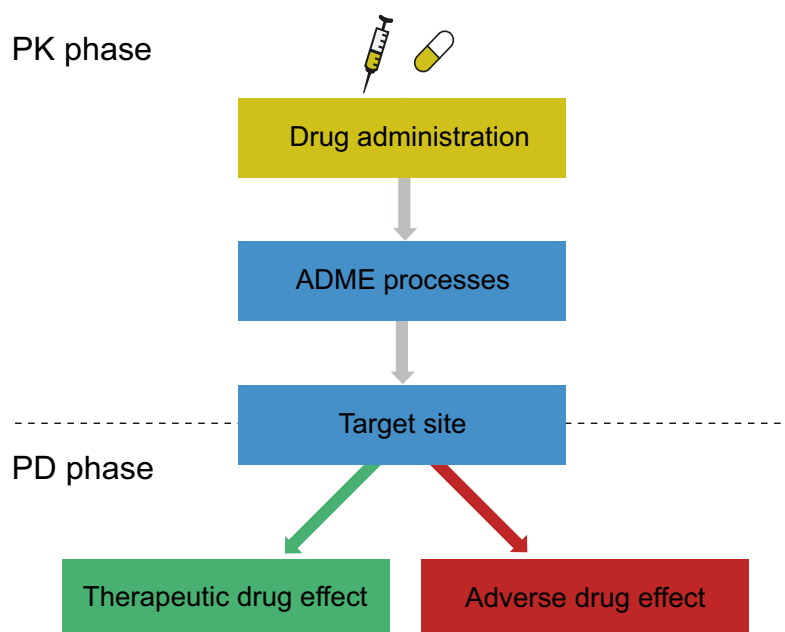


Figure 3.6: Basic concept of PBPK/PD modeling. Schematic representation of the relationship between PK and PD processes after drug administration in vivo. PBPK modeling can be used to estimate the drug concentrations at the target site where therapeutic or, in the worst case, adverse drug effects occur. (adapted from [Mutschler et al., 2001])

The overall goal of physiologically-based pharmacokinetic/pharmacodynamic (PBPK/PD) modeling approaches is a quantitative relationship between drug concentrations over time following drug administration of various doses in humans with drug effects observed in vitro for different drug exposures (Figure 3.6). These modeling concepts allow a better understanding of the mechanisms underlying the pharmacological activity and, in case of acute overdoses, the drug-induced toxicity. This in turn may help to improve the development processes of new drugs, on the one hand, and to reduce drug toxicity, on the other hand.

3.6 Modeling software

Several software solutions exist to model pharmacokinetic processes of various compounds based on prior knowledge about species-specific physiology and anatomy. Some of these frameworks also allow the modeling of drug-drug interactions, PBPK/PD modeling, or the simulation of pharmacokinetic profiles for different populations. Prominent PBPK modeling frameworks are listed below.

- PK-SimTM [Willmann et al., 2003] is a comprehensive PBPK software package developed by Bayer Technology Services GmbH that enables simulations of pharmacokinetics for different compounds in different animals or humans in a mechanistic way.
- SimcypTM Simulator [Jamei et al., 2009] is a population-based pharmacokinetic modeling software for simulating ADME processes of drugs and drug candidates.
- GastroPlusTM [Agoram et al., 2001; Yu et al., 1996], a module-based PBPK modeling software package, allows mechanistic simulations of pharmacokinetic processes in particular for several administration routes such as intravenous, oral, intramuscular, subcutaneous, or inhalation.
- PKQuest [Levitt, 2002], a Java-based, free, and intuitive PBPK program, provides the simulation of concentration time-profiles of several drugs in humans and rats.

Drug-drug interactions

Nowadays, several patients are prescribed multiple drugs for the treatment of their diseases. This is in particular true for elderly people. A European study of about 2700 elderly patients showed, for instance, that 34-68 % of the patients with a mean age of about 80 years are taking at least six drugs [Fialová et al., 2005]. The concomitant administration of multiple drugs may induce adverse events, on the one hand, and may reduce the clinical efficacy, on the other hand, due to interactions between the applied drugs. Drug-drug interactions (DDIs) are thus one of the most common causes of medication error and have become a major problem in clinical practice with respect to patient safety and drug efficacy.

A drug interaction is defined as an event in which one drug affects the pharmacological activity of another drug following administration of both drugs at the same time. This can directly or indirectly provoke (i) additive, (ii) synergistic, or (iii) antagonistic drug effects (Figure 4.1). The situation where two co-administered drugs are inducing a total pharmacological effect the same as the sum of their individual effects is referred to as additive effect. An antagonistic and a synergistic effect, on the contrary, result in a reduced and an increased pharmacological action within the organism, respectively, when both substances are administered concomitantly. In this regard, a synergistic effect might be detrimental when the increased pharmacological response exceeds the effect level observed for the MTD. In this case, a co-medication could be the trigger for the onset of adverse drug events. In contrast, an antagonistic effect would be particularly significant, if the reduced pharmacological action drops below the effect level caused by the MED. This basically provokes an ineffective drug treatment.

In combination therapy, interactions between two or multiple drugs can lead to alterations of the drug concentration levels within the body (pharmacokinetic drug interaction), the desired drug effects at the target site (pharmacodynamic drug interaction), or both. Since in most cases one drug is affecting the PK or PD behavior of another drug but not vice versa, the terms 'perpetrator drug' and 'victim drug' are often used in that sense and also in regulatory agencies [Prueksaritanont et al., 2013].

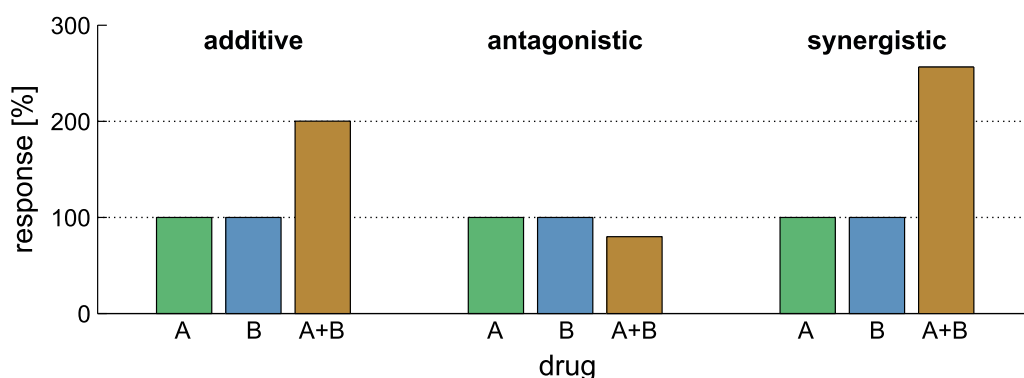


Figure 4.1: Different effects caused by co-administration of multiple drugs. The co-administration of multiple drugs may lead to additive, antagonistic, or synergistic drug effects.

4.1 Pharmacokinetic drug interactions

The impact on pharmacokinetic processes of one drug caused by the co-application of another drug is referred to as pharmacokinetic drug interaction. This mostly results in an altered drug-concentration time profile of the victim drug induced by co-administration of the perpetrator drug. Pharmacokinetic drug interactions may influence different ADME processes, which are outlined in more detail in the following (Figure 4.2).

In the absorption phase, drugs slowing or hastening the gastric emptying time such as atropine or erythromycin may modify the absorption rate of another drug [Brown and Tomlin, 2010]. For instance, the co-medication of acetaminophen with atropine, for which is known to have a pronounced effect on gastric emptying, significantly reduced the rate of absorption of acetaminophen in young and elderly subjects (Figure 4.2) [Rashid and Bateman, 1990].

Plasma protein binding is a key determinant of how well a drug is distributed between the blood pool and the different organs. The fraction unbound of a drug can increase in the circumstances of a competition for plasma protein binding sites with the co-administered drug (Figure 4.2). As a consequence, the pharmacological activity might be indirectly enhanced due to a higher drug concentration at the target site. Co-application of drugs having relatively high F_u values are not susceptible to such modifications due to a sufficiently high free drug concentration in plasma. However, a displacement in plasma protein binding, also for highly bound drugs, often have a minor or even no effect on the pharmacological action of involved drugs [Brown and Tomlin, 2010].

Pharmacokinetic drug interactions are of utmost importance in the metabolism phase. Several drugs are extensively metabolized in the liver, primarily by CYP enzymes, that strongly contributes to the hepatic clearance of administered drugs. The co-administration of one or multiple drugs may disturb the

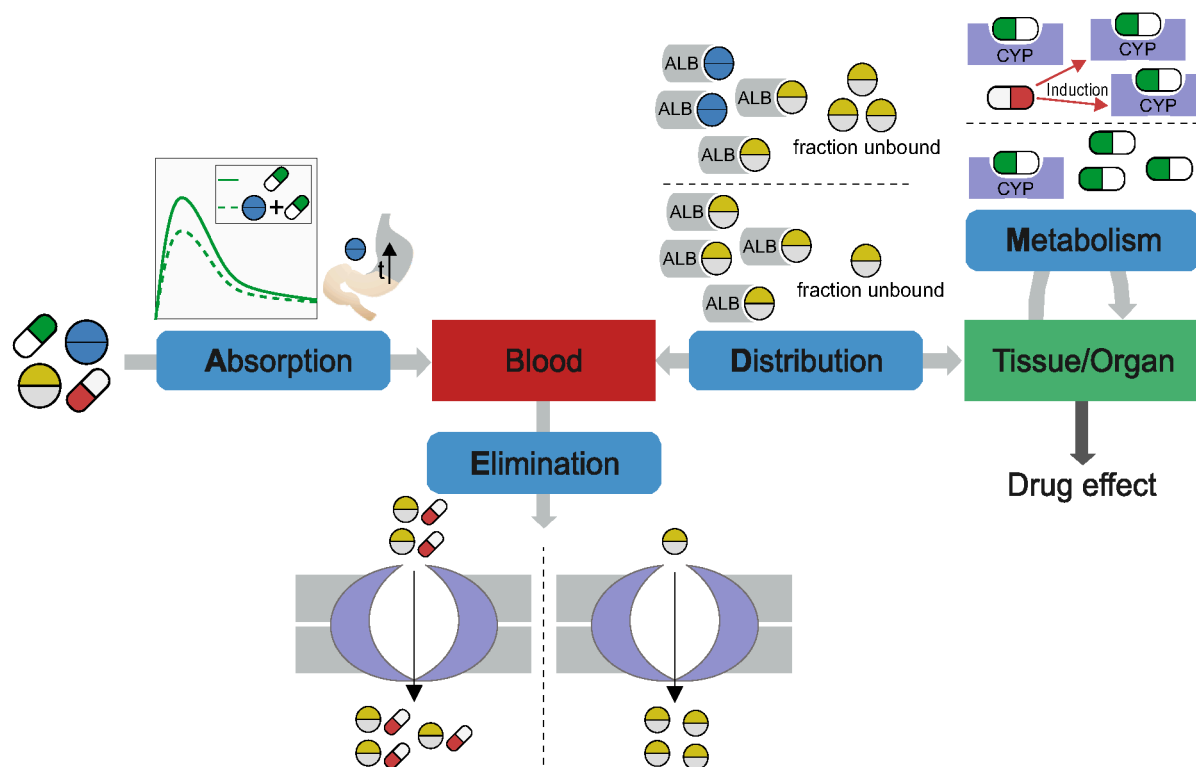


Figure 4.2: Pharmacokinetic drug interactions. Potential pharmacokinetic drug interactions may occur in different ADME processes: (i) hastening of gastric emptying during absorption, (ii) competition for plasma protein (e.g., albumin [ALB]) binding sites during distribution, (iii) induction of CYP enzymes during metabolism, and (iv) competition with the same low-specificity carrier system during elimination.

metabolism and ultimately the PK behavior of another drug by inducing or inhibiting metabolic enzymes involved. This regulation might occur by changing the expression level and, subsequently, the amount of enzyme that is available for the specific chemical process. (Figure 4.2). For instance, rifampicin is hepatically metabolized and a well-known inducer for several CYP enzymes such as CYP3A4, CYP1A2, or CYP2C9 [Wishart et al., 2006]. Since rifampicin decreased the blood levels of cyclosporine A by inducing its hepatic metabolism, a dose adjustment of cyclosporine A was consequently suggested when co-applied with rifampicin to preserve its therapeutic efficacy, i.e., to prevent allograft rejection [Capone et al., 1996].

In the elimination phase, pharmacokinetic drug interactions play a minor role compared to interactions observed during drug metabolism. Nevertheless, drugs that substantially induce or inhibit transporters involved in active excretion processes of other drugs, such as the ABC-transporter MDR2, might change their elimination behavior and further their residence time within the organism. Moreover, drugs that compete with the same low-specificity carrier system during tubular secretion might affect their renal clearance. This was observed for digoxin administered concomitantly with quinidine (Figure 4.2) [Bigger and Leahey, 1982].

4.2 Pharmacodynamic drug interactions

In contrast to pharmacokinetic drug interactions, pharmacodynamic drug interactions describe interactions between drugs that occur at the site of action within the target organ. Such interactions directly modulate the drug efficacy. Since pharmacodynamic drug interactions are not measurable by altered drug concentrations at the target site, these type of interactions are much harder to detect than pharmacokinetic drug interactions. Furthermore, the mode of action of several drugs is diverse and the understanding of the underlying mechanisms is rather unknown, which both clearly complicate the identification process of pharmacodynamic drug interactions.

In clinical application, pharmacodynamic drug interactions are sometimes desired, if the concomitant administration evokes a synergistic therapeutic effect compared to the individual effects after single drug treatment. For instance, a combination of acetaminophen and tramadol showed a synergism of their analgesic effects in order to relieve pain, and a prolongation of their pharmacological action [Medve et al., 2001]. In contrast, combination therapies may also induce severe side effects. In the treatment of cardiovascular diseases, the administration of the anti-thrombotic agent warfarin together with heparin, aspirin, or spironolactone, for instance, might lead to excessive bleeding [Teklay et al., 2014].

Toxicogenomics

The identification and characterization of adverse events induced by xenobiotic substances (e.g., drugs) administered to a living organism is of great relevance in clinical pharmacology and toxicology. In that regard, toxicogenomics is defined as the study of such toxic events by the application of different omics technologies such as transcriptomics, proteomics, or metabolomics. The overall goal of a toxicogenomics study involves (i) the elucidation of the mechanisms underlying drug-induced toxicity, and (ii) the identification of predictive biomarkers [Heijne et al., 2005; Waters and Fostel, 2004].

In an animal-free toxicogenomics study, transcriptomic, proteomic and metabolomic profiles can be measured simultaneously for a low and high drug concentration after different exposure durations in an appropriate in vitro system (Figure 5.1). The high concentration that is associated with the onset of toxicity might be identified by measuring global cell viability markers such as DNA, or Lactatdehydrogenase (LDH) activity. Ideally, the measurements obtained at all omics levels are then analyzed in an integrative way to get insights into the mechanistic understanding of the drug-induced toxic events. Significant changes in molecular expression patterns of the transcriptome, proteome and metabolome can be thereby used to identify biomarkers of toxicity [Waters and Fostel, 2004].

Prominent examples of public toxicogenomics projects are Open TG-GATEs (Toxicogenomics Project-Genomics Assisted Toxicity Evaluation System) [Igarashi et al., 2015], or the ToxCast programme carried out by the US Environmental Protection Agency [Dix et al., 2007]. The Japanese toxicogenomics project Open TG-GATEs, for instance, provides a large-scale toxicogenomics database containing time-resolved gene expression data for more than 160 compounds obtained in human and rat hepatocytes. For each drug, transcriptional changes were measured after drug exposure of three different in vitro concentrations and after different exposure durations (see more in Appendix A.1). In the following, transcriptomics is reviewed in more detail since gene expression data from TG-GATEs have been used in research chapters 7, 8, and 9.

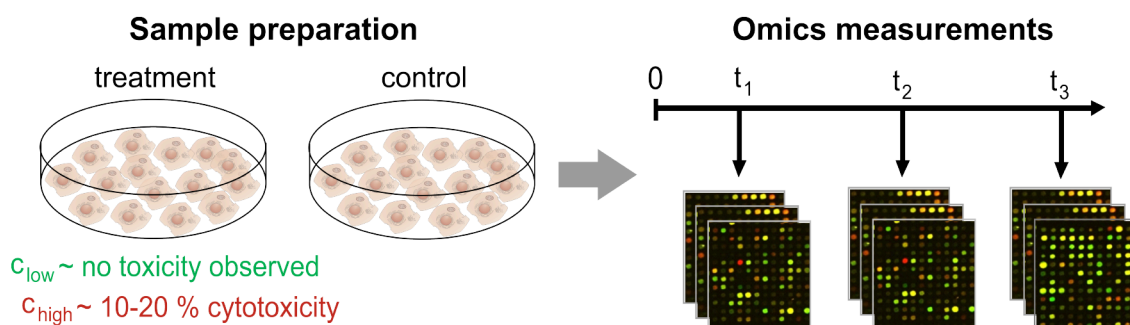


Figure 5.1: Toxicogenomics study. A toxicogenomics study involves measurements obtained by single- or multiple omics technologies (transcriptomics, proteomics, and/or metabolomics) after different exposure durations (t_1 , t_2 , and t_3) for different drug concentrations (low, high) as well as for a control group.

5.1 Transcriptomics

While in proteomics and metabolomics a set of proteins and metabolites can be measured in a cell or a tissue at a certain time for specific treatments or control groups, transcriptomics allows a quantitative identification of mRNA transcripts in principle by use of oligonucleotide or DNA microarrays [Waters and Fostel, 2004]. Moreover, a relatively new technology used in the field of transcriptomics called 'RNA-Seq' provides a more comprehensive view on the transcriptome compared to basic microarray experiments. Although structural variations such as alternative splicing events, single nucleotide variants, or small insertions and deletions are detectable by RNA-Seq, data analysis and storage is still more complex and more challenging as in basic DNA microarray studies. Also due to the lower costs, several transcriptomics experiments using DNA microarray analyses, in particular high-throughput studies applied for a wide range of compounds.

5.1.1 Workflow of a microarray experiment

In a basic two-channel DNA microarray experiment, complementary DNA (cDNA) samples of the treatment and control group are obtained from isolated RNA using reverse transcriptase (Figure 5.2). Treatment and control samples are labeled with different fluorophores and are pipetted in an equal amount onto the microarray. During the hybridization, the sample sequences are binding complementary to the known sequences fixed on the array. Intensity values of RNA transcripts of the control and treatment group are finally detectable by a dual-wavelength microarray scanner based on laser confocal principle (Figure 5.2). Afterwards the resulting images are analyzed to eventually monitor the expression of thousands of genes for each sample.

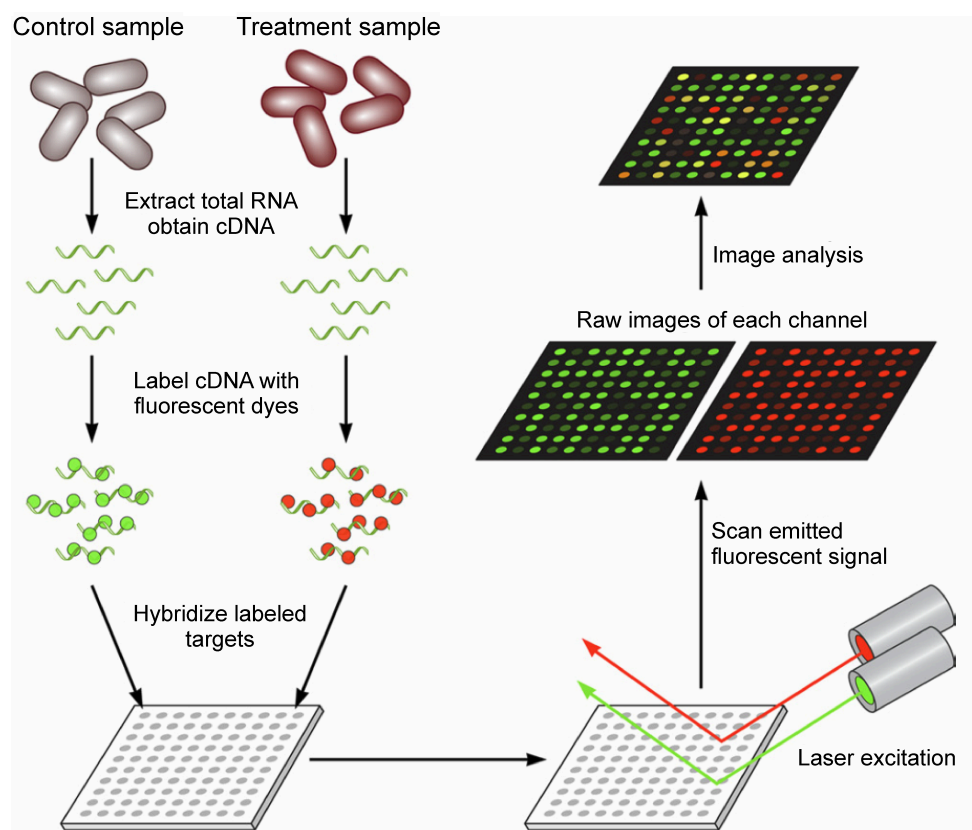


Figure 5.2: Simple workflow of a microarray experiment. Schematic representation of a simple workflow of a two-channel DNA microarray experiment. (adapted from [Miller and Tang, 2009])

5.1.2 Analysis of microarray data

The analysis of microarray data generally consists of three important steps: data preprocessing, a differential expression analysis, and a functional analysis.

Data preprocessing

A standard procedure for analyzing the measured raw data of a microarray experiment involves several data pre-processing steps including quality control assessment as well as data normalization. A widely-used background adjustment method, for instance, is the GC Robust Multi-array Average (GC-RMA) that uses quantile normalization and median polishing summarization [Wu et al., 2004]. These pre-processing steps are important due to several reasons such as systematic biases in the measured expression levels, or differences in labeling and detection efficiencies of the fluorescent dyes [Quackenbush, 2002].

Fold change values are often used to quantitatively describe the change in gene expression between a treatment and a control experiment. A fold change value for a specific gene i is calculated as follows:

$$FC_i = \frac{T_i}{C_i} \quad (5.1)$$

where FC represents fold change, T and C represents expression levels of the treatment and control for a gene i , respectively. In order to describe up- and down-regulation of genes in a similar way, fold changes are often expressed as log2 values [Quackenbush, 2002]. As a consequence, for instance, a two-fold up- and down-regulated gene has a $\log_2(FC)$ of 1 and -1 instead of a FC of 2 and 0.5, respectively.

Differential expression analysis

A main result of a microarray analysis is the identification of differentially expressed genes (DEGs) between one or more pairs of samples (e.g., between a high and a low dose, or between two timepoints). A widely-used method to assess differential expression of genes is called Limma (Linear models for microarray data) using moderated t-statistic [Smyth, 2004]. DEGs can be identified, for instance, by using fold change and p-value cutoffs reflecting the biological and statistical significance, respectively. Volcano plots help to quickly identify and visualize DEGs in a large dataset (Figure 5.3).

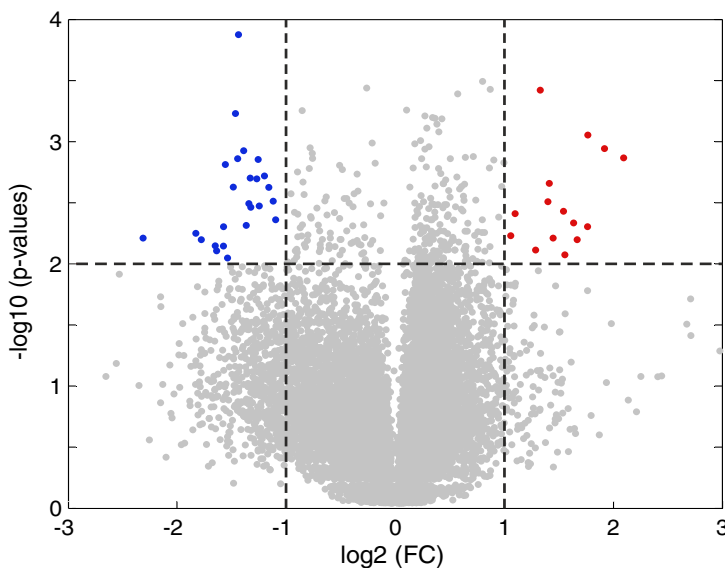


Figure 5.3: Volcano plot. Identification of differentially expressed genes (absolute $\log_2 FC > 1$ and $p\text{-value} \leq 0.01$) using a volcano plot. Cutoff values are represented by dashed lines. Blue, significantly down-regulated genes; Red, significantly up-regulated genes.

Functional analysis

In a last step, a functional analysis can be performed on the identified sets of DEGs with respect to the functional annotations of the genes such as their involvement in biological pathways or processes. The application of hypergeometric testing, for instance, enables to check whether the distribution of the genes belonging to a certain biological term in a set of DEGs is statistically significant. The association of enriched biological terms with a set of DEGs, thus, allows an interpretation at the functional level. Gene enrichment analysis is often applied for pathways from the Kyoto Encyclopedia of Genes and Genomes (KEGG) [Kanehisa and Goto, 2000], or on the gene ontology (GO) database, which is built up on a controlled vocabulary covering molecular functions, cellular components, and biological processes of genes and gene products [Ashburner et al., 2000].

Biomarkers

As proposed by the National Institute of Health, a biomarker is defined as a 'characteristic that is objectively measured and evaluated as an indicator of normal biological processes, pathogenic processes, or pharmacologic responses to a therapeutic intervention or other health care intervention' [Biomarkers Definitions Working Group., 2001]. If the biomarker represents high clinical relevance, one can also speak of 'clinical biomarker'. A major goal of biomarker identification is the improvement of drug efficacy and patient safety. At the same time, high attrition rates of newly developed drugs during the clinical phases I-III can be reduced [Frank and Hargreaves, 2003]. Biomarkers can be helpful at multiple stages of a disease process thereby representing the potential for (i) disease detection and risk assessment (diagnostic), (ii) the estimation of the disease development in untreated individuals (prognostic); and (iii) the monitoring of the therapy success by predicting responses to drug treatment (predictive) [Winter et al., 2013; Pfaffl, 2013].

In clinical application, a biomarker ideally reflects therapeutic success by indicating changes of a specific biomarker induced by drug treatment, which is associated to a positive alteration of the patient's disease state. A serious problem in the identification process of such biomarkers are false positives or false negatives. These are represented, for instance, by changes in the specific biomarker (i) that reflect the mechanism of action of the drug but are irrelevant for the pathophysiology of the disease (false positive), or (ii) that reflect clinically relevant changes in the pathophysiology of the disease but do not capture the mechanisms of the drug intervention (false negative) [Frank and Hargreaves, 2003].

In cardiology, prominent examples of clinical biomarkers are blood pressure and cholesterol. A reduction of both are associated with cardiovascular diseases like heart attack or stroke. Furthermore, the acute-phase reactant C-reactive-peptide was recommended to be a promising biochemical biomarker to assess the risk of coronary heart diseases [Pearson et al., 2003], independent on measurements of serum cholesterol [Frank and Hargreaves, 2003].

6.1 Transcriptional biomarkers

Powerful omics technologies such as transcriptomics, proteomics, and metabolomics allow the measurement of thousands of genes, proteins, and metabolites within a cell or a tissue at a certain time. A major aim of these experiments is to answer questions concerning drug efficacy and patient safety. Since transcription of genes is a highly dynamic process, transcriptomics presents snapshots of the current status of perturbed cells at different timepoints following various drug exposures [Pfaffl, 2013]. Gene expression profiling, thus, provides an effective opportunity to identify clinically relevant transcriptional biomarkers that describe drug action under toxic conditions in a mechanistic way. These biomarkers may have the potential to early detect a disease and, furthermore, to monitor the patient status, as well as the efficacy of applied drugs for the entire patient evolution [Pfaffl, 2013]. A workflow for the identification of transcriptional biomarkers is illustrated in Figure 6.1.

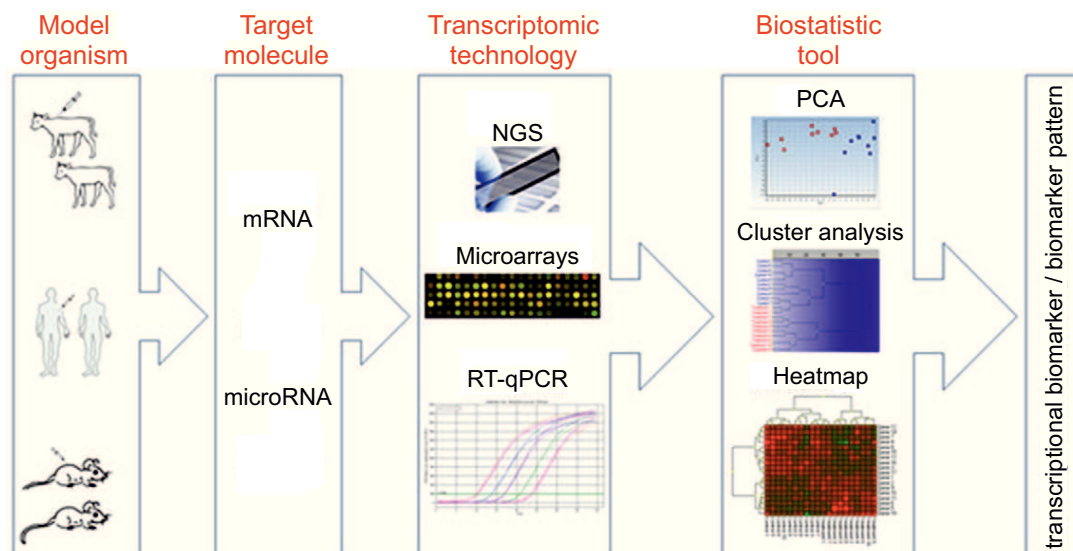


Figure 6.1: Simple workflow for the identification of transcriptional biomarkers. After selecting a model organism and treating it with a drug of interest, the target molecules (e.g., mRNA or microRNA) are isolated and analyzed using a transcriptomic technique. After applying statistics like hierarchical cluster analysis or principal component analysis (PCA), transcriptional biomarkers can be identified. NGS, next-generation sequencing; RT-qPCR, reverse transcriptase quantitative polymerase chain reaction; PCA, principal component analysis. (taken from [Riedmaier and Pfaffl, 2013a])

Although omics approaches generate several biomarker candidates for future investigations, the suggested biomarkers have a clear limited practical use due to lack of validation. The low amount of available in vivo data for humans clearly makes biomarker validation approaches quite challenging in clinical practice. Due to the limited access to tissue biopsies from patients and thus to human in vivo data, translational approaches extrapolating findings about biomarker candidates attained in vitro or during animal studies into a human context are of great relevance [Mendrick, 2011].

6.2 Biomarkers for drug-induced hepatotoxicity

In hepatology, enzyme levels of biochemical markers such as alanine transaminase (ALT), aspartate transaminase (AST), and gamma-glutamyltransferase (GGT), are measured as standard to assess the hepatic function. All three enzymes are mostly expressed in the liver and are highly involved in liver metabolism. In case of liver damage, these enzymes get released and enter the blood circulation. Significant elevations of enzyme levels measured in blood plasma, which obviously exceed reference levels of healthy people, hence indicate a potential hepatotoxicity, for instance, induced by drug treatment.

Besides ALT, AST, and GGT, other enzymes such as LDH5 or glutamate dehydrogenase (GDH) have been proposed as new biomarkers for drug-induced hepatotoxicity. Measuring LDH is a popular method to investigate in vitro cytotoxicity in hepatocytes [Ramachandran and Kakar, 2009]. Moreover, due to a prolonged serum half-life and a higher sensitivity, GDH might outperform ALT [O'Brien et al., 2002]. However, both enzymes are rarely used as biomarker to detect drug-induced liver toxicity since both lack of specificity. Furthermore, LDH5 is difficult to measure, on the one hand, while GDH is an allosteric enzyme that might be regulated by several activators or inhibitors, on the other hand.

A clear drawback of the aforementioned biomarkers are the inadequate sensitivity and specificity, and a lack of mechanistic understanding of drug action as well as disease onset and development. These circumstances might impair the evaluation of the hepatotoxic potential during in vitro or in vivo experiments [Shi et al., 2010].

Cytokines or microRNAs such as interleukine-6 or miR-122 seem to be promising and highly-specific biomarkers associated with inflammation and hepatocellular injury [Shi et al., 2010]. For instance, serum cytokines such as $\text{TNF}\alpha$ or interferon γ have been successfully used as DILI biomarkers to assess liver function in mice exposed to an overdose of acetaminophen [Saha and Nandi, 2009]. Micro RNAs such as miR-122 even performed more reliable and with less variations than standard biomarkers (e.g., ALT) [Shi et al., 2010]. Furthermore, numerous marker genes could be identified in vitro or in laboratory animals for biological events that are involved in drug-induced liver toxicity such as oxidative stress, glutathione depletion, or phospholipidosis [Shi et al., 2010].

Acetaminophen is a well-known hepatotoxic drug. In case of acetaminophen intoxication, analyzing gene expression patterns from rat blood cells showed to be a powerful and even better predictor for acute exposure levels than classical biochemical parameters such as ALT [Bushel et al., 2007]. In addition, translating the findings to humans by using ortholog information helped to discriminate between an untreated group and humans exposed to an acetaminophen overdose. Toxic exposure levels of acetaminophen could be identified earlier in comparison to the use of standard biochemical parameters, which nicely demonstrates the powerful usage of transcriptional biomarkers in potential clinical application [Bushel et al., 2007].

Results

Model-based contextualization of in vitro toxicity data quantitatively predicts in vivo drug response in patients

Abstract

Understanding central mechanisms underlying drug-induced toxicity plays a crucial role in drug development and drug safety. However, a translation of cellular in vitro findings to an actual in vivo context remains challenging. Here, PBPK modeling was used for PBPK-based in vivo contextualization of in vitro toxicity data (PICD) to quantitatively predict in vivo drug response over time by integrating multiple levels of biological organization. Explicitly, in vitro toxicity data at the cellular level were integrated into whole-body PBPK models at the organism level by coupling in vitro drug exposure with in vivo drug concentration-time profiles simulated in the extracellular environment within the organ. PICD was exemplarily applied on the hepatotoxicant azathioprine to quantitatively predict in vivo drug response of perturbed biological pathways and cellular processes in rats and humans. The predictive accuracy of PICD was assessed by comparing in vivo drug response predicted for rats with observed in vivo measurements. To demonstrate clinical applicability of PICD, in vivo drug responses of a critical toxicity-related pathway were predicted for eight patients following acute azathioprine overdoses. Moreover, acute liver failure after multiple dosing of azathioprine was investigated in a patient case study by use of own clinical data. Simulated pharmacokinetic profiles were thereby related to in vivo drug response predicted for genes associated with observed clinical symptoms and to clinical biomarkers measured in vivo. PICD provides a generic platform to investigate drug-induced toxicity at a patient level and thus may facilitate individualized risk assessment during drug development.

published as:

Thiel, C., Cordes, H., Conde, I., Castell, J. V., Blank, L. M., and Kuepfer, L. (2016). Model-based contextualization of in vitro toxicity data quantitatively predicts in vivo drug response in patients. *Archives of Toxicology*.

Author contributions:

Writing - original draft: Thiel, C., Conde, I., Castell, J. V., and Kuepfer, L.; Writing - review & editing: Thiel, C., Cordes, H., Conde, I., Castell, J. V., Blank, L. M., and Kuepfer, L.; Project design: Thiel, C., and Kuepfer, L.; Analysis & implementation: Thiel, C.

7.1 Introduction

Drug-induced toxicity is a major clinical problem [Schuster et al., 2005] with cardiotoxicity and hepatotoxicity being the most frequent clinical cases [Von Hoff et al., 1977; Andrade et al., 2005; Takikawa et al., 2009]. The predictability of specific toxic events is a major challenge in pharmaceutical development since the underlying origins are almost unforeseeable [Kaplowitz, 2004]. In drug development, whole-body PBPK models are nowadays routinely used [Jones et al., 2006; Maharaj et al., 2013; Lippert et al., 2013]. Whole-body PBPK modeling describes biological processes underlying drug pharmacokinetics at a large scale of physiological detail and may be used amongst others to simulate interstitial concentration-time profiles in the extracellular environment of various organs [Jones et al., 2009; Kuepfer, 2010]. PBPK modeling aims for a mechanistic understanding of physiological processes describing drug ADME within the body based on prior physiological and anatomical knowledge. Different organs are explicitly represented in PBPK models and are connected by blood flow (Figure 3.1). Since PBPK models describe the physiology of an organism at a high level of detail, they can be used to simulate pharmacokinetic PK profiles of specific patient subgroups with individualized physiology [Maharaj et al., 2013; Lippert et al., 2013].

In order to detect drug-induced injury at an early stage, reliable predictions of toxic events as well as representative diagnostic biomarkers are of key relevance for patient safety [Shi et al., 2010]. This also requires a mechanistic understanding of the underlying cellular processes [Bissell et al., 2001; Schimmel et al., 2004; Holt and Ju, 2006; Russmann et al., 2009]. Current advances in systems toxicology provide novel insights into central mechanisms involved in drug-induced toxicity [Waters and Fostel, 2004; Heijne et al., 2005; Chen et al., 2012]. Changes at different biological levels can nowadays be measured by omics technologies to describe cellular alterations in response to toxic drug concentrations. Transcriptome profiling was successfully applied before to study adverse effects of toxic agents [Hockley et al., 2006; Brynildsen and Liao, 2009; Michaelson et al., 2011; Zhang et al., 2012; Van Delft et al., 2012; Iskar et al., 2013; Doktorova et al., 2013; Zhang et al., 2014; Herpers et al., 2016].

Combined application of different profiling techniques allows linking cellular changes at multiple levels of biological organization that finally facilitates the characterization of molecular mechanisms of toxic events [Carreras Puigvert et al., 2013; Wilmes et al., 2013; Pillai et al., 2014]. Furthermore, reverse toxicokinetics were used before to identify steady state blood concentrations for correlations of in vivo equivalent doses with in vitro bioactivity data [Dix et al., 2007; Judson et al., 2011; Wetmore et al., 2013; Judson et al., 2014]. In another study, physiologically-based kinetic models developed for different glycol ethers were used to estimate dose-response curves in rats and humans [Louisse et al., 2010]. However, a systematic consideration of in vitro toxicity data into an in vivo context thereby reflecting temporal cellular changes induced by drugs administered in vivo remains still challenging.

In this article, PBPK-based in vivo contextualization of in vitro toxicity data (PICD) is presented (Figure 7.1). PICD integrates in vitro toxicity data into drug-specific whole-body PBPK models to translate drug-induced in vitro findings to an actual in vivo situation thereby predicting drug-specific response profiles induced by different dose levels administered in vivo (Figure 7.1). At the cellular level, in vitro toxicity data are coupled with equivalent PBPK-simulated concentration-time profiles at the organism level to allow a quantitative description of time-resolved in vivo drug response of key cellular processes and biological pathways. Applying PICD in clinical research allows the quantitative prediction of patient-specific drug response by specifically incorporating patient physiology in individualized PBPK models. In brief, PICD aims for a translation of preclinical in vitro toxicity data into an in vivo context and hence allows risk assessment for individual patients during drug development.

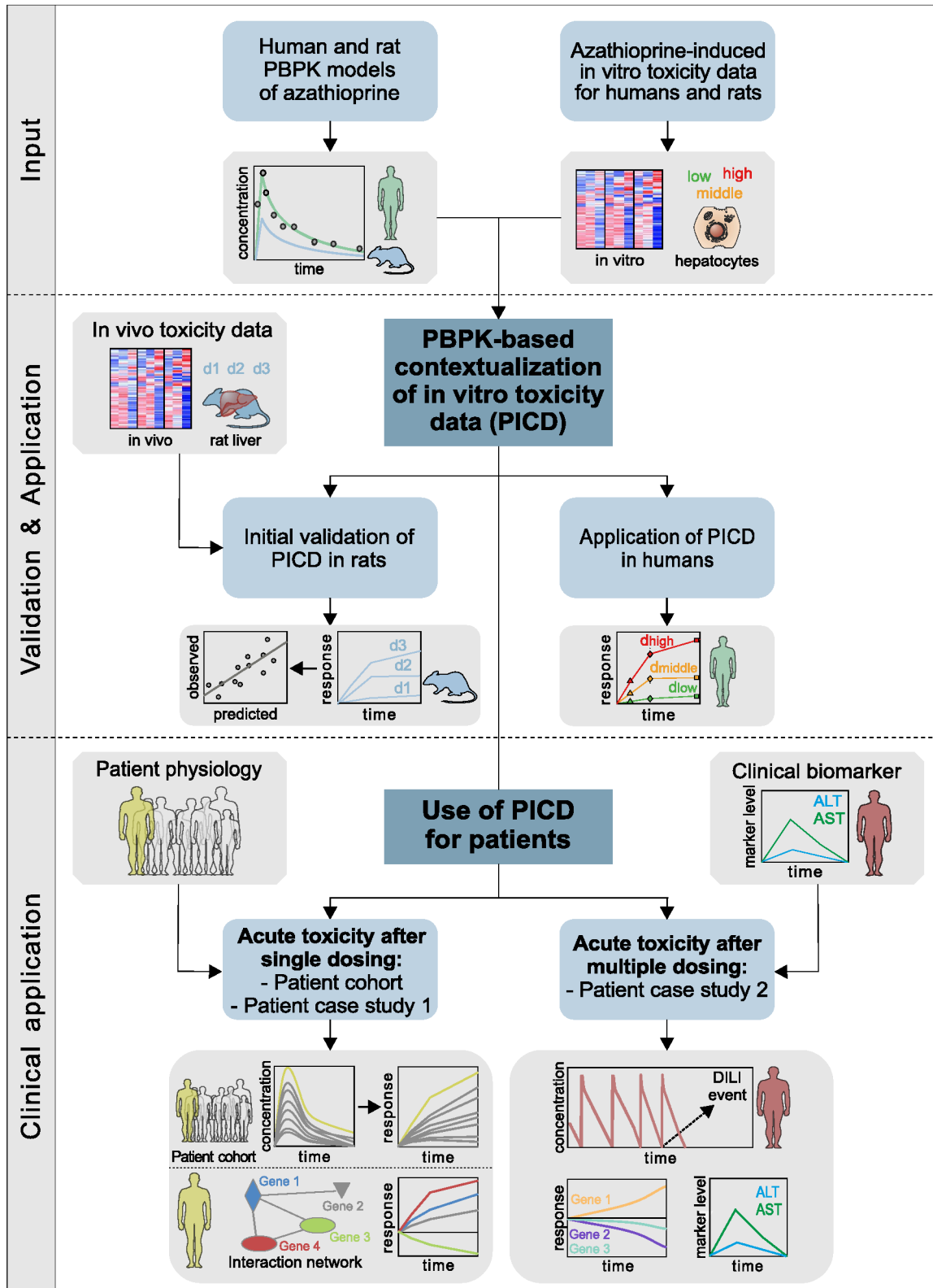


Figure 7.1: Overview of the use of PICD. **Input:** Human and rat PBPK models of azathioprine were developed and in vitro toxicity data of primary human and rat hepatocytes were analyzed [Igarashi et al., 2015]. **Validation & Application:** Before applying PICD on humans, in vivo toxicity data obtained in rat livers were used to validate predicted in vivo drug response. **Clinical application:** To demonstrate clinical applicability, PICD was firstly applied on eight clinical cases and, further, in a patient case study to predict in vivo drug response induced by acute azathioprine overdoses [Gregoriano et al., 2014]. In a second patient case study, acute toxicity after multiple dosing of azathioprine at therapeutic dose was investigated thereby relating simulated drug concentrations for the entire therapy to in vivo response predicted for symptoms-related genes and to own data.

PICD is exemplarily applied on the hepatotoxicant azathioprine in humans and rats. As input, human and rat PBPK models of azathioprine are developed and in vitro toxicity data are analyzed (Figure 7.1). Explicitly, time-series gene expression profiles of primary human and rat hepatocytes from Open TG-GATEs [Igarashi et al., 2015], a large-scale toxicogenomics database, represents the in vitro toxicity data. The predictive quality of PICD is assessed by in vivo response data measured in rat livers [Igarashi et al., 2015], thus exploring whether predicted in vivo drug response shows in vivo relevance (Figure 7.1). To assess the predictive accuracy of PICD, in vivo data is necessary for validation purposes. Since in vivo response data from liver biopsies were available in rats [Igarashi et al., 2015], PICD was applied on rats to assess whether predicted drug response shows in vivo relevance (Figure 7.1). PICD is then applied for humans to predict in vivo drug response over time for doses estimated to be the in vivo equivalents for concentrations exposed in vitro (Figure 7.1). Note that the application of PICD in rats and humans is fully independent since apart from the validation step no information from the animal study was further used for the human case.

To demonstrate the potential of PICD for clinical applications in humans, acute toxicity is investigated after single and multiple dosing of azathioprine. Patient-specific in vivo drug response over time following documented cases of acute azathioprine overdose are predicted specifically considering patient physiology [Gregoriano et al., 2014] (Figure 7.1). The patient, who received the highest overdose [Gregoriano et al., 2014], is further considered in a first patient case study (Figure 7.1). In a second patient case study, PICD is applied on own clinical data to get insights into acute toxicity after multiple dosing of azathioprine at the therapeutic dose. Simulated drug concentration-time profiles, predicted responses of symptoms-related genes, as well as clinical biomarkers measured in vivo are thereby analyzed (Figure 7.1).

7.2 Materials and methods

7.2.1 Analysis of in vitro toxicity data

Raw data were downloaded from TG-GATEs [Igarashi et al., 2015] (Appendix A.1). Gene expression profiles measured with Affymetrix Human Genome U133 Plus 2.0 and Affymetrix Rat Genome 230 2.0 GeneChip arrays were normalized by applying the GC-RMA method [Wu et al., 2004]. Probe sets on the chip were mapped to Entrez Gene IDs using BrainArray custom CDF files (version 19.0.0, ENTREZG) [Dai et al., 2005]. For each treatment, differential gene expression analysis was performed by linear models using limma [Smyth, 2004]. Compound-treated hepatocytes exposed to different concentrations were thereby compared to their respective time-matched controls. P-values were adjusted by Benjamini-Hochberg correction for multiple testing [Benjamini and Hochberg, 1995]. Fold change values were calculated to indicate gene expression changes compared to the time-matched controls. Gene expression profiles of primary human and rat hepatocytes were further analyzed by applying hypergeometric testing [Falcon and Gentleman, 2007] on each subset of differentially expressed genes identified for each treatment to determine significantly overrepresented terms (GO) and pathways (KEGG, TOX) (Table B.1). P-values were adjusted by Benjamini-Hochberg correction. Terms and pathways with a size of assigned genes lower than five were filtered out. To investigate only GO terms with a high level of specialization, an additional filtering step was performed on significant results (see more in Appendix B.1.1, Table B.2).

7.2.2 Physiologically-based pharmacokinetic model development

In the PBPK model structure (Figure 3.4), compound-specific properties and physiological parameters of the organism such as organ volumes can be considered independently. The latter parameters describing the physiology and anatomy of the organism are provided by the PBPK modeling software [Willmann

Table 7.1: Dose identification. In vitro concentration, exposure time, resulting in vitro exposure, and identified in vivo dose for the specific treatments for rats and humans.

Species	Treatment	In vitro concentration [$\mu\text{mol/l}$]	Exposure time [h]	In vitro exposure [$\mu\text{mol/l/h}$]	In vivo dose [mg/kg]
Human	Low - 2 h	2.9	2	5.8	9.0
Human	Low - 8 h	2.9	8	23.2	18.8
Human	Low - 24 h	2.9	24	69.6	34.4
Human	Middle - 2 h	14.6	2	29.2	21.4
Human	Middle - 8 h	14.6	8	116.8	46.6
Human	Middle - 24 h	14.6	24	350.4	91.8
Human	High - 2 h	72.8	2	145.6	53.4
Human	High - 8 h	72.8	8	582.4	126.8
Human	High - 24 h	72.8	24	1747.2	248.3
Rat	Low - 2 h	0.14	2	0.28	2.2
Rat	Low - 8 h	0.14	8	1.1	5.6
Rat	Low - 24 h	0.14	24	3.4	10.1
Rat	Middle - 2 h	0.72	2	1.5	6.5
Rat	Middle - 8 h	0.72	8	5.8	13.3
Rat	Middle - 24 h	0.72	24	17.3	23.5
Rat	High - 2 h	3.6	2	7.2	14.9
Rat	High - 8 h	3.6	8	28.8	31.2
Rat	High - 24 h	3.6	24	86.4	58.0

et al., 2003] (Appendix A.2). Besides physicochemical properties like the lipophilicity or plasma protein binding values influencing in particular drug disposition in absorption and distribution processes, active drug transport or metabolizing reactions were integrated to describe the drug clearance in the body. K_m and v_{max} were used to characterize the kinetic behavior of such active processes. Abundances of relevant enzymes and transporters in multiple compartments were quantified by using tissue-specific gene expression data [Meyer et al., 2012].

In this study, the quality of the developed PBPK model of azathioprine was assessed by comparing simulated PK data with different experimental concentration-time profiles from literature [Odland et al., 1986; Van Os et al., 1996; Zins et al., 1997]. To indicate the model quality, PBPK models were evaluated by calculating a root-mean-square deviation (RMSD) whereby the differences of measured and simulated concentrations were normalized by respective experimental values [Thiel et al., 2015]. Moreover, a linear regression was performed for simulated and observed concentrations. Coefficient of determination (R^2), as well as the slope a and the intercept b of the linear equation were then additionally used to evaluate the 'goodness of fit'.

7.2.3 Prediction of in vivo drug responses in humans and rats

PICD was applied on rats and humans to quantify in vivo responses for different time points and dose levels. Gene expression values (log2 fold change) and cell viability values, both measured in vitro [Igarashi et al., 2015], as well as gene response values (defined as absolute log2 fold change) were mapped to the nine identified in vivo doses (Table 7.1), and were linearly interpolated to determine respective dose-response profiles for the different time points (2 h, 8 h, and 24 h) [Igarashi et al., 2015]. Note that the identification of the in vivo doses is dependent on the underlying PBPK model and the specific dosage regimen.

Time-resolved in vivo response profiles were then predicted for arbitrary doses by assigning gene expression, cytotoxicity, or gene response values after 2 h, 8 h, and 24 h. In vivo drug responses of all terms (GO) and pathways (KEGG, TOX) (Table B.4) that were significantly overrepresented in at least one treatment (e.g., Middle - 2h) (Table B.3) were predicted by computing the mean gene response level of all genes assigned to a specific term or pathway. Significant increase in drug response values after the

early time point was evaluated by one-sample t-test, while changes between individual time points were assessed by using one-way ANOVA followed by Tukey-Kramer multiple comparison test.

7.2.4 Validation of predicted in vivo drug responses in rats

To validate PICD, predicted in vivo drug responses were linearly interpolated to perform a correlation with time-matched drug responses observed in the in vivo study [Igarashi et al., 2015]. All cellular processes or biological pathways that were significantly affected in rats for at least one treatment (Table B.1) were considered for this correlation. Predicted expression profiles for all genes considered in the two case studies were analogously validated with in vivo gene expression profiles observed in rats [Igarashi et al., 2015]. All Correlation analyses were performed by calculating Pearson's correlation coefficient r and the corresponding p-value p .

7.2.5 Clinical cases of acute toxicity after single dosing of azathioprine

PICD was used for different clinical cases of acute azathioprine overdose reported between 1995 and 2013 [Gregoriano et al., 2014]. Patients showing symptoms most likely caused by other drugs than azathioprine [Gregoriano et al., 2014] were not taken into account. Moreover, only patients for whom no decontamination measures were undertaken after exposure to a single oral overdose were considered leading to a total of eight clinical cases (Table 7.2). Consequently, eight PBPK models were developed incorporating individual anthropometric parameters (age, sex, and weight).

PICD was then applied on each patient thereby simulating drug concentration-time profiles in the interstitial space of the liver following oral administration of the specific overdose. In a next step, drug response in the most responsive toxicity-related pathway (DNA Damage & repair) and cytotoxicity values were predicted at every time point. Finally, in vivo drug responses were correlated with global cytotoxic observations by calculating Pearson's correlation coefficient r , while PSS values were correlated with drug response values after one day by calculating Spearman's rank correlation coefficient ρ . In the latter correlation analysis, patient 17 was not considered, since she remained asymptomatic after a heavy overdose of azathioprine (Table 7.2). Furthermore, patient 19 was considered in a patient case study thereby investigating acute toxicity after single dosing of azathioprine.

Table 7.2: Clinical cases of acute azathioprine overdose. Anthropometric parameters (age, weight, and sex), administered dose, and observed symptoms including assigned Poisoning Severity Scores (PSS) [Persson et al., 1998]. The clinical data were taken from [Gregoriano et al., 2014].

Patient ID	Age [years]	Weight [kg]	Sex	Dose [mg/kg]	Symptoms (PSS)
33	28	65	Male	6.9	Asymptomatic (0)
13	23	63	Female	11.9	Vomiting (1)
4	39	50	Female	16.0	Asymptomatic (0)
16	44	75	Female	26.7	Sinus tachycardia (1)
21	39	73	Male	27.0	Headache (1), Vomiting (1)
28	49	76	Male	32.9	Increased GGT ($< 2 \times$) (1)
17	53	60	Female	107.5	Asymptomatic (0)
19	28	71	Male	180.1	Nausea (1), Abdominal pain (1), Headache (1), Fall in leucocyte count (7.2-3.9 G/l) (1), Increased liver enzymes (10-fold increase in transaminases from baseline) (2), Dyspnoea (2)

7.3 Results

7.3.1 PBPK-based in vivo contextualization of in vitro toxicity data (PICD)

Here, the development of PBPK-based in vivo contextualization of in vitro toxicity data (PICD) - an integrative multiscale approach - is shown. The application of PICD allows predicting in vivo drug response by integrating multiple levels of biological organization thereby using whole-body PBPK models, at the organism level, to couple interstitial PK profiles, at the organ level, with in vitro toxicity data, at the cellular level (Figure 7.2).

The use of PICD thus allows the prediction of drug response over time in an in vivo context. Gene expression data of primary human and rat hepatocytes treated with specific drugs at different concentration levels over different time ranges from Open TG-Gates are used exemplarily as in vitro toxicity data to quantify drug-induced toxicity at the cellular level (Figure 7.2). In the in vitro assay of TG-Gates, the highest concentration was selected such that cell viability was decreased by 10-20 % [Igarashi et al., 2015]. PICD is basically applicable on any drug of interest, provided that correspondent in vitro response data for the same compound is available. Note that the application of PICD is here exemplarily shown for the liver since the in vitro toxicity data was obtained in primary hepatocytes. To translate in vitro findings to an in vivo situation, PBPK modeling is used here to contextualize these cellular gene expression data at an organism level.

In an initial step, a drug-specific PBPK model is developed to identify in vivo doses that are directly related to in vitro drug exposure (Figure 7.2). The in vitro assay setup is explicitly represented in the PBPK models by specifically adjusting in vivo drug plasma protein binding in the PBPK model correspondent to the in vitro concentrations. PK profiles simulated in the interstitial space of the liver are then coupled with in vitro toxicity data to predict in vivo drug response, at the cellular level, following in vivo drug administration, at the organism level (Figure 7.2).

To couple interstitial concentration-time profiles with in vitro toxicity data, in vivo doses are identified by PBPK simulations for intravenous drug administration such that the in vitro drug exposure in the assay equals the interstitial area under the curve (AUC) in the liver at each experimental time point (Figure 7.2). Note that by using validated PBPK models, potential non-linearities in ADME processes affecting the interstitial drug concentration are implicitly considered such that dose estimations are accurate across different dosage regimens. Dose-response curves are then generated for all time points by mapping in vitro toxicity data to the identified in vivo doses (Figure 7.2).

The identified in vivo doses are averaged horizontally to three doses (d_{low} , d_{middle} and d_{high}), which thus represent the in vivo equivalents to in vitro concentrations (low, middle, and high). Drug response values are next calculated and assigned to doses d_{low} , d_{middle} and d_{high} by linearly interpolating dose-response curves (Figure 7.2) to predict in vivo drug response in relevant Gene Ontology (GO) [Ashburner et al., 2000] terms, as well as in human pathways from the Kyoto Encyclopedia of Genes and Genomes (KEGG) [Kanehisa and Goto, 2000], and in toxicity-related pathways (TOX) (SABiosciences) (Table B.4).

The use of PICD enables a time-resolved description of drug-induced in vivo response at the organism level by the integration of several levels of biological organization and, hence, allows considering various aspects of translational research in drug development.

7.3.2 Use of PICD for individual patients

PBPK modeling allows, amongst others, the consideration of patient-specific differences in the anatomy and physiology between various individuals by incorporating the anthropometry of patients (e.g., body weight). Moreover, since validated PBPK models allow extrapolating PK simulations to different dosage

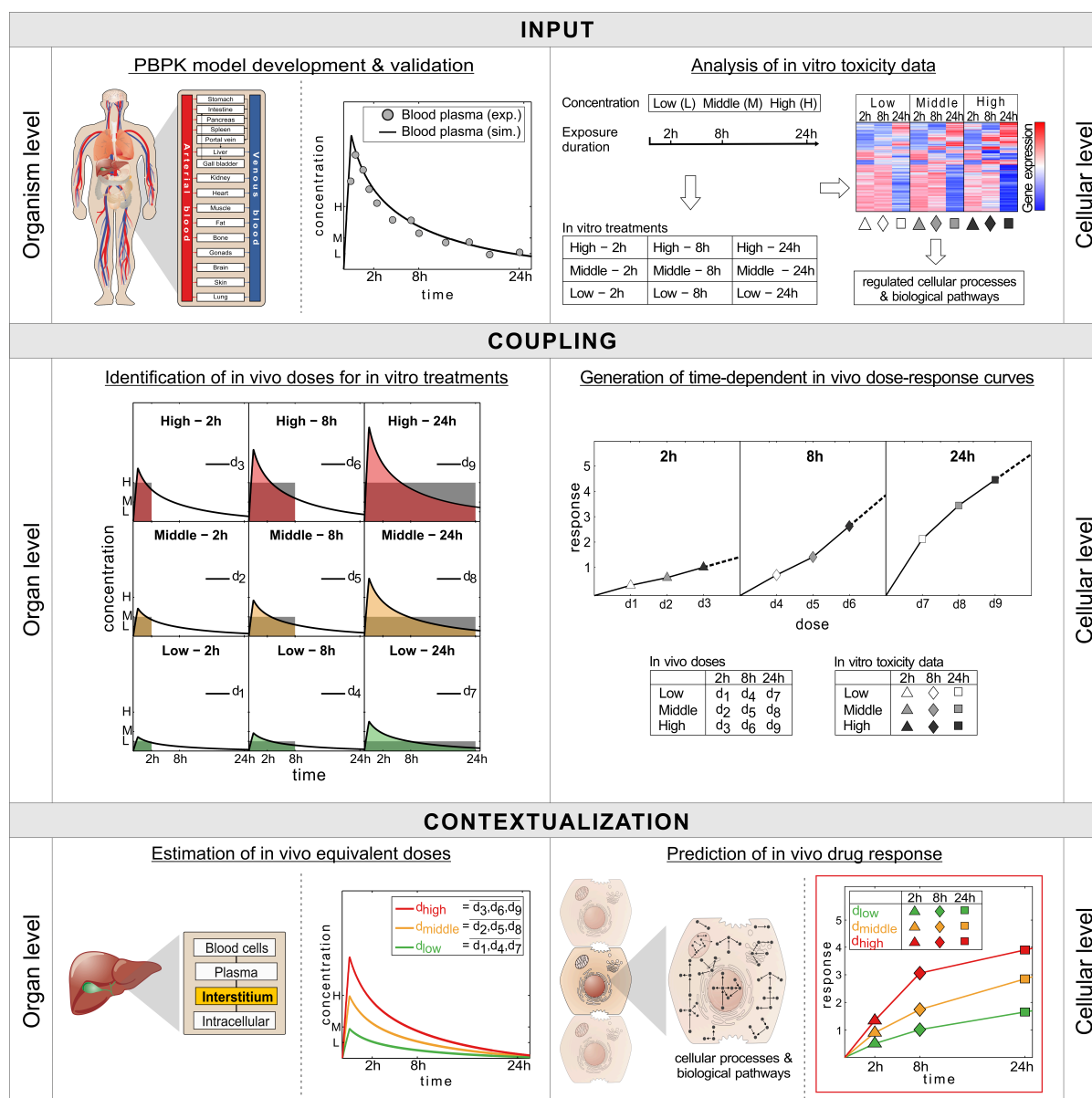


Figure 7.2: Workflow of PICD. **Input:** At the organism level, PBPK models are developed and validated by comparing simulated (sim.) and experimental (exp.) drug concentrations. At the cellular level, gene expression data of drug-treated primary hepatocytes are analyzed for nine different treatments (white-gray colored symbols) [Igarashi et al., 2015]. Functional enrichment analysis was then applied to find regulated cellular processes and biological pathways. **Coupling:** In vivo doses d_1 - d_9 are identified for all treatments such that the in vivo exposure simulated in the interstitial space of the liver (colored AUC) matched the in vitro exposure (gray rectangular area). Identified in vivo doses d_1 - d_9 together with in vitro toxicity data (white-gray colored symbols) are used to generate dose-response curves for all considered time points of the in vitro experiment. **Contextualization:** In vivo doses d_1 - d_9 are averaged horizontally along the same in vitro concentration to determine three in vivo equivalent doses d_{low} , d_{middle} , and d_{high} (colored lines) for exposed in vitro concentrations (low, middle, high). At the cellular level, in vivo drug response over time reflecting changes in cellular processes and biological pathways are then predicted (colored symbols) for the in vivo equivalent doses (d_{low} , d_{middle} and d_{high}) (colored lines) by using time-dependent in vivo dose-response curves. AUC, area under the curve

regimens, PICD is not only applicable to predict drug response for the in vivo equivalent doses administered intravenously (Figure 7.2), but also for other dose levels and administration routes. Thus, PICD can be applied in a patient-specific manner to allow the simulation and interpretation of clinical observations following drug administration over time at the patient level (Figure 7.3). Anthropometric parameters of patients (e.g., age or weight) are thereby used to build individualized PBPK models specifically consider-

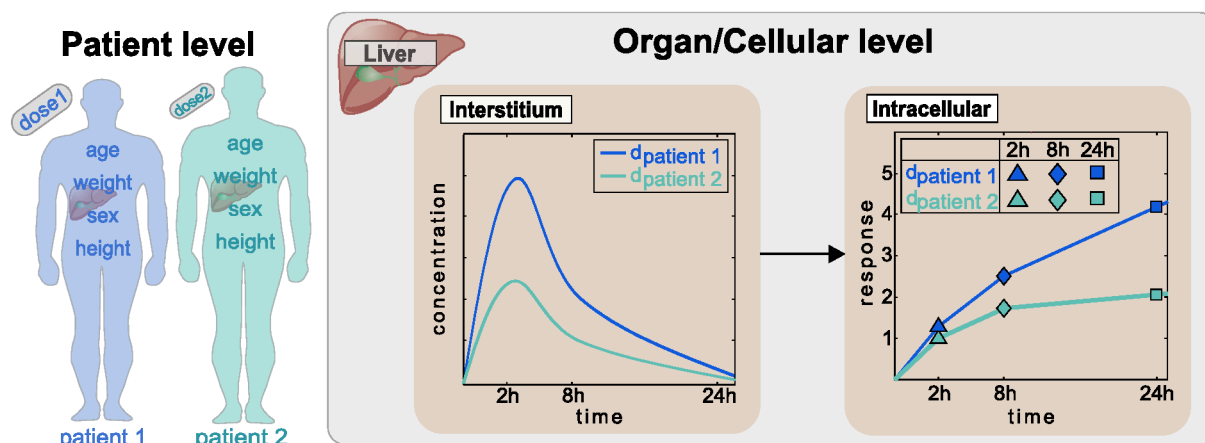


Figure 7.3: Use of PICD for patients. At the patient level, individualized PBPK models are developed by incorporating anthropometric parameters of patients (e.g., weight). PICD is then applied individually on each patient-specific PBPK model by taking into account the respective dosage regimen (administration route, and dose level). Concentration-time profiles are thereby simulated in the interstitial space of the liver and correspondent in vivo drug response profiles are predicted at the cellular level following administration of the specific dose.

ing patient physiology. Time-dependent dose-response curves (Figure 7.2) are generated analogously for each clinical case by simulating PK profiles in the interstitial space of the liver taking into account the specific administration route (Figure 7.3).

Finally, patient-specific in vivo drug response can be predicted following administration of the respective dosage regimen in each patient (Figure 7.3). The application of PICD therefore facilitates the consideration of in vitro toxicity data within the context of human patients described in turn by patient-specific PBPK models [Maharaj et al., 2013; Lippert et al., 2013]. PICD thus provides a generic platform for translational research in clinical drug development.

7.3.3 Organism level: Physiologically-based pharmacokinetic models

At the organism level, PICD initially requires the establishment of validated PBPK models (Figure 7.2). The immunosuppressant azathioprine [Elion, 1993] was chosen here as an exemplary use case for a hepatotoxic compound since the drug label gives a severity level of 3 for drug-induced liver injury [Chen et al., 2011; Björnsson, 2015]. Compound-specific physicochemical properties and the F_u of the drug in plasma were used to parametrize the initial reference PBPK model for humans (Figure 7.4, Figure 7.5, Table 7.3).

Furthermore, patient physiology was considered in the human PBPK model to characterize the specific patient physiology (Table 7.4) [Odlind et al., 1986; Van Os et al., 1996; Zins et al., 1997]. The compound-specific parameters (Table 7.3) together with the specific information about the clinical studies (Table 7.4) [Odlind et al., 1986; Van Os et al., 1996; Zins et al., 1997] are sufficient to reproduce the PBPK models of azathioprine since all anatomical and physiological parameters for both rats and humans are already provided in the modeling software. Likewise compound-specific parameters such as membrane permeabilities or partition coefficients are directly calculated by the formulas underlying the chosen distribution model.

First, plasma concentration data were used for initial model establishment [Van Os et al., 1996]. The PBPK model considered both the prodrug azathioprine that is quickly converted in the liver by glutathione-s-transferase [Kaplowitz and Kuhlenkamp, 1978; Watanabe et al., 1978; Eklund et al., 2006] and its metabolite 6-mercaptopurine, which is in turn mostly metabolized by xanthine oxidase to 6-thiouric acid [Aberra and Lichtenstein, 2005]. Since a negligible amount of both drugs, azathioprine and 6-mercaptopurine, were excreted unchanged in urine [Elion, 1972; Bergan et al., 1994], renal elimination

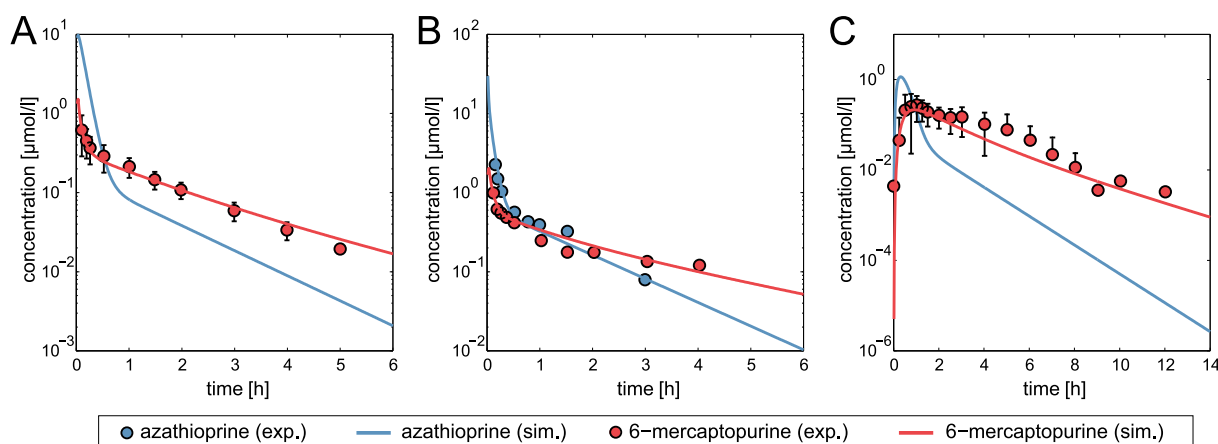


Figure 7.4: PBPK model development and validation. Simulated concentration-time curves (lines) for azathioprine (blue) and 6-mercaptopurine (red) were assessed with experimental PK profiles (circles) [Van Os et al., 1996]. The reference PBPK model was then validated by evaluating simulated PK profiles with experimental PK data from different clinical studies not used to establish the reference model [Odlind et al., 1986; Zins et al., 1997] (Table 7.4). Azathioprine was either administered intravenously or orally. (A) Reference, 50 mg IV. (B) Validation, 100 mg IV. (C) Validation, 100 mg PO.

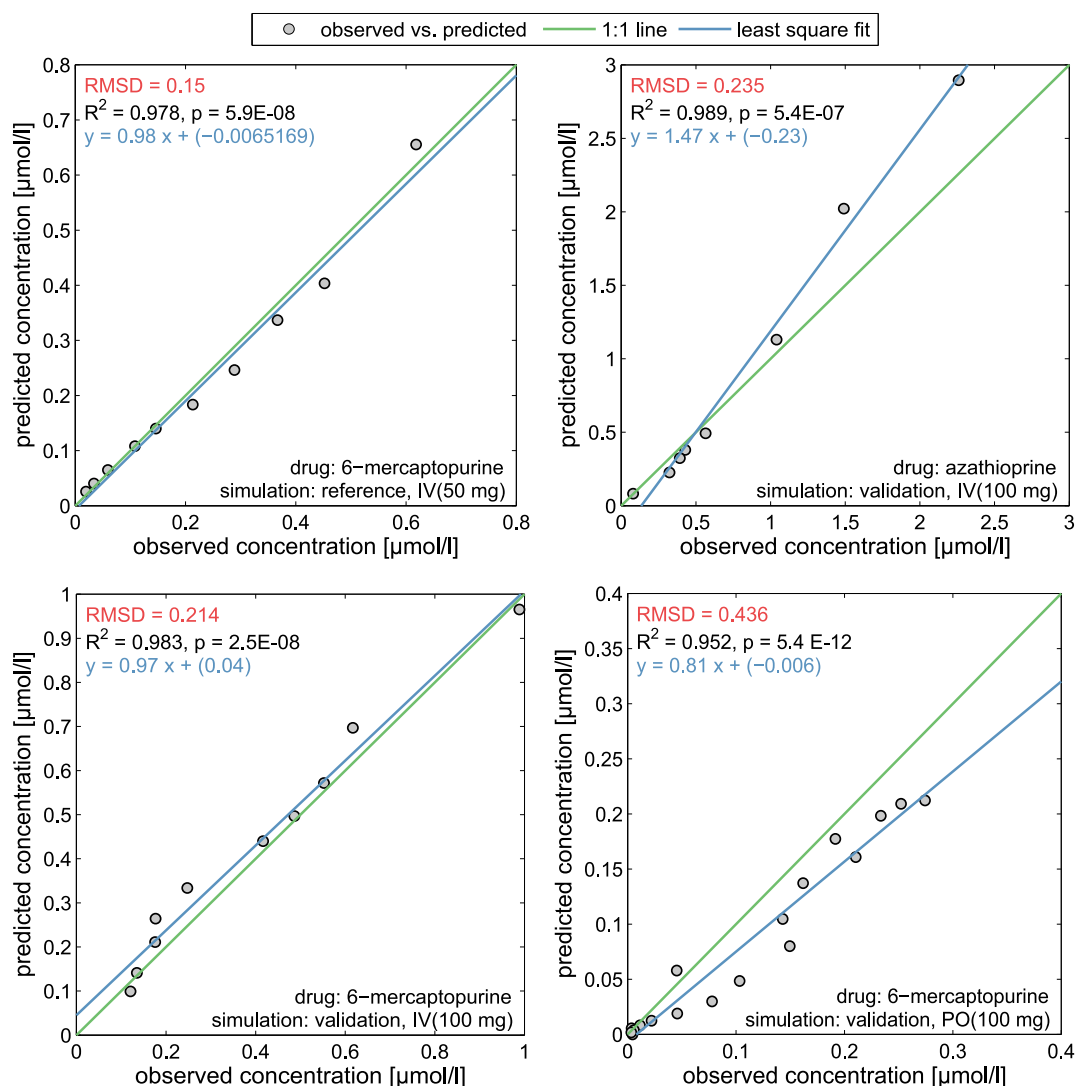


Figure 7.5: PBPK model assessment. Simulated concentration-time profiles were compared to experimental data. Observed vs. predicted plots including RMSE and R^2 values, and the equation of the linear regression were generated for the reference and validated PBPK model.

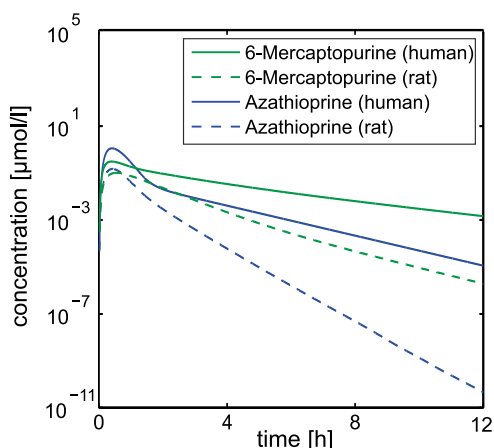


Figure 7.6: Cross-species extrapolation.

Blood plasma concentration-time profiles of azathioprine and 6-mercaptopurine were simulated for rats (dashed blue line, dashed green line) and for humans (solid blue line, solid green line) after oral administration of 100 mg of azathioprine. The rat PBPK model of azathioprine was developed by considering rat-specific anatomy and physiology in the human PBPK model according to [Thiel et al., 2015].

Table 7.3: PBPK model parameters. Molecular weight (MW), pKa, logP, F_u , and integrated metabolic process consisting of metabolic enzyme and corresponding kinetic parameters (v_{max} , K_m) used for the developed PBPK model. The experimental logP value for 6-mercaptopurine was slightly adjusted, while the experimentally measured lipophilicity for azathioprine was used unchanged.

Drug	MW [g/mol]	pKa	logP	F_u	Metabolic enzyme	K_m [$\mu\text{mol/l}$]	v_{max} [$\mu\text{mol/l/min}$]
Azathioprine	277.26 [Wishart et al., 2006]	7.87 [Wishart et al., 2006]	0.10 [Wishart et al., 2006]	0.70 [Wishart et al., 2006]	Glutathione S-transferase A1 [Eklund et al., 2006]	7.0*	60.0*
6-Mercapto- purine	152.18 [Wishart et al., 2006]	9.50 (acid), 2.99 (base) [Wishart et al., 2006]	1.85 [Czyrski and Kupczyk, 2013]	0.81 [Wishart et al., 2006]	Xanthine oxidase [Abera and Lichtenstein, 2005]	41.5*	410.0*

* Estimated

Table 7.4: Experimental conditions. Administration route, respective doses, health state and number of subjects. The experimental PK data were either used for establishment of the reference PBPK model (Reference) or for model validation (Validation).

Administration route	Dose	Subjects	Usage	Reference
Intravenous bolus	50 mg	Healthy (n=24)	Reference	[Van Os et al., 1996]
Intravenous bolus	100 mg	Uremic patient (n=1)	Validation	[Odland et al., 1986]
Oral	100 mg	Healthy (n = 10)	Validation	[Zins et al., 1997]

was not considered in the underlying PBPK model. To appropriately validate simulated concentration-time profiles of different compounds, experimental PK data are necessary. The metabolite 6-thiouric acid was not included in the PBPK model because no experimental measurements were performed in the used clinical studies.

After model establishment, the simulated plasma concentrations showed an excellent agreement with clinical PK data used for the initial model identification (Figure 7.4, Figure 7.5). For model validation, additional experimental PK data were next used (Table 7.4), which were accurately described without further model modifications (Figure 7.4, Figure 7.5) thereby ensuring an adequate quality of the PBPK model for further predictions.

The validated human PBPK model was next used to develop a PBPK model for rats that is needed for the initial validation of PICD. Recently, it was shown that species-specific physiology has the highest influence on the predictive quality of PBPK-based cross-species extrapolation [Thiel et al., 2015]. The rat PBPK model of azathioprine (Figure 7.6) was hence developed by considering species-specific differences in the physiology and anatomy in the human PBPK model of azathioprine (Figure 7.4).

7.3.4 Cellular Level: In vitro toxicity data

At the cellular level, in vitro toxicity data is required for PICD to predict in vivo drug response over time. Human and rat gene expression and enrichment analysis was performed in the same way. Time-course gene expression profiles of primary human and rat hepatocytes from Open TG-GATEs were analyzed to obtain quantitative toxicity data of azathioprine [Igarashi et al., 2015]. Notably, toxicity data generated by other profiling techniques [Waters and Fostel, 2004; Heijne et al., 2005] can analogously be used to predict drug-specific response profiles. For each treatment, subsets of differentially expressed genes were identified (absolute fold change > 1.5 , Benjamini-Hochberg corrected $p < 0.01$) (Figure 7.7A, Figure 7.7B). Functional enrichment analysis was then applied to find significantly overrepresented terms (GO) and pathways (KEGG, TOX) (Benjamini-Hochberg corrected $p < 0.01$) (Table B.1). Gene response values defined as absolute log2 fold change were calculated to quantify changes in significantly affected terms and pathways. Since the drug response values reflect the extent of activation or inhibition of functionally related genes in an in vivo situation, they were used to predict drug-induced cellular changes over time in both rats and humans.

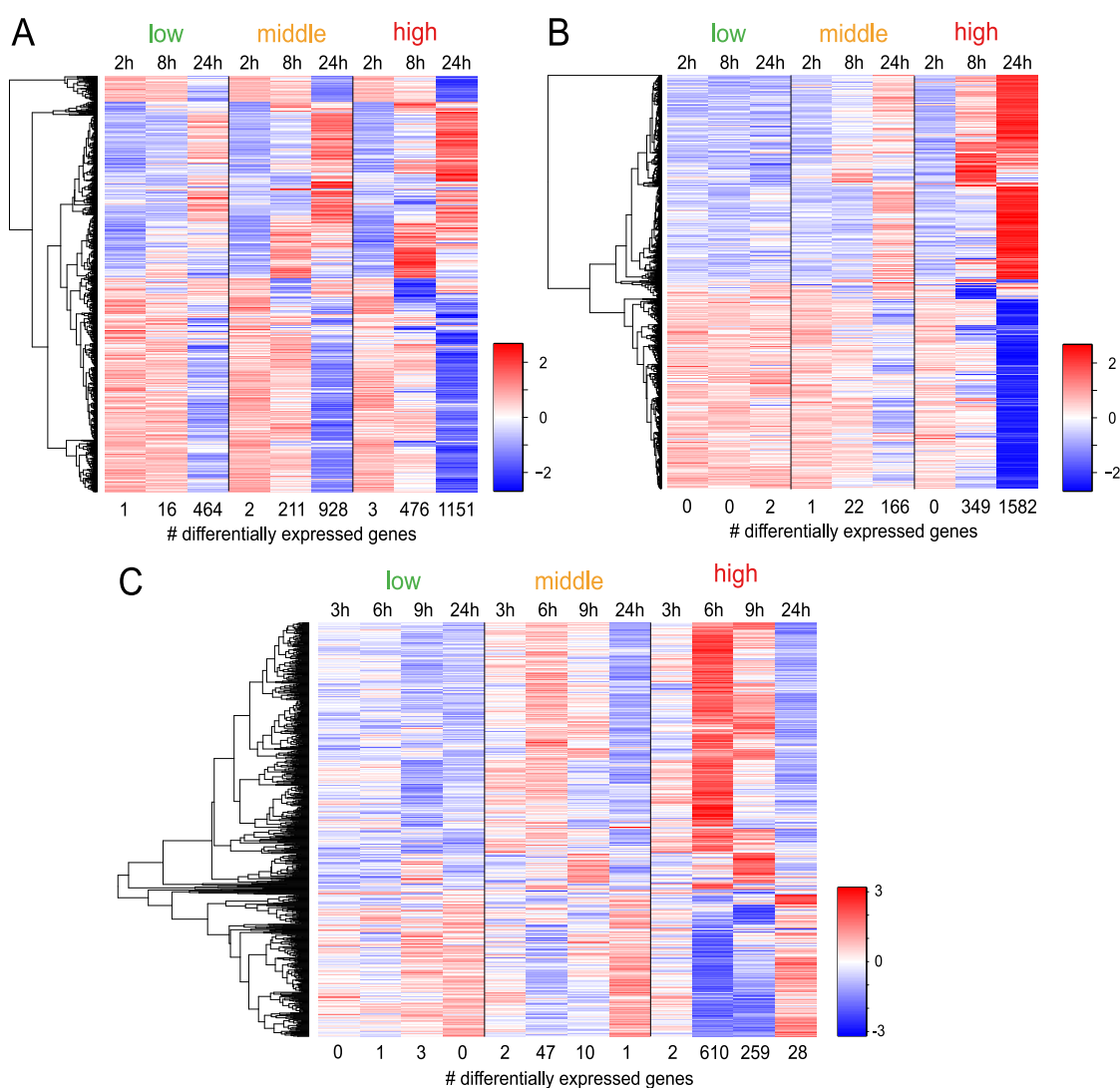


Figure 7.7: Azathioprine-induced gene expression data. In vitro and in vivo expression data of genes differentially expressed in at least one treatment of the specific experiment. Three exposure levels of azathioprine were administered (low (green), middle (orange), high (red)). The number below each column indicates the number of DEGs identified in the specific treatment. Gene expression values in each row were z-score normalized. (A) In vitro, primary human hepatocytes. (B) In vitro, primary rat hepatocytes. (C) In vivo, rat livers.

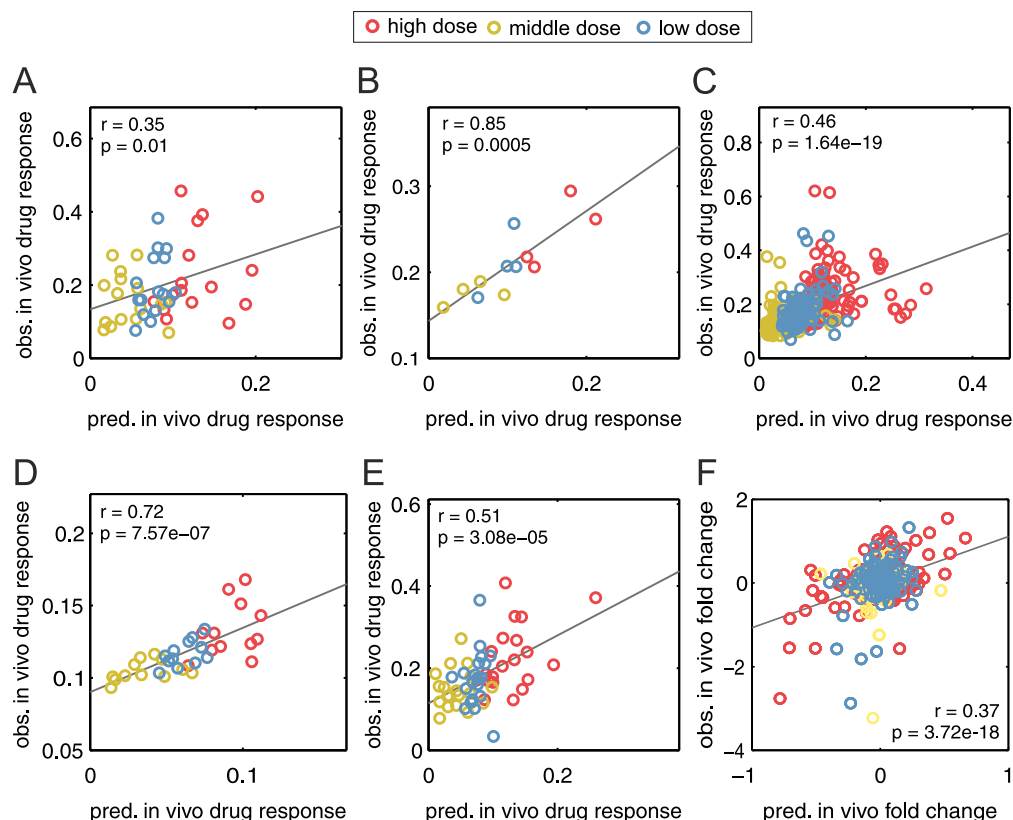


Figure 7.8: Correlation of predicted drug response profiles with in vivo measurements in rats. Correlation between predicted (pred.) in vivo profiles of drug response and gene expression with observed (obs.) profiles measured in vivo following oral administration of the three doses used in the rat study (low dose = yellow, middle dose = blue, high dose = red) [Igarashi et al., 2015]. All cellular processes or biological pathways that were significantly regulated in at least one treatment (Table B.1) and all genes analyzed in the case studies (Table B.5, Table B.7) were considered for the correlation of drug response and gene expression, respectively. Correlation analyses were performed by calculating Pearson's correlation coefficient r and the corresponding p-value p . (A) KEGG pathways. (B) Toxicity-related pathways. (C) Biological processes. (D) Cellular components. (E) Molecular functions. (F) Genes considered in both case studies.

7.3.5 Validation of PICD in rats

To assess the predictive accuracy of PICD, in vivo toxicity data measured in rat livers (Figure 7.7C) were used. The developed rat PBPK model (Figure 7.6) together with the in vitro toxicity data obtained in rat hepatocytes (Figure 7.7B) served as input for the application of PICD to predict in vivo drug response in rats. When applying PICD on rats, a corresponding in vivo dose was determined for each of the nine in vitro treatments (e.g., High - 8h) (Table 7.1). In the in vivo rat study, the minimum toxic dose identified in a 4-week toxicity study was used as highest dose while the low and middle dose were selected by diluting the high dose with a factor of three and ten, respectively [Igarashi et al., 2015]. Consequently, PICD was applied to predict drug responses induced by the three doses used in the in vivo rat study. In vivo drug response of cellular processes and biological pathways significantly regulated in rats (Table B.1) were then predicted for all three doses orally administered in the in vivo rat study and were subsequently correlated with corresponding in vivo observations (Pearson's $r = [0.35, 0.85]$, $p \leq 0.01$) (Figure 7.8A-E).

To check whether the application of PICD actually improved in vivo predictions compared to the in vitro situation, temporal in vitro patterns and predicted in vivo drug responses were both correlated to respective in vivo observations. In vitro drug response profiles of perturbed biological pathways (KEGG,

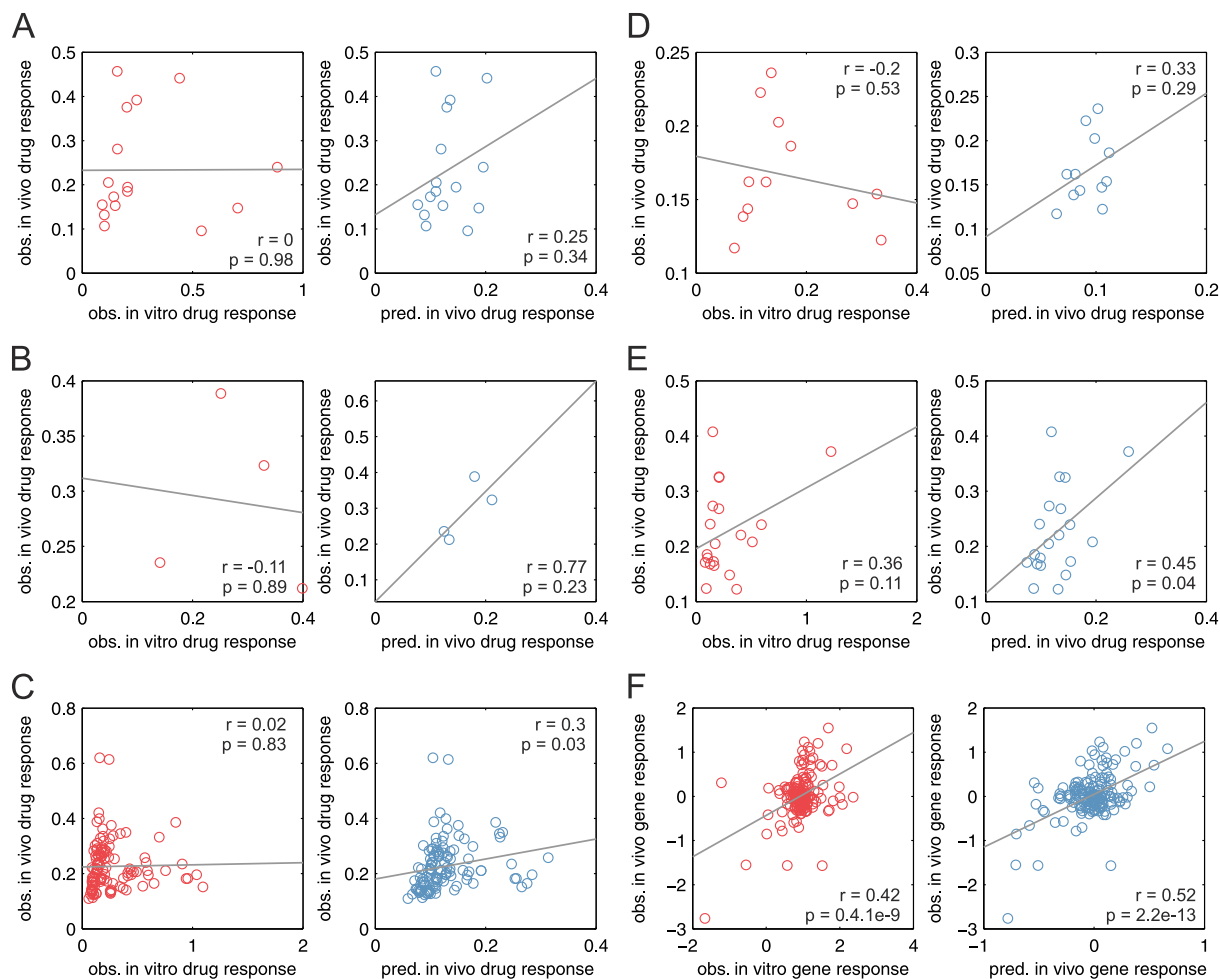


Figure 7.9: Correlation between observed in vivo, in vitro and predicted in vivo drug responses. Predicted in vivo drug response (blue) induced by the identified toxic dose, as well as corresponding in vitro profiles (red) induced by the toxic concentration were correlated with measurements observed in vivo [Igarashi et al., 2015]. All cellular processes or biological pathways that were significantly regulated in at least one treatment (Table B.1) and all genes analyzed in both case studies (Table B.5, Table B.7) were considered for the correlation of drug response and gene expression, respectively. Correlation analyses were performed by calculating Pearson's correlation coefficient r and the corresponding p -value p . (A) Correlation of significantly affected KEGG pathways. (B) Correlation of significantly affected toxicity-related pathways. (C) Correlation of significantly affected biological processes. (D) Correlation of significantly affected cellular components. (E) Correlation of significantly affected molecular functions. (F) Correlation of genes considered in both case studies.

TOX) and biological processes showed almost no relevance for the in vivo situation (Pearson's $r = [-0.2, 0.36]$, $p > 0.05$). In contrast, applying PICD obviously increased the concordance with in vivo measurements for all biological pathways and cellular processes ($r = [0.2, 0.77]$, $p = [0.02, 0.34]$) (Figure 7.9A-E). The correlation results for the individual pathways and cellular processes can be found in Table B.3.

In both patient case studies, expression profiles of considered genes were predicted for clinically-relevant doses to investigate acute liver toxicity after single and multiple dosing of azathioprine. To test whether predictions have in vivo relevance in rats, predicted gene expression profiles were correlated with respective profiles observed in vivo (Pearson's $r = 0.37$, $p = 3.7e-18$) (Figure 7.8F). In vitro-in vivo extrapolation of gene expression profiles was also improved by using PICD (Figure 7.9F). The in vivo relevance of predictions in rats thus verified the application of PICD in humans. Independent of the use of PICD in rats, reliable in vivo profiles of drug response and gene expression were predicted following administration of azathioprine in humans.

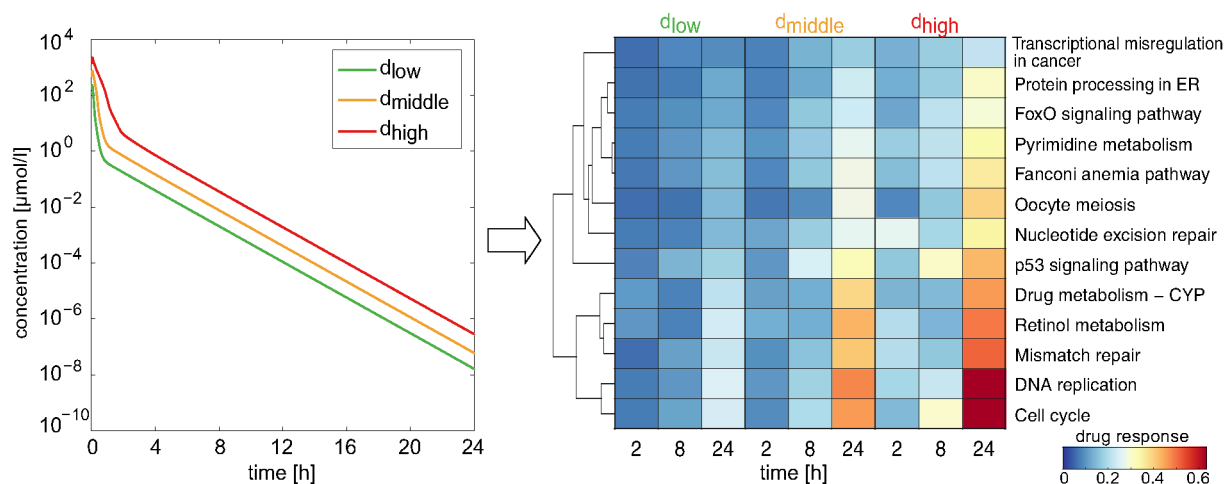


Figure 7.10: Application of PICD on the hepatotoxicant azathioprine in humans. At the organ level, liver interstitial PK profiles were simulated for doses d_{low} , d_{middle} , and d_{high} (colored lines). At the cellular level, correspondent drug response profiles were predicted for significant affected human pathways from KEGG following in vivo drug administration of azathioprine. The color scale depicts predicted in vivo drug response.

7.3.6 Application of PICD in humans

In order to now predict in vivo drug response in humans, in vitro toxicity data from azathioprine treated hepatocytes (Figure 7.7A) were coupled with interstitial PK profiles simulated in the liver for the same drug (Figure 7.2). To this end, three estimates of in vivo doses were averaged horizontally to obtain doses representing the in vivo equivalents ($d_{low} = 20.7$ mg/kg, $d_{middle} = 53.3$ mg/kg, and $d_{high} = 142.8$ mg/kg) to concentrations exposed in vitro (Table 7.1). Since the highest in vitro concentration was defined at the onset of toxicity [Igarashi et al., 2015], administration of the identified high dose (d_{high}) was expected to cause the experimentally observed toxic effects at the cellular level. The remaining two concentrations were further selected by diluting the toxic concentration by a factor of five and twenty-five, respectively [Igarashi et al., 2015]. Interestingly, the identified low dose was seven times higher compared to the therapeutic dose (3 mg/kg) used in clinical trials [Shapiro et al., 1993]. Still, various toxic effects induced by dose levels in the range of the identified doses were reported in clinical studies (Table 7.2) [Gregoriano et al., 2014].

Drug response values after 2 h, 8 h, and 24 h were next calculated to quantify the in vivo response in enriched GO terms and biological pathways (KEGG, TOX) following administration of the in vivo equivalent doses (Figure 7.10, Figure 7.11). By considering a dense number of hypothetical intermediate doses, correspondent in vivo drug response can be further extended to calculate drug response maps as such reflecting cellular changes over time for multiple dose levels applied in vivo (Figure 7.12).

In general, in vivo drug response values show low response after 2 h and 8 h as opposed to larger changes after 24 h indicating a delayed regulatory response at the cellular level (Figure 7.10, Figure 7.11). Nonetheless, the initial increase of drug response was significant at the early time point in any regulated KEGG pathway and in 85 % of any perturbed toxicity-related pathway and GO term ($p < 0.05$, one-sample t-test). High responsive pathways induced by all equivalent in vivo doses after one day showed significant increases in drug response between 8 h and 24 h (DNA replication, cell cycle, mismatch repair, drug metabolism – cytochrome P450, nucleotide excision repair and retinol metabolism, $p < 0.05$, one-way ANOVA with post-hoc Tukey-Kramer) (Figure 7.10). Furthermore, high cellular activity was identified in biological processes regulating cell replication (Figure 7.11A), as well as in processes involved in chromosome condensation (Figure 7.11B). Analyzing enriched toxicity-related pathways revealed high

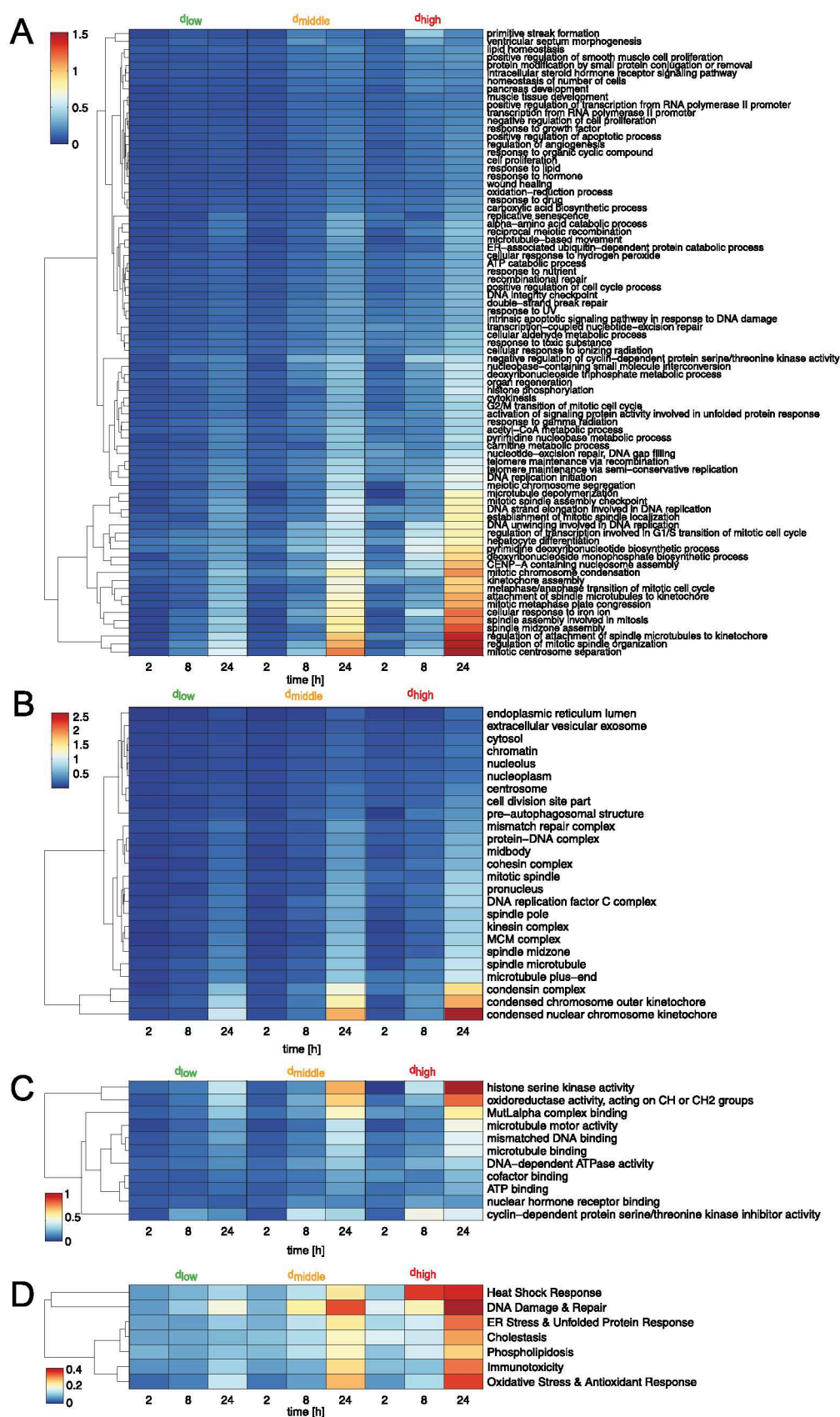


Figure 7.11: Predicted in vivo drug responses in humans. In vivo drug responses of significantly affected GO terms and toxicity-related pathways (Benjamini-Hochberg corrected $p < 0.01$) following in vivo drug administration of d_{low} , d_{middle} , and d_{high} . The color scale depicts predicted in vivo drug responses. (A) Go terms of biological processes. (B) Go terms of cellular components. (C) Go terms of molecular functions. (D) Toxicity-related pathways.

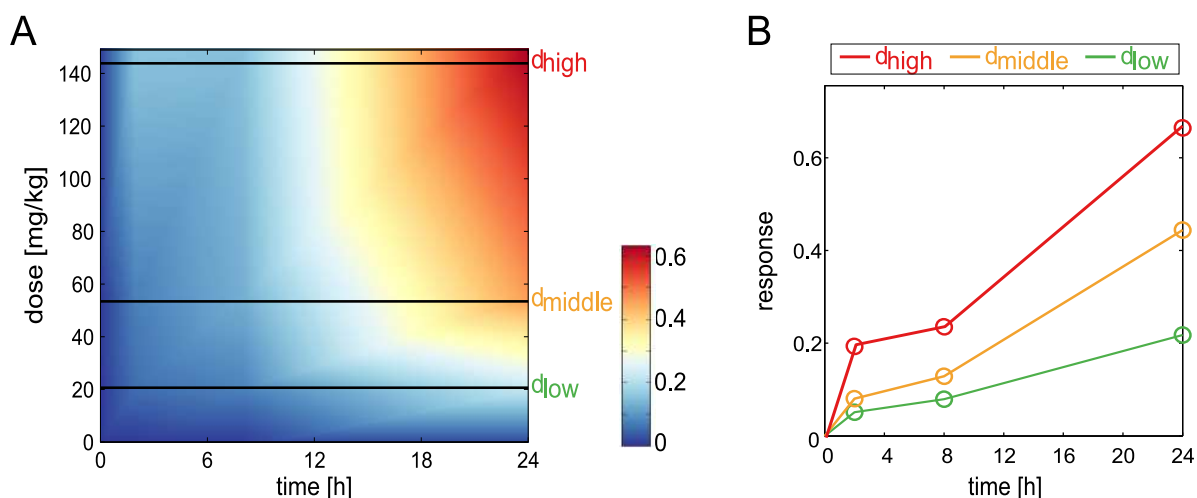


Figure 7.12: Predicted in vivo drug responses for DNA replication. (A) Drug response map exemplarily shown for DNA replication reflects time- and dose-dependent effects following administration of azathioprine at dose levels d_{low} , d_{middle} and d_{high} (black lines). The color scale depicts predicted in vivo drug response. (B) Predicted in vivo drug response over time induced by doses d_{low} , d_{middle} and d_{high} .

response in mechanisms related to DNA damage and repair (Figure 7.11D) as suggested by another study [Karran, 2006].

Here, PICD was applied to predict in vivo drug response in humans induced by in vivo doses derived from in vitro concentrations [Igarashi et al., 2015]. In a next step, PICD was used for different patients by specifically considering individual physiology and various dosage regimens.

7.3.7 Acute toxicity after single dosing of azathioprine: Patient cohort study

An overview of previous cases of acute azathioprine overdoses has recently been reported [Gregoriano et al., 2014]. Since all cases are clinically documented, PICD could be applied to study azathioprine-induced toxicity in a patient-specific manner. In particular, individualized azathioprine PBPK models were developed by explicitly considering patient physiology (Figure 7.13A, Table 7.2). PICD was then applied on each clinical case thereby calculating in vivo drug response of processes involved in DNA damage and repair (Figure 7.13A) following oral administration of the respective overdose. In addition, correspondent cytotoxicity values describing cell viability over time were predicted for all clinical cases to allow a correlation with patient-specific drug responses (Figure 7.13A).

Analyzing patient-specific drug response profiles indicated an early increase in gene response for every patient ($p < 0.001$, one-sample t-test) (Figure 7.13A). Further analysis revealed a significant change between 8 h and 24 h for patient 16, 21, 28, 17, and 19 ($p < 0.05$, one-way ANOVA with post-hoc Tukey-Kramer). To assess the increase in toxicity, drug response values calculated at different time points were correlated with global cytotoxicity values (Figure 7.13B). Excellent correlation results were found at 24 h ($r = 0.99$, $p = 2.73e-6$). Comparing clinically applied Poisoning Severity Scores (PSS) [Persson et al., 1998] with individual drug response after 24 h confirms this observation (Spearman's $\rho = 0.78$, $p = 0.057$). For this correlation analysis, patient 17, who remained asymptomatic after receiving a heavy overdose, was not considered (Table 7.2).

In the following, patient 19, who was exposed to the highest overdose (180.1 mg/kg), was regarded in a patient case study to investigate acute toxicity after single dosing of azathioprine.

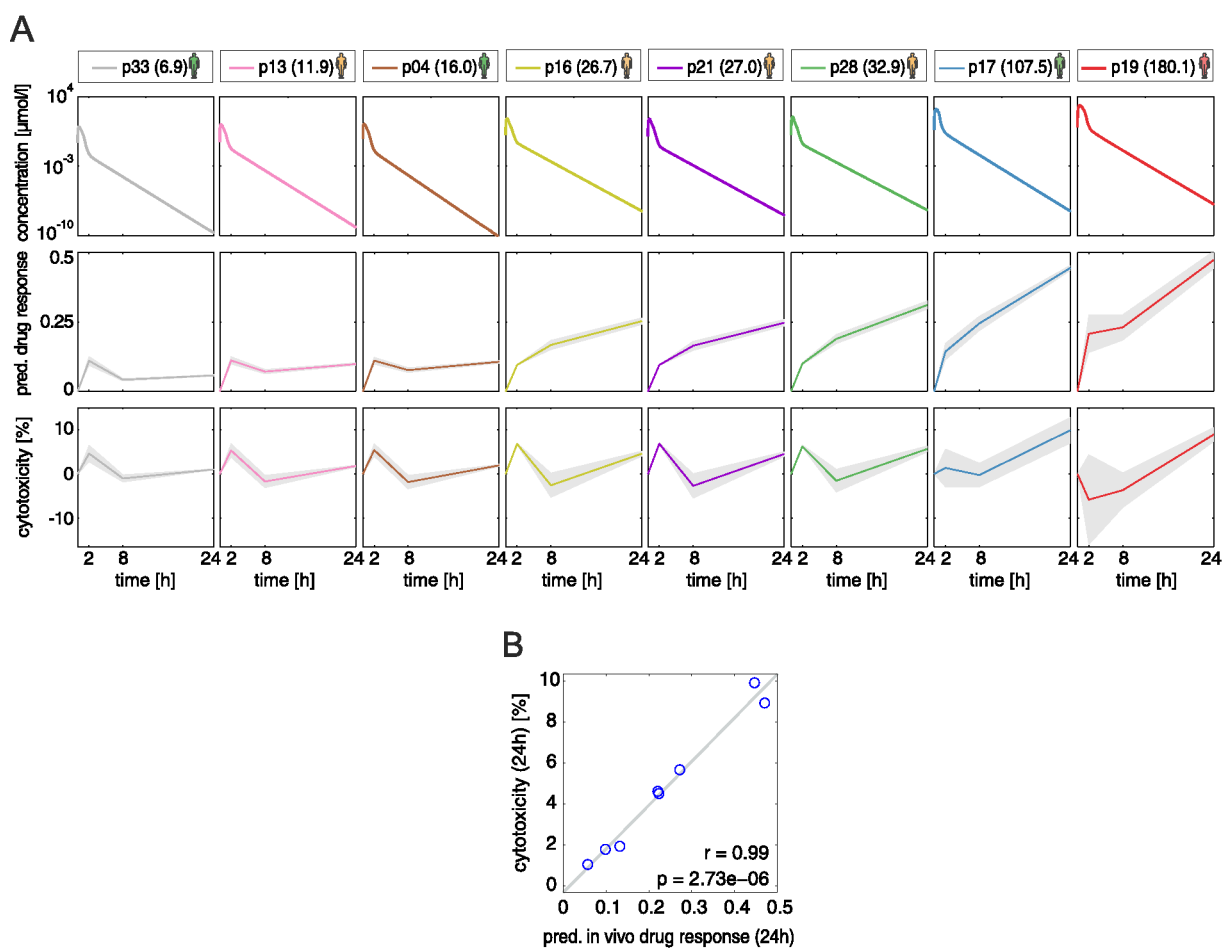


Figure 7.13: Application of PICD on eight clinical cases of acute azathioprine overdose. (A) Simulated drug concentration-time profiles, corresponding predicted in vivo drug response of a critical toxicity-related pathway (DNA damage & repair), as well as predicted cytotoxicity for eight clinical cases following oral administration of different azathioprine overdoses (Table 7.2). In vivo drug responses and cytotoxicity were predicted for both replicates to represent the variability (gray area) [Igarashi et al., 2015]. The mean drug responses are shown as solid lines. Colors of patients indicate the highest Poisoning Severity Score (PSS) [Persson et al., 1998] of the occurred symptoms (none (green) = 0, minor (yellow) = 1, moderate (red) = 2). The overdoses (mg/kg) are shown in brackets. **(B)** Correlation results of predicted in vivo drug response of DNA damage and repair at 24 h with predicted cytotoxicity values. Correlation analysis was performed by calculating Pearson's correlation coefficient r and the corresponding p-value p .

7.3.8 Acute toxicity after single dosing of azathioprine: Patient case study 1

When regarding the various cases of acute azathioprine overdoses the highest overdose was observed for patient 19, considered in the first patient case study [Gregoriano et al., 2014] (Table 7.2). Drug response in the most responsive toxicity-related pathway (DNA damage & repair) was thereby analyzed following oral administration of the specific overdose in this patient (180.1 mg/kg). Additionally, drug response was considered for the therapeutic dose (3 mg/kg) [Shapiro et al., 1993] to study changes between the toxic case and the therapeutic situation (Figure 7.14A).

Clinical symptoms with minor (e.g., headache) and moderate severity (e.g., dyspnoea) were observed for patient 19 (Table 7.2). PK profiles (Figure 7.14A) as well as predicted cytotoxic response patterns (Figure 7.14B) were calculated for both dose levels. In vivo drug responses for DNA damage and repair processes were separated into responses of different functional groups (Figure 7.14C, Table B.5). A slight increase in drug response was identified after 2 h followed by stable drug response to 24 h for nearly any functional category (enzyme, other, transcription regulator) except for kinases that were strongly affected by azathioprine overdose between 8 h and 24 h (Figure 7.14C). In contrast, only a slight response in all

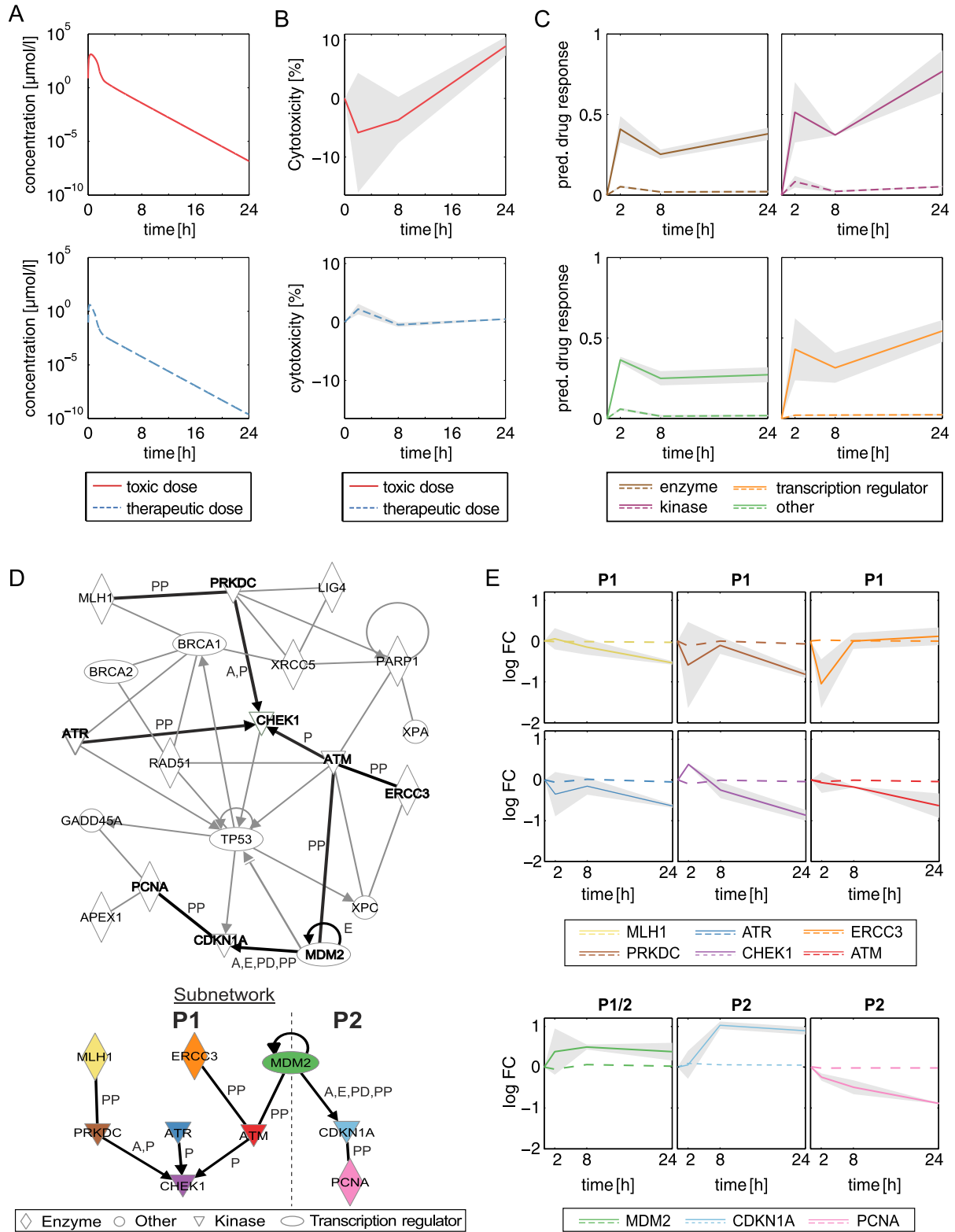


Figure 7.14: Acute liver toxicity after single dosing of azathioprine. (A) Concentration-time profiles simulated for patient 19 (Table 7.2) following oral administration of the toxic dose (solid red line) and the therapeutic dose (dashed blue line). (B) Cytotoxicity values over time predicted for the toxic dose (solid red line) and the therapeutic dose (dashed blue line). The predictions were made for both replicates to represent the variability (gray area). The mean cytotoxicity is shown as solid line. (C) Predicted in vivo drug response induced by oral administration of the therapeutic dose (dashed colored lines) and the toxic dose (solid colored lines). In vivo drug responses were separated into different functional categories (enzyme, other, kinase, and transcription regulator) (Table B.5). The predictions were made for both replicates to represent the variability (gray area). The mean drug responses are shown as solid lines. \Rightarrow

Figure 7.14: ⇒ (D) Interaction network and processed subnetwork of genes involved in DNA damage and repair processes (Table B.6). Since no expression data were available for CHEK2 and ERCC5, interactions between these genes and other were excluded. The subnetwork (thick black lines) was identified by considering only interactions between genes that were strongly regulated (absolute log2 fold change > 0.5) in at least one timepoint. The interaction types (A = Activation, E = Expression, P = Phosphorylation, PD = Protein-DNA interaction, PP = Protein-Protein interaction) were highlighted next to the specific edges. The interaction network was generated through the use of QIAGENs Ingenuity Pathway Analysis (IPA®, QIAGEN Redwood City, www.qiagen.com/ingenuity). (E) Predicted temporal expression patterns induced by the therapeutic and toxic dose were simulated for patient 19. Two critical processes (P1, P2) extracted from the subnetwork were considered separately (dashed line indicates separation). The first process (involved genes: MLH1, ERCC5, MDM2, PRKDC, ATR, ATM, CHEK1) resulted in the inhibition of CHEK1 that is required to initiate cell cycle arrest in response to DNA damage. The second process (involved genes: MDM2, CDKN1A, PCNA) induced the inhibition of PCNA leading to an impairment of DNA repair processes. The predictions were made for both replicates to represent the variability (gray area). The mean gene expressions are shown as solid lines.

functional categories was identified when azathioprine was administered at the therapeutic dose (Figure 7.14C).

Furthermore, an interaction network was generated and a subnetwork was extracted by considering all interactions between genes that were substantially perturbed (absolute log2 fold change > 0.5) by azathioprine in at least one timepoint (Figure 7.14D, Table B.6). Temporal expression patterns of genes involved in two critical processes inducing DNA repair were then analyzed and compared for both dose levels (Figure 7.14E). In both processes, very low changes in gene expression were identified when azathioprine was administered at the therapeutic dose contrarily to substantial changes induced by the toxic dose (Figure 7.14E). Considering the first process following acute azathioprine overdose, CHEK1 responsible for cell cycle arrest and repairing damaged DNA [Goto et al., 2012; McNeely et al., 2014; Kim et al., 2015] was activated after 2 h (Figure 7.14E). Then, CHEK1 was continuously inhibited as consequence of the inhibition of kinases (ATM, ATR, PRKDC) activating CHEK1 and enzymes (MLH1, ERCC3) interacting with ATM and ATR (Figure 7.14E). The inactivation of CHEK1 potentially indicates mitotic catastrophe [Zhivotovsky and Kroemer, 2004]. The regulation of DNA repair after 24 h was reflected by an increased cell death measured in vitro (Figure 7.14B) [Igarashi et al., 2015].

In the second process (Figure 7.14E), MDM2, a transcription regulator, interacts with the kinase inhibitor CDKN1A [Sánchez-Aguilera et al., 2006] leading to a constant activation, whereas the proliferating cell nuclear antigen (PCNA) was strongly inhibited over 24 h (Figure 7.14E). Since PCNA is required for DNA replication and repair [Shivji et al., 1992; Essers et al., 2005], cell viability was detrimentally affected (Figure 7.14B). Analyzing both processes induced by the therapeutic dose showed very low response, which reveals no deficiency in DNA repair or cell cycle arrest (Figure 7.14E). This observation was confirmed by the cell viability profile predicted for the therapeutic dose only showing slight variations compared to the control (Figure 7.14B).

For this patient case study, PICD provided important insights into changes in gene expression for acute toxicity after acute azathioprine overdose at the patient level.

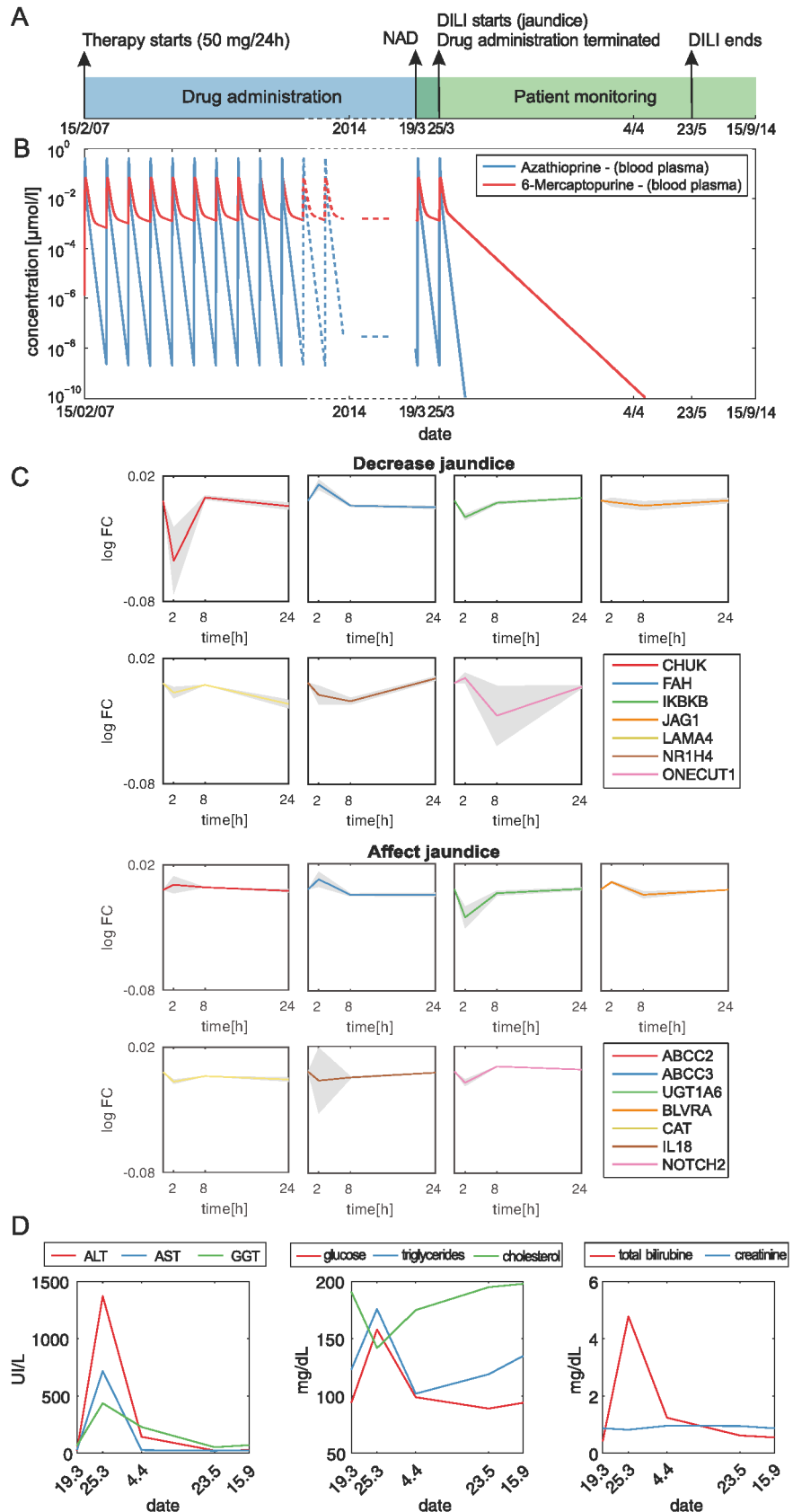
7.3.9 Acute toxicity after multiple dosing of azathioprine: Patient case study 2

In contrast to acute toxicity after acute overdosing of azathioprine, in this second case study, acute liver injury was observed in the context of a chronic treatment with azathioprine at therapeutic dose by using own clinical data. A 37 year-old man with a history of thrombocytopenic purpura (TTP) was treated orally with 50 mg of azathioprine once-daily over a period of seven years (Figure 7.15A). During this period liver parameters were always within normal range. Blood plasma concentrations of azathioprine and 6-mercaptopurine were simulated for the entire evolution of the patient (Figure 7.15B).

The patient was seen for urgent consultation in the outpatient hepatology clinic for evaluation of new onset of jaundice and elevated liver enzymes, associated with general malaise, weakness and nausea

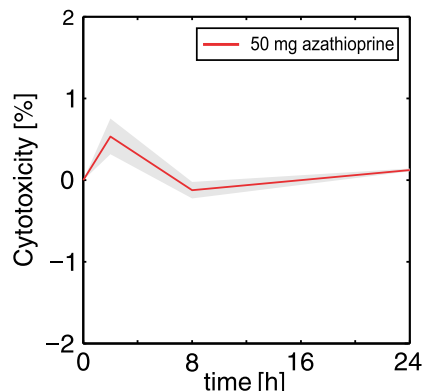
Figure 7.15: Acute liver failure after multiple dosing of azathioprine.

(A) Therapy process. The 37 year-old male patient received 50 mg of azathioprine orally every day over a period of seven years. Measurements of clinical biomarkers (e.g., ALT) were started one week before DILI symptoms (jaundice) occurred. At that time, no abnormality was detected (NAD). Azathioprine treatment was terminated at the onset of liver toxicity. About nine weeks later, jaundice disappeared. (B) Blood plasma concentrations of azathioprine (blue line) and 6-mercaptopurine (red line) were simulated for the whole therapy process following oral administration of 50 mg every 24 h. When DILI occurs, azathioprine treatment was terminated leading to a rapid clearance of both compounds within the body. (C) Expression levels of fifteen genes related to jaundice (Table B.7) were exemplarily simulated over one day following single dosing of 50 mg of azathioprine to reflect the cellular effects at the transcriptional level induced by the permanent drug treatment (Table B.7). The predictions were made for both replicates to represent the variability (gray area). (D) Eight different clinical biomarkers (total bilirubin, creatinine, glucose, cholesterol, triglycerides, ALT, AST, and GGT) were measured at five different dates over a period of about six months. The first measurement was started about one week before DILI was observed in the specific patient.



within 5 days evolution. When jaundice has started, azathioprine treatment was terminated resulting in an instantaneous wash-out of the drug from the body within a few days (Figure 7.15B). The diagnosis of DILI was carried out based on a scale specifically designed for DILI causality assessment, the Rousell Uctaf

Figure 7.16: Predicted in vivo cytotoxicity over time. In vivo cytotoxicity values over time induced by the therapeutic dose were predicted for both replicates (gray area). The mean cytotoxicity values are shown as solid line.



Causality Assessment Model (RUCAM) [Danan and Benichou, 1993], with a score of 7 (probable), by ruling out other possible etiologies (viral hepatitis, excessive alcohol use, metabolic diseases, autoimmune disorders and biliary diseases).

To compare changes at the cellular level with observed clinical symptoms, temporal expression patterns following oral administration of azathioprine were predicted for fifteen genes that are associated with jaundice (Figure 7.15C, Table B.7). Notably, no drug accumulation occurred during multiple dosing for both azathioprine and 6-mercaptopurine since both compounds were extensively metabolized and almost completely cleared from the body within 24 h (Figure 7.15B). This was also observed for the simulated drug concentrations in the intracellular space of the liver. Since additionally no in vitro response data were available for repeated dosing, drug-induced adaption due to multiple dosing was hence assumed to be negligible and the predicted gene expression profiles (Figure 7.15C) were thus to be assumed to reflect the drug response at the cellular level. In addition, cell viability values predicted for the therapeutic dose disclosed no relevant elevations (Figure 7.16). Investigating the response of genes affecting jaundice (Table B.7) revealed no remarkable changes (Figure 7.15C).

Biochemical markers measured shortly before, during and after the occurrence of jaundice, indicated significant elevations (Figure 7.15D). Levels of ALT (1373 U/L), AST (718 U/L), and GGT (437 U/L) clearly exceeded clinically-relevant reference levels [Ceriotti et al., 2010] (Figure 7.15D). Moreover, laboratory studies yielded a total bilirubin of 4.78 mg/dL reflecting a substantial increase compared to measurements before and after jaundice occurred. While concentrations of glucose and triglycerides were increased, total cholesterol (142 mg/dL) was notably diminished (Figure 7.15D). The patient reported substantial improvement in his health status, and liver biochemical tests a few days after the discontinuation of azathioprine, and follow-up visits after two months revealed subsequent normal laboratory tests and lack of symptoms (Figure 7.15D).

In this second patient case study, PICD provided the contextualization of simulated pharmacokinetics, predicted gene expression changes induced by the therapeutic dose and in vivo measurements of biochemical markers.

7.4 Discussion

In this study, the integrative multiscale approach PICD is presented, which allows a time-resolved description of drug-specific response profiles at the cellular level induced by in vivo drug administration at the organism level. Conceptually, PBPK models validated with blood plasma concentration-time data were used to simulate unbound drug concentrations in the interstitial space of the liver that in turn corresponds directly to the extracellular medium of in vitro experiments. Applied consistently, the systematic

approach of using PBPK modeling for contextualization of *in vitro* toxicity data, which was exemplarily applied here for azathioprine, thus enables a generic workflow for the analysis of toxic effects of arbitrary drugs at patient level.

Predicted *in vivo* drug response induced by the identified doses (Figure 7.10, Figure 7.11) reflect the *in vivo* results of temporal cellular alterations observed for drug concentrations administered *in vitro* (Table 7.1). Considering oral administration [Zins et al., 1997], identified doses are in the range of toxic dose levels reported in clinical studies [Gregoriano et al., 2014] as such highlighting clinical relevance of the presented approach. Similar findings were observed when comparing the high dose (61.5 mg/kg) estimated for the rat with the minimum toxic dose determined in the *in vivo* study [Igarashi et al., 2015]. The presented concept of coupling *in vitro* toxicity data with simulated interstitial concentration-time curves is based on the identification of *in vivo* doses that best represents the *in vitro* drug exposure. For this identification process, various pharmacokinetic parameters like the maximal observed concentration (C_{max}) could alternatively be considered. Here, the area under curve was selected since it represents a quantitative measure for drug exposure [Igarashi et al., 2015].

To initially validate PICD, a rat PBPK model was built (Figure 7.6) by performing a cross-species extrapolation from humans to rats using the validated human PBPK model (Figure 7.4). This mechanistic translation was based on recent findings [Thiel et al., 2015] and helped to compensate the unavailability of adequate PK data for the rat in the literature. Gene expression data of azathioprine-treated rats (Figure 7.7C) and rat hepatocytes (Figure 7.7B) together with the developed rat PBPK model were then used to assess the predictive quality of PICD by correlating predicted *in vivo* drug response of regulated cellular processes and biological pathways (Table B.1) with findings observed *in vivo* [Igarashi et al., 2015]. The correlation results showed high *in vivo* relevance of predicted *in vivo* drug responses in rats (Figure 7.8) considering that *in vitro-in vivo* extrapolation is still a challenging issue [Boess et al., 2003; Heise et al., 2012; Stegeman et al., 2012; Cebola et al., 2015]. Overlooking potential inter-species differences, this validation was indispensable to verify the reliability of predicted *in vivo* drug response for human patients since no *in vivo* toxicity data was available for humans. The comparison of both *in vitro* patterns and predicted response profiles with *in vivo* observations was evaluated. Correlation results obviously revealed that the extrapolation of *in vitro* toxicity data into an *in vivo* context was clearly improved by use of PICD (Figure 7.9). PICD can generally be used for any laboratory animal (e.g., rat, dog, or monkey) used in the preclinical phase during drug development, since PBPK modeling allows the simulation of concentration-time profiles for several species by incorporating prior knowledge about their specific anatomy and physiology. Notably, the application of PICD on any species occurs independently meaning that no species-specific findings were extrapolated from one species to another species.

Prediction of drug-induced cellular changes in response to interstitial PK profiles is not limited to hepatotoxicants. The compartmentalization of PBPK models enables the prediction of interstitial drug concentrations in multiple tissues or organs such as, for example, the heart. In this case, cellular changes obtained from compound-treated cardiomyocytes could likewise be used to get insights into adverse effects of cardiotoxic compounds in an *in vivo* context. Time-series gene expression profiles from a toxicogenomics database [Igarashi et al., 2015] were considered here to quantify drug response over time at the cellular level. Transcriptome analysis is a powerful technique to determine changes in gene expression by measuring mRNA abundances in order to predict protein levels and activity. However, correlations between the transcriptome and proteome can be low and gene expression analysis may have limitations in elucidating stress response [Feder and Walser, 2005; Haider and Pal, 2013]. Since *in vitro* data obtained by other functional omics techniques such as proteomics or metabolomics can be analogously incorporated in the presented approach, this integrative analysis would provide a more comprehensive description of complex

biological processes induced by drug administration in vivo. Likewise, in vitro toxicity data from different high-throughput technologies could also be taken into account [Dix et al., 2007].

To demonstrate future potential of PICD in clinical application, individualized PBPK models considering specific patient physiology were developed to predict in vivo drug response for clinical cases of acute azathioprine overdose [Gregoriano et al., 2014] (Table 7.2). Notably, drug response of processes involved in DNA damage and repair after one day was highly correlated with measured cytotoxicity (Figure 7.13B) indicating that changes at the transcriptional level might be directly related to cytotoxic measurements observed in vitro. High correlation determined between PSS values and corresponding drug response pointed out the relation between the drug-induced response in a critical toxicity pathway and the severity of observed clinical symptoms. Availability of additional individualized information such as patients' genotype [Lippert et al., 2013] might be useful to further specify the translation for potential clinical applications and analysis of idiosyncratic hepatotoxicity. Genetic heterogeneity, like variants in cytochrome P450 enzymes [Dandara et al., 2011], may alter the catalytic activity of drug-related enzymes, which in turn affect drug distribution and elimination processes. For instance, genetic polymorphisms in crucial metabolic enzymes involved in the metabolism of isoniazid substantially influenced relevant pharmacokinetic processes, which may change drug efficacy at the target site or may increase the risk of toxicity [Kinzig-Schippers et al., 2005; Vuilleumier et al., 2006; Perwitasari et al., 2015]. Coupling individualized PBPK models developed for different genotypes with in vitro toxicity data obtained by omics technologies that may consider genetic diversity could therefore have a beneficial effect for individually tailored drug therapy and patient safety.

Two patient case studies have been performed to demonstrate the application of PICD on clinical cases of acute toxicity induced by different dosage regimens (Figure 7.14, Figure 7.15). In vivo relevance of all genes considered in both case studies was verified by assessing predicted gene expression profiles in rats. In the first patient case study, in vitro toxicity data could be directly used to simulate drug response of DNA damage and repair processes following acute azathioprine overdose (Figure 7.14) [Gregoriano et al., 2014]. Analyzing the drug response for different functional categories identified kinases as high responsive when azathioprine was administered at the toxic dose (Figure 7.14C). Further analysis of two critical processes allowed comparing drug response between toxic and therapeutic dose levels (Figure 7.14D).

In the second patient case study own data was used to study drug-induced liver failure elicited by multiple dosing of azathioprine at therapeutic dose over more than seven years (Figure 7.15A). Here, genes affecting the development of jaundice (Table B.7) were specifically considered and could thus be correlated to observed clinical symptoms (Figure 7.15C, Figure 7.15D). Since PK analysis showed no drug accumulation in the therapy process, the predicted response profiles (Figure 7.15C) were assumed to reflect the drug activity at the cellular level for each day. Over 24 hours only low transcriptional changes induced by the therapeutic dose were predicted for jaundice-related genes. This clearly indicates that more data is needed to actually predict the sudden emergence of jaundice following long-term azathioprine administration. Such data could be, for instance, additional patient information or response data obtained by other functional omics techniques like proteomics or metabolomics. Moreover, further analyses are necessary to elucidate the molecular mechanism of the adverse reaction leading to jaundice, in particular when the toxicity was induced by chronic drug administration over a long period of time. For a mechanistic analysis, gene expression data from liver biopsies after repeated dosing would be required here to adequately investigate such toxic events. Further patient data involving, amongst others, medical history or patient lifestyle would also be necessary. Still, the application of PICD here allowed a description of how cellular drug response profiles are induced by a clinically relevant dose. Thus, this patient case study provided an integrated analysis of patient-specific pharmacokinetics, drug response following oral administration of the therapeutic dose, as well as the relation to several clinical biomarkers measured before, during and after the occurrence of jaundice. Finding crucial changes between predicted

gene expression profiles for therapeutic and toxic dose levels could thus enhance the identification of useful biomarkers in patients and subsequently lead to an early detection of potential toxicity.

Clearly, the *in vivo* predictions in the rat are not fully accurate and the application of PICD inhibits some inherent level of uncertainty. However, it should be noted that the approach presented provides a generic workflow for quantitative analyses of *in vitro* measurements within an *in vivo* context. The PBPK models at the organism level were carefully qualified by validating the model with clinical data for different doses and different administration routes. Furthermore, the expression data at the cellular scale were taken from TG-GATEs [Igarashi et al., 2015], which is one of the most systematic and best curated toxicological databases in the world. Hence, despite some inherent yet inevitable uncertainty in the input, the predictions made by PICD represents nevertheless a sound extrapolation of *in vitro* data to an *in vivo* environment. Please note also that PICD allows an animal-free assessment of drug-induced toxicity which is fully in line with 3R principles. Assuming that appropriate *in vitro* toxicity tests were concluded, the use of PICD for laboratory animals may improve the predictability of toxic events in an *in vivo* context and may facilitate the identification of a safe dose. The demand for animal sacrifice is thereby reduced since PICD is an *in silico*-based approach.

To conclude, PICD allows describing temporal changes at the cellular level induced by drug administration *in vivo* and hence provides a generic platform to contextualize *in vitro* measurements of different omics studies at the organism level. Therefore, changes in cellular events induced by clinically-relevant or toxic dose levels can be predicted for humans and thus might facilitate the investigation of *in vitro* findings within a patient context for clinical applications in the future.

A comparative analysis of drug-induced hepatotoxicity in clinically relevant situations

Abstract

Drug-induced toxicity is a significant problem in clinical care. A key problem here is a general understanding of the molecular mechanisms accompanying the transition from desired drug effects to adverse events following administration of either therapeutic or toxic doses, in particular within a patient context. Here, a comparative toxicity analysis was performed for fifteen hepatotoxic drugs by evaluating toxic changes reflecting the transition from therapeutic drug responses to toxic reactions at the cellular level. By use of physiologically-based pharmacokinetic modeling, in vitro toxicity data were first contextualized to quantitatively describe time-resolved drug responses within a patient context. Comparatively studying toxic changes across the considered hepatotoxicants allowed the identification of subsets of drugs sharing similar perturbations on key cellular processes, functional classes of genes, and individual genes. The identified subsets of drugs were next analyzed with regard to drug-related characteristics and their physicochemical properties. Toxic changes were finally evaluated to predict both molecular biomarkers and potential drug-drug interactions. The results may facilitate the early diagnosis of adverse drug events in clinical application.

published as:

Thiel, C., Cordes, H., Fabbri, L., Aschmann, H. E., Baier, V., Smit, I., Atkinson, F., Blank, L. M., and Kuepfer, L. (2017). A comparative analysis of drug-induced hepatotoxicity in clinically relevant situations. *PLoS Computational Biology*.

Author contributions:

Writing - original draft: Thiel, C., and Kuepfer, L.; Writing - review & editing: Thiel, C., Cordes, H., Baier, V., Smit, I., Atkinson, F., Blank, L. M., and Kuepfer, L.; Conceptualization: Thiel, C., and Kuepfer, L.; Software & validation: Thiel, C.; Resources: Smit, I., Atkinson, F., Thiel, C., Cordes, H., Fabbri, L., Aschmann, H. E.; Formal analysis & implementation: Thiel, C.

8.1 Introduction

Drug-induced hepatotoxicity poses a significant problem in drug development and public health [Schuster et al., 2005; Kaplowitz, 2004]. Extensive drug exposure due to overdosing or patient idiosyncrasy may lead to hepatotoxic effects such as drug-induced steatosis or cholestasis [Bernal et al., 2010; Lee, 1993, 1995]. Such adverse events may even be aggravated through drug interactions during patient co-medication leading to additive, synergistic, or antagonist drug effects [Askgaard et al., 1995; Deray et al., 1987; Chen and Raymond, 2006; Sato et al., 1985].

Understanding the molecular mechanisms underlying the transition from desired drug effects to adverse events induced by therapeutic and toxic doses, respectively, is of general importance for both clinical diagnostics and curative intervention strategies [Park et al., 2004]. In this regard, robust clinical biomarkers may significantly improve patient safety and health [Shi et al., 2010; Wang et al., 2013; Riedmaier and Pfaffl, 2013b; Mendrick, 2011; Salminen et al., 2011] by the initial identification of cellular mechanisms indicating drug toxicity in order to implement appropriate interventions at an early stage [Wilmes et al., 2013; Iskar et al., 2013; Herpers et al., 2016; Zhang et al., 2014]. Comparatively analyzing cellular responses following the transition from therapeutic to toxic doses supports the identification of molecular biomarkers and would clearly help to investigate to what extent specific drugs similarly contribute to characteristic toxicological processes and, furthermore, to find out potential interactions between those drugs, which might act on a mutual target gene.

A comparative study of molecular responses in human cell lines in the face of therapeutic and toxic doses for a set of known hepatotoxic drugs could be used to better characterize drug-induced toxicity. A severe drawback of such in vitro analyses, however, is often the limited translatability to the in vivo situation in patients in actual clinical practice. Recently, we have developed an integrative multiscale approach called PICD for the in vivo contextualization of in vitro toxicity data based on PBPK modeling, which significantly supports translations to an in vivo situation in patients (Figure 8.1) [Thiel et al., 2016]. Importantly, PBPK modeling aims for a mechanistic representation of ADME processes governing drug pharmacokinetics within the human body. Since PBPK models include a large amount of mechanistic information, these models are well-suited for extrapolations to different treatment scenarios.

The main goal of this study was the analysis of drug-induced toxicity following administration of therapeutic and toxic doses of different hepatotoxicants in humans. Thus, toxic changes reflecting drug-induced toxicity during the transition from therapeutic to toxic doses were comparatively evaluated for fifteen hepatotoxicants to quantitatively identify subsets of drugs, which share similar perturbations on (i) key cellular processes, (ii) functional classes of genes, and (iii) individual genes (Figure 8.2). To predict drug responses in clinically relevant situations following administration of therapeutic and toxic doses, PICD (Figure 8.1) was applied on a set of fifteen known hepatotoxic drugs: acetaminophen (APAP), amiodarone (AD), azathioprine (AZA), cyclophosphamide (CPA), cyclosporine A (CSA), diclofenac (DFN), erythromycin (ERY), flutamide (FT), haloperidol (HPL), isoniazid (INH), phenobarbital (PB), phenytoin (PHE), rifampicin (RIF), simvastatin (SST), valproic acid (VPA).

The drugs were selected based on pharmaceutical and chemical diversity, physicochemical properties, availability of in vitro toxicity data and experimental drug concentration-time profiles, as well as concern for DILI. Transcriptome data obtained in primary human hepatocytes from Open TG-GATEs [Igarashi et al., 2015] was used as in vitro toxicity data at the cellular level, while human PBPK models were developed at the organism level. In the comparative toxicity analysis, toxic changes were evaluated in three different analyses (Figure 8.2).

In the first analysis, toxic changes between the fifteen hepatotoxic drugs were investigated for a large number of key cellular processes (Table C.1). In the second analysis, toxic changes calculated for different

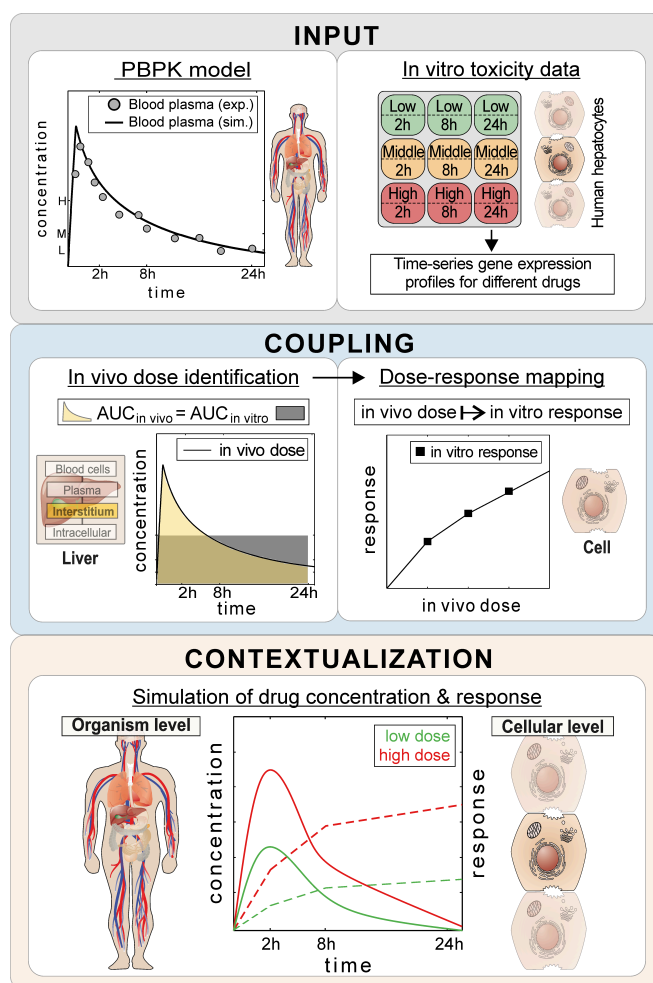


Figure 8.1: PBPK-based in vivo contextualization of in vitro toxicity data (PICD). **Input:** At the organism level, PBPK models are developed for specific drugs. At the cellular level, in vitro response data of compound-treated primary hepatocytes are analyzed [Igarashi et al., 2015]. **Coupling:** In vivo doses are identified, which are directly related to in vitro drug exposure ($AUC_{in\ vivo} = AUC_{in\ vitro}$). Time-dependent dose-response curves are built by mapping in vivo doses to in vitro responses. **Contextualization:** By use of the time-dependent dose-response curves, drug responses over time are predicted for PK profiles simulated for different doses.

functional classes of genes were evaluated for a subset of key cellular processes strongly perturbed by an identified set of high-responsive drugs. In the third analysis, toxic changes were evaluated for a set of individual genes thereby quantitatively discovering molecular biomarkers and potential DDIs for the high-responsive drugs.

8.2 Materials and methods

8.2.1 Set of drugs

In this study, fifteen hepatotoxic drugs (APAP, AD, AZA, CPA, CSA, DFN, ERY, FT, HPL, INH, PB, PHE, RIF, and SST) were analyzed. The drugs have been selected based on pharmaceutical and chemical diversity, physicochemical properties, availability of in vitro toxicity data and experimental drug concentration-time profiles, as well as concern for DILI (Table 8.1). The drugs were categorized into drugs with most-DILI or less-DILI-concern [Chen et al., 2011; Herpers et al., 2016]. Assigned severity scores were between two and eight [Chen et al., 2011; Herpers et al., 2016]. The World Health Organization's Anatomical Therapeutic Chemical (ATC) classification system [Skrbo et al., 2004] was used to separate

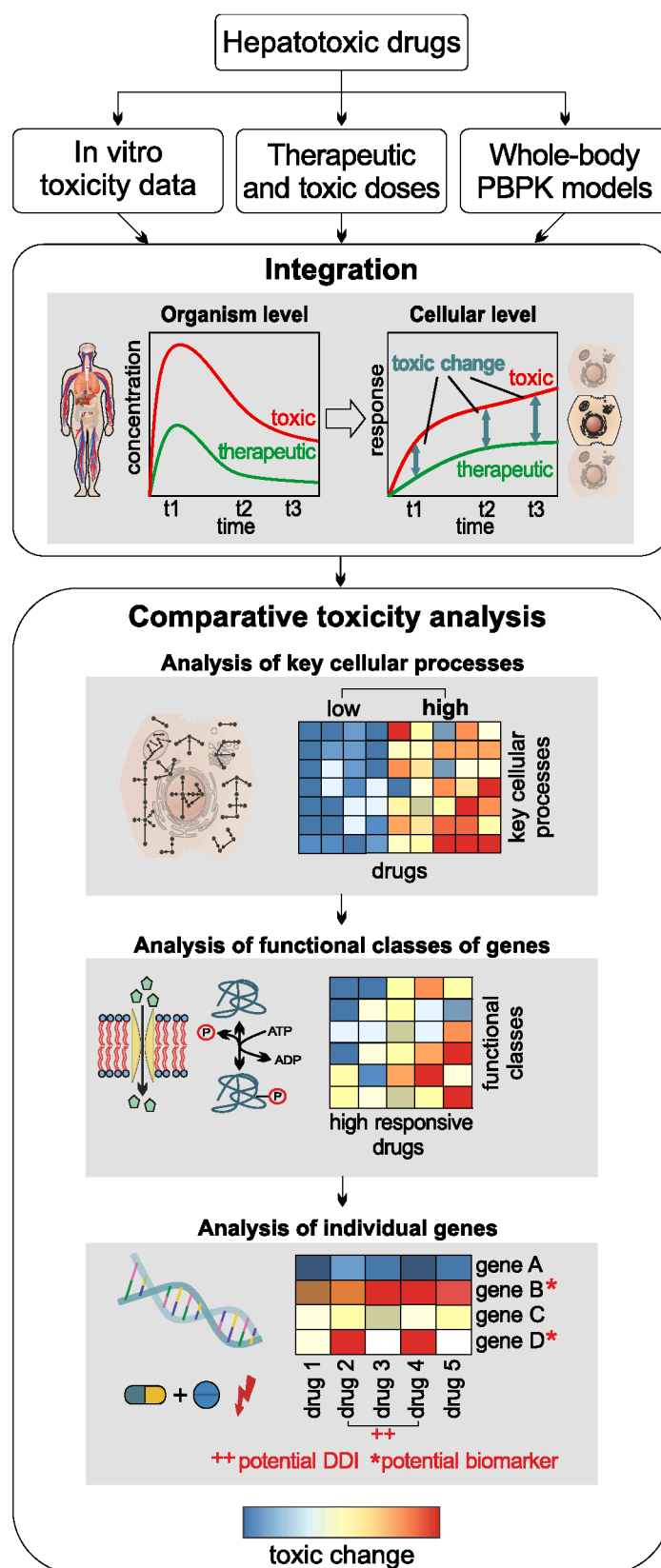


Figure 8.2: General workflow. For a set of hepatotoxic drugs, in vitro toxicity data from Open TG-GATEs [Igarashi et al., 2015] were analyzed, therapeutic and toxic doses were identified in the literature, and whole-body PBPK models were developed and validated. Toxic changes were then predicted at different timepoints (2 h, 8 h, 24 h) by comparing cellular response following drug administration of therapeutic and toxic doses. Toxic changes were subsequently evaluated with regard to key cellular processes, functional classes of genes, and individual genes.

Table 8.1: Drug-specific annotations. DILI-potential, severity score, anatomical main group, therapeutic and chemical subgroup, as well as BCS class of the fifteen considered drugs.

Drug	DILI-potential	Severity score	Anatomical main group	Therapeutic subgroup	Chemical subgroup	BCS class
APAP	Most-DILI-concern	5	Nervous system	Analgesics	Anilides	class 4
AD	Most-DILI-concern	8	Cardiovascular system	Cardiac therapy	Antiarrhythmics, class III	class 2
AZA	Less-DILI-concern	3	Antineoplastic and immunomodulating agents	Immunosuppressants	Other immunosuppressants	class 4
CPA	Less-DILI-concern	5	Antineoplastic and immunomodulating agents	Antineoplastic agents	Nitrogen mustard analogues	class 3
CSA	Less-DILI-concern	2	Antineoplastic and immunomodulating agents	Immunosuppressants	Calcineurin inhibitors	class 2
DFN	Most-DILI-concern	7	Musculo-skeletal system	Antiinflammatory and antirheumatic products	Acetic acid derivatives and related substances	class 2
ERY	Most-DILI-concern	5	Antiinfectives for systemic use	Antibacterials for systemic use	Macrolides	class 2
FT	Most-DILI-concern	8	Antineoplastic and immunomodulating agents	Endocrine therapy	Anti-androgens	class 2
HPL	Less-DILI-concern	5	Nervous system	Psycholeptics	Butyrophenone derivatives	class 2
INH	Most-DILI-concern	8	Antiinfectives for systemic use	Antimycobacterials	Hydrazides	class 3
PB	Less-DILI-concern	3	Nervous system	Antiepileptics	Barbiturates and derivatives	class 4
PHE	Less-DILI-concern	3	Nervous system	Antiepileptics	Hydantoin derivatives	class 1
RIF	Most-DILI-concern	8	Antiinfectives for systemic use	Antimycobacterials	Antibiotics	class 2
SST	Less-DILI-concern	3	Cardiovascular system	Lipid modifying agents	HMG coa reductase inhibitors	class 2
VPA	Most-DILI-concern	8	Nervous system	Antiepileptics	Fatty acid derivatives	class 3

the drugs into different groups according to the organ or system on which they act, and their pharmacological and chemical properties (ATC index available at http://www.whocc.no/atc_ddd_index/, [Accessed 2015 November 27]) (Table 8.1). The Biopharmaceutics Classification System (BCS) [Benet, 2013] was used to classify the drugs based on their solubility and permeability properties (Table 8.1). The BCS classification of drugs was obtained from the Therapeutic System Research Laboratories website (<http://www.tsrlinc.net/search.cfm>, [Accessed 2015 October 30]) and from literature [Kasim et al., 2004; Value and Samy, 2012]

8.2.2 Key cellular processes

Seventy-four hand-curated toxicity lists were extracted from QIAGENs Ingenuity Pathway Analysis (IPA® QIAGEN Redwood City, www.qiagen.com/ingenuity) (Table C.1) to represent key cellular processes. These toxicity lists consist of gene sets contributing to a specific type of toxicity and were generated based on crucial biological processes and key toxicological responses. Furthermore, all genes associated to a certain toxicity list were functionally classified into one of the following groups: Cytokine, growth factor, metabolic enzyme, G-protein-coupled receptor, ion channel, kinase, ligand-dependent nuclear receptor, other, peptidase, phosphatase, transcription regulator, translation regulator, transmembrane protein, or transporter.

8.2.3 Therapeutic and toxic dose levels

The therapeutic doses were taken from the clinical studies used to develop the PBPK models for oral administration (Table 8.2). The databases from LiverTox® [Hoofnagle et al., 2013] and ACuteTox [Clemedson et al., 2007], as well as literature [Gregoriano et al., 2014; Tenenbein and Tenenbein, 2005; Aguiar Bujanda et al., 2006; Spalding and Buss, 1986; von Mach et al., 2005] were screened to set a toxic dose

Table 8.2: Experimental conditions. Administration route (IV, or PO), respective doses, number of subjects, and health state. The experimental PK data were either used for establishment of the reference PBPK model (Reference) or for model validation (Validation).

Drug	Route	Dose	Subjects	Health state	Model type	Reference
APAP	po	1000 mg	5	Healthy	Reference	[Shinoda et al., 2007]
APAP	po	20 mg/kg	8	Healthy	Validation	[Prescott, 1980]
AD	iv	400 mg	7	Sick	Reference	[Andreasen et al., 1981]
AD	po	400 mg	7	Sick	Reference	[Andreasen et al., 1981]
AZA	iv	100 mg	15	Sick	Validation	[Odland et al., 1986]
AZA	iv	50 mg	24	Healthy	Reference	[Van Os et al., 1996]
AZA	po	100 mg	10	Healthy	Reference	[Zins et al., 1997]
CPA	iv	800 mg	12	Healthy	Reference	[Haubitz et al., 2002]
CPA	iv	800 mg	1	Healthy	Validation	[Juma et al., 1981]
CPA	iv	200 mg	1	Sick	Validation	[Juma et al., 1981]
CPA	po	300 mg	1	Healthy	Reference	[Juma et al., 1979]
CSA	iv	4 mg/kg	1	Sick	Reference	[Aweeka et al., 1994]
CSA	iv	4 mg/kg	1	Healthy	Validation	[Gupta et al., 1990]
CSA	po	10 mg/kg	1	Sick	Reference	[Aweeka et al., 1994]
CSA	po	10 mg/kg	1	Healthy	Validation	[Gupta et al., 1990]
DFN	iv	50 mg	7	Healthy	Reference	[Willis et al., 1979]
DFN	po	50 mg	7	Healthy	Validation	[Willis et al., 1979]
DFN	po	100 mg	3	Healthy	Reference	[Degen et al., 1988]
ERY	iv	500 mg	6	Healthy	Reference	[Barre et al., 1987]
ERY-PED	po	400 mg	24	Healthy	Reference	[Zakeri-Milani et al., 2010]
FT	po	250 mg	6	Healthy	Reference	[Anjum et al., 2001]
HPL	iv	3.5 mg	1	Sick	Reference	[Cheng et al., 1987]
HPL	po	2 mg	1	Sick	Reference	[Cheng et al., 1987]
INH	iv	670 mg	1	Healthy	Reference	[Boxenbaum and Riegelman, 1974]
INH	iv	681 mg	1	Healthy	Validation	[Boxenbaum and Riegelman, 1974]
INH	po	300 mg	8	Healthy	Reference	[Bing et al., 2011]
INH	po	300 mg	8	Healthy	Validation	[Bing et al., 2011]
PB	iv	2.6 mg/kg	6	Healthy	Reference	[Nelson et al., 1982]
PB	po	2.9 mg/kg	6	Healthy	Reference	[Nelson et al., 1982]
PB	po	5.2 mg/kg	1	Healthy	Validation	[Boréus et al., 1978]
PB	po	4.3 mg/kg	1	Healthy	Validation	[Boréus et al., 1978]
PHE	iv	5 mg/kg	2	Healthy	Reference	[Lund et al., 1974]
PHE	po	5 mg/kg	2	Healthy	Reference	[Lund et al., 1974]
PHE	po	300 mg	6	Healthy	Validation	[Velpandian et al., 2001]
RIF	iv	300 mg	12	Healthy	Reference	[FDA, 2015b]
RIF	iv	600 mg	12	Healthy	Validation	[FDA, 2015b]
RIF	po	150 mg	8	Healthy	Validation	[Riess and W, 1968]
RIF	po	300 mg	8	Healthy	Validation	[Riess and W, 1968]
RIF	po	450 mg	8	Healthy	Reference	[Riess and W, 1968]
RIF	po	600 mg	8	Healthy	Validation	[Riess and W, 1968]
SST	po	40 mg	10	Healthy	Reference	[Lilja et al., 2004]
VPA	iv	800 mg	6	Healthy	Reference	[Perucca et al., 1978]
VPA	po	800 mg	6	Healthy	Reference	[Perucca et al., 1978]
VPA	po	600 mg	6	Healthy	Validation	[Gugler et al., 1977]
VPA	po	1000 mg	6	Healthy	Validation	[Bialer et al., 1985]

level for the fifteen hepatotoxic drugs (Table 8.3). During the screening process, only sub-lethal doses were used while lethal doses were neglected. In case of multiple identified doses, the mean value was set as therapeutic and toxic dose, respectively.

Toxic doses for SST and FT were scaled from minimum toxic doses observed in rats [Igarashi et al., 2015] since no appropriate doses could be found in literature. Thereby, a mean scaling factor was computed between minimum toxic doses from rats [Igarashi et al., 2015] and mean toxic doses found in humans for all remaining drugs.

Table 8.3: Toxic dose levels. Toxic dose levels for the fifteen drugs were identified by database and literature screening. To determine a toxic dose for SST and FT, toxic rat doses [Igarashi et al., 2015] were scaled since no appropriate doses were found in literature.

Drug	Mean toxic dose	References
APAP	465 mg/kg	[Clemmedson et al., 2007; Hoofnagle et al., 2013]
AD	58.7 mg/kg	[Clemmedson et al., 2007; Hoofnagle et al., 2013]
AZA	46.4 mg/kg	[Gregoriano et al., 2014]
CPA	221.9 mg/kg	[Aguiar Bujanda et al., 2006]
CSA	134.7 mg/kg	[Clemmedson et al., 2007]
DFN	13.7 mg/kg	[von Mach et al., 2005]
ERY	39 mg/kg	[Tenenbein and Tenenbein, 2005; Hoofnagle et al., 2013]
FT	21.2 mg/kg	*
HPL	378.2 mg/kg	[Henderson et al., 1991; Clemmedson et al., 2007]
INH	203.3 mg/kg	[Clemmedson et al., 2007]
PB	68.5 mg/kg	[Clemmedson et al., 2007]
PHE	153 mg/kg	[Clemmedson et al., 2007]
RIF	99 mg/kg	[Spalding and Buss, 1986; Clemmedson et al., 2007]
SST	56.6 mg/kg	*
VPA	606 mg/kg	[Clemmedson et al., 2007]

* Scaled

8.2.4 In vitro toxicity data

Time-series gene expression profiles from Open TG-GATEs [Igarashi et al., 2015] (ArrayExpress accession numbers: E-MTAB-797, E-MTAB-798, E-MTAB-799) (Appendix A.1), a large-scale toxicogenomics database, were used to obtain quantitative drug response data measured in human and rat hepatocytes as well as in rat livers. Gene expression was measured for three exposed concentrations (low, middle, high) after three exposure durations (2 h, 8 h and 24 h) in the in vitro study and after four exposure durations (3 h, 6 h, 9 h, 24 h) in the in vivo study, respectively, by use of Affymetrix Human Genome U133 Plus 2.0 and Affymetrix Rat Genome 230 2.0 GeneChip arrays. Data normalization was performed by applying the GC-RMA method [Wu et al., 2004]. Probe sets on the chip were mapped to Entrez Gene IDs using BrainArray custom CDF files (version 19.0.0, ENTREZG) [Dai et al., 2005]. Fold change values were calculated to indicate gene expression changes compared to the time-matched controls [Igarashi et al., 2015].

For each in vitro measurement in primary human and rat hepatocytes, differential gene expression analysis was performed (absolute fold change > 1.5 , Benjamini-Hochberg corrected p-value < 0.01) by linear models using limma [Smyth, 2004] and hypergeometric testing was further applied on each subset of differentially expressed genes to determine significantly overrepresented key cellular processes (Benjamini-Hochberg corrected p-value < 0.01) (Table C.2, Table C.3). P-values were adjusted by Benjamini-Hochberg correction for multiple testing [Benjamini and Hochberg, 1995].

8.2.5 Identification of significantly perturbed key cellular processes

In the first analysis of the comparative toxicity study, a set of strongly perturbed key cellular processes was extracted by considering all processes that were found to be significantly overrepresented (Benjamini-Hochberg corrected p < 0.01) in the in vitro experiment [Igarashi et al., 2015] by at least one third of the hepatotoxic drugs, irrespectively of the timepoints (Table C.2).

In the second analysis, a toxic change of at least 10 %, on average, was required to identify a set of key cellular processes significantly affected at certain timepoints by the high-responsive drugs but not by the low-responsive drugs. At this threshold, no key cellular process was perturbed at any timepoint by the low-responsive drugs.

8.2.6 Development of whole-body physiologically-based pharmacokinetic models

The whole-body PBPK models of the fifteen considered drugs were built by use of the software PK-Sim® [Willmann et al., 2003; Kuepfer et al., 2016] (Appendix A.2). PBPK models describe ADME processes based on prior information about the physicochemical properties of a drug and the physiology and anatomy of the organism (Table 8.4). In the PBPK model structure, relevant tissues and organs are represented by compartments and are connected by blood flow. These compartments are usually subdivided into plasma, red blood cells, interstitial and intracellular space. Distribution models describing mass transfer are parameterized based on physicochemical drug properties and are used to determine partition coefficients as well as cellular permeabilities between these compartments [Rodgers and Rowland, 2006; Rodgers et al., 2005; Schmitt, 2008; Willmann et al., 2005]. The best-performing calculation methods provided in the modeling software were used in the developed PBPK models (Table C.5).

Table 8.4: Physicochemical drug properties used in the developed PBPK models. MW, logP, F_u , pKa, and water solubility used in the developed PBPK models. Molecular weights are taken from DrugBank [Wishart et al., 2006], references for other properties were explicitly presented. In some cases, logP and F_u values were slightly adjusted to best describe the experimental data.

ID	Drug/ Metabolite	MW [g/mol]	logP	F_u	Compound type	pKa	Water Solubility [mg/l]	References
1	APAP	151.16	0.33	0.81	Acid	9.38	14000	[Wishart et al., 2006]
1	APAPC	254.31	0.4	0.6*	[Acid, base]	[1.93, 9.09]	337	[Wishart et al., 2006]
1	APAPG	327.29	-0.98	0.98*	Acid	3.17	27700	[Wishart et al., 2006]
1	APAPS	231.23	-0.52	0.8*	Acid	10.46	1540	[Bento et al., 2014; Swain, 2012]
1	NAPQI	149.15	0.1	0.02	Neutral	-	987	[Wishart et al., 2006; Bond, 2009; Swain, 2012]
2	AD	645.31	4.67	0.0032	Base	6.56	4.76	[Waldhauser et al., 2006; Veronese et al., 1988; Latini et al., 1984; Wishart et al., 2006]
3	6-MP	152.18	1.85	0.81	[Acid, base]	[9.50, 2.99]	68500	[Czyrski and Kupczyk, 2013; Wishart et al., 2006]
3	AZA	277.26	0.1	0.7	Base	7.87	1007	[Wishart et al., 2006]
4	CPA	261.09	0.8	0.8	Acid	6	30000	[Mahoney et al., 2003; Wishart et al., 2006]
5	CSA	1202.61	3.88	0.09	Acid	11.83	5.81	[Wishart et al., 2006; Lucangioli et al., 2003; Legg et al., 1988]
6	DFN	296.15	4.1	0.0035	Acid	4.15	2.37	[Wishart et al., 2006; Davies and Anderson, 1997]
7	ERY	733.93	3.06	0.18	Base	8.88	2000	[Wishart et al., 2006]
7	ERY-PED	862.06	3.84*	0.18	Acid	7.1	2000*	[Osol, A. and J.E. Hoover, 1976; Wishart et al., 2006]
8	2-hydroxy FT	292.21	2.08	0.028	Acid	3.8	5.56	[Anjum et al., 2001; Wishart et al., 2006]
8	FT	276.21	3.05	0.052	Acid	13.17	9.45	[Anjum et al., 2001; Wishart et al., 2006]
9	HPL	375.86	3.6	0.06	Base	8.66	14	[Wishart et al., 2006]
10	Acetyl-INH	179.18	-0.9	0.9*	[Acid, base]	[6.77, 3.02]	1770	[Wishart et al., 2007]
10	INH	137.14	-0.67	0.9	[Acid, base]	[13.61, 3.35]	140000	[Wishart et al., 2006]
11	PB	232.24	0.13	0.57	Acid	7.3	1110	[Wishart et al., 2006]
12	PHE	252.27	2.26	0.098	Acid	8.33	32	[Peterson et al., 1982; Wishart et al., 2006]
13	RIF	822.94	2.93	0.195	Acid	1.7	1400	[Acocella, 1978; Wishart et al., 2006]
14	SST	418.57	4.68	0.03	Neutral	-	0.76	[García et al., 2003; Lippert et al., 2013; Wishart et al., 2006]
14	SST-acid	436.58	4.3	0.056	Acid	4.31	11	[Wishart et al., 2006, 2007; Lippert et al., 2013]
15	Hydroxyl-VPA	160.21	1.42	0.04*	Acid	4.81	45100	[Wishart et al., 2007]
15	VPA	114.21	1.85	0.04	Acid	5.14	1300	[Gugler et al., 1977; Wishart et al., 2006]
15	VPA- β -glucuronide	320.33	0.85	0.04*	Acid	3.41	22200	[Wishart et al., 2007, 2006]

* Adjusted/adopted from parent drug

Table 8.5: Active drug transport and metabolic processes. Metabolic and active drug transport processes either consist of the metabolic enzyme and the corresponding metabolite, or of the transporter and the corresponding transporter type (efflux, influx). Kinetic parameters K_m and v_{max} were used to characterize the kinetic behavior of active processes. A liver plasma clearance of 11.5 ml/min/kg was estimated for the clearance of 2-hydroxy-FT. For INH, NAT2 polymorphism was considered by estimating two different v_{max} values to best describe clinical data available for fast and slow metabolizers [Boxenbaum and Riegelman, 1974; Bing et al., 2011].

ID	Drug/ Metabolite	Metabolite/ Transporter Type	Metabolic enzyme/ Transporter	K_m [$\mu\text{mol/l}$]	v_{max} [$\mu\text{mol/l/min}$]	Reference
1	APAP	APAP-glucuronide	UGT1A9	19742*	5343.10*	[Mutlib et al., 2006]
1	APAP	APAP-sulfate	SULT1A1	9963.80*	192.97*	[Riches et al., 2007]
1	APAP	NAPQI	CYP2E1	41.26*	2.40*	[Shinoda et al., 2007]
1	APAPG	Efflux	ABCG2	96.30*	21.80*	[Mazaleuskaya et al., 2015]
1	APAPS	Efflux	ABCG2	94.49*	21500.41*	[Mazaleuskaya et al., 2015]
1	NAPQI	APAPC	GSTT1	25.00*	569.00*	[Shinoda et al., 2007]
2	AD	Desethyl-AD	CYP1A1	15.9	30.00*	[Elsherbiny et al., 2008]
3	6-MP	6-thiouric acid	XO	41.50*	410.00*	[Aberra and Lichtenstein, 2005]
3	AZA	6-MP	GSTA1	7.00*	60.00*	[Kaplowitz and Kuhlenkamp, 1978]
4	CPA	4-hydroxy-CPA	CYP2B6	91.00*	3.70*	[Huang et al., 2000; Gervot et al., 1999; McDonald et al., 2003]
5	CSA	M1, M9, M4n	CYP3A4	2.3	108.00*	[Vickers et al., 1995; Wishart et al., 2006]
6	DFN	4-hydroxy-DFN	CYP2C9	9	530.00*	[Leemann et al., 1993; Bort et al., 1999a]
7	ERY	N-desmethyl ERY	CYP3A4	46	23.00*	[Wang et al., 1997; Zhang et al., 2009]
7	ERY-PED	N-desmethyl ERY	CYP3A4	46	23.00*	[Wang et al., 1997; Zhang et al., 2009]
8	FT	2-hydroxy-FT	CYP1A2	10.00*	17.30*	[Shet et al., 1997]
9	HPL	Reduced HPL, HPL pyridinium derivative, 4-Fluorobenzoyl- propionic-acid	CYP3A4	34	47.00*	[Avent et al., 2006; Froemming et al., 1989]
10	Acetyl-INH	Isonicotinicacid, Acetylhydrazine	NAAA	500.00*	30.00*	[Ellard and Gammon, 1976]
10	INH	Acetyl-INH	NAT2	1950.00*	400.00* ^{+,++}	[Ellard and Gammon, 1976]
10	INH	Acetyl-INH	NAT2	1950.00*	70.00* ^{+,+}	[Ellard and Gammon, 1976]
10	INH	Isonicotinic acid, Hydrazine	NAAA	2000.00*	4.00*	[Ellard and Gammon, 1976]
11	PB	P-hydroxy-PB	CYP2C19	147.00*	0.27*	[Wishart et al., 2006]
12	PHE	5-(p-hydroxy- phenyl-), 5-phenylhydantoin	CYP2C19	16.9	2.40*	[Cuttle et al., 2000; Yukawa and Mamiya, 2006]
13	RIF	25-desacetyl-RIF	CES2	39.20*	1.95*	[Sousa et al., 2008; Song et al., 2013; Jamis-Dow et al., 1997]
14	SST	SST-acid	CES2	10	223.92*	[Lilja et al., 2004; Lippert et al., 2013; García et al., 2003]
14	SST	6-hydroxy-SST, 3-hydroxy-SST, 6-exomethylene	CYP3A4	10	10.25*	[Lilja et al., 2004; García et al., 2003; Lippert et al., 2013]
14	SST-acid	SST-acid- metabolites	CYP3A4	10	223.90*	[Lilja et al., 2004; García et al., 2003; Lippert et al., 2013]
14	SST-acid	Influx	OATP1B1	10	276.00*	[Kameyama et al., 2005; Lippert et al., 2013]
15	VPA	Hydroxy-VPA	CYP2C9	40.00*	0.90*	[Kiang et al., 2006; Wishart et al., 2006]
15	VPA	VPA- β -glucuronide	UGT1A8	60.00*	0.90*	[Ethell et al., 2003; Wishart et al., 2006]

* Estimated

++ Fast metabolizer

+ Slow metabolizer

A reference PBPK model for intravenous administration was first developed and assessed by comparing simulated drug concentrations with experimental data from literature (Table 8.2). For FT, only a reference PBPK model for oral administration of 250 mg was developed, since this is the major therapeutic dose level and administration route. K_m and v_{max} representing the kinetic behavior of active processes were mainly fitted to best describe the experimental data used for model establishment. However, experimentally measured K_m values for several metabolic reactions could be identified in literature and were used unchanged in the model structure (Table 8.5). In the PBPK model of INH, two different v_{max} values were estimated for the enzymatic reaction catalyzed by N-acetyltransferase 2 (NAT2) to characterize fast and slow metabolizers, for which clinical data were available [Boxenbaum and Riegelman, 1974; Bing et al., 2011]. Note that NAT2 polymorphism may extensively influence the pharmacokinetic and pharmacodynamic behavior of INH for specific patient subgroups. To describe the elimination of the drugs and their metabolites, renal and biliary clearance processes were incorporated into the PBPK models

Table 8.6: Renal and biliary clearance processes. Renal and biliary clearance processes of the developed PBPK models.

ID	Drug/Metabolite	Route	Process type	Clearance	Reference
1	APAP	Renal	Kidney plasma clearance	13.62 ml/h/kg	[Critchley et al., 1986]
1	APAPC	Renal	Kidney plasma clearance	300.00 ml/h/kg	[Critchley et al., 1986]
1	APAPG	Renal	Kidney plasma clearance	126.00 ml/h/kg	[Critchley et al., 1986]
1	APAPS	Renal	Kidney plasma clearance	10.12 ml/h/kg	[Critchley et al., 1986]
1	NAPQI	Renal	Kidney plasma clearance	120.00 ml/h/kg	[Krauss et al., 2012]
4	CPA	Renal	Kidney plasma clearance	15.30 ml/h/kg	[Wishart et al., 2006]
4	CPA	Biliary	Biliary plasma clearance	3.90 ml/h/kg	[Wishart et al., 2006]
6	DFN	Renal	Kidney plasma clearance	16.80 ml/h/kg	[Wishart et al., 2006]
7	ERY	Renal	Kidney plasma clearance	61.00 ml/h/kg	[FDA, 2015a]
7	ERY-PED	Renal	Kidney plasma clearance	61.00 ml/h/kg	[Periti et al., 1989]
8	2-hydroxy-FT	Renal	Kidney plasma clearance	0.26 ml/h/kg	[Anjum et al., 2001]
8	FT	Renal	Kidney plasma clearance	5.22 ml/h/kg	[Anjum et al., 2001]
9	HPL	Renal	Kidney plasma clearance	4.80 ml/h/kg	[Froemming et al., 1989]
10	INH	Renal	Tubular secretion*	$K_m = 300.00 \mu\text{mol/l}$ $v_{\max} = 45.69 \mu\text{mol/l/min}$	[Mitchell et al., 1975]
10	Acetyl-INH	Renal	Tubular secretion*	$K_m = 20.00 \mu\text{mol/l}$ $v_{\max} = 0.69 \mu\text{mol/l/min}$	[Mitchell et al., 1975]
11	PB	Renal	Kidney plasma clearance	0.99 ml/h/kg	[Boréus et al., 1978]
12	PHE	Renal	Tubular secretion**	0.22 l/h	[Borgå et al., 1979]
13	RIF	Renal	Kidney plasma clearance	16.80 ml/h/kg	[FDA, 2015b]
14	SST	Renal	Kidney plasma clearance	420.00 ml/h/kg	[García et al., 2003]
15	VPA	Renal	Kidney plasma clearance	0.30 ml/h/kg	[Gugler et al., 1977]

* Michaelis-Menten

** First-order

(Table 8.6) In the case of AZA, 6-MP, AD and CSA, renal elimination was not considered since negligible amounts were found in urine [Vickers et al., 1995; Wishart et al., 2006].

Once a sufficient model quality was reached, a reference PBPK model for oral administration was developed thereby using all parameters identified for the intravenous reference PBPK model. Only the intestinal permeability was adjusted in some cases to best describe the absorption phase after oral drug intake (Table C.4). In general, an endothelial barrier between the plasma and the interstitial space is assumed for large molecules like proteins but not for small molecules [Rippe and Haraldsson, 1994]. In the PBPK model of DFN, however, the rate of permeation through this endothelial barrier was limited in all organs except in the liver (brain: 0.004 cm/s, other organs/tissues: 0.04 cm/s), since DFN is highly bound to plasma proteins (Table 8.4).

The established reference PBPK models for both administration routes were further validated dependent on the availability of experimental data from other clinical studies. Since APAP and SST are mostly administered orally, only one administration route was considered in the specific PBPK models (Figure 8.2). In the case of ERY, erythromycin ethylsuccinate (ERY-PED) [FDA, 2016], an ester of the base form, was orally administered. In the validation step, all parameters of the specific reference PBPK model were left unchanged, except parameters characterizing the specific individuals and the dosage regimen. In the validated PBPK model established for intravenous administration of 200 mg of CPA (Figure 8.2, Table 8.2), kidney plasma clearance was reduced to 5.1 ml/h/kg for renally-impaired patients [Juma et al., 1981]. Finally, a normalized RMSD as well as R^2 identified after linear regression were calculated for all human PBPK models to assess the model quality [Thiel et al., 2016].

To develop rat PBPK models used for the validation cross-species extrapolation was applied. Thereby, pharmacokinetics were extrapolated from humans to rats by taking into account physiological and anatomical differences between both species [Thiel et al., 2015].

8.2.7 Prediction and validation of in vivo drug responses

The integrative multiscale approach called PICD allows a time-resolved description of drug-induced in vivo response at the patient level by integrating in vitro toxicity data into whole-body PBPK models [Thiel et al., 2016]. Here, PICD was applied on fifteen hepatotoxic drugs to predict in vivo drug responses of key cellular processes, functional classes of genes, and individual genes, induced by oral administration of therapeutic and toxic doses in humans.

When applying PICD, bioavailability values calculated from the developed human PBPK model were used to consider oral administration (Table C.6). In the case of AZA, the bioavailability found in literature was used since the difference between the literature value and the calculated value was significantly high [Van Os et al., 1996].

In vivo drug responses after 2 h, 8 h and 24 h for therapeutic and toxic dose administration were then calculated by computing the mean gene response level (gene response is defined as absolute log2 fold change) of all genes assigned to a specific key cellular process (Table C.1). In the case where in vitro data only exist for 8 h and 24 h [Igarashi et al., 2015], the predicted response patterns were interpolated to determine response values at 2 h. When analyzing functional classes of genes, in vivo drug responses were predicted for the different functional classes of genes involved in a specific key cellular process by calculating the mean gene response level of all genes assigned to a certain functional category.

To validate PICD in rats, significantly enriched key cellular processes (Benjamini-Hochberg corrected $p < 0.01$) were first identified for each drug (Table C.3), and correspondent in vivo drug responses were then predicted following oral administration of the three doses applied in the in vivo rat study [Igarashi et al., 2015]. Here, the highest dose was identified in a 4-week toxicity study.

According to [Thiel et al., 2016], predictions were subsequently compared to in vivo observations by calculating the Pearson correlation coefficient r , the coefficient of determination R^2 and corresponding confidence intervals (CI) between predicted drug response profiles and measurements obtained in rat livers [Igarashi et al., 2015]. Predicted drug response profiles were linearly interpolated to be comparable to time-matched in vivo measurements (3 h, 6 h, 9 h, and 24 h).

8.2.8 Calculation of toxic changes

In the comparative toxicity analysis (Figure 8.2), toxic changes were calculated at different timepoints (2 h, 8 h and 24 h) for key cellular processes, functional classes of genes within a key cellular process, and single genes. Here, a toxic change at a timepoint t for a drug d is defined as follows:

$$\text{toxic change}_{t,x,d} = \text{in vivo drug response}(\text{toxic})_{t,x,d} - \text{in vivo drug response}(\text{therapeutic})_{t,x,d} \quad (8.1)$$

where x denotes a key cellular process, a functional class within a key cellular process, or a single gene. In vivo drug responses induced by therapeutic and toxic dose administration were predicted by calculating gene response levels (defined as absolute log2 fold change) for single genes, and by calculating the mean gene response level of all genes assigned to a key cellular process or to a functional class within a key cellular process, respectively [Thiel et al., 2016].

In order to compare the toxic behavior of AZA and VPA in cell cycle checkpoint regulation, differences of toxic changes for all involved genes were calculated between both drugs and were mapped onto the pre-defined pathway 'cell cycle G2/M DNA damage checkpoint regulation' taken from QIAGENs Ingenuity Pathway Analysis (IPA® QIAGEN Redwood City, www.qiagen.com/ingenuity). Note that differentially responding genes (absolute difference of toxic change > 0.15) of AZA and VPA are reflected by a positive and a negative value, respectively. All differentially responding genes as well as genes with toxic changes higher than 15 % for both drugs were finally used to build differential response pathways.

8.2.9 Prediction of molecular biomarkers and potential drug interactions

All genes involved in the strongly affected key cellular processes analyzed in the functional analysis were considered to identify potential molecular biomarkers and DDIs. A gene g was marked as common molecular biomarker for all high-responsive drugs if the following condition was fulfilled:

$$\mu(\text{toxic change})_g > 1.5 * \mu(\text{toxic change}) \text{ AND } \sigma(\text{toxic change})_g < 0.5 * \sigma(\text{toxic change}) \quad (8.2)$$

μ , mean response of all genes considered; σ , respective standard deviation. In contrast, a gene g was marked as individual molecular biomarker for only a single drug d if the more stringent requirement was fulfilled:

$$(\text{toxic change})_{d,g} > 7 * \mu(\text{toxic change}) \quad (8.3)$$

Several thresholds deviating from ± 5 % of the used thresholds above did not significantly alter the number of identified common molecular biomarkers (± 14 %) or individual molecular biomarkers (± 4 %). All common molecular biomarkers were additionally compared between the low and high-responsive drugs by evaluating the correspondent toxic changes between both groups.

All individual molecular biomarkers were used to identify potential DDIs. Thereby, a potential DDI was assumed, if at least one individual molecular biomarker was identified for both drugs. These DDIs were then compared with known DDIs from DrugBank [Wishart et al., 2006] and from www.drugs.com [Accessed 2016 March 3rd] by calculating the accuracy, sensitivity, specificity and the precision that were formulated as follows:

$$\text{Accuracy} = \frac{(TP + TN)}{(TP + FP + TN + FN)} \quad (8.4)$$

$$\text{Sensitivity} = \frac{TP}{(TP + FN)} \quad (8.5)$$

$$\text{Specificity} = \frac{TN}{(TN + FP)} \quad (8.6)$$

$$\text{Precision} = \frac{TP}{(TP + FP)} \quad (8.7)$$

where TP represents true positive, TN represents true negative, FP represents false positive, FN represents false negative. Types of DDIs ('pharmacokinetic interaction' and 'pharmacodynamic interaction') were assigned according to [Huang et al., 2013], if the interaction type was not unknown. The BioInteractor tool from DrugBank was used to confirm predicted drug-enzyme associations for two corresponding drugs involved in a potential DDI [Wishart et al., 2006].

8.3 Results

8.3.1 Whole-body physiologically-based pharmacokinetic models

Whole-body PBPK models were initially established for a set of fifteen hepatotoxic drugs and were carefully validated with human experimental data from literature (Figure 8.3, Figure 8.4, Table 8.2). The validated PBPK models served as input for PICD [Thiel et al., 2016] to quantify in vivo drug responses induced by therapeutic and toxic doses administered in humans.

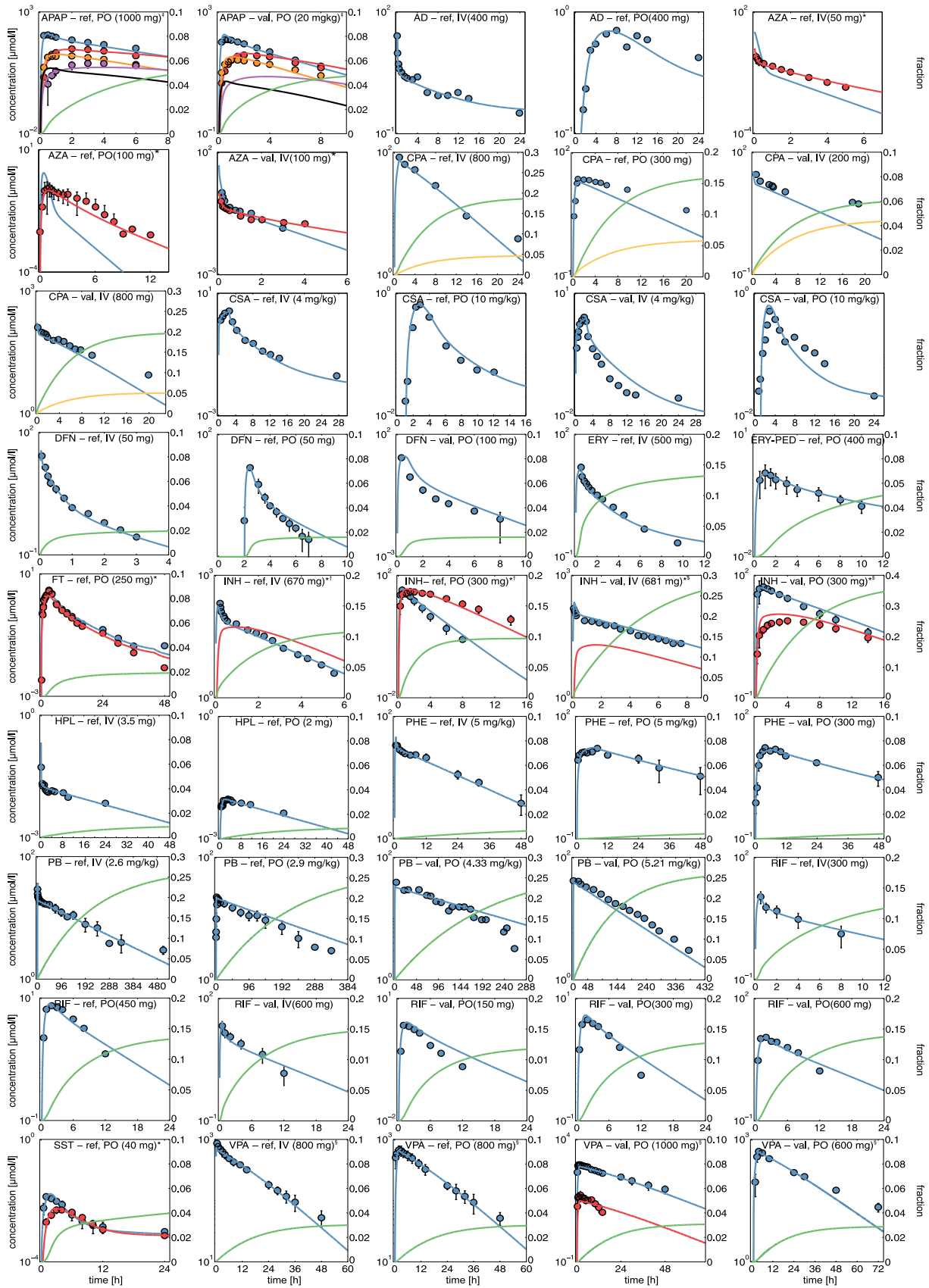


Figure 8.3: Human PBPK models. Simulated (lines) and experimental (circles) PK data of parent drugs (blue) were evaluated to develop reference (ref) or validated (val) human PBPK models. Green, renal excretion; dark yellow, biliary excretion; * Primary metabolites (red) 6-MP, 2-hydroxy-FT, acetyl-INH, and SST-acid; † APAP-glucuronide (APAPG) (red), APAP-sulfate (APAPS) (orange), APAP-cysteine (APAPC) (purple), and NAPQI (black); ‡ Rapid metabolizer; § Slow metabolizer; § Unbound plasma concentrations (red).

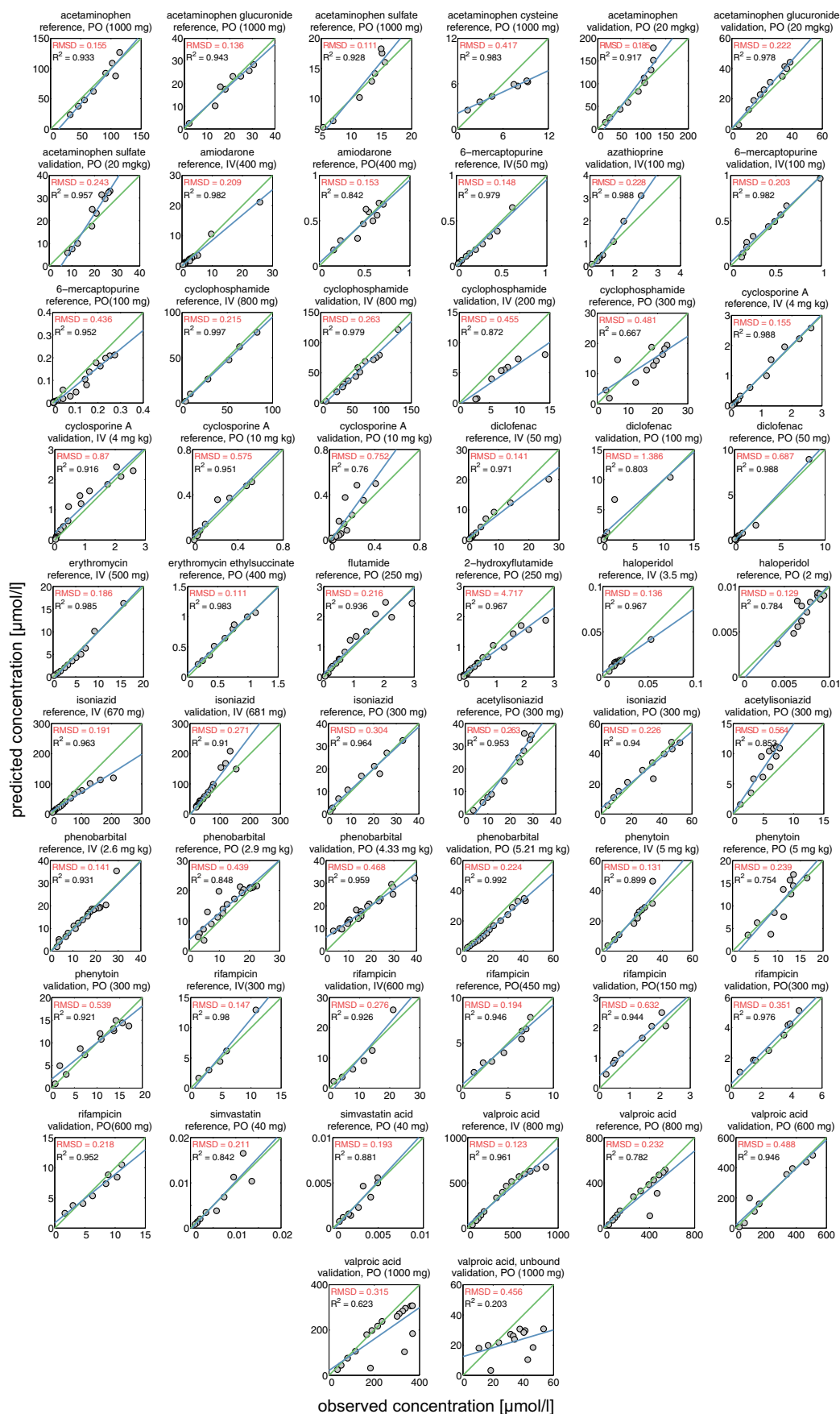


Figure 8.4: PBPK model assessment. Simulated concentration-time profiles of parent drugs and their metabolites were compared to experimental PK data. Observed vs. predicted plots including the RMSD and R^2 value were generated for all reference and validated PBPK models

Physicochemical properties, plasma protein binding, and lipophilicity of the different drugs and their metabolites were obtained from literature and were used to develop the reference PBPK model for intravenous administration in humans (Table 8.4). Key metabolic reactions and active drug transport were integrated into the human PBPK models to represent the main ADME processes (Table 8.5). Relative tissue-specific abundances of relevant enzymes and transporters were estimated using tissue-specific gene expression data [Meyer et al., 2012]. To describe the elimination of the drugs and their metabolites, renal and biliary clearance processes were incorporated into the human PBPK models (Table 8.6) and parametrized such that simulations are in agreement with experimental observations (Table 8.6). After model establishment, the simulated drug concentrations in plasma showed an excellent agreement with *in vivo* PK data measured in humans (Figure 8.3, Figure 8.4).

To validate the established reference PBPK models, experimental PK data from different studies, which had not been used during initial model establishment, were next used to simulate concentration-time profiles for additional dosage regimens and patient subgroups (Figure 8.3, Figure 8.4). Notably, model parameters were left unchanged for model validation except the intestinal permeability where the initial reference value was slightly adjusted in some cases, when the drug was given orally (Table C.4).

The PBPK model parameters (Table 8.4, Table 8.5, Table 8.6, Table C.4, Table C.5) together with the specific information about the clinical studies (Table 8.2) are sufficient to fully reproduce all developed human PBPK models due to the large degree of prior information, which is already included in PBPK models. Importantly, the validated PBPK models allow accurate simulations for different dose levels, including therapeutic or toxic doses, since potential non-linearities in ADME processes are implicitly represented through the underlying model structure.

8.3.2 Integrating *in vitro* toxicity data into physiologically-based pharmacokinetic models

To analyze and compare drug-induced hepatotoxicity of the fifteen drugs within a patient context, toxic changes reflecting the transition from desired drug effects to adverse events were considered by predicting time-dependent *in vivo* responses for humans following drug administration of therapeutic and toxic doses. *In vitro* toxicity data from Open TG-GATEs measured in primary human hepatocytes for the fifteen hepatotoxic drugs were therefore analyzed [Igarashi et al., 2015]. Toxicity lists from QIAGENs Ingenuity Pathway Analysis (IPA®), QIAGEN Redwood City, www.qiagen.com/ingenuity) were used to represent biological processes associated to critical toxicological responses and are further referred to as 'key cellular processes' (Table C.1). Drug concentration-time profiles were simulated for therapeutic and toxic doses identified in literature (Figure 8.5, Table 8.2, Table 8.3) by using the developed human PBPK models (Figure 8.3).

PICD was next applied to translate *in vitro* findings to an *in vivo* situation within patients. In brief, the basic concept of PICD is the identification of *in vivo* doses such that the simulated drug exposure in the interstitial space of the liver is equal to the *in vitro* drug exposure of the assay. The identified *in vivo* doses were mapped to the *in vitro* toxicity data in order to describe time-dependent *in vivo* drug responses at different dose levels (Figure 8.1) [Thiel et al., 2016]. After applying PICD, *in vivo* drug responses for humans induced by therapeutic and toxic doses could be predicted for the considered key cellular processes.

8.3.3 Validation of predicted *in vivo* drug responses in rats

To validate the predictive accuracy of the PICD-based *in vitro-in vivo* translations, PICD was next applied for rats, because *in vivo* data were only available for rats but not for humans [Igarashi et al., 2015]. Since PICD requires PBPK models as input at the organism level, rat PBPK models were developed by

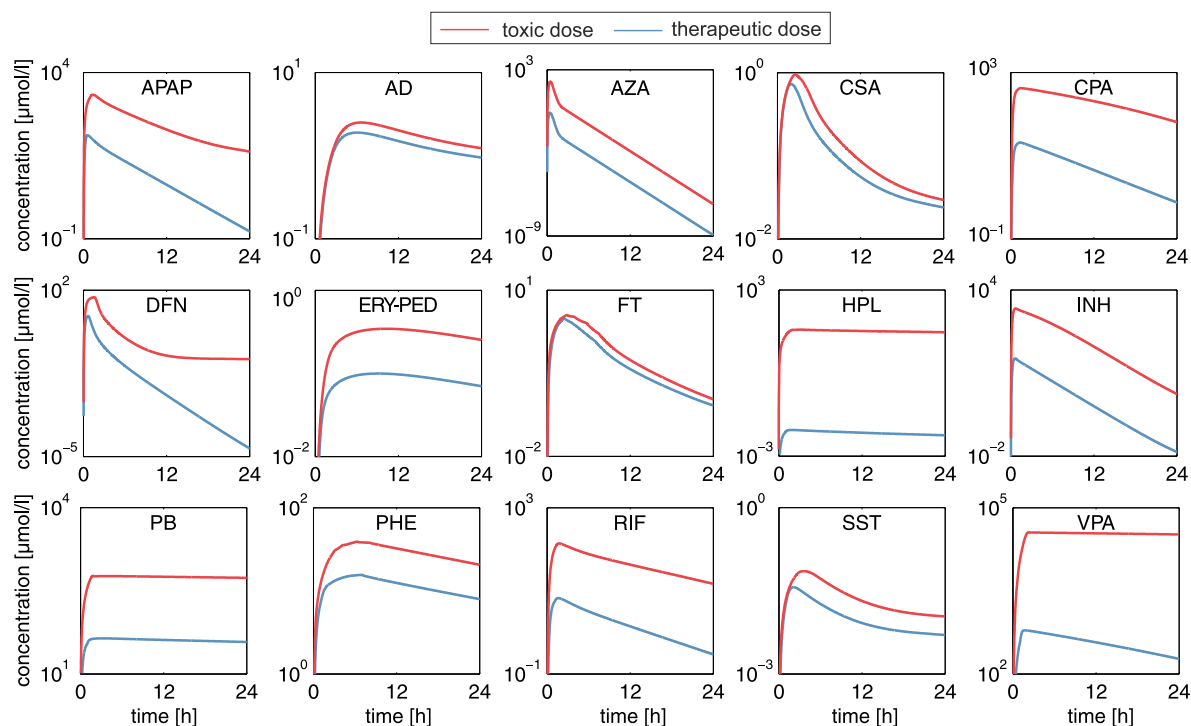


Figure 8.5: Therapeutic and toxic pharmacokinetic profiles. Plasma concentration-time profiles simulated for drug administration of the therapeutic (blue) and the toxic (red) doses in humans (Table 8.2, Table 8.3).

applying cross-species extrapolation thereby taking into account species-specific differences to extrapolate PK profiles between humans and rats [Thiel et al., 2015].

In vitro toxicity data measured in rat hepatocytes [Igarashi et al., 2015] were then translated to an in vivo situation by applying PICD on rat PBPK models. For each drug, significantly perturbed key cellular processes for rats were identified (Table C.3) and correspondent in vivo drug responses were subsequently predicted for the relevant doses that have been administered in the in vivo rat study [Igarashi et al., 2015]. Finally, predicted drug responses were correlated with in vivo observations.

Correlation analyses between predicted and observed in vivo rat data revealed moderate correlations ($r = 0.27-0.76$, $p < 0.05$, $R^2 = 0.07-0.58$) (Figure 8.6) for all drugs apart from PB ($r = 0.03$, $p = 0.6$, 95 % CI = $[-0.07, 0.13]$, $R^2 = 9.4E-4$) and APAP ($r = -0.05$, $p = 0.35$, 95 % CI = $[-0.16, 0.06]$, $R^2 = 0.0025$) (Figure 8.6). These correlations obtained in a preparatory proof-of-concept analysis in rats are mostly statistically significant albeit not that strong in some cases. A general validity of further PICD-based analyses in humans can nevertheless be assumed.

8.3.4 Comparative toxicity analysis

In the comparative toxicity analysis, drug-induced hepatotoxicity was investigated within a patient context to identify subsets of drugs, which share similar perturbation on key cellular processes, functional classes of genes, as well as individual genes. Toxic changes reflecting the transition from desired drug effects to adverse events were therefore calculated for humans and were compared among the set of fifteen hepatotoxic drugs (Table 8.1).

The application of PICD allowed predicting time-dependent drug responses of therapeutic and toxic doses in an in vivo context [Thiel et al., 2016]. Note that all in vivo drug response values predicted for the toxic dose were higher than the respective values predicted for the therapeutic dose, such that all toxic changes are positive.

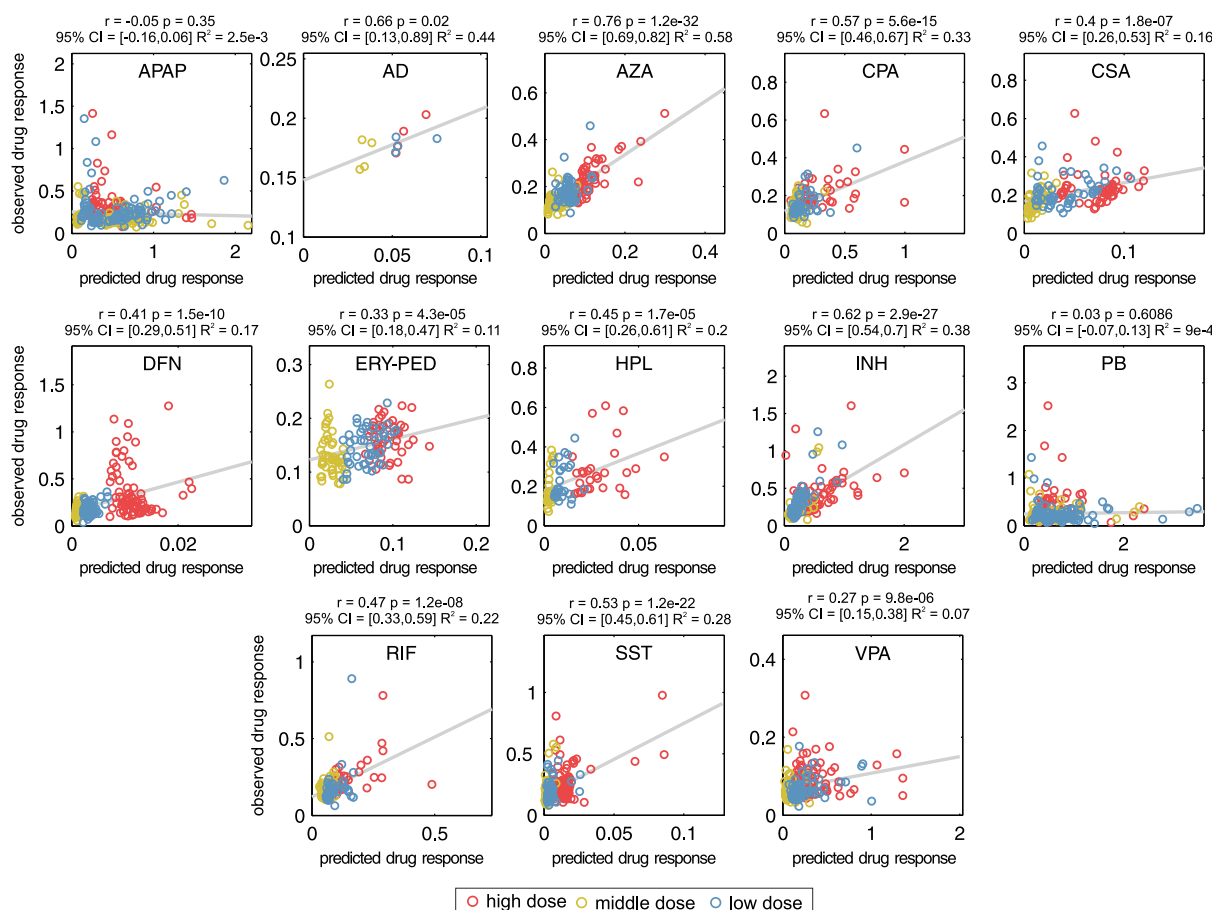


Figure 8.6: Validation of predicted drug response with in vivo measurements in rats. In vivo drug responses of significantly perturbed key cellular processes (Table C.3) predicted for the three doses used in the in vivo rat study were compared to observations measured in vivo [Igarashi et al., 2015].

Analysis of key cellular processes

In the first analysis, toxic changes calculated for humans were evaluated at three different time points (2 h, 8 h, and 24 h) for key cellular processes that were significantly overrepresented in at least one third of the drugs (Figure 8.7, Table C.2).

Hierarchical clustering identified three major groups, which showed a clear separation between the considered timepoints (Figure 8.7). This observation was also confirmed by applying a principal component analysis (Figure 8.8). Interestingly, low toxic changes were observed for SST, DFN, and AD at all timepoints. In contrast, high toxic changes (e.g., for genes involved in liver damage, liver hepatitis, liver steatosis, and liver proliferation) were found already at 2 h for HPL, APAP, VPA, AZA, and INH. AZA and VPA further depicted a high impact on genes involved in hepatocellular hypertrophy resulting in glutathione depletion (Figure 8.7). At 8 h, VPA and APAP revealed substantially high activity on several key cellular processes in particular on liver proliferation, liver damage, and liver hyperplasia (Figure 8.7). Furthermore, the regulation of the cell cycle G2/M DNA damage checkpoint, on the one hand, as well as the activation of the FXR/RXR and CAR/RXR heterodimers, on the other hand, were clearly perturbed after 8 h by APAP and AZA, respectively (Figure 8.7). At 24 h, VPA primarily affected all considered key cellular processes (Figure 8.7).

Hierarchical clustering was next performed to classify the fifteen hepatotoxic drugs according to similar hepatotoxic potential. Two main clusters could be identified where the first cluster (SST, DFN, AD, ERY, FT, CSA, and PHE) basically showed a lower response on key cellular processes than the second one (RIF,

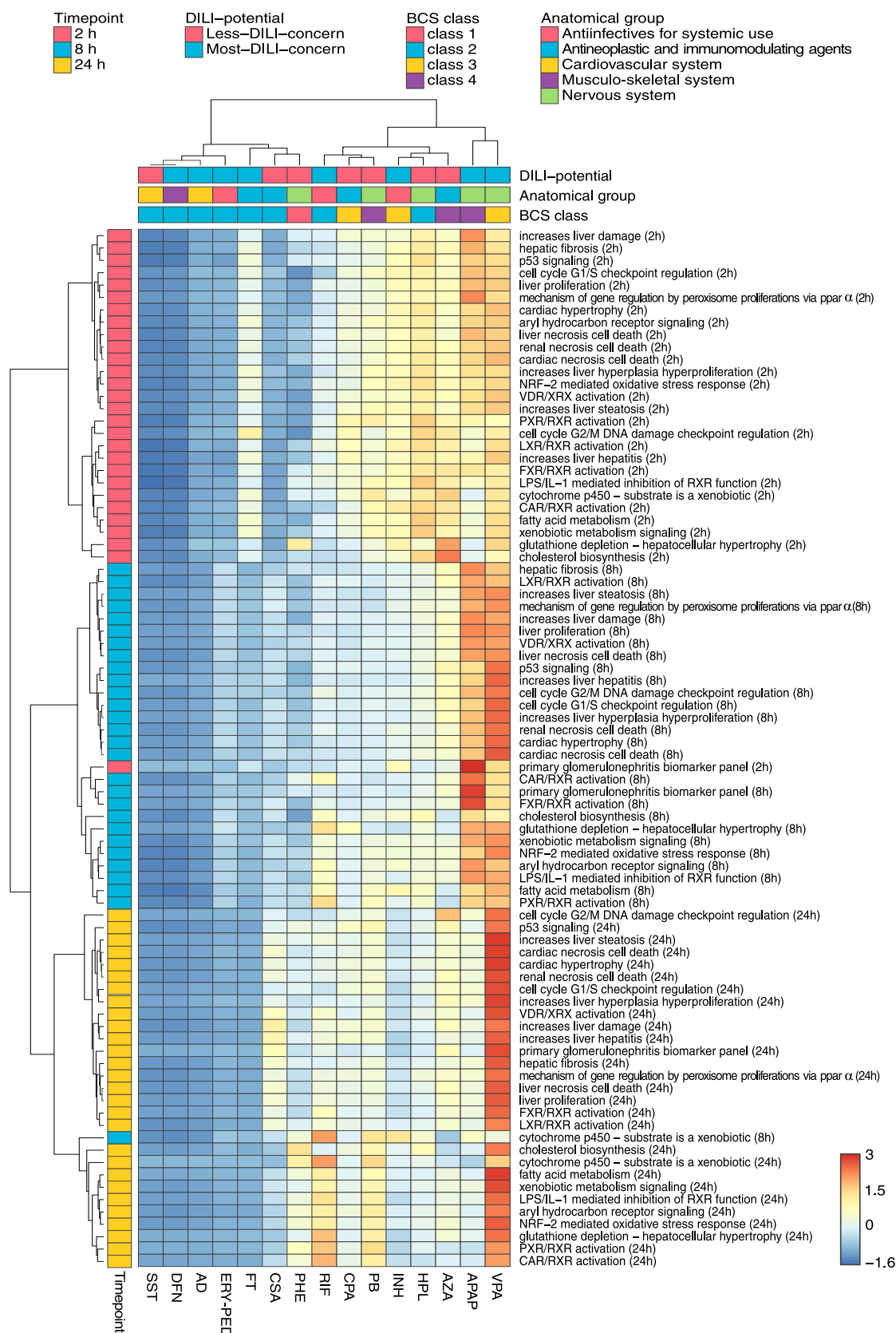


Figure 8.7: Comparative toxicity analysis of key cellular processes. Toxic changes in perturbed key cellular processes (Table C.1) were calculated for fifteen hepatotoxic drugs at 2 h, 8 h and 24 h. The drugs were annotated with their respective DILI-potential, the BCS class and the target organ or system. The dendrograms were constructed using Ward's minimum variance algorithm. The color scale depicts normalized toxic changes. The heatmap was visualized by use of the web tool ClustVis [Metsalu and Vilo, 2015]. Row-normalization is performed by subtracting the mean and by dividing the respective standard deviation.

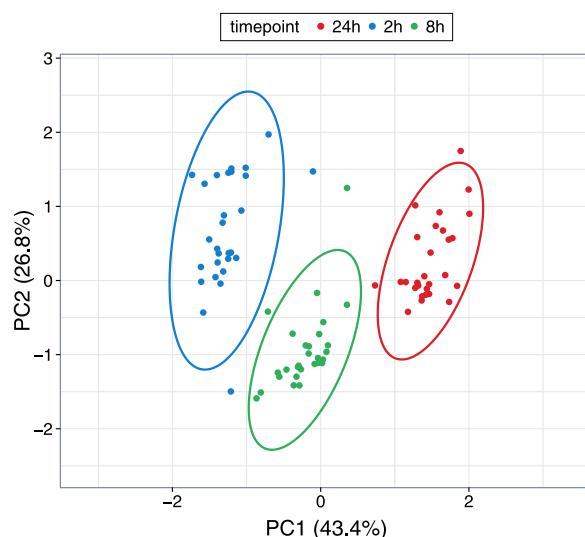


Figure 8.8: Principal component analysis. Principal component analysis was applied on all toxic changes predicted at 2 h (blue), 8 h (green), and 24 h (red). Percentage of explained variance of principal components one (PC1) and two (PC2) are shown in brackets. Ellipses around the different groups are generated with a confidence level of 0.95. Results of principal component analysis were visualized by use of the web tool ClustVis [Metsalu and Vilo, 2015].

CPA, PB, INH, HPL, AZA, APAP, and VPA) ($p = 9\text{E-}66$, 95 % CI = [0.079, 0.098], two-sample t-test). The low-responsive group was further subclustered into SST, DFN, AD and ERY, on the one hand, and into FT, CSA and PHE, on the other hand. The high-responsive group could be further subdivided into three smaller subclusters: the first consists of RIF, CPA, and PB; the second of AZA, HPL, and INH; the third only of APAP and VPA.

The hierarchical clustering results were further analyzed to test whether the low- and high-responsive drugs could be attributed to (i) pharmacokinetic parameters, (ii) drug permeability and solubility properties (BCS class) [Benet, 2013], (iii) their target organ or system (anatomical main group), or (iv) their concern for causing DILI (DILI-potential) (Table 8.1). Results from this analysis show that the low-responsive drugs were significantly higher bound to plasma proteins ($p = 0.0098$, 95 % CI = [0.15, 0.74], two-sample t-test), were more lipophilic ($p = 0.0013$, 95 % CI = [1.24, 4.05], two-sample t-test), and tended to be less soluble than drugs from the high-responsive group ($p = 0.21$, 95 % CI = [-16964.77, 63585.33], two-sample t-test) (Table 8.4). Interestingly, toxic changes calculated for both groups were independent from both the ratio of toxic and therapeutic doses ($p = 0.33$, 95 % CI = [-1509.31, 3929.78], two-sample t-test) (Table 8.2, Table 8.3) and from the ratio of correspondent area under the curve values ($\text{AUC}_{0-24\text{h}}$: $p = 0.35$, 95 % CI = [-2341.65, 5798.28], two-sample t-test) (Figure 8.5).

Comparison of both main clusters also showed no clear distinction of annotated DILI-potentials (Figure 8.7) with regard to drug-specific characteristics, which was also observed for the assigned severity scores ($p = 0.7$, 95 % CI = [-2.12, 3.09], two-sample t-test) (Figure 8.7, Table 8.1). Contrarily, the drugs classified as BCS class 3 (low permeability, high solubility) and class 4 (low permeability, low solubility) tended to belong to the high-responsive drugs while the low-responsive group was enriched with drugs annotated with BCS class 2 (low solubility, high permeability). Furthermore, drugs were not clearly separable based on their target organ or system (Figure 8.7). Nevertheless, drugs acting on the cardiovascular system (SST and AD) or on the musculo-skeletal system (DFN) were clustered together, while anti-infectives and drugs acting on the nervous system were rather assigned to the high-responsive group (Figure 8.7, Table 8.1).

Analysis of functional classes of genes

Next, toxic changes were analyzed at the functional level to quantitatively describe to what extent single drugs or subset of drugs perturbed different functional classes of genes (e.g. kinases or metabolic enzymes) associated to key cellular processes (Figure 8.9). Note that only the previously identified set of the high-

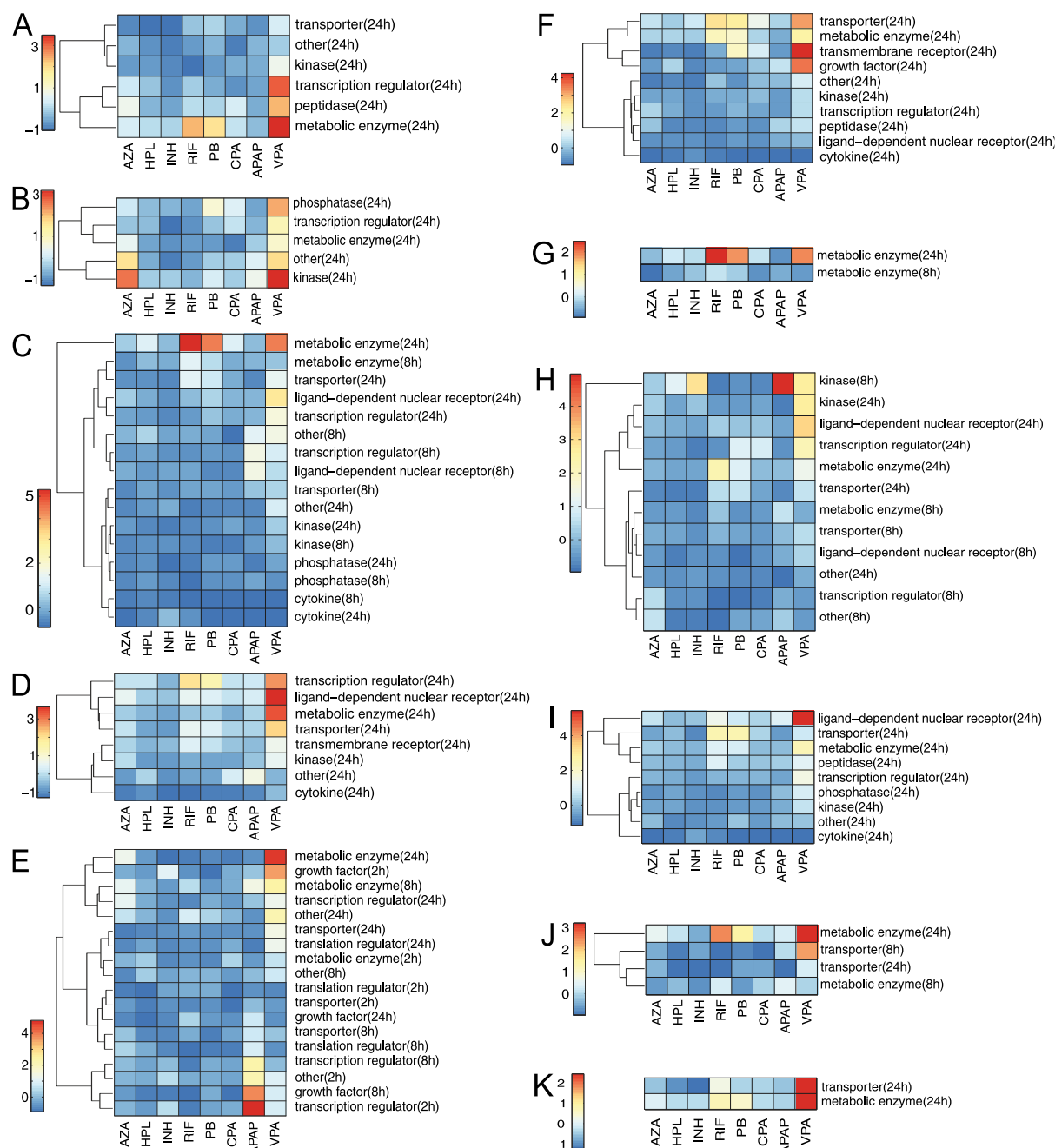


Figure 8.9: Toxic changes predicted for functional classes of genes involved in key cellular processes. The toxic changes were predicted for different functional classes of genes involved in the respective key cellular processes. All drugs belonging to the high-responsive group were considered. The color scale depicts toxic changes that were normalized over each heatmap. Normalization for each key cellular process is performed by subtracting the mean and by dividing the respective standard deviation. (A) 'Nrf2 mediated oxidative stress response'. (B) 'Cell cycle G2/M DNA damage checkpoint regulation'. (C) 'PXR/RXR activation'. (D) 'LPS/IL-1 mediated inhibition of RXR function'. (E) 'Primary glomerulonephritis biomarker panel'. (F) 'Aryl hydrocarbon receptor signalling'. (G) 'Cytochrome P450 - substrate is a xenobiotic'. (H) 'CAR/RXR activation'. (I) 'Xenobiotic metabolism signalling'. (J) 'Glutathione depletion - hepatocellular hypertrophy'. (K) 'Fatty acid metabolism'.

responsive drugs and a subset of key cellular processes, which were strongly induced by these drugs, were here considered in the following.

RIF, PB and VPA demonstrated a high impact on metabolic enzymes involved in the Nrf2-mediated oxidative stress response (Benjamini-Hochberg corrected $p = 0.001$, 95 % CI = [0.11, 0.36], two-sample t-test), in particular on cytochrome P450 enzymes and transferases (Figure 8.9A). VPA further affected

transcription regulators (Benjamini-Hochberg corrected $p = 0.05$, two-sample t-test, 95 % CI = [0.06, 0.58]) particularly FOSL1 and KEAP1 (Figure 8.9A). A significant toxic change on kinases by AZA and VPA was observed at 24 h when focusing on processes of cell cycle G2/M DNA damage checkpoint regulation (Benjamini-Hochberg corrected $p = 0.0002$, 95 % CI = [0.19, 0.45], two-sample t-test) (Figure 8.9B). A high toxic change of RIF, PB and VPA at 24 h was detected for metabolic enzymes involved in xenobiotic cytochrome P450 metabolism (Benjamini-Hochberg corrected $p = 0.003$, 95 % CI = [0.38; 1.36], two-sample t-test) (Figure 8.9G), glutathione depletion induced by hepatocellular hypertrophy (Benjamini-Hochberg corrected $p = 0.069$, 95 % CI = [0.05; 0.78], two-sample t-test) (Figure 8.9J), as well as in fatty acid metabolism (Benjamini-Hochberg corrected $p = 0.0001$, 95 % CI = [0.12, 0.30], two-sample t-test) (Figure 8.9K), and in the activation of the PXR/RXR heterodimer (Benjamini-Hochberg corrected $p = 0.001$, 95 % CI = [0.34, 1.02], two-sample t-test) (Figure 8.9C). Moreover, PB, VPA and RIF strongly perturbed BAX (Benjamini-Hochberg corrected $p = 0.0016$, 95 % CI = [0.24, 0.47], two-sample t-test), an apoptosis regulator that modulates the mitochondrial permeability of the transporter VDAC [Shi et al., 2003] (Figure 8.9F). Investigating toxic changes of biomarkers referred to primary glomerulonephritis revealed a substantial impact of APAP on the heparin-binding growth factor HBEGF at 8 h (Benjamini-Hochberg corrected $p = 0.0026$, 95 % CI = [0.42, 0.96], two-sample t-test) (Figure 8.9E).

Amongst others, a high impact of AZA and VPA on the regulation of the cell cycle G2/M DNA damage checkpoint was found in this second analysis (Figure 8.9B). Building on this observation, the cellular response on cell cycle regulation induced by both drugs was analyzed in more detail at the level of single genes and pathways in the following.

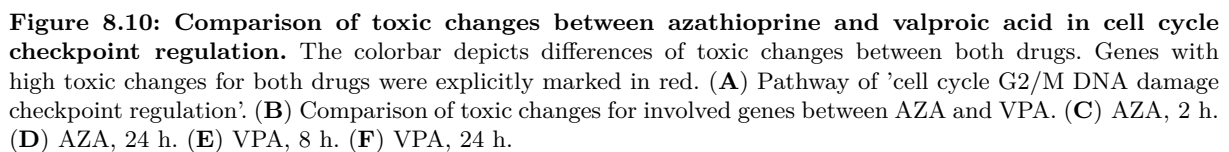
Comparative toxicity analysis of azathioprine and valproic acid in cell cycle checkpoint regulation

The previous analysis of functional classes of genes revealed similar toxic behavior of AZA and VPA in the regulation of the cell cycle G2/M DNA damage checkpoint (Figure 8.9B) despite a significant pharmaceutical and chemical diversity (Table 8.4, Table 8.1). We therefore considered the toxic behavior between AZA and VPA at the gene level in an exemplary use case by individually analyzing toxic changes of involved genes.

The G2/M DNA damage checkpoint represents the second checkpoint in the cell cycle and ensures that genomic stability is maintained by repairing damaged DNA before entering the mitosis phase (Figure 8.10A) [Löbrich and Jeggo, 2007]. Hence, this pathway is crucially involved in DNA replication, recombination, and repair, respectively, and is consequently essential for cell viability [Kastan and Bartek, 2004]. A key role for the transition from the G2 phase to the M phase forms the cyclin-dependent kinases and several transcription regulators (Figure 8.10A) [Nigg, 1995].

To directly compare the toxic behavior between both drugs, the differences of toxic change were calculated for all involved genes (Figure 8.10B). In this way, differentially responding genes of AZA and VPA reflected by a positive or negative value, respectively, could be identified. Analyzing differences in toxic changes revealed similar effects at 2 h for several genes (Figure 8.10B). Interestingly, only the p53 regulator MDM4, and the phosphatase PPM1D, the kinases CKS2 and CDC2 as well as the stress sensor GADD45, demonstrated high differences of toxic change for VPA and AZA, respectively (Figure 8.10B).

Furthermore, a set of similarly responding genes was observed at 2 h, 8 h and 24 h (ATM, PLK1, p19Arf, RPRM, p300, 14-3-3(β,ϵ), CDC25B, WEE1 and CHEK1) (Figure 8.10B). Although these similarly responding genes showed only slight differences of toxic change, both drugs considerably affect ATM, CDC25B, WEE1 and CHEK1, and in particular PLK1 and cyclin B1 and B2 (Figure 8.10B). In contrast



The differentially responding genes were next used to build differential response pathways at given time-points (Figure 8.10C-F). Note that none of these pathways could be found for AZA and VPA alone at

2 h and 8 h, respectively, but can only be identified through a comparative analysis. Exploring these pathways helps to compare dynamic changes between AZA and VPA in the regulation of the cell cycle G2/M DNA damage checkpoint when switching from therapeutic to toxic dose administration.

Analyzing differential response pathways of AZA at 2 h (Figure 8.10C) and VPA at 8 h (Figure 8.10E) revealed that AZA highly perturbed GADD45 and CKS2, which regulates CDC2-cyclin B complex, while VPA affected the same key complex by strongly perturbing p53 via HIPK2, on the one hand, and p90RSK, Myt1, and CDK7, on the other hand. Interestingly, GADD45 and CKS2 were involved in both pathways but in a time-shifted manner. In order to regulate key processes of the cell cycle G2/M checkpoint at 24 h, BORA and DNA-PK were highly affected by AZA (Figure 8.10D). In contrast, a significantly higher activity due to VPA administration was observed at the same timepoint thereby regulating all major processes mostly via p53, MDM2 and CDC2 (Figure 8.10F).

The comparative analysis of similarly- and differentially responding genes might help to identify either individually or commonly affected molecular biomarkers that reflect toxic drug action, which is either exclusively induced by a single drug (e.g., BORA at 24 h for AZA) or simultaneously by both drugs (e.g., cyclin B1 and B2 at 24 h). Genes that are simultaneously affected by two drugs might also be a common target during drug co-administration as such leading to an additive drug effect.

Analysis of individual genes

To conclude our analysis, toxic changes were calculated for individual genes that were involved in the key cellular processes strongly affected by the high-responsive drugs (Figure 8.9). These gene-related toxic changes were then used to quantitatively explore which genes were similarly perturbed by which drugs. This knowledge was finally used to identify individual and common molecular biomarkers for single drugs and subset of drugs, respectively. Molecular biomarkers play a key role in clinical risk assessment and the early prediction of drug toxicity. To identify robust common molecular biomarkers within the cluster of high-responsive drugs, a significant and similar toxic change (at least one and a half-fold increase and less than half of the standard deviation) at a certain timepoint was required (Table 8.7). To test whether the common molecular biomarkers were sensitive, the respective toxic changes of an identified biomarker were compared between the low- and high-responsive drugs.

In total, twelve common molecular biomarkers were detected for the set of high-responsive drugs (Table 8.7). Nine genes demonstrated statistical significant changes (Benjamini-Hochberg corrected $p < 0.05$): the metabolizing enzymes EPHX1, CYP2C9, SULT1A2, and GSTP1, the transporter ABCA1, as well as the kinases PRKACA and MAP3K14, and the ligand-dependent nuclear receptors AHR and NR0B2 (Table 8.7). These biomarkers are involved in key cellular processes such as in the activation of the PXR/RXR heterodimer, in the LPS and IL-1 mediated inhibition of the RXR function, or in the aryl hydrocarbon receptor signaling (Table 8.7). In contrast, the transcription regulator ELF3, the growth factor TGFB2 and the kinase PKMYT1 were not found to be significant (Benjamini-Hochberg corrected $p \geq 0.05$, two-sample t-test) indicating that these genes show similar toxic change for both the high- and the low-responsive drugs (Table 8.7).

To identify individual molecular biomarkers for each of the high-responsive drugs, a very strong toxic change (at least seven-fold increase compared to mean toxic change) was required. The majority of the individual molecular biomarkers belong to the cytochrome P450 family, transcription regulators, or they are transporters (Table C.7). These drug-specific molecular biomarkers were finally analyzed to identify potential DDIs between the high-responsive drugs in the case of co-administration. To this end, a potential DDI between two drugs was assumed, if both drugs share at least one biomarker (Table C.8).

The consequently identified pairs of drugs were then compared with known DDIs from DrugBank [Wishart et al., 2006] and from Drugs.com (Figure 8.11). Strikingly, the prediction of DDIs reaches an accuracy of

Table 8.7: Common molecular biomarkers. Common molecular biomarkers were identified in different key cellular processes at different timepoints for the drugs of the high-responsive group. Benjamini-Hochberg corrected p-values p were calculated by comparing the correspondent toxic changes between the low and high-responsive group. Functional types were taken from QIAGENs Ingenuity Pathway Analysis (IPA®), QIAGEN Redwood City, www.qiagen.com/ingenuity).

Gene	Functional type	P-value	Key cellular processes (timepoint)
EPHX1	peptidase	0.001*	xenobiotic metabolism signaling (24 h), NRF-2 mediated oxidative stress response (24 h)
CYP2C9	enzyme	0.003*	cytochrome p450 - substrate is a xenobiotic (8 h), PXR/RXR activation (8 h), CAR/RXR activation (8 h)
ABCA1	transporter	0.003*	LPS/IL-1mediated inhibition of RXR function (24 h)
GSTP1	enzyme	0.004*	xenobiotic metabolism signaling (24 h), aryl hydrocarbon receptor signaling (24 h), LPS/IL-1 mediated inhibition of RXR function (24 h), NRF-2 mediated oxidative stress response (24 h)
SULT1A2	enzyme	0.004*	xenobiotic metabolism signaling (24 h), LPS/IL-1mediated inhibition of RXR function (24 h)
AHR	ligand-dependent nuclear receptor	0.005*	xenobiotic metabolism signaling (24 h), aryl hydrocarbon receptor signaling (24 h)
PRKACA	kinase	0.008*	PXR/RXR activation (24 h)
MAP3K14	kinase	0.016*	xenobiotic metabolism signaling (24 h)
NR0B2	ligand-dependent nuclear receptor	0.022*	PXR/RXR activation (24 h), aryl hydrocarbon receptor signaling (24 h), LPS/IL-1 mediated inhibition of RXR function (24 h)
TGFB2	growth factor	0.086	aryl hydrocarbon receptor signaling (24 h)
PKMYT1	kinase	0.186	cell cycle G2/M DNA damage checkpoint regulation (24 h)
ELF3	transcription regulator	0.212	primary glomerulonephritis biomarker panel (8 h)

* Benjamini-Hochberg corrected $p < 0.05$

68 % and a precision of 71 % with respect to DDIs known from the literature (Figure 8.11). The number of correctly predicted DDIs and non-DDIs was found to be 75 % and 58 %, respectively. Analyzing all potential DDIs, 35 out of the 42 DDIs were identified based on high toxic changes on cytochrome P450 enzymes for both drugs (Table C.8). Interestingly, in 72 % of these cases predicted cytochrome P450 enzymes are in accordance with literature data [Wishart et al., 2006] underlining the general validity of the approach.

8.4 Discussion

In this article, a comparative study of drug-induced hepatotoxicity was presented, which enables the investigation and evaluation of the hepatotoxic potential of several drugs within a patient context. Toxic changes reflecting time-resolved cellular responses induced by oral drug administration of therapeutic and toxic doses in humans were thereby predicted to study changes in key cellular processes, functional classes of genes, and individual genes, as well as to identify molecular biomarkers and potential DDIs. Notably, toxic changes describe the transition from therapeutic drug response to adverse events and thus allow a quantitative representation of clinically relevant situations within a patient context.

By applying PICD (Figure 8.1) [Thiel et al., 2016], in vitro toxicity data obtained in primary human hepatocytes from Open TG-GATEs [Igarashi et al., 2015] could be contextualized to predict in vivo drug response patterns of key cellular processes for the simulated therapeutic and toxic PK profiles (Figure 8.5, Figure 8.7). As input for PICD, drug-specific human PBPK models were developed and validated with different dosage regimens used in previous clinical studies (Figure 8.3, Table 8.2). This validation step ensures reliable predictions of PK profiles for a wide range of in vivo doses since potential non-linearities are explicitly taken into account. Therapeutic and toxic drug concentrations over time were

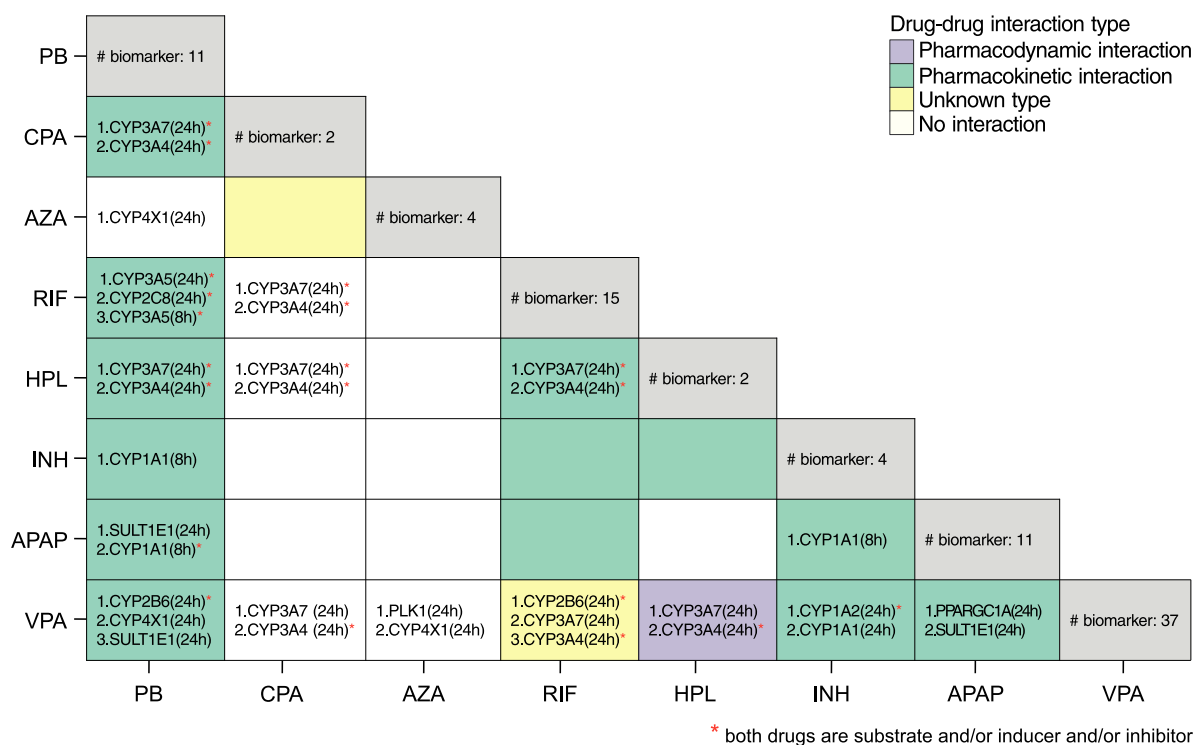


Figure 8.11: Potential drug interactions between the high-responsive drugs. The total number of identified biomarkers for each drug is shown on the diagonal. The biomarkers were ranked according to the absolute differences of toxic change between both considered drugs. Measures of the performance were additionally calculated by comparing predicted DDIs with known DDIs from literature: accuracy = 68 %, sensitivity = 75 %, specificity = 58 %, and precision = 71 %.

then simulated (Figure 8.5). The toxic doses were identified from clinical cases for which toxic events occurred (Table 8.3). Two large databases as well as literature were screened to reasonably cover a wide range of toxic doses (Table 8.3). Moreover, it should be noted that the in vivo doses considered here reflect the range of drug exposure occurring in clinical practice (Table 8.2, Table 8.3).

When evaluating the toxic behavior between the fifteen hepatotoxic drugs, no significant toxic change was observed in the case of SST, AD or DFN (Figure 8.7). However, it is known that these drugs may still have a high hepatotoxic potential [Bort et al., 1999b; Horsmans et al., 1990; Lewis et al., 1989]. Notably, these three drugs are highly bound to plasma proteins in vivo and are rapidly metabolized such that high in vivo doses are necessary to reach the in vitro exposure when applying PICD [Thiel et al., 2016]. The identified toxic in vivo doses are therefore probably higher than those provided in the literature (Table 8.3). As a consequence, the drug responses predicted by PICD for the toxic doses may be very low. Hence, a future application of drug-specific pharmacokinetics in in vitro assay design might improve the in vivo relevance of certain in vitro outcomes. To validate predicted drug response profiles of all considered drugs, in vivo rat data from Open TG-GATEs were used [Igarashi et al., 2015].

In a preparatory proof-of-concept analysis, correlation results in rats demonstrated that PICD-based predictions were generally in concordance with in vivo observations (Figure 8.6). Although uncertainties were observed in some cases, it can still be assumed that the predicted drug responses in humans have in vivo relevance since such uncertainties are almost unavoidable due to (i) the high variability of physicochemical properties and pharmacological diversity of the considered drugs, (ii) the several differences potentially influencing the response data observed in vitro and in vivo (e.g., different plasma protein binding and enzyme and transporter activity, crosstalk between relevant tissues and organs in the in vivo situation), (iii) the time-dependent interpolation that was necessary to make the predictions comparable to the in vivo observations [Igarashi et al., 2015].

In the first analysis of the comparative toxicity study, toxic changes in significantly perturbed key cellular processes were compared between the fifteen hepatotoxic drugs (Figure 8.7). One objective of this study was to investigate whether subsets of drugs exist, which share similar perturbations of key cellular processes, and whether these subsets have common pharmacokinetic parameters or drug-specific characteristics such as DILI-potential, solubility and permeability properties, and the target organ or system. Surprisingly the analyses showed that the low-responsive drugs primarily belong to the BCS class 2 (high permeability, low solubility), except PHE (class 1: high permeability, high solubility). In contrast, high-responsive drugs were rather less permeable with statistically significant differences for lipophilicity but not for water solubility. This finding might imply that a low permeability plays an important role in the hepatotoxic potential of the considered drugs in contrast to the results of other studies that showed a correlation between high lipophilicity and toxicological outcomes [Waring, 2010; Stolerma, 2010]. This could be due to the fact that in our multiscale approach additional drug properties such as plasma protein binding or doses applied *in vivo* are implicitly taken into account in the whole-body PBPK models and set in relation to actual *in vitro* omics data for known hepatotoxicants. Also, it could be hypothesized that hydrophilic drugs tend to have more polar functional groups and thus are more prone to enzyme-mediated adverse chemical modifications since these drugs present several potential interaction targets within the cell. Statistically significant differences between both groups were identified for the plasma protein binding but not for the ratio of toxic and therapeutic AUCs and dose levels, respectively. The latter result is important, since it demonstrates that the hepatotoxic potential is not affected by the selection of the therapeutic and toxic dose levels and the resulting concentration-time courses. Interestingly, the low-responsive drugs tend to have a narrow therapeutic index (defined as the ratio between toxic and therapeutic dose) (Figure 8.5, Table 8.3) [Muller and Milton, 2012], which increases the risk of adverse reactions following high drug exposure due to overdosing or idiosyncrasy.

Next, the toxic changes between the high-responsive drugs were predicted in terms of functionally-related genes involved in key cellular processes. In this way, toxic changes of functional classes (e.g., phosphatases or transcription regulators) that are mainly contributing to a certain key cellular process could be identified. For instance, a high toxic change of growth factors at 8 h was found for APAP, which highly increases the risk of renal impairment as described in previous studies [Mitić-Zlatković and Stefanović, 1999; Fruchter et al., 2011] (Figure 8.9E). In the case of AZA and VPA, a high toxic change in kinases was found at 24 h, which were involved in the regulation of the cell cycle G2/M DNA damage checkpoint (Figure 8.9B). This is in striking accordance with previous studies [Han et al., 2013; Yagi et al., 2010; Karran, 2006; van Furth et al., 1975] where both drugs were also reported to have a substantial impact on the cell cycle regulation. The hepatotoxic potential of AZA and VPA in this crucial pathway was hence exemplarily investigated in more detail to compare toxic changes of involved genes. Focusing on the cyclins B1 and B2 or the kinase PLK1, for instance, revealed similar toxic changes and especially high drug responses at 24 h for both drugs. This suggests a potential key role of these genes in the drug-induced hepatotoxicity of AZA and VPA. In contrast, differentially responding genes for both drugs could be found at different timepoints (Figure 8.10B). Interestingly, AZA and VPA similarly perturbed central biological processes of the G2/M DNA damage checkpoint (Figure 8.10). However, the initiation of these processes is complementary and preferably occurred by DNA-PK, GADD45 and BORA for AZA, and CDC2, p53 and MDM2 for VPA (Figure 8.10).

Finally, the calculated toxic changes were used to discover common and individual molecular biomarkers for the high-responsive drugs. A set of nine common molecular biomarkers could be identified, which showed significant differences to the low-responsive drugs indicating a high sensitivity of the identified biomarkers (Table 8.7). Moreover, individual molecular biomarkers mostly enzymes of the cytochrome P450 family, were found and further used to detect potential DDIs. Here, the identification of potential DDIs was based on high toxic changes reflecting differences between therapeutic and toxic drug response.

Known DDIs from literature could be predicted with a precision of 71 % (Figure 8.11). In some cases, known DDIs from literature (e.g., between RIF and INH) were not identified as such (Figure 8.11), which might indicate that these interactions are only significant after therapeutic drug administration. In contrast, predicted DDIs not found in literature might present newly discovered drug interactions, which only occur under toxic conditions. The consideration of more toxic and non-toxic drugs in a future extension of our analysis could further improve the identification and validation of molecular biomarkers and DDIs discovered in an *in vivo* situation. Moreover, it is also conceivable to apply the workflow on a set of candidate drugs during early drug development. In this regard, measured time-series gene expression profiles could be contextualized in human PBPK models parametrized based on molecular modeling to identify potential toxic and non-toxic compounds before entering the clinical phases.

To conclude, the hepatotoxic potential of a set of known hepatotoxic drugs was studied and compared by predicting toxic changes for humans, which reflect the transition from therapeutic drug response to toxic reactions. We therefore analyzed primary human hepatocytes, at the cellular level, and developed human PBPK models, at the organism level, and coupled both levels by the application of the recently developed approach called PICD (Figure 8.1). Hence, the analysis of toxic changes allows a quantitative evaluation of clinically relevant situations within a patient context. Altogether, toxic changes after 2 h, 8 h and 24 h in significantly affected key cellular processes could be analyzed thereby identifying a low-responsive (SST, DFN, AD, ERY, FT, CSA and PHE) and a high-responsive group (RIF, CPA, PB, INH, HPL, AZA, APAP and VPA) (Figure 8.7). For the latter, molecular biomarkers and potential DDIs could be identified. An accuracy, specificity, sensitivity, and precision of 67 %, 58 %, 75 %, and 71 %, respectively, has been reached when comparing the potential DDIs with known DDIs from literature. Notably, 72 % of the predicted cytochrome P450 enzymes could be identified in known drug-enzyme association for both drugs involved in the specific DDI [Wishart et al., 2006].

This article provides a systematic analysis of drug-induced hepatotoxicity by coupling *in vitro* toxicity data measured in primary human hepatocytes [Igarashi et al., 2015] with *in vivo* pharmacokinetics, and thus allows an investigation of differences in drug response following oral administration of therapeutic and toxic doses in humans. Drug-induced hepatotoxicity could be hence analyzed within a patient context to investigate drug effects between therapeutic and toxic conditions, and to discover molecular biomarkers as well as potential DDIs for several hepatotoxic drugs. The results of our study might help to improve clinical risk assessment and patient safety during a drug development process in the future.

Multiscale modeling reveals inhibitory and stimulatory effects of caffeine on acetaminophen-induced toxicity in humans

Abstract

Acetaminophen is a widely used analgesic drug that is frequently co-administered with caffeine in the treatment of pain. It is well-known that acetaminophen may cause severe liver injury after an acute overdose. However, the understanding of whether and to what extent caffeine inhibits or stimulates acetaminophen-induced hepatotoxicity in humans is still lacking. Here, a multiscale analysis is presented that quantitatively models the pharmacodynamic response of acetaminophen during co-medication with caffeine. Drug-drug interaction processes were therefore integrated into physiologically-based pharmacokinetic models at the organism level, while drug-specific pharmacodynamic response data were contextualized at the cellular level. The results provide new insights into the inhibitory and stimulatory effects of caffeine on acetaminophen-induced hepatotoxicity for crucially affected key cellular processes and individual genes at patient level. This study might facilitate the risk assessment of drug combination therapies in humans and thus may improve patient safety in clinical practice.

published as: 'Thiel, C., Cordes, H., Baier, V., Blank, L. M., and Kuepfer, L. (2017). Multiscale modeling reveals inhibitory and stimulatory effects of caffeine on acetaminophen-induced toxicity in humans. *CPT: Pharmacometrics & Systems Pharmacology*.'

Author contributions:

Writing - original draft: Thiel, C., and Kuepfer, L.; Writing - review & editing: Thiel, C., Cordes, H., Baier, V., Blank, L. M., and Kuepfer, L.; Research design: Thiel, C.; Data analysis & implementation: Thiel, C.; PBPK model development: Thiel, C., and Cordes, H.

9.1 Introduction

Acetaminophen (APAP) is a widely used over-the-counter drug with analgesic and antipyretic activities [Nelson, 1990]. In therapeutic applications, APAP is an effective and safe drug mostly used in the treatment of pain. However, in humans acute overdosing of APAP increases the risk of hepatotoxic events leading to severe liver damage or even to death [Nelson, 1990]. The specific molecular mechanisms underlying APAP-induced hepatotoxicity are still not well understood. However, it was suggested that an accumulation of NAPQI, which is supposed to be the reactive intermediate of APAP [Walubo et al., 2004], causes the toxic reactions [Sato and Izumi, 1989; Nelson, 1990]. NAPQI is a phase I metabolite of APAP that is mostly formed by CYP enzymes, in particular CYP1A2, CYP2E1, and CYP3A4 [Walubo et al., 2004]. When APAP is administered at toxic doses, the conjugation of NAPQI with glutathione and the subsequent conversion to APAP cysteine (APAPC) is decreased, which leaves NAPQI as potential binding partner for proteins within the cell [Jaw and Jeffery, 1993]. Furthermore, APAP and its metabolites are involved in active drug transport across extra- and intracellular membranes mediated by ABC transporters, in particular ABCB1 and ABCG2 [Wishart et al., 2006; Mazaleuskaya et al., 2015].

Caffeine (CAF) is a stimulant of the central nervous system and is daily consumed in hot or cold beverages. CYP enzymes, particularly CYP1A2 and CYP2E1, are predominantly involved in the metabolism of CAF [Gu et al., 1992]. Moreover, CAF showed inhibitory effects on active drug transport mediated by ABCB1 [Wishart et al., 2006]. CAF is often administered as combination therapy in the treatment of pain since CAF is supposed to enhance the analgesic effects evoked by APAP or other analgesic agents [Sawynok and Yaksh, 1993; Renner et al., 2007; Palmer et al., 2010]. In this regard, CAF may alter APAP pharmacokinetics at the organism level [Iqbal et al., 1995; Renner et al., 2007] and may influence APAP-induced pharmacodynamic responses at the cellular scale [Sawynok and Yaksh, 1993]. In this context, CAF and APAP may thus be considered as perpetrator and victim drug, respectively [Prueksaritanont et al., 2013]. Notably, the unintentional co-administration of CAF together with other drugs is mostly unavoidable, since coffee is one of the most popular drinks in the world. In clinical practice, simultaneous administration of multiple drugs is often a standard treatment. In such combination therapies, drug interactions may inevitably occur and may potentially have a substantial impact on the PK behavior and the resulting PD effect of the administered drugs eventually leading to additive, synergistic, or antagonistic drug effects [Sato and Izumi, 1989; Sawynok and Yaksh, 1993; Iqbal et al., 1995; Renner et al., 2007; Coors and De Meester, 2008].

In vitro drug response data measured at toxic concentrations may help to investigate the cellular effects induced by different drugs in cellular assays. However, a major challenge of such in vitro experiments is the translatability to patients. Recently, we have developed an integrative multiscale approach called PICD [Thiel et al., 2016] that allows the translation of such in vitro findings to an in vivo context by coupling in vitro toxicity data with whole-body PBPK models (Figure 9.1).

PBPK modeling allows a mechanistic description of ADME processes governing the fate of a drug within the body. PBPK models are particularly well suited for extrapolation to different dosage regimens and, moreover, to consider DDIs of co-administered drugs influencing their ADME processes and, hence, altering their concentration-time courses within the blood or the organs [Zhou et al., 2016].

In recent studies, the concomitant administration of APAP and CAF in rats and mice resulted in either a potentiation or a reduction of APAP-induced hepatotoxicity, respectively [Sato et al., 1985; Sato and Izumi, 1989; Lee et al., 1991; Raińska et al., 1992; Jaw and Jeffery, 1993]. A possible explanation of these observations is the impact of CAF on the formation of NAPQI either due to inhibitory or stimulatory effects. Results obtained in rat and mice liver microsomes suggested an involvement of CAF on APAP metabolism mediated by CYP enzymes [Nouchi et al., 1986; Lee et al., 1991; Jaw and Jeffery, 1993]. In rat liver microsomes, for instance, co-administration of CAF led to a reduced or an accelerated NAPQI

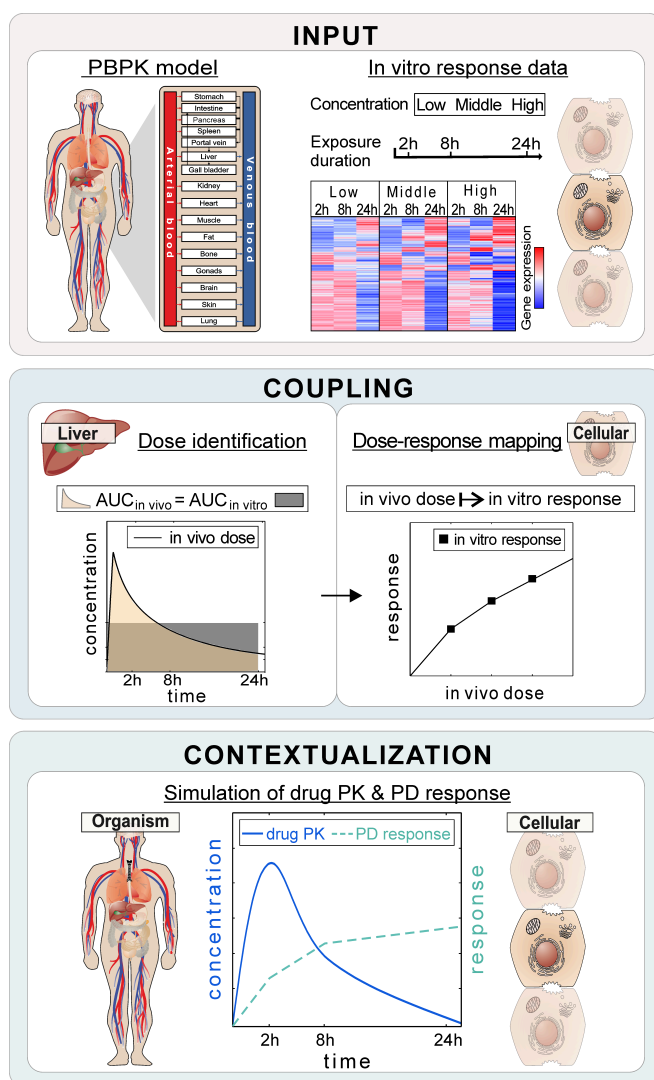


Figure 9.1: Overview of the use of PICD. **Input:** Drug-specific PBPK models are developed at the organism level, while in vitro response data of compound-treated primary hepatocytes are analyzed at the cellular level [Igarashi et al., 2015]. **Coupling:** In vivo doses are identified that are directly related to in vitro drug exposure ($AUC_{in\ vivo} = AUC_{in\ vitro}$). Time-dependent dose-response curves are generated by mapping in vivo doses to in vitro response data. **Contextualization:** PD responses over time are predicted for simulated PK profiles following drug administration of specific dose levels by use of time-dependent dose-response curves.

formation dependent on the applied concentration by affecting CYP enzymes such as CYP1A1, CYP3A2, or CYP2E1 [Lee et al., 1991]. However, the interaction of CAF with APAP in humans, particularly at toxic dose levels, is still not well understood.

The aim of this study was a model-based investigation of the PK and PD interactions of CAF on APAP-induced toxicity during co-medication in humans, through the consideration of drug interactions at the organism level, and the contextualization of drug-specific PD response data at the cellular level, respectively. PD responses of CAF and APAP were therefore predicted for an in vivo situation by the application of PICD [Thiel et al., 2016] thereby coupling in vitro toxicity data with drug-specific PBPK models. To validate the PBPK models, simulated drug concentrations of APAP, CAF, and their main metabolites APAPC, acetaminophen glucuronide (APAPG), acetaminophen sulfate (APAPS), paraxanthine (PX), theophylline (TP), and theobromine (TB) were first assessed with clinical PK profiles from several studies obtained for different dosage regimens [Rawlins et al., 1977; Prescott, 1980; Newton et al., 1981; Tang-Liu et al., 1983; Blanchard and Sawers, 1983; Lelo et al., 1986; Iqbal et al., 1995; Kaplan et al., 1997; Renner et al., 2007; Shinoda et al., 2007]. Using an additive PD response model, the influence of CAF on APAP-induced hepatotoxicity was analyzed for key cellular processes and individual genes. Dose escalation studies were finally performed to evaluate the transition from desired therapeutic effects to undesired toxic events thereby quantitatively describing clinically relevant situations.

9.2 Materials and methods

9.2.1 Physiologically-based pharmacokinetic model development

To develop the PBPK models of APAP and CAF, physicochemical drug properties of APAP, CAF and their metabolites were obtained from the literature (Table 9.1). Reference PBPK models were first developed and assessed by comparing simulated drug concentrations with clinical PK data from literature [Lelo et al., 1986; Blanchard and Sawers, 1983; Kaplan et al., 1997; Renner et al., 2007; Shinoda et al., 2007] (Figure 9.2, Appendix A.2).

Intestinal permeability values originally provided by PK-Sim® were slightly adjusted for APAP (1.9E-05 cm/min) and CAF (3E-05 cm/min) (Figure 9.2). The standard distribution model of PK-Sim® was used to calculate partition coefficients and cellular permeabilities [Willmann et al., 2003]. K_m and v_{max} representing the kinetic behavior of active transport processes and metabolizing reactions were either taken from literature [Chen et al., 1998; Ha et al., 1995; Gates and Miners, 1999; Gu et al., 1992; Labedzki et al., 2002; Mutlib et al., 2006; Adjei et al., 2008] or were fitted to best describe the experimental data (Table 9.2). Relative abundance of relevant ADME enzymes and transporters (Table 9.2) was estimated by using tissue-specific gene expression data (Table D.1) [Meyer et al., 2012]. Kidney plasma clearances were parametrized such that urinary excretion rates were in accordance with results observed in human clinical studies [Critchley et al., 1986; Wishart et al., 2006; Tang-Liu et al., 1983] (Table 9.3).

A competitive inhibition of CAF on CYP2E1 [Nouchi et al., 1986; Gu et al., 1992] and ABCB1 [Wishart et al., 2006] with dissociation constants (K_d) of 48.5 $\mu\text{mol/l}$ and 0.06 $\mu\text{mol/l}$, respectively, were modeled to consider the PK interaction of CAF on APAP [Renner et al., 2007; Iqbal et al., 1995]. Respective reaction rates in the competitive inhibition processes were calculated as follows:

$$v = \frac{v_{max} * S}{K_m * (1 + \frac{I}{K_d}) + S} \quad (9.1)$$

where v represents reaction rate, v_{max} represents maximal reaction rate, S represents free substrate (APAP) concentration, I represents free inhibitor (CAF) concentration, and K_m represents Michaelis-Menten constant in absence of the inhibitor.

The established reference PBPK models were further validated by using clinical PK data not used for model establishment [Newton et al., 1981; Rawlins et al., 1977; Prescott, 1980; Tang-Liu et al., 1983; Iqbal et al., 1995] (Figure 9.2) thereby leaving all model parameters unchanged, except parameters characterizing the specific design of the clinical studies (Table 9.4). The model quality was evaluated by calculating normalized RMSD values, R^2 values [Thiel et al., 2016], and by comparing observed vs. predicted AUCs and cMax values of the different simulations.

9.2.2 Analysis of in vitro toxicity data

The analysis of time-series gene expression profiles from Open TG-GATEs [Igarashi et al., 2015] (ArrayExpress accession numbers: E-MTAB-798) (Appendix A.1) including data pre-processing and normalization, differential expression analysis of single genes and overrepresentation analysis of key cellular processes, were performed as explained before [Thiel et al., 2016]. Fold change values were calculated to indicate gene expression changes compared to time-matched controls. To represent key cellular processes, seventy-four hand-curated toxicity lists were extracted from QIAGENs Ingenuity Pathway Analysis (IPA®), QIAGEN Redwood City, www.qiagen.com/ingenuity) (Table C.1). Since primary human hepatocytes were analyzed [Igarashi et al., 2015], key cellular processes representing cardiac or renal toxicity were not considered. Genes with unknown functions were also not taken into account.

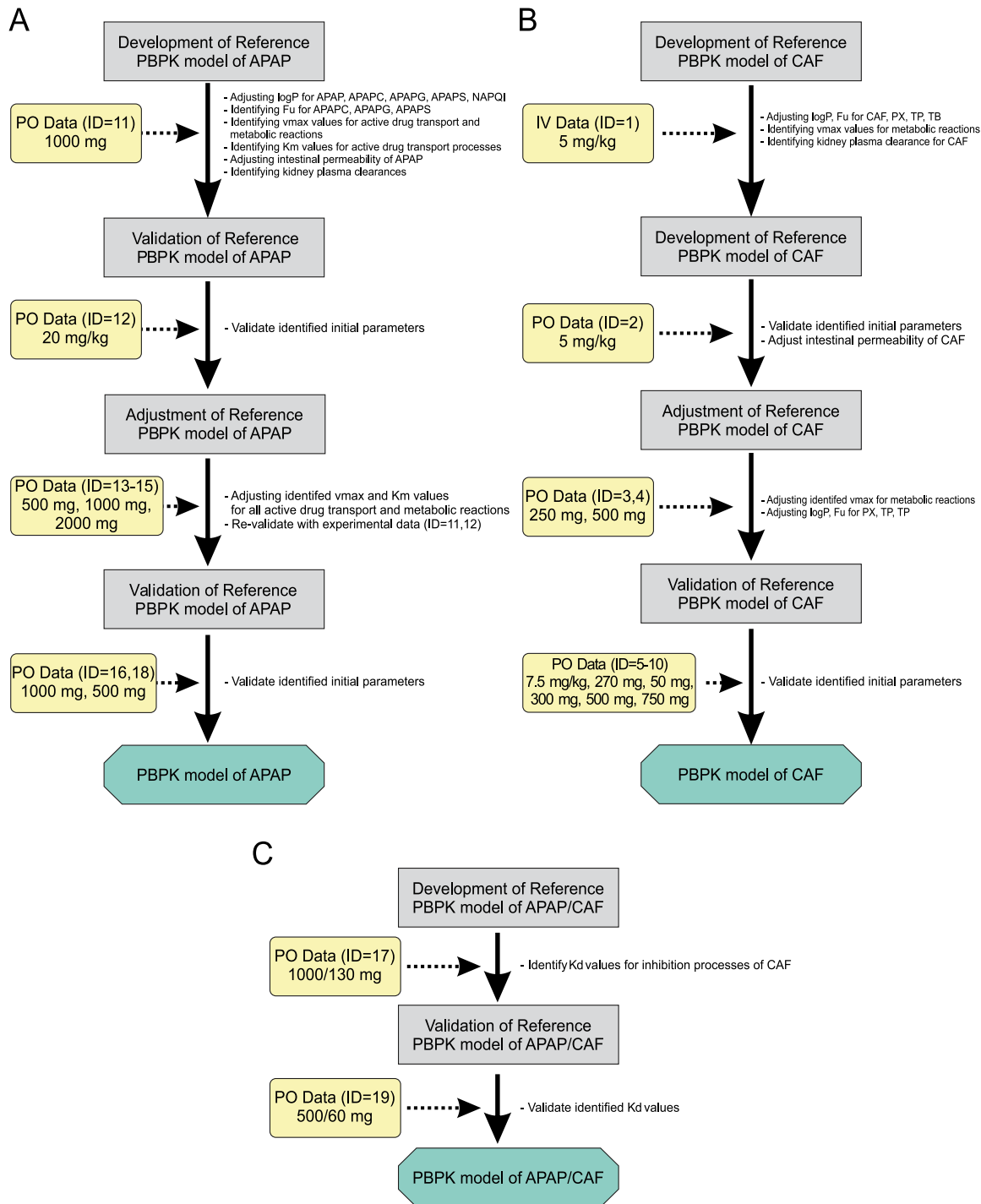


Figure 9.2: Workflow of PBPK model development and validation. Workflow of PBPK model development and validation including experimental data and modeling steps for (A) single administration of APAP, (B) single administration of CAF, and (C) co-administration of APAP and CAF.

9.2.3 Predicting the pharmacodynamic responses of acetaminophen and caffeine

PICD allows a quantitative description of drug responses at patient level by integrating in vitro toxicity data from Open TG-GATEs [Igarashi et al., 2015] into whole-body PBPK models [Thiel et al., 2016]. In short, the basic concept of PICD is the identification of in vivo doses such that the simulated drug exposure in the interstitial space of the liver is equal to the in vitro drug exposure of the in vitro assay

Table 9.1: Physicochemical properties of acetaminophen, caffeine, and their metabolites used in the developed PBPK models. MW, logP, F_u , pKa, and water solubility used in the developed PBPK models of APAP and CAF. MWs, logP values and water solubilities are taken from DrugBank [Wishart et al., 2006] and Human Metabolome Database [Wishart et al., 2007]. In some cases, logP and F_u values were slightly adjusted to best describe the experimental PK data.

Drug/ Metabolite	MW [g/mol]	logP	Water solubility [mg/l]	F_u	Reference	Compound type	pKa	Reference
APAP	151.16	0.46	14000.0	0.81	[Wishart et al., 2006]	Acid	9.38	[Wishart et al., 2006]
APAPC	254.31	0.33	337.0	0.6	*	[Acid, base]	[1.93, 9.09]	[Wishart et al., 2006]
APAPG	327.29	-1.04	27700.0	0.98	*	Acid	3.18	[Wishart et al., 2006]
APAPS	231.23	-0.372	1540.0	0.8	*	Acid	10.46	[Bento et al., 2014]
NAPQI	149.15	0.01	987.0	0.02	[Bond, 2009]	Neutral	-	[Swain, 2012]
CAF	194.2	-0.07	21600.0	0.65	[Lelo et al., 1986]	Base	10.4	[Wishart et al., 2006]
PX	180.16	-0.63	9130.0	0.52	[Lelo et al., 1986]	Acid	10.76	[Wishart et al., 2007]
TB	180.16	-0.78	9740.0	0.86	[Lelo et al., 1986]	Acid	9.28	[Wishart et al., 2007]
TP	180.16	-0.02	22900.0	0.58	[Lelo et al., 1986]	Acid	7.82	[Wishart et al., 2007]

* Estimated

Table 9.2: Active drug transport and metabolic reactions. Metabolic and active drug transport processes, which were considered in the PBPK models of APAP and CAF, either consist of the metabolic enzyme and the corresponding metabolite, or of the transporter and the corresponding transporter type (efflux is defined as transport of a substance from the intracellular space to the interstitial space or the lumen). Kinetic parameters K_m and v_{max} were used to characterize the kinetic behavior of active processes.

Drug/ Metabolite	Metabolite/ Transporter	Enzyme/ Transporter type	K_m [$\mu\text{mol/l}$]	v_{max} * [$\mu\text{mol/l/min}$]	Reference
APAP	APAPG	UGT1A9	9200.0	1078.88	[Mutlib et al., 2006]
APAP	APAPS	SULT1A1	2400.0	51.0	[Riches et al., 2007; Adjei et al., 2008]
APAP	NAPQI	CYP2E1	1300.0	51.02	[Chen et al., 1998; Shinoda et al., 2007]
APAP	Efflux	ABCB1	20308.5*	1220.0	[Mazaleuskaya et al., 2015; Wishart et al., 2006]
APAPG	Efflux	ABCG2	96.33*	24.51.0	[Mazaleuskaya et al., 2015]
APAPS	Efflux	ABCG2	94.49*	1200.0	[Mazaleuskaya et al., 2015]
NAPQI	APAPC	GSTT1	25.0*	20.16.0	[Shinoda et al., 2007]
CAF	PX	CYP1A2	400.0	19.0	[Gu et al., 1992]
CAF	TB	CYP1A2	280.0	4.8	[Gu et al., 1992]
CAF	TP	CYP2E1	2800.0	9.0	[Gu et al., 1992]
PX	1X	CYP1A2	2500.0	260.0	[Labeledzki et al., 2002]
TB	7X	CYP1A2	4200.0	280.0	[Gates and Miners, 1999]
TP	13U	CYP2E1	15300.0	350.0	[Ha et al., 1995]

* Estimated

Table 9.3: Elimination processes. Renal clearance processes considered in the developed PBPK models of APAP and CAF. Kidney plasma clearances were parameterized in order to match experimental observations.

Drug/Metabolite	Plasma clearance [l/min/kg]	Reference
APAP	1.27E-04	[Critchley et al., 1986; Wishart et al., 2006]
APAPC	4.38E-04	[Critchley et al., 1986]
APAPG	1.19E-03	[Critchley et al., 1986]
APAPS	4.56E-03	[Critchley et al., 1986]
NAPQI	4.62E-03	adjusted from [Krauss et al., 2012]
CAF	3.00E-03	[Tang-Liu et al., 1983]

(Figure 9.1). The identified in vivo doses were mapped to the in vitro drug response data to quantitatively describe PD responses for different dose levels applied in vivo (Figure 9.1) [Thiel et al., 2016].

Here, PICD was applied separately on single doses of APAP and CAF to predict PD responses for genes (defined as log2 fold change) and key cellular processes (defined as mean absolute log2 fold change of all involved genes) at 8 h and 24 h. Note that in TG-GATEs in vitro response data of APAP and CAF was measured at these timepoints [Igarashi et al., 2015]. Bioavailability values calculated from the developed PBPK models (APAP = 92 %, CAF = 100 %) were used to consider oral administration.

Table 9.4: Experimental conditions. Administration route (IV, or PO), respective doses, and number of subjects (n) and their gender, age, and weight. The experimental PK data were either used for establishment of the reference PBPK model (Reference) or for model validation (Validation).

Study ID	Drug(s)	Route	Dose	n	Gender (M,F)	Age [years]	Weight [kg]	Model type	Reference
1	CAF	iv	5 mg/kg	8	M	20.52	75±6	Reference	[Blanchard and Sawers, 1983]
2	CAF	po	5 mg/kg	8	M	20.5±2	75±6	Reference	[Blanchard and Sawers, 1983]
3	CAF	po	250 mg	12	5 M/7 F	28.8±6	66.8±10	Reference	[Kaplan et al., 1997]
4	CAF	po	500 mg	12	5 M/7 F	28.8±6	66.8±10	Reference	[Kaplan et al., 1997]
5	CAF	po	270 mg	6	M	19-21	62-104	Validation	[Lelo et al., 1986]
6	CAF	po	7.5 mg/kg	6	5 M/1 F	24-32	73±7	Validation	[Tang-Liu et al., 1983]
7	CAF	po	50 mg	6	5 M/1 F	21-36	54-84	Validation	[Newton et al., 1981]
8	CAF	po	300 mg	6	5 M/1 F	21-36	54-84	Validation	[Newton et al., 1981]
9	CAF	po	500 mg	6	5 M/1 F	21-36	54-84	Validation	[Newton et al., 1981]
10	CAF	po	750 mg	6	5 M/1 F	21-36	54-84	Validation	[Newton et al., 1981]
11	APAP	po	1000 mg	5	1 M/4 F	55±13	60±11	Reference	[Shinoda et al., 2007]
12	APAP	po	20 mg/kg	8	n/a	n/a	n/a	Validation	[Prescott, 1980]
13	APAP	po	500 mg	6	M	n/a	65-72	Validation	[Rawlins et al., 1977]
14	APAP	po	1000 mg	6	M	n/a	65-72	Validation	[Rawlins et al., 1977]
15	APAP	po	2000 mg	6	M	n/a	65-72	Validation	[Rawlins et al., 1977]
16	APAP	po	1000 mg	24	12 M/12 F	18-45	67-86/51-66	Reference	[Renner et al., 2007]
17	APAP/CAF	po/po	1000/130 mg	24	12 M/12 F	18-45	67-86/51-66	Reference	[Renner et al., 2007]
18	APAP	po	500 mg	10	M	22-32	50-70	Validation	[Iqbal et al., 1995]
19	APAP/CAF	po/po	500/60 mg	10	M	22-32	50-70	Validation	[Iqbal et al., 1995]

9.2.4 Modeling the pharmacodynamic response of acetaminophen co-administered with caffeine

PICD was applied for a co-administration of APAP and CAF with a relative dose ratio of 1000:130 according to therapeutic indications [Renner et al., 2007; Palmer et al., 2010]. When both drugs were given concomitantly, the PICD-based PD response of APAP ($PD\ response_{DDI}(APAP)$) were adjusted according to its changed concentration-time profile caused by the competitive inhibition of CAF on ABCB1- and CYP2E1-mediated transport and metabolism of APAP, respectively [Nouchi et al., 1986; Lee et al., 1991; Wishart et al., 2006; Gu et al., 1992]. Furthermore, the predicted PD response of CAF ($PD\ response(CAF)$) was considered separately. The total PD response of APAP during co-administration with CAF ($PD\ response(APAP + CAF)$) was thus calculated as follows:

$$PD\ response(APAP + CAF)_{x,t,d} = PD\ response_{DDI}(APAP)_{x,t,d} + PD\ response(CAF)_{x,t,d} \quad (9.2)$$

where x represents a gene or a key cellular process, t represents the timepoint, and d represents the oral dose level. An additive PD response model was used here to calculate the PD response of APAP for co-administration with CAF since the in vitro data was only available for single drug administration such that potential synergistic or antagonistic effects induced by co-medication of both drugs beyond pure additional effects could not be described. The relative PD effect of CAF co-administered with APAP compared to the PD response predicted for single administration of APAP alone ($PD\ response(APAP)$) was computed as follows:

$$\begin{aligned} relative\ PD\ effect(APAP + CAF, APAP)_{x,t,d} = \\ \frac{PD\ response(APAP + CAF)_{x,t,d} - PD\ response(APAP)_{x,t,d}}{PD\ response(APAP)_{x,t,d}} * 100 \end{aligned} \quad (9.3)$$

Note that a positive or negative relative PD effect value means that CAF increases and decreases the PD response of APAP, respectively, while a value of zero indicates no effect of CAF.

9.2.5 Other systems biology models for acetaminophen

Several systems biology models of APAP were published in literature and applied for different purposes such as toxicology [Woodhead et al., 2012; Krauss et al., 2012; Howell et al., 2012; Ben-Shachar et al., 2012] or pediatric scaling [Jiang et al., 2013] (Table D.3).

Here, a subset of five different models [Krauss et al., 2012; Howell et al., 2012; Ben-Shachar et al., 2012; Woodhead et al., 2012; Jiang et al., 2013] is briefly explored (Table D.3) thereby focusing on (i) the underlying model structure including the modeling framework and the implemented biochemical processes, (ii) the clinical data used for model development and validation, and (iii) the modeling purpose and the results. All models consider clearance processes of APAP and its metabolites, while Jiang et al. [Jiang et al., 2013] and Ben-Shachar et al. [Ben-Shachar et al., 2012] additionally considers several UGT and CYP enzymes for the metabolism of APAP (Table D.3). In our model active drug transport processes by ABCB1 and ABCG2 were additionally considered.

9.3 Results

9.3.1 Physiologically-based pharmacokinetic models of acetaminophen and caffeine

At first, reference PBPK models for APAP and CAF were established by using clinical PK data (Table 9.4) [Kaplan et al., 1997; Renner et al., 2007; Blanchard and Sawers, 1983; Shinoda et al., 2007]. Twenty-one biochemical processes were implemented in the PBPK models of CAF and APAP (Figure 9.3, Figure 9.4) to represent key metabolic reactions, active drug transport (Table 9.2), as well as elimination processes (Table 9.3).

To consider the influence of CAF on APAP pharmacokinetics [Renner et al., 2007; Iqbal et al., 1995], an inhibitory effect of CAF on CYP2E1-mediated NAPQI formation and on ABCB1-mediated active drug transport of APAP was mechanistically represented by incorporating competitive inhibition processes in

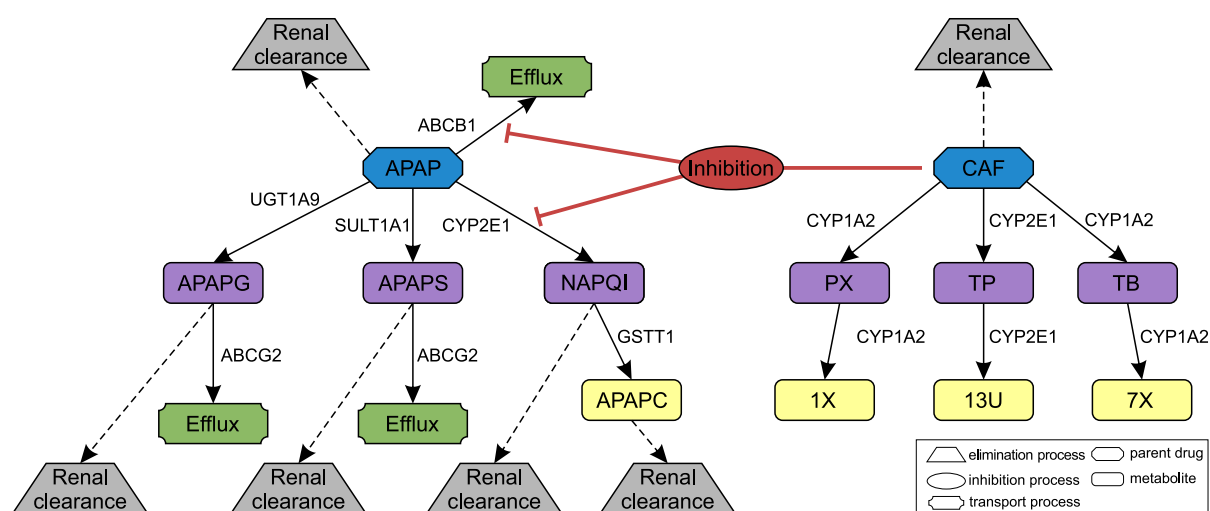


Figure 9.3: Reaction diagram of biochemical processes implemented in the PBPK models of acetaminophen and caffeine Reaction diagram of twenty-one biochemical processes implemented in the PBPK models of APAP and CAF illustrating active drug transport (green), metabolizing reactions for phase I (purple) and phase II (yellow) metabolites, kidney plasma clearance (gray), and inhibition processes (red). Metabolic enzymes and transporters are shown next to the respective reaction. APAPC, acetaminophen cysteine; APAPG, acetaminophen glucuronide; APAPS, acetaminophen sulfate; NAPQI, N-acetyl-p-benzoquinoneimine; CAF, caffeine; PX, paraxanthine; TB, theobromine; TP, theophylline; 13U, 1,3,dimethyluric acid; 7X, 7-methylxanthine; 1X, 1-methylxanthine.

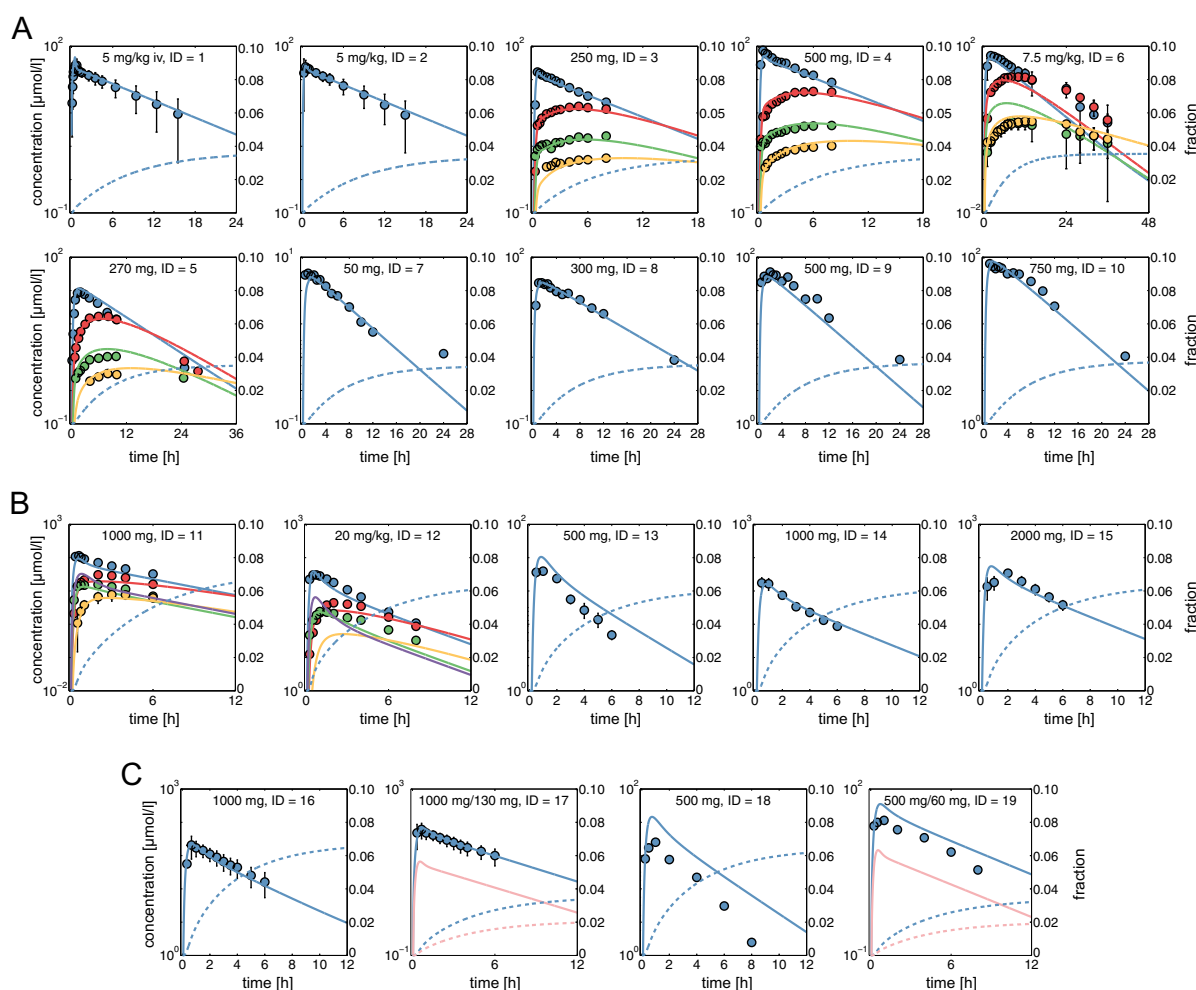


Figure 9.4: PBPK models of acetaminophen and caffeine. Simulated drug concentration-time curves (lines) were assessed with experimental PK profiles (circles). Renal excretion rates were additionally simulated for APAP and CAF (dashed lines). Study IDs and dose levels of the experimental data are shown within each plot (Table 9.4). (A) PBPK model of CAF (CAF, blue; PX, red; TB, green; TP, yellow). (B) PBPK model of APAP (APAP, blue; APAPG, red; APAPC, green; APAPS, yellow; NAPQI, purple). (C) PBPK model for single administration of APAP and for co-administration of APAP and CAF (APAP, blue; CAF, pink).

the developed PBPK models [Nouchi et al., 1986; Lee et al., 1991; Wishart et al., 2006; Gu et al., 1992]. Notably, PK simulations following co-administration of APAP and CAF at toxic dose levels resulted in a decrease of NAPQI concentrations in plasma (Figure 9.6), which is in accordance with experimental observations obtained in rat liver microsomes [Lee et al., 1991].

After model establishment, the simulated drug concentrations in plasma showed an excellent agreement with in vivo PK data for both single doses of CAF and APAP alone as well as for concomitant administration of both drugs (Figure 9.4, Figure 9.5, Table D.2). The relative contribution of phase I CYP isoforms versus phase II enzymes in the PBPK models of APAP and CAF was 70:30, and 100:0, respectively (Figure 9.4). The established reference PBPK models were validated for additional doses and individual subgroups by using clinical PK data from different studies not used for developing the reference PBPK models [Lelo et al., 1986; Tang-Liu et al., 1983; Newton et al., 1981; Prescott, 1980; Rawlins et al., 1977; Iqbal et al., 1995]. Note that all model parameters were left unchanged in this validation step except study parameters specifying the design of the clinical trials. Importantly, the validated PBPK models allow accurate predictions for different doses, since potential non-linearities in ADME processes [Kaplan et al., 1997; Sahajwalla and Ayres, 1991] are implicitly considered through the underlying model structure.

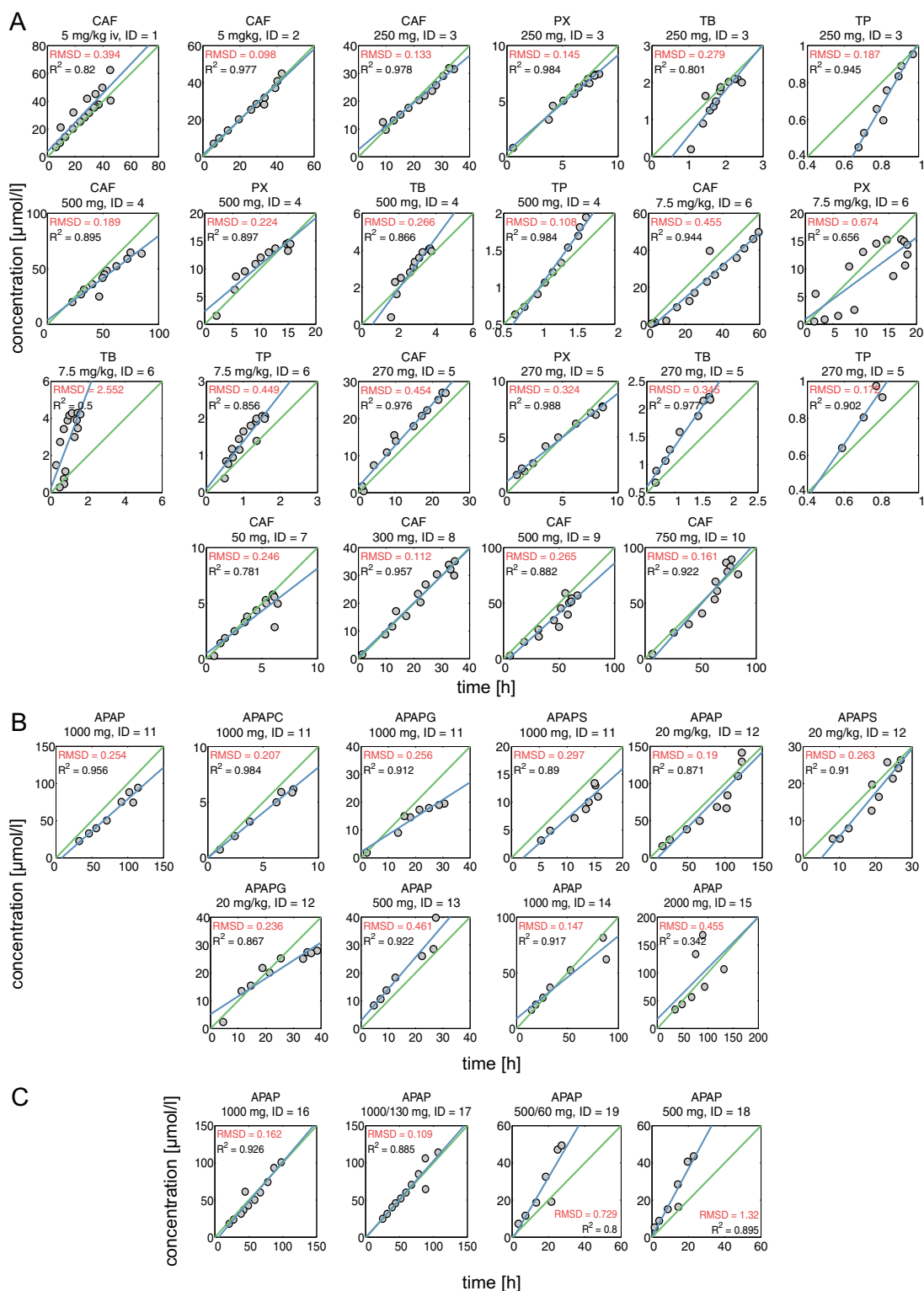
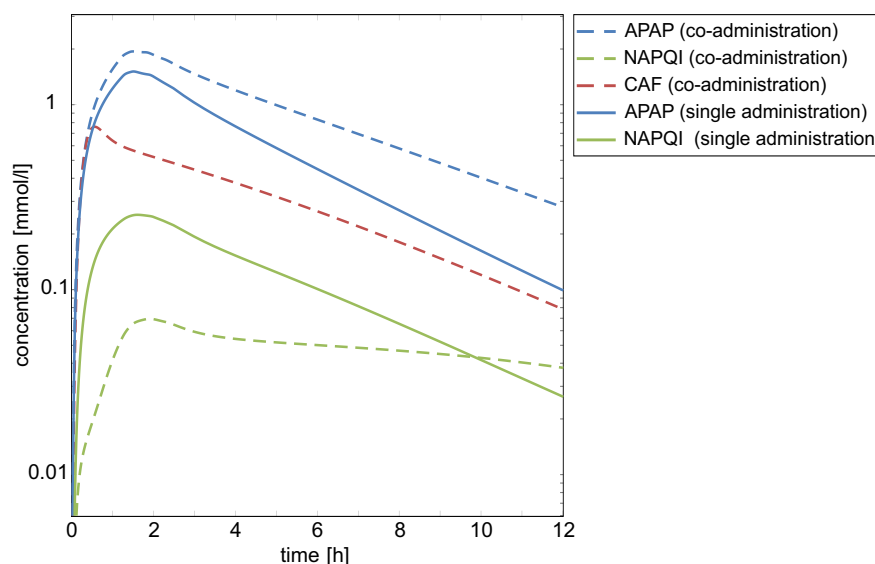


Figure 9.5: PBPK model assessment. Observed vs. predicted plots, RMSD and R^2 values determined by comparing experimental PK data with simulated drug concentration-time profiles. Study IDs and dose levels of the experimental data are shown within each plot (Table 9.4). (A) PBPK model of CAF. (B) PBPK model of APAP. (C) PBPK model for single administration of APAP and for co-administration of APAP with CAF.

The validated PBPK models were next used in the application of PICD to predict PD responses induced by single administration of APAP alone as well as by co-administration of APAP and CAF. Note that the PD response is here based on transcriptome data from Open TG-GATEs [Igarashi et al., 2015].

Figure 9.6: Simulated plasma concentrations for single administration of acetaminophen and co-administration of caffeine. Plasma concentrations were simulated for APAP (blue) and NAPQI (green) following a single toxic dose of APAP (solid lines) and a co-administered dose (dashed lines) of APAP and CAF (red).



9.3.2 Analyzing pharmacodynamic responses induced by single administration of acetaminophen and by co-administration of caffeine

Drug-specific PD responses following oral administration of APAP and CAF were predicted at the cellular level to investigate acute hepatotoxicity induced by a single toxic dose of APAP and by a co-administered dose with CAF.

Relative PD effect values of CAF on APAP were therefore computed, which notably reflect both (i) the influence of CAF on the concentration-time course of APAP at the organism level represented by competitive inhibition processes of CAF on ABCB1- and CYP2E1-mediated transport and metabolism of APAP, respectively (PK interaction); (ii) the changed PD response of APAP at the cellular level implemented by additively contributing the PD response predicted for CAF (PD interaction).

A mean toxic dose of APAP (34 g) was identified in literature at a sub-lethal level [Clemenson et al., 2007; Hoofnagle et al., 2013], while the dose level of CAF (4.4 g) was derived from a relative dose ratio of 1000:130 according to therapeutic indications used in drug combination therapy [Renner et al., 2007; Palmer et al., 2010; Sawynok and Yaksh, 1993]. Note that APAP and CAF are frequently co-administered since CAF is supposed to enhance the analgesic effect of APAP [Renner et al., 2007; Palmer et al., 2010; Sawynok and Yaksh, 1993].

In the following, PD responses and relative PD effects induced by a single toxic dose of APAP and by a co-administered dose of CAF were analyzed for genes expressed differentially (absolute fold change > 1.5, Benjamini-Hochberg corrected $p < 0.01$) at 8 h and 24 h, and for key cellular processes significantly overrepresented (Benjamini-Hochberg corrected $p < 0.01$) at any timepoint. Note that these subsets were identified for both APAP and CAF.

Analysis of key cellular processes

Overall, the co-administration of CAF led to a statistically significant perturbation ($p < 0.01$, two-sample t-test) of all considered key cellular processes (Figure 9.7). Analyzing PD responses at 8 h following single administration of APAP revealed a substantial impact on cell cycle G1/S and G2/M checkpoint regulation as well as on liver necrosis, while a co-administration of CAF resulted in a significantly increased PD response of these cellular processes by about 22 %, 16 %, and 43 %, respectively (Figure 9.7). Note that an increased PD response of a key cellular process may result from both inhibition and activation of genes involved, since absolute log2 fold changes were considered for calculation purposes.

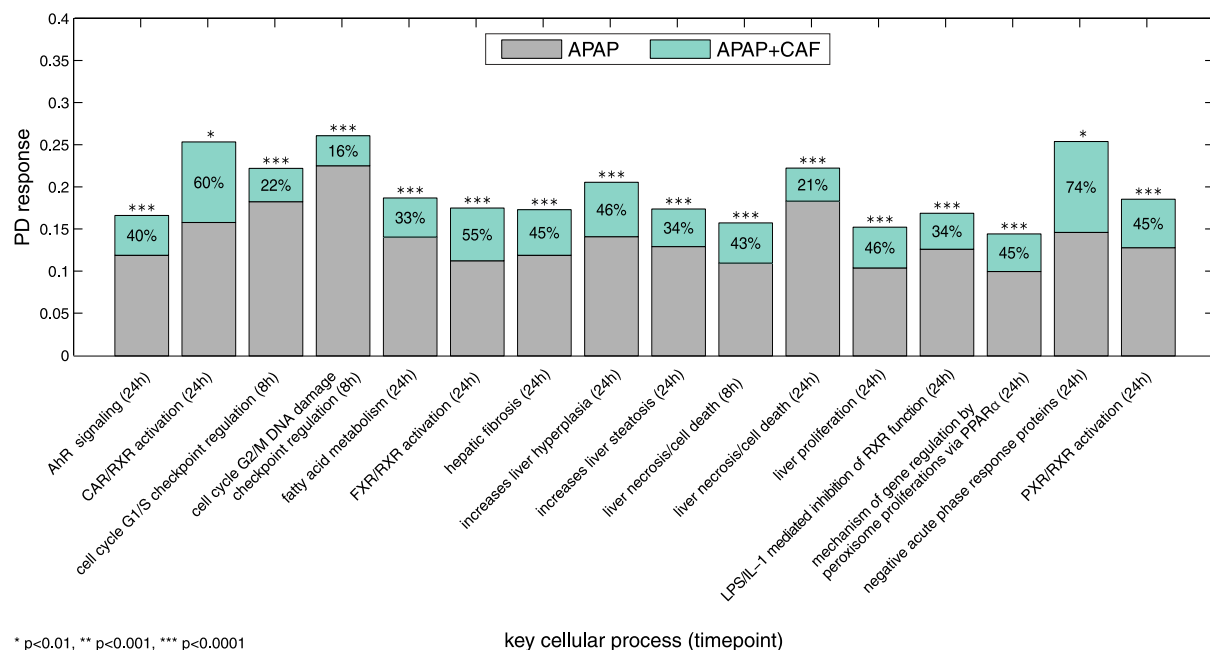


Figure 9.7: Pharmacodynamic response of key cellular processes. PD responses for significantly perturbed key cellular processes following drug administration of APAP as single toxic dose (gray) or co-administered with CAF (mint green). Percentages indicate relative PD effects of CAF.

At 24 h, high PD responses of APAP administered alone were found in particular for fatty acid metabolism, liver necrosis, as well as for the promotion of hepatic steatosis, and for negative acute phase response proteins (Figure 9.7). These key cellular processes were additionally affected by 33 %, 21 %, 34 %, and 74 %, respectively, due to the co-administration of CAF (Figure 9.7). Furthermore, the activation of CAR/RXR, FXR/RXR, and PXR/RXR heterodimers as well as the inhibition of the RXR function mediated by LPS and IL-1 were strongly perturbed by APAP and were further significantly induced by 60 %, 55 %, 45 % and 34 %, respectively, when CAF was given concomitantly (Figure 9.7). Moreover, a relative PD effect of about 45 % was observed for CAF on PD responses of APAP inducing hepatic fibrosis, liver proliferation, and liver hyperplasia at 24 h (Figure 9.7).

Analysis of individual genes

When analyzing the impact of single administration of APAP and co-administration together with CAF on individual genes, the analyzed genes were additionally subdivided into their corresponding functional classes to allow a functional interpretation. In this context, a positive and negative PD effect value means that CAF increases or reduces the PD responses of APAP at the cellular level.

Comparing the PD responses of APAP at both timepoints following single administration revealed both an increased inhibition and activation of individual genes after 8 h independently from the considered functional classes (Figure 9.8, Figure 9.9). Likewise, calculated PD effects of CAF showed only minor changes on significantly perturbed genes at 24 h in contrast to observations at 8 h (Figure 9.8, Figure 9.9).

At 8 h, APAP induced the inhibition of several genes belonging to different functional classes, among which the following were found to be noteworthy due to a substantial impact of one or both drugs: the kinases PBK, PCK1, and IP6K3 (Figure 9.8A); the cytokines TNFSF10 and CXCL6 (Figure 9.8B); the ligand-dependent nuclear receptor NR1H4 (Figure 9.8C); the ion channel KCNJ8 and the transporter SLC38A4 (Figure 9.8D); the metabolic enzymes GPAM, and TAT (Figure 9.8E); the transcription factor ATOH8 (Figure 9.8F); CDC20, and RTP3 (Figure 9.9). On the other hand, a few genes were highly

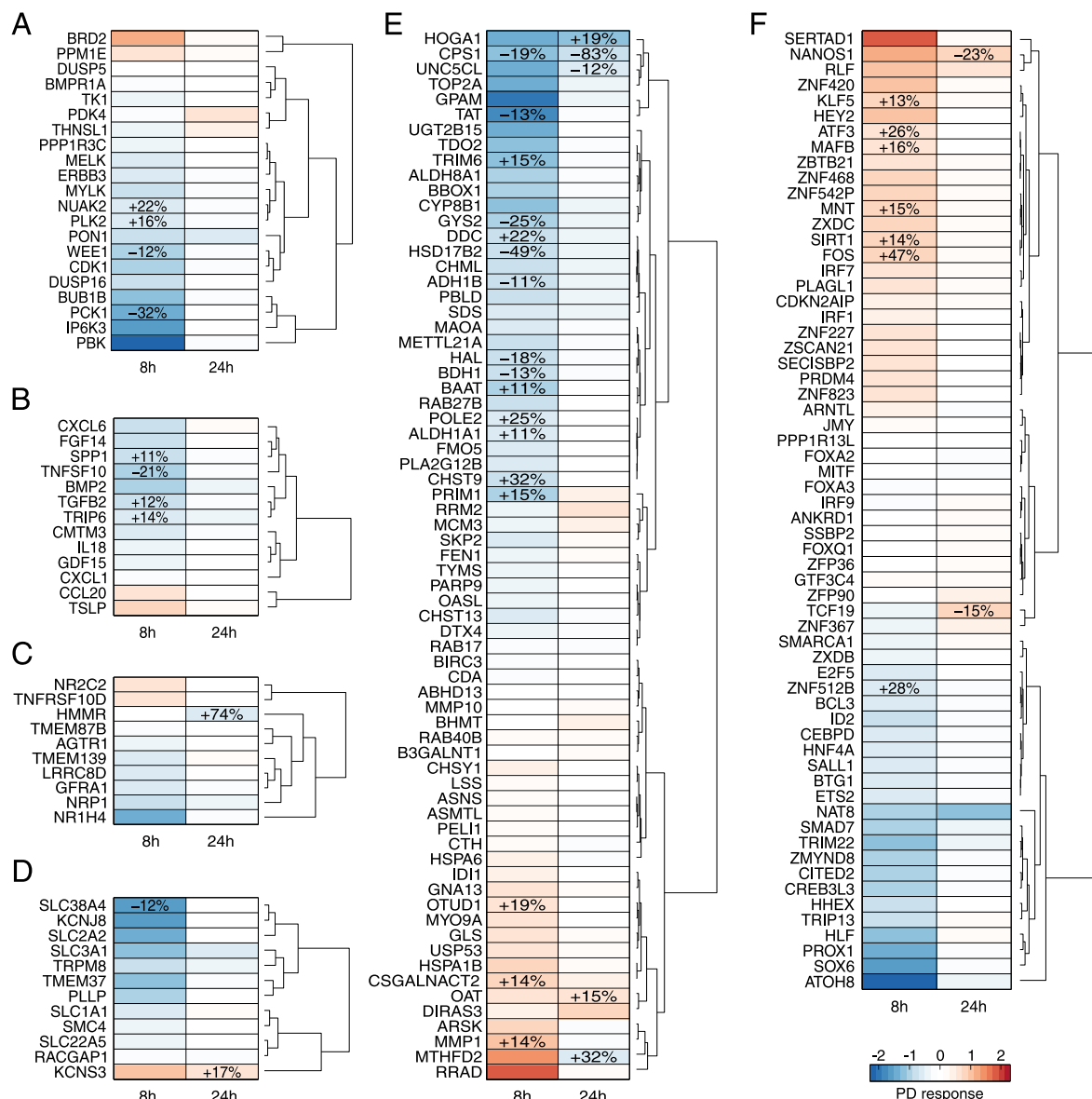
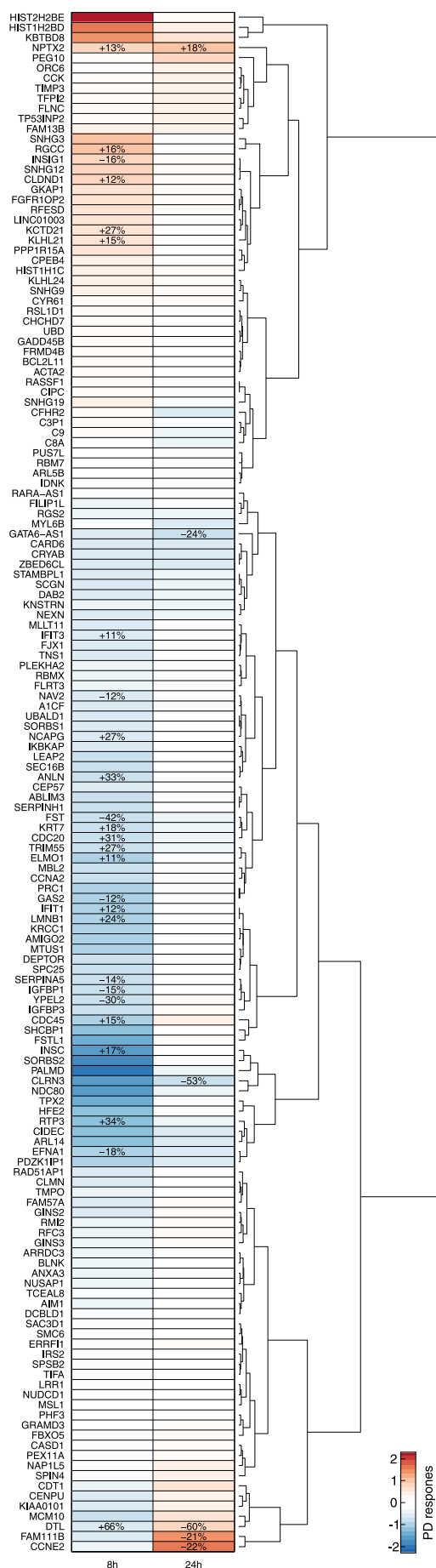


Figure 9.8: Pharmacodynamic response of individual genes. PD responses of significantly perturbed genes following drug administration of APAP as single toxic dose and correspondent PD effects induced by co-administration of CAF. Genes were classified according to their functional classes. Relative PD effect values indicated by percentages were only shown for highly regulated genes (absolute fold change > 1.5 and absolute relative PD effect > 10 %). (A) Kinase/phosphatase. (B) Cytokine/growth factor. (C) Receptor. (D) Ion channel/transporter. (E) Metabolic enzyme. (F) Transcription/translation regulator.

activated, for instance the kinase BRD2 (Figure 9.8A), the metabolic enzymes MMP1, MTHFD2 and RRAD (Figure 9.8E), the transcription regulator FOS, and SERTAD1 (Figure 9.8F), as well as the histone cluster HIST2H2BE and HIST1H2BD (Figure 9.9). At 24 h, only a few genes were substantially activated or inhibited by APAP, such as the kinase PDK4 (Figure 9.8A), the receptor HMMR (Figure 9.8C), the ion channel KCNS3 (Figure 9.8D), the metabolic enzymes HOGA1, CPS1, and MTHFD2 (Figure 9.8E), the transcription regulators TCF19 (Figure 9.8F), as well as Cyclin E2 (Figure 9.9). Analyzing PD effects of CAF on APAP elucidated both a reduced inhibitory effect (21-83 %) of APAP on specific genes such as TNFSF10, PCK1, CPS1, GYS2, HSD17B2, FST, and CLRN3 as well as an enhanced inhibitory effect (19-74 %) on other genes such as NUKA2, HMMR, HOGA1, DDC, CHST9, ZNF512B, RTP3, and CDC20 (Figure 9.8, and Figure 9.9). The activation of APAP on individual genes was mostly potentiated by CAF particularly on FOS and ATF3 by 47 % and 26 %, respectively (Figure 9.8F).

Figure 9.9: Pharmacodynamic response of additional individual genes. Pharmacodynamic response of significantly perturbed genes following drug administration of APAP as single toxic dose and correspondent PD effects induced by co-administration of CAF. Genes were classified into the functional class 'other'. Relative PD effect values indicated by percentages were only shown for highly regulated genes (absolute fold change > 1.5 and absolute relative PD effect > 10 %).



In this gene-level analysis, PD responses of significantly perturbed genes induced by a single toxic dose of APAP and the corresponding PD effects provoked by a co-administration of CAF were analyzed. Besides the identification of genes crucially affected by APAP, inhibitory and stimulatory effects of CAF on APAP were thereby investigated.

9.3.3 Dose escalation study – Transition from therapeutic to toxic conditions

In the dose escalation study, an exemplary set of genes (at 8 h: ATF3, PCK1, TNFSF10, SLC38A4, HSD17B2, FOS, and ZNF512B; at 24 h: HMMR, KCNS3, CPS1, CCNE2, and CDC20; at both time-points: DTL) and key cellular processes (at 8 h: regulation of cell cycle G1/S and G2/M DNA damage checkpoint; at 24 h: activation of CAR/RXR heterodimer, and liver hyperplasia) were next analyzed, which were substantially affected by a single toxic dose of APAP and by a co-administered dose of CAF (Figure 9.8, and Figure 9.9). The dose escalation study was performed on these genes and key cellular processes to quantitatively explore the transition from desired therapeutic effects to undesired toxic events (Figure 9.10). In this regard, the initial therapeutic dose was stepwise increased by 1000 mg until the considered toxic dose level was reached thereby simultaneously monitoring PD responses following single administration of APAP and its co-administration with CAF.

Analyzing dose-response curves for single genes revealed that the co-administration of CAF at high doses near the toxic range resulted in the strongest impact on PD responses of APAP, as expected, in comparison to doses around the therapeutic range (Figure 9.10A). However, opposing PD effects of CAF were observed with regard to diminishing or enhancing the regulatory effects of APAP. The up- or down-regulations of the kinase PCK1, the dehydrogenase HSD17B2, the synthase CPS1, or cyclin E2, which were strongly induced by high doses of APAP, were attenuated by co-administration of CAF. In contrast, perturbations of APAP on the transcription regulator FOS, ATF3 and ZNF512B, the transmembrane receptor HMMR, or CDC20 were obviously increased by CAF (Figure 9.10A). Interestingly, studying PD effects of CAF on DTL, which is involved in the detection of DNA damage and repair mechanisms,

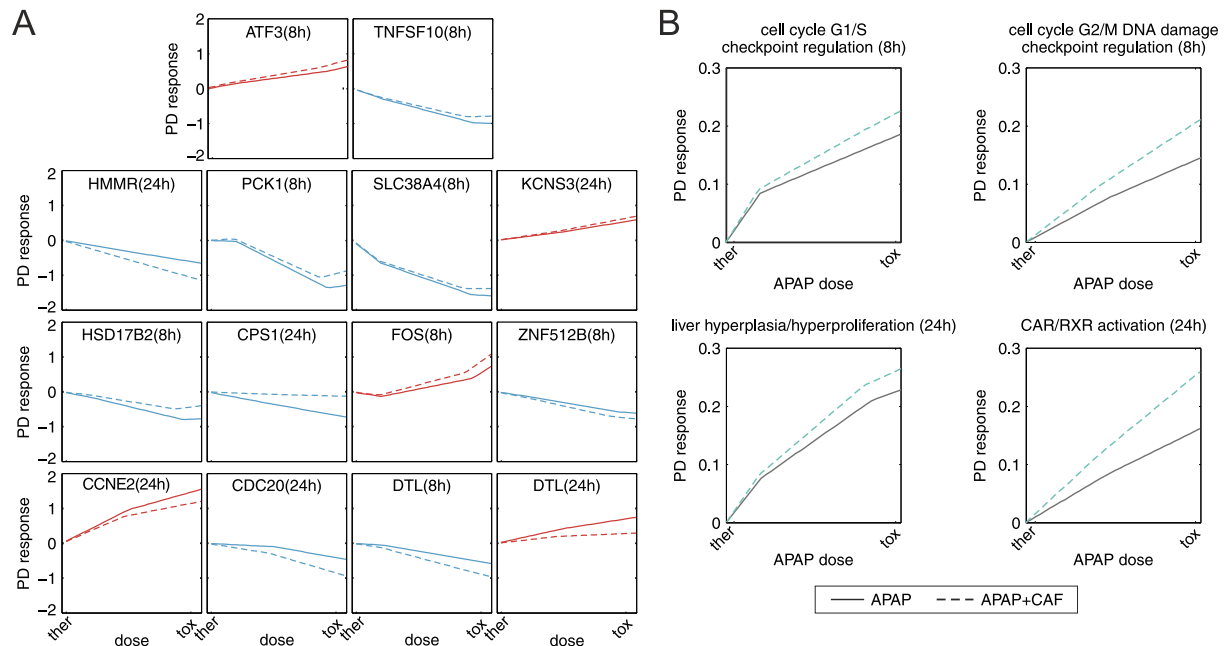


Figure 9.10: Dose escalation study. PD responses were predicted following single administration of APAP (solid lines) and co-administration of APAP and CAF (dashed lines). The doses were stepwise increased from therapeutic to toxic dose levels. (A) Individual genes. (B) Key cellular processes.

elucidated an enhanced inhibitory effect of APAP at 8 h, while the up-regulation at 24 h was rigorously reduced (Figure 9.10A).

Next, dose-response curves for an exemplary set of four key cellular processes were analyzed (Figure 9.10B). During the escalation from therapeutic to toxic doses a high perturbation of APAP on the cell cycle checkpoints G1/S and G2/M was observed at 8h, which was additionally increased due to a co-administration of CAF (Figure 9.10B). At 24 h, gradually increasing the therapeutic to the toxic dose led to a significant perturbation of APAP on genes associated with an increased hyperplasia of the liver and with the activation of the CAR/RXR heterodimer that transcriptionally activates the promoters of CYP2B and CYP3A gene expression (Figure 9.10B) [Chen et al., 2010]. Moreover, these key cellular processes were additionally affected when both drugs were administered concomitantly (Figure 9.10B). This dose escalation study allows the simultaneous investigation of cellular perturbations induced by single administration of APAP or co-administration with CAF to quantitatively describe drug-induced changes in clinically relevant situations, which hence may have important implications for dose decisions in the future.

9.3.4 Investigating the effect of caffeine on the analgesic action of acetaminophen under therapeutic conditions

From a therapeutic perspective, CAF is expected to increase the analgesic effect of APAP in humans [Renner et al., 2007; Palmer et al., 2010; Sawynok and Yaksh, 1993]. To explore this effect in our model, PD responses on pain-related genes [Foulkes and Wood, 2008] were predicted for single- and co-administration of APAP and CAF, respectively, by applying dose levels up to a maximum daily dose (APAP: 4000 mg, Drugs.com; APAP/CAF: 4000 mg/520 mg, [Renner et al., 2007]) (Figure 9.11). Here, CAF showed a slight but significant effect on the PD response of APAP on pain-related genes, particularly at 8 h (Figure 9.11A). Note that the therapeutic PD response was here analogously calculated as before for the key cellular processes (mean absolute log2 fold change of all involved genes).

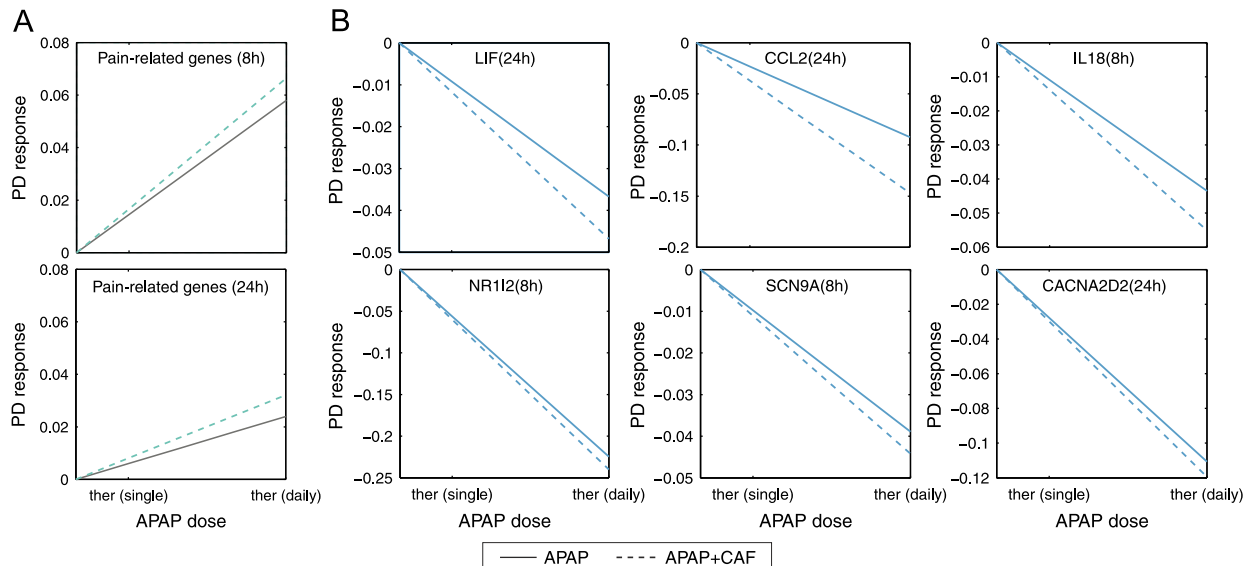


Figure 9.11: Pharmacodynamic response of genes associated to pain. PD response of genes associated to pain were predicted following single administration of APAP (solid lines) and co-administration of APAP and CAF (dashed lines). The doses were stepwise increased from a therapeutic single dose to the maximum daily dose. (A) Pharmacodynamic response of a set of pain-related genes. (B) PD response of individual genes involved in pain modulation as well as in pain conduction & synaptic transmission.

PD responses were further investigated for an exemplary set of six genes (LIF, CCL2, IL18, NR1I2, SCN9A, CACNA2D2), which are involved in pain modulation as well as in pain conduction and synaptic transmission. It was found that CAF slightly enhances the inhibitory effect of APAP on these pain-related genes (Figure 9.11B). Interestingly, the effect of CAF at 24 h was most prominent on the chemokine CCL2 that is supposed to mediate the activation of pain pathways [Foulkes and Wood, 2008].

9.4 Discussion

In this article, the impact of CAF on APAP-induced hepatotoxicity was investigated at patient level by evaluating the effects of CAF on the PK and PD behavior of APAP induced by co-medication of both drugs.

A mean toxic dose level of APAP was identified by collecting non-fatal toxic doses from public databases [Hoofnagle et al., 2013; Clemenson et al., 2007]. The co-administered dose of CAF was selected according to relative dose ratios applied in combination therapy [Renner et al., 2007; Palmer et al., 2010], and was found to be in the lower range of clinical observations about sub-lethal acute poisoning [Clemenson et al., 2007] indicating a low toxic potential caused by the single dose of CAF. Hence, the *in vivo* doses used here reflect clinically relevant situations for which toxic events were observed.

Drug interaction processes between CAF and APAP were considered in the PBPK models by incorporating competitive inhibition in ADME-related processes to reflect the inhibitory effect of CAF on ABCB1-mediated active transport of APAP, and on CYP2E1-mediated metabolism of APAP to NAPQI, respectively (Figure 9.3) [Wishart et al., 2006]. APAP-induced hepatotoxicity may occur due to an accumulation of NAPQI [Jaw and Jeffery, 1993]. Here, simulations of NAPQI concentrations were significantly decreased when both drugs were administered concomitantly (Figure 9.6), which is in accordance to experimental observations from rat liver microsomes [Lee et al., 1991]. This might indicate a favourable effect of the co-administration of CAF for the reduction of acute liver failure induced by extensive exposure of APAP.

Several ADME processes were further included in the PBPK models of APAP and CAF to describe the processes governing a drug PK with a high level of detail (Figure 9.3, Figure 9.4). The PBPK models were carefully validated and showed excellent agreement with experimental data from literature obtained for different dosage regimens in human clinical studies [Blanchard and Sawers, 1983; Kaplan et al., 1997; Lelo et al., 1986; Tang-Liu et al., 1983; Newton et al., 1981; Shinoda et al., 2007; Renner et al., 2007; Prescott, 1980; Rawlins et al., 1977; Iqbal et al., 1995]. (Figure 9.4, Figure 9.5, Table D.2). This validation step ensures reliable predictions of PK profiles following drug administration of doses ranging from therapeutic to toxic levels.

The previously established multiscale approach PICD allows a quantitative description of drug-induced toxicity at patient level [Thiel et al., 2016] (Figure 9.1) by coupling whole-body PBPK models (Figure 9.4) with *in vitro* toxicity data from Open TG-GATEs [Igarashi et al., 2015], an exceptional large-scale toxicogenomics database. In this study, PD responses were analyzed at 8 h and 24 h since *in vitro* response data for CAF had only been measured at these timepoints [Igarashi et al., 2015]. Although estimating PD responses induced by multiple dosing would also be very interesting, only single drug administration was here considered since no adequate *in vitro* response data for repeated dosing was available [Igarashi et al., 2015]. Instead of using time-resolved gene expression profiles to represent PD responses at the cellular level, PICD also allows contextualizing *in vitro* drug response data obtained at different omics levels like proteomics or metabolomics, as well as incorporating other functional or clinical endpoints.

Here, PICD was applied for single administration of APAP and CAF, respectively, as well as for co-administration of both drugs. To predict PD responses of APAP in combination therapy with CAF,

both the PK and PD interaction of CAF were considered: (i) the implemented competitive inhibition processes of CAF led to an altered PK profile of APAP and consequently to a changed PD response when applying PICD (PK interaction); (ii) the predicted PD response of CAF was added separately to the PD responses of APAP (PD interaction). Although the co-administration of different drugs may lead not only to additive drug effects but also to synergistic or antagonistic effects, an additive PD response model was used since no adequate *in vitro* data was available to identify or differentiate potential synergism or antagonism.

PD responses of APAP and correspondent PD effects of CAF were evaluated for single genes and key cellular processes, which were significantly affected by both drugs. Amongst other things, it was found that a single toxic dose of APAP highly affected the G1/S and G2/M DNA damage checkpoint of the cell cycle at 8 h, which was further increased by the co-administration of CAF (Figure 9.7). At 24 h, CAF strongly enhanced the effect of APAP on heterodimerization of the receptors CAR and RXR, which transcriptionally induce the expression of P450 enzymes, as well as bilirubin and thyroid hormone metabolism (Figure 9.7). The transcription regulator FOS was substantially upregulated at 8h by a single dose administration of APAP (Figure 9.8F). This observation is in agreement with earlier experimental results where FOS expression was induced by APAP in MCF-7 breast cancer cells [Gadd et al., 2002]. Moreover, the PD effect of CAF revealed an enhancement on the activation of FOS, which may potentiate the APAP-induced hepatotoxicity, since FOS seems to favour the development of toxic events [Fernandez et al., 2005; Gillardon et al., 1996].

The validated PBPK models and the generic application of PICD here allowed considering drug interactions between APAP and CAF and monitoring PD responses induced by single or co-administration of several doses. In the dose escalation study, the therapeutic dose was stepwise increased until the considered toxic dose was reached thereby investigating the transition from desired drug effects to adverse events. The predicted dose-response curves provided insights into the inhibitory or stimulatory effects of APAP and enabled to check whether these regulatory effects were enhanced or diminished by co-administration of CAF. For DTL, which supports the detection of DNA damage and repair, an increased and decreased impact of CAF on the inhibitory and stimulatory effect of APAP was found at 8 h and 24 h, respectively (Figure 9.10A). This might indicate a potentiation of the APAP-induced hepatotoxicity, since DTL plays an essential role in the detection of DNA damage. However, a potential reduction of the toxicity caused by APAP would also be possible, because a decreased expression of DTL might also be related to a reduced DNA damage after drug exposure within the cell.

In a further dose escalation study, the effect of CAF on the analgesic action on APAP was investigated under therapeutic conditions. It was found that CAF slightly enhances the inhibitory effects of APAP on genes involved in pain perception and modulation (Figure 9.11). These results may explain the observed increase in the clinical efficacy of APAP at the cellular scale induced by co-administration of CAF [Renner et al., 2007; Palmer et al., 2010; Sawynok and Yaksh, 1993].

In conclusion, the impact of CAF on APAP-induced hepatotoxicity was here investigated in humans by simultaneously considering drug effects of CAF on APAP at both the PK and the PD level. It was shown that CAF has a significant effect on APAP-induced hepatotoxicity due to a co-administration of both drugs. Key results demonstrate, on the one hand, that CAF might favour a reduction of APAP-induced hepatotoxicity in humans at the PK and the PD level by reducing the concentrations of NAPQI, which is supposed to be the reactive metabolite of APAP [Walubo et al., 2004], as well as by positively regulating genes playing an essential role in the development of toxicity, respectively. On the other hand, CAF might also potentiate APAP-induced toxicity by affecting crucial genes such as FOS that may support the activation of cell death pathways.

Although key outcomes of the study demonstrated inhibitory and stimulatory effects of CAF on APAP, the question if CAF potentiates or diminishes the hepatotoxicity caused by extensive exposure of APAP partly remains open. To adequately address this question, more *in vitro* data would be required such as measurements of other omics levels like proteomics or metabolomics, as well as *in vitro* response data obtained in an appropriate cell system after simultaneous exposure to multiple drugs. This would obviously help to improve the understanding of the molecular mechanisms following co-administration of APAP and CAF, and would clearly facilitate to discover potential synergistic or antagonistic drug effects. As presented here, dose escalation studies might further enhance the development of safe and efficient dosage regimens in drug combination therapy. Moreover, the concept used to consider DDIs at the PK and PD level is generically applicable for different drug combinations in clinically relevant situations. Hence, this might help to explore the PK and PD interactions caused by drug combination therapies at patient level and, thus, may improve patient safety in clinical practice.

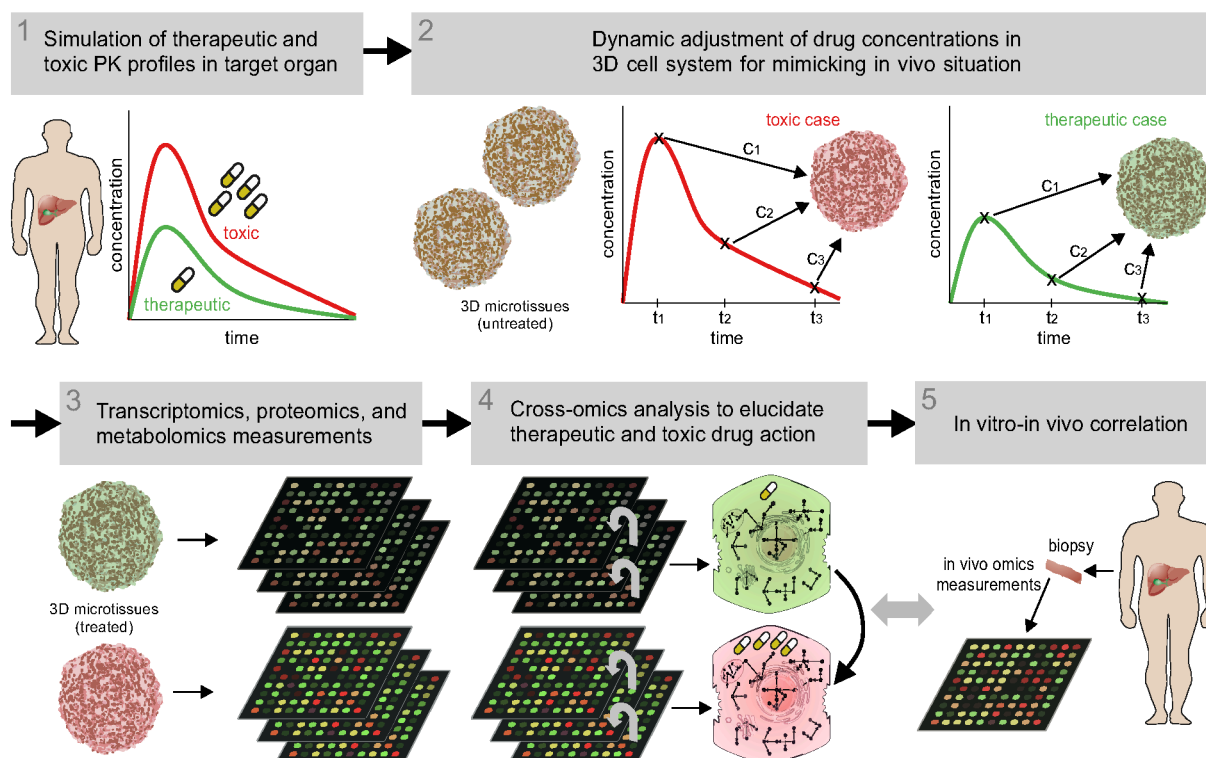
General conclusions and outlook

The benefit of multiscale modeling of drug-induced toxicity in humans was considered in the presented thesis. The integrative multiscale approach PICD was developed that integrates in vitro toxicity data, at the cellular level, into drug-specific whole-body PBPK models, at the organism level (Chapter 7) [Thiel et al., 2016]. In vitro toxicity data from Open-TG GATEs, a large-scale transcriptomics database [Igarashi et al., 2015], were therefore analyzed, and drug-specific whole-body PBPK models were developed and validated with human clinical data. The developed multiscale approach was then used in three different studies:

- (i) PICD was applied in a proof-of-principle study on the hepatotoxicant azathioprine to analyze drug-induced toxicity caused by different dosage regimens in humans. Changes in cellular events induced by therapeutic or toxic dose levels could be thereby evaluated (Chapter 7) [Thiel et al., 2016].
- (ii) PICD was applied in a comparative analysis of drug-induced hepatotoxicity for fifteen drugs in the face of therapeutic and toxic drug administration in humans (Chapter 8) [Thiel et al., 2017a].
- (iii) PICD was used to explore drug interactions between acetaminophen and caffeine at patient level. The simultaneous consideration of drug effects at the PK and the PD level allowed studying the impact of caffeine on acetaminophen-induced hepatotoxicity during co-medication with caffeine in humans (Chapter 9) [Thiel et al., 2017b].

The multiscale approach PICD aims for a detailed representation of cellular changes over time following drug administration in vivo and provides a generic platform to investigate in vitro measurements of different omics studies within a patient context. The use of PICD, thus, facilitates in vitro-to-in vivo extrapolations (IVIVE) and supports clinical translations. Since PICD is an in silico-based approach, its application also allows an animal-free assessment of drug-induced toxicity, which is fully in line with 3R principles (replacement, reduction, and refinement) [Kroeger, 2006]. A potential application of PICD on laboratory animals might further enhance the early detection of adverse drug reactions in an in vivo situation. The identification of non-toxic dose levels might be, hence, improved under the assumption that appropriate in vitro toxicity assays were conducted during drug development.

The use of PICD for humans might facilitate the investigation of in vitro findings at patient level for clinical applications in future as shown in the three presented studies (Chapter 7, 8, and 9) [Thiel et al., 2016, 2017a,b]. In the comparative toxicity analysis, the hepatotoxic potential of a set of fifteen known hepatotoxicants was evaluated and compared by predicting toxic changes reflecting the transition from therapeutic drug response to unwanted adverse reactions. Therefore, clinically relevant situations describing oral drug administration in humans could be mimicked and further assessed to explore drug effects between therapeutic and toxic conditions and finally to discover molecular biomarkers and potential DDIs. This might improve clinical risk assessment and patient safety during the drug development process (Figure 1.1). Furthermore, the performed dose escalation studies for single and co-administration of acetaminophen and caffeine might amend the identification of safe and efficient doses in drug combination therapy. Moreover, the presented concept of using PICD to consider drug interactions at both, the PK



Perspective Figure: A potential workflow of a comprehensive systems toxicology study in future. In a first step, drug concentration-time profiles would be simulated for therapeutic and toxic doses in the interstitial space of a target organ such as the liver. To reflect the pharmacokinetic behavior of the compound of interest, a dynamic adjustment of concentrations exposed to 3D microtissues might be performed. Omics measurement at different timepoints could be obtained by applying different technologies such as transcriptomics, proteomics, or metabolomics. The dynamic dose-response curves of genes, proteins and metabolites might be related by an advanced cross-omics analysis to elucidate therapeutic and toxic mode of actions. Such findings might be validated by comparisons to in vivo measurements gathered in liver biopsies.

and PD level is generically applicable for various drug combinations in clinically relevant situations. This might facilitate the analysis of PK and PD interactions caused by drug combination therapies within a patient context and, thus, may also enhance patient safety in clinical practice.

Key outcomes of the thesis have demonstrated the benefits of coupling cellular in vitro drug response data with drug concentration-time profiles to determine dose-response relationships at patient level. In this respect, accurate predictions of potential drug-induced toxicity events are indispensable in clinical risk assessment to guarantee patient safety in first-in-human trials and in following clinical phases of drug development. In future studies, however, a direct integration of simulated animal or human pharmacokinetic profiles in the in vitro assay design might represent a situation that is closer to the actual in vivo case (Perspective Figure).

In this thesis, transcriptomic-based drug response data was successfully analyzed within a human context to get insights into drug-induced cellular perturbations at the transcriptional level. Understanding toxic events induced by extensive drug exposure at a systems level, however, requires a better understanding of the dynamic interplay between genes, proteins, and metabolites, as well as robust correlations of such temporal molecular signatures with physiological outcomes associated with a specific disease. This requires, inter alia, the application of more omics technologies (e.g., proteomics, and metabolomics) covering a long period of time to improve the understanding of the dynamic mechanisms underlying drug-induced toxicity (Perspective Figure).

Three-dimensional (3D) cell culture systems are very interesting in drug discovery since these systems provide a lot of physiological and predictive data for in vivo testing [Edmondson et al., 2014]. 3D microtissues consist of multiple cells that reflect a small part of an organ or tissue and are developed in such a way that their functionality and morphology is as close as possible to the native environment. In vitro experiments, in which therapeutic and toxic drug concentrations are exposed to 3D microtissues, may thus outperform in vitro tests conducted in standard two-dimensional (2D) monolayer cell cultures in terms of representing an organotypic in vivo-like environment (Perspective Figure).

Combined applications of different omics technologies applied for 3D cell culture systems that include drug concentrations over time might be very useful to perform valuable cross-omics analyses taking into account in vivo pharmacokinetics. This would clearly help to elucidate and predict the molecular mechanisms underlying adverse drug reactions with a high level of detail following drug administration in humans (Perspective Figure). In vitro-to-in vivo correlations might ultimately ensure a high accordance to the in vivo situation, whereby potential modes of action or toxicity might be validated with in vivo data from biopsies. Overall, such comprehensive experiments and analyses may significantly improve animal and patient safety in future approaches applied in drug development.

To conclude, in this thesis multiscale modeling was successfully applied to study drug-induced toxicity in humans [Thiel et al., 2016, 2017a,b]. The presented results demonstrate advances in translational medicine by contextualizing in vitro toxicity data into a patient situation. This might improve patient safety in future drug development.

References

- Aberra, F. N. and Lichtenstein, G. R. (2005). Review article: Monitoring of immunomodulators in inflammatory bowel disease. *Alimentary Pharmacology and Therapeutics*, 21(4):307–319.
- Acocella, G. (1978). Clinical pharmacokinetics of rifampicin. *Clinical Pharmacokinetics*, 3(2):108–127.
- Adjei, A. A., Gaedigk, A., Simon, S. D., Weinshilboum, R. M., and Leeder, J. S. (2008). Interindividual variability in acetaminophen sulfation by human fetal liver: implications for pharmacogenetic investigations of drug-induced birth defects. *Birth Defects Research*, 82(3):155–65.
- Agoram, B., Woltosz, W. S., and Bolger, M. B. (2001). Predicting the impact of physiological and biochemical processes on oral drug bioavailability. *Advanced Drug Delivery Reviews*, 50 Suppl 1:S41–67.
- Aguiar Bujanda, D., Cabrera Suárez, M. Á. A., Bohn Sarmiento, U., and Aguiar Morales, J. (2006). Successful recovery after accidental overdose of cyclophosphamide. *Annals of Oncology*, 17(8):1334.
- Andrade, R. J., Lucena, M. I., Fernández, M. C., Pelaez, G., Pachkoria, K., García-Ruiz, E., García-Muñoz, B., González-Grande, R., Pizarro, A., Durán, J. A., Jiménez, M., Rodrigo, L., Romero-Gomez, M., Navarro, J. M., Planas, R., Costa, J., Borrás, A., Soler, A., Salmerón, J., and Martín-Vivaldi, R. (2005). Drug-induced liver injury: An analysis of 461 incidences submitted to the Spanish registry over a 10-year period. *Gastroenterology*, 129(2):512–521.
- Andreasen, F., Agerbaek, H., Bjerregaard, P., and Gøtzsche, H. (1981). Pharmacokinetics of amiodarone after intravenous and oral administration. *European Journal of Clinical Pharmacology*, 19(4):293–9.
- Anjum, Swan, Lambrecht, Radwanski, Cutler, Affrime, and Halstenson (2001). Pharmacokinetics of flutamide in patients with renal insufficiency. *British Journal of Clinical Pharmacology*, 47(1):43–47.
- Ashburner, M., Ball, C. A., Blake, J. A., Botstein, D., Butler, H., Cherry, J. M., Davis, A. P., Dolinski, K., Dwight, S. S., Eppig, J. T., Harris, M. A., Hill, D. P., Issel-Tarver, L., Kasarskis, A., Lewis, S., Matese, J. C., Richardson, J. E., Ringwald, M., Rubin, G. M., and Sherlock, G. (2000). Gene ontology: tool for the unification of biology. The Gene Ontology Consortium. *Nature Genetics*, 25(1):25–9.
- Askgaard, D. S., Wilcke, T., and Døssing, M. (1995). Hepatotoxicity caused by the combined action of isoniazid and rifampicin. *Thorax*, 50(2):213–4.
- Avent, K. M., DeVoss, J. J., and Gillam, E. M. J. (2006). Cytochrome P450-mediated metabolism of haloperidol and reduced haloperidol to pyridinium metabolites. *Chemical Research in Toxicology*, 19(7):914–920.
- Aweeka, F. T., Tomlanovich, S. J., Prueksaritanont, T., Gupta, S. K., and Benet, L. Z. (1994). Pharmacokinetics of orally and intravenously administered cyclosporine in pre-kidney transplant patients. *Journal of Clinical Pharmacology*, 34(1):60–7.

- Bailey, D. G., Malcolm, J., Arnold, O., and Spence, J. D. (1998). Grapefruit juice-drug interactions. *British Journal of Clinical Pharmacology*, 46(2):101–10.
- Barre, J., Mallat, A., Rosenbaum, J., Deforges, L., Houin, G., Dhumeaux, D., and Tillement, J. P. (1987). Pharmacokinetics of erythromycin in patients with severe cirrhosis. Respective influence of decreased serum binding and impaired liver metabolic capacity. *British Journal of Clinical Pharmacology*, 23(6):753–757.
- Barron, M. G., Stehly, G. R., and Hayton, W. L. (1990). Pharmacokinetic modeling in aquatic animals i. models and concepts. *Aquatic Toxicology*, 18(2):61–85.
- Ben-Shachar, R., Chen, Y., Luo, S., Hartman, C., Reed, M., and Nijhout, H. F. (2012). The biochemistry of acetaminophen hepatotoxicity and rescue: a mathematical model. *Theoretical Biology & Medical Modelling*, 9:55.
- Benet, L. Z. (2013). The role of BCS (biopharmaceutics classification system) and BDDCS (biopharmaceutics drug disposition classification system) in drug development. *Journal of Pharmaceutical Sciences*, 102(1):34–42.
- Benjamini, Y. and Hochberg, Y. (1995). Controlling the false discovery rate: A practical and powerful approach to multiple testing. *Journal of the Royal Statistical Society*, 57(1):289–300.
- Bento, A. P., Gaulton, A., Hersey, A., Bellis, L. J., Chambers, J., Davies, M., Krüger, F. A., Light, Y., Mak, L., McGlinchey, S., Nowotka, M., Papadatos, G., Santos, R., and Overington, J. P. (2014). The ChEMBL bioactivity database: an update. *Nucleic Acids Research*, 42(Database issue):D1083–90.
- Bergan, S., Rugstad, H. E., Bentdal, O., Endresen, L., and Stokke, O. (1994). Kinetics of mercaptopurine and thioguanine nucleotides in renal transplant recipients during azathioprine treatment. *Therapeutic Drug Monitoring*, 16(1):13–20.
- Bernal, W., Auzinger, G., Dhawan, A., and Wendon, J. (2010). Acute liver failure. *The Lancet*, 376(9736):190–201.
- Bhattacharya, S., Shoda, L. K. M., Zhang, Q., Woods, C. G., Howell, B. A., Siler, S. Q., Woodhead, J. L., Yang, Y., McMullen, P., Watkins, P. B., and Andersen, M. E. (2012). Modeling drug- and chemical-induced hepatotoxicity with systems biology approaches. *Frontiers in Physiology*, 3(462).
- Bialer, M., Hussein, Z., Raz, I., Abramsky, O., Herishanu, Y., and Pachys, F. (1985). Pharmacokinetics of valproic acid in volunteers after a single dose study. *Biopharmaceutics & Drug Disposition*, 6(1):33–42.
- Bigger, J. T. and Leahey, E. B. (1982). Quinidine and digoxin. An important interaction. *Drugs*, 24(3):229–39.
- Bing, C., Xiaomeia, C., and Jinhenga, L. (2011). Gene dose effect of NAT2 variants on the pharmacokinetics of isoniazid and acetylisoniazid in healthy Chinese subjects. *Drug Metabolism and Drug Interactions*, 26(3):113–8.
- Biomarkers Definitions Working Group. (2001). Biomarkers and surrogate endpoints: preferred definitions and conceptual framework. *Clinical Pharmacology and Therapeutics*, 69(3):89–95.
- Bissell, D. M., Gores, G. J., Laskin, D. L., and Hoofnagle, J. H. (2001). Drug-induced liver injury: mechanisms and test systems. *Hepatology*, 33(4):1009–1013.
- Björnsson, E. S. (2015). Drug-induced liver injury: an overview over the most critical compounds. *Archives of Toxicology*, 89(3):327–34.
- Blanchard, J. and Sawers, S. J. (1983). Comparative pharmacokinetics of caffeine in young and elderly men. *Journal of Pharmacokinetics and Biopharmaceutics*, 11(2):109–26.

- Boess, F., Kamber, M., Romer, S., Gasser, R., Muller, D., Albertini, S., and Suter, L. (2003). Gene expression in two hepatic cell lines, cultured primary hepatocytes, and liver slices compared to the in vivo liver gene expression in rats: Possible implications for toxicogenomics use of in vitro systems. *Toxicological Sciences*, 73(2):386–402.
- Bond, G. R. (2009). Acetaminophen protein adducts: A review. *Clinical Toxicology*, 47(1):2–7.
- Boréus, L. O., Jalling, B., and Kållberg, N. (1978). Phenobarbital metabolism in adults and in newborn infants. *Acta Paediatrica Scandinavica*, 67(2):193–200.
- Borgå, O., Hoppel, C., Odar-Cederlöf, I., and Garle, M. (1979). Plasma levels and renal excretion of phenytoin and its metabolites in patients with renal failure. *Clinical Pharmacology and Therapeutics*, 26(3):306–314.
- Bort, R., Macé, K., Boobis, A., Gómez-Lechón, M. J., Pfeifer, A., and Castell, J. (1999a). Hepatic metabolism of diclofenac: role of human CYP in the minor oxidative pathways. *Biochemical Pharmacology*, 58(5):787–96.
- Bort, R., Ponsoda, X., Jover, R., Gómez-Lechón, M. J., and Castell, J. V. (1999b). Diclofenac toxicity to hepatocytes: a role for drug metabolism in cell toxicity. *The Journal of Pharmacology and Experimental Therapeutics*, 288(1):65–72.
- Boxenbaum, H. G. and Riegelman, S. (1974). Determination of isoniazid and metabolites in biological fluids. *Journal of Pharmaceutical Sciences*, 63(8):1191–7.
- Brater, D. C. (2002). Measurement of renal function during drug development. *British Journal of Clinical Pharmacology*, 54(1):87–95.
- Brodie, B. B., Gillette, J. R., and La Du, B. N. (1958). Enzymatic metabolism of drugs and other foreign compounds. *Annual Review of Biochemistry*, 27(3):427–54.
- Brown, D. and Tomlin, M. (2010). *Pharmacology & Pharmacokinetics*. Competency-Based Critical Care. Springer London, London.
- Brynildsen, M. P. and Liao, J. C. (2009). An integrated network approach identifies the isobutanol response network of *Escherichia coli*. *Molecular Systems Biology*, 5(277):277.
- Bushel, P. R., Heinloth, A. N., Li, J., Huang, L., Chou, J. W., Boorman, G. A., Malarkey, D. E., Houle, C. D., Ward, S. M., Wilson, R. E., Fannin, R. D., Russo, M. W., Watkins, P. B., Tennant, R. W., and Paules, R. S. (2007). Blood gene expression signatures predict exposure levels. *Proceedings of the National Academy of Sciences of the United States of America*, 104(46):18211–6.
- Capone, D., Aiello, C., Santoro, G. A., Gentile, A., Stanziale, P., D'Alessandro, R., Imperatore, P., and Basile, V. (1996). Drug interaction between cyclosporine and two antimicrobial agents, josamycin and rifampicin, in organ-transplanted patients. *International Journal of Clinical Pharmacology Research*, 16(2-3):73–6.
- Carreras Puigvert, J., von Stechow, L., Siddappa, R., Pines, A., Bahjat, M., Haazen, L. C. J. M., Olsen, J. V., Vrieling, H., Meerman, J. H. N., Mullenders, L. H. F., van de Water, B., and Danen, E. H. J. (2013). Systems biology approach identifies the kinase Csnk1a1 as a regulator of the DNA damage response in embryonic stem cells. *Science Signaling*, 6(259):ra5.
- Cebola, I., Rodríguez-Seguí, S. a., Cho, C. H.-H., Bessa, J., Rovira, M., Luengo, M., Chhatriwala, M., Berry, A., Ponsa-Cobas, J., Maestro, M. A., Jennings, R. E., Pasquali, L., Morán, I., Castro, N., Hanley, N. a., Gomez-Skarmeta, J. L., Vallier, L., and Ferrer, J. (2015). TEAD and YAP regulate the enhancer network of human embryonic pancreatic progenitors. *Nature Cell Biology*, 17(5):615–626.

- Cerioti, F., Henny, J., Queralto, J., Ziyu, S., Özarda, Y., Chen, B., Boyd, J. C., and Panteghini, M. (2010). Common reference intervals for aspartate aminotransferase (AST), alanine aminotransferase (ALT) and γ -glutamyl transferase (GGT) in serum: Results from an IFCC multicenter study. *Clinical Chemistry and Laboratory Medicine*, 48(11):1593–1601.
- Chen, J. and Raymond, K. (2006). Roles of rifampicin in drug-drug interactions: underlying molecular mechanisms involving the nuclear pregnane X receptor. *Annals of Clinical Microbiology and Antimicrobials*, 5(1):3.
- Chen, M., Vijay, V., Shi, Q., Liu, Z., Fang, H., and Tong, W. (2011). FDA-approved drug labeling for the study of drug-induced liver injury. *Drug Discovery Today*, 16(15-16):697–703.
- Chen, M., Zhang, M., Borlak, J., and Tong, W. (2012). A decade of toxicogenomic research and its contribution to toxicological science. *Toxicological Sciences*, 130(2):217–228.
- Chen, S., Wang, K., and Wan, Y.-j. Y. (2010). Retinoids activate RXR/CAR-mediated pathway and induce CYP3A. *Biochemical Pharmacology*, 79(2):270–6.
- Chen, W., Koenigs, L. L., Thompson, S. J., Peter, R. M., Rettie, A. E., Trager, W. F., and Nelson, S. D. (1998). Oxidation of acetaminophen to its toxic quinone imine and nontoxic catechol metabolites by baculovirus-expressed and purified human cytochromes P450 2E1 and 2A6. *Chemical Research in Toxicology*, 11(4):295–301.
- Cheng, Y. F., Paalzow, L. K., Bondesson, U., Ekblom, B., Eriksson, K., Eriksson, S. O., Lindberg, A., and Lindström, L. (1987). Pharmacokinetics of haloperidol in psychotic patients. *Psychopharmacology*, 91(4):410–414.
- Chiacchio, F., Pennisi, M., Russo, G., Motta, S., and Pappalardo, F. (2014). Agent-based modeling of the immune system: NetLogo, a promising framework. *BioMed Research International*, 2014:907171.
- Clemenson, C., Kolman, A., and Forsby, A. (2007). The integrated acute systemic toxicity project (ACuteTox) for the optimisation and validation of alternative in vitro tests. *Alternatives to Laboratory Animals*, 35(1):33–8.
- Coors, A. and De Meester, L. (2008). Synergistic, antagonistic and additive effects of multiple stressors: predation threat, parasitism and pesticide exposure in *Daphnia magna*. *Journal of Applied Ecology*, 45(6):1820–1828.
- Cordes, H., Thiel, C., Aschmann, H. E., Baier, V., Blank, L. M., and Kuepfer, L. (2016). A Physiologically Based Pharmacokinetic Model of Isoniazid and Its Application in Individualizing Tuberculosis Chemotherapy. *Antimicrobial Agents and Chemotherapy*, 60(10):6134–6145.
- Critchley, J. a., Nimmo, G. R., Gregson, C. a., Woolhouse, N. M., and Prescott, L. F. (1986). Inter-subject and ethnic differences in paracetamol metabolism. *British Journal of Clinical Pharmacology*, 22(6):649–657.
- Cuttle, L., Munns, a. J., Hogg, N. a., Scott, J. R., Hooper, W. D., Dickinson, R. G., and Gillam, E. M. J. (2000). Phenytoin metabolism by human cytochrome P450: Involvement of P450 3A and 2C forms in secondary metabolism and drug-protein adduct formation. *Drug Metabolism and Disposition*, 28(8):945–950.
- Czyrski, A. and Kupczyk, B. (2013). The Determination of Partition Coefficient of 6-Mercaptopurine Derivatives by Thin Layer Chromatography. *Journal of Chemistry*, 2013:1–4.
- Dai, M., Wang, P., Boyd, A. D., Kostov, G., Athey, B., Jones, E. G., Bunney, W. E., Myers, R. M., Speed, T. P., Akil, H., Watson, S. J., and Meng, F. (2005). Evolving gene/transcript definitions significantly alter the interpretation of GeneChip data. *Nucleic Acids Research*, 33(20):e175.

- Danan, G. and Benichou, C. (1993). Causality assessment of adverse reactions to drugs – I. A novel method based on the conclusions of international consensus meetings: application to drug-induced liver injuries. *Journal of Clinical Epidemiology*, 46(11):1323–30.
- Dandara, C., Lombard, Z., Du Plooy, I., McLellan, T., Norris, S. A., and Ramsay, M. (2011). genes in a black South African population: a window into diversity. *Pharmacogenomics*, 12(12):1663–1670.
- Davies, N. M. and Anderson, K. E. (1997). Clinical pharmacokinetics of diclofenac. Therapeutic insights and pitfalls. *Clinical Pharmacokinetics*, 33(3):184–213.
- Degen, P. H., Dieterle, W., Schneider, W., Theobald, W., and Sinterhauf, U. (1988). Pharmacokinetics of Diclofenac and Five Metabolites After Single Doses in Healthy Volunteers and After Repeated Doses in Patients. *Xenobiotica*, 18(12):1449–1455.
- Deray, G., Le Hoang, P., Aupetit, B., Achour, A., Rottembourg, J., and Baumelou, A. (1987). Enhancement of cyclosporine A nephrotoxicity by diclofenac. *Clinical Nephrology*, 27(4):213–4.
- Dix, D. J., Houck, K. a., Martin, M. T., Richard, A. M., Setzer, R. W., and Kavlock, R. J. (2007). The toxcast program for prioritizing toxicity testing of environmental chemicals. *Toxicological Sciences*, 95(1):5–12.
- Doktorova, T. Y., Yildirimman, R., Vinken, M., Vilardell, M., Vanhaecke, T., Gmuender, H., Bort, R., Brolen, G., Holmgren, G., Li, R., Chesne, C., van Delft, J., Kleinjans, J., Castell, J., Bjorquist, P., Herwig, R., and Rogiers, V. (2013). Transcriptomic responses generated by hepatocarcinogens in a battery of liver-based in vitro models. *Carcinogenesis*, 34(6):1393–402.
- Edmondson, R., Broglie, J. J., Adcock, A. F., and Yang, L. (2014). Three-dimensional cell culture systems and their applications in drug discovery and cell-based biosensors. *Assay and Drug Development Technologies*, 12(4):207–18.
- Eissing, T., Kuepfer, L., Becker, C., Block, M., Coboeken, K., Gaub, T., Goerlitz, L., Jaeger, J., Loosen, R., Ludewig, B., Meyer, M., Niederal, C., Sevestre, M., Siegmund, H. U., Solodenko, J., Thelen, K., Telle, U., Weiss, W., Wendl, T., Willmann, S., and Lippert, J. (2011). A computational systems biology software platform for multiscale modeling and simulation: Integrating whole-body physiology, disease biology, and molecular reaction networks. *Frontiers in Physiology*, 2(4).
- Eklund, B. I., Moberg, M., Bergquist, J., and Mannervik, B. (2006). Divergent activities of human glutathione transferases in the bioactivation of azathioprine. *Molecular Pharmacology*, 70(2):747–754.
- Elion, G. B. (1972). Significance of azathioprine metabolites. *Proceedings of the Royal Society of Medicine*, 65(3):257–260.
- Elion, G. B. (1993). The Pharmacology of Azathioprine. *Annals New York Academy of Sciences*, 685(1):401–407.
- Ellard, G. A. and Gammon, P. T. (1976). Pharmacokinetics of isoniazid metabolism in man. *Journal of Pharmacokinetics and Biopharmaceutics*, 4(2):83–113.
- Elsherbiny, M. E., El-Kadi, A. O. S., and Brocks, D. R. (2008). The metabolism of amiodarone by various CYP isoenzymes of human and rat, and the inhibitory influence of ketoconazole. *Journal of Pharmacy & Pharmaceutical Sciences*, 11(1):147–59.
- Essers, J., Theil, A. F., Baldeyron, C., van Cappellen, W. A., Houtsmuller, A. B., Kanaar, R., and Vermeulen, W. (2005). Nuclear dynamics of PCNA in DNA replication and repair. *Molecular and Cellular Biology*, 25(21):9350–9359.

- Ethell, B. T., Anderson, G. D., and Burchell, B. (2003). The effect of valproic acid on drug and steroid glucuronidation by expressed human UDP-glucuronosyltransferases. *Biochemical Pharmacology*, 65(9):1441–9.
- Falcon, S. and Gentleman, R. (2007). Using GOstats to test gene lists for GO term association. *Bioinformatics*, 23(2):257–258.
- FDA (2015a). Food and Drug Administration. Drugs@FDA http://www.accessdata.fda.gov/drugsatfda_docs/label/2008/050609s0251b1.pdf [Accessed 26 August 2015].
- FDA (2015b). Food and Drug Administration. Drugs@FDA http://www.accessdata.fda.gov/drugsatfda_docs/label/2010/050420s073,050627s0121b1.pdf [Accessed 29 September 2015].
- FDA (2016). Food and Drug Administration. Drugs@FDA https://www.accessdata.fda.gov/drugsatfda_docs/label/2011/050207s0641b1.pdf [Accessed 18 March 2016].
- Feder, M. E. and Walser, J. C. (2005). The biological limitations of transcriptomics in elucidating stress and stress responses. *Journal of Evolutionary Biology*, 18(4):901–910.
- Fernandez, M., Pirondi, S., Antonelli, T., Ferraro, L., Giardino, L., and Calzà, L. (2005). Role of c-Fos protein on glutamate toxicity in primary neural hippocampal cells. *Journal of Neuroscience Research*, 82(1):115–25.
- Fialová, D., Topinková, E., Gambassi, G., Finne-Soveri, H., Jónsson, P. V., Carpenter, I., Schroll, M., Onder, G., Sørbye, L. W., Wagner, C., Reissigová, J., Bernabei, R., and AdHOC Project Research Group (2005). Potentially inappropriate medication use among elderly home care patients in Europe. *The Journal of the American Medical Association*, 293(11):1348–58.
- Foulkes, T. and Wood, J. N. (2008). Pain Genes. *PLoS Genetics*, 4(7):e1000086.
- Frank, R. and Hargreaves, R. (2003). Clinical biomarkers in drug discovery and development. *Nature Reviews Drug Discovery*, 2(7):566–80.
- Froemming, J. S., Lam, Y. W., Jann, M. W., and Davis, C. M. (1989). Pharmacokinetics of haloperidol. *Clinical Pharmacokinetics*, 17(6):396–423.
- Fruchter, L. L., Alexopoulou, I., and Lau, K. K. (2011). Acute interstitial nephritis with acetaminophen and alcohol intoxication. *Italian Journal of Pediatrics*, 37(1):17.
- Gadd, S. L., Hobbs, G., and Miller, M. R. (2002). Acetaminophen-induced proliferation of estrogen-responsive breast cancer cells is associated with increases in c-myc RNA expression and NF-kappaB activity. *Toxicological Sciences*, 66(2):233–43.
- García, M. J., Reinoso, R. F., Sánchez Navarro, A., and Prous, J. R. (2003). Clinical pharmacokinetics of statins. *Methods and Findings in Experimental and Clinical Pharmacology*, 25(6):457–81.
- Gates, S. and Miners, J. O. (1999). Cytochrome P450 isoform selectivity in human hepatic theobromine metabolism. *British Journal of Clinical Pharmacology*, 47(3):299–305.
- Gervot, L., Rochat, B., Gautier, J. C., Bohnenstengel, F., Kroemer, H., de Berardinis, V., Martin, H., Beaune, P., and de Waziers, I. (1999). Human CYP2B6: expression, inducibility and catalytic activities. *Pharmacogenetics*, 9(3):295–306.
- Gillard, F., Skutella, T., Uhlmann, E., Holsboer, F., Zimmermann, M., and Behl, C. (1996). Activation of c-Fos contributes to amyloid beta-peptide-induced neurotoxicity. *Brain Research*, 706(1):169–72.

- Goto, H., Izawa, I., Li, P., and Inagaki, M. (2012). Novel regulation of checkpoint kinase 1: Is checkpoint kinase 1 a good candidate for anti-cancer therapy? *Cancer Science*, 103(7):1195–1200.
- Gregoriano, C., Ceschi, A., Rauber-Lüthy, C., Kupferschmidt, H., Banner, N. R., Krähenbühl, S., and Taegtmeier, A. B. (2014). Acute thiopurine overdose: Analysis of reports to a national poison centre 1995–2013. *PLoS ONE*, 9(1):e86390.
- Gu, L., Gonzalez, F. J., Kalow, W., and Tang, B. K. (1992). Biotransformation of caffeine, paraxanthine, theobromine and theophylline by cDNA-expressed human CYP1A2 and CYP2E1. *Pharmacogenetics*, 2(2):73–7.
- Guengerich, F. P. (2011). Mechanisms of drug toxicity and relevance to pharmaceutical development. *Drug Metabolism and Pharmacokinetics*, 26(1):3–14.
- Gugler, R., Schell, A., Eichelbaum, M., Fröscher, W., and Schulz, H. U. (1977). Disposition of valproic acid in man. *European Journal of Clinical Pharmacology*, 12(2):125–32.
- Gupta, S. K., Manfro, R. C., Tomlanovich, S. J., Gambertoglio, J. G., Garovoy, M. R., and Benet, L. Z. (1990). Effect of food on the pharmacokinetics of cyclosporine in healthy subjects following oral and intravenous administration. *Journal of Clinical Pharmacology*, 30(7):643–53.
- Ha, H. R., Chen, J., Freiburghaus, A. U., and Follath, F. (1995). Metabolism of theophylline by cDNA-expressed human cytochromes P-450. *British Journal of Clinical Pharmacology*, 39(3):321–326.
- Haider, S. and Pal, R. (2013). Integrated analysis of transcriptomic and proteomic data. *Current Genomics*, 14(2):91–110.
- Hamon, J., Renner, M., Jamei, M., Lukas, A., Kopp-Schneider, A., and Bois, F. Y. (2015). Quantitative in vitro to in vivo extrapolation of tissues toxicity. *Toxicology in vitro*, 30:203–16.
- Han, B. R., You, B. R., and Park, W. H. (2013). Valproic acid inhibits the growth of HeLa cervical cancer cells via caspase-dependent apoptosis. *Oncology Reports*, 30(6):2999–3005.
- Haubitz, M., Bohnenstengel, F., Brunkhorst, R., Schwab, M., Hofmann, U., and Busse, D. (2002). Cyclophosphamide pharmacokinetics and dose requirements in patients with renal insufficiency. *Kidney International*, 61(4):1495–1501.
- Heijne, W. H. M., Kienhuis, A. S., van Ommen, B., Stierum, R. H., and Groten, J. P. (2005). Systems toxicology: applications of toxicogenomics, transcriptomics, proteomics and metabolomics in toxicology. *Expert Review of Proteomics*, 2(5):767–780.
- Heise, T., Schug, M., Storm, D., Ellinger-Ziegelbauer, H., J. Ahr, H., Hellwig, B., Rahnenfuhrer, J., Ghallab, a., Guenther, G., Sisnaiske, J., Reif, R., Godoy, P., Mielke, H., Gundert-Remy, U., Lampen, a., Oberemm, a., and G. Hengstler, J. (2012). In Vitro - In Vivo Correlation of Gene Expression Alterations Induced by Liver Carcinogens. *Current Medicinal Chemistry*, 19(11):1721–1730.
- Henderson, R. A., Lane, S., and Henry, J. A. (1991). Life-threatening ventricular arrhythmia (torsades de pointes) after haloperidol overdose. *Human & Experimental Toxicology*, 10(1):59–62.
- Herpers, B., Wink, S., Fredriksson, L., Di, Z., Hendriks, G., Vrieling, H., de Bont, H., and van de Water, B. (2016). Activation of the Nrf2 response by intrinsic hepatotoxic drugs correlates with suppression of NF- κ B activation and sensitizes toward TNF α -induced cytotoxicity. *Archives of Toxicology*, 90(5):1163–79.

- Hockley, S. L., Arlt, V. M., Brewer, D., Giddings, I., and Phillips, D. H. (2006). Time- and concentration-dependent changes in gene expression induced by benzo(a)pyrene in two human cell lines, MCF-7 and HepG2. *BMC Genomics*, 7:260.
- Holt, M. P. and Ju, C. (2006). Mechanisms of drug-induced liver injury. *The AAPS journal*, 8(1):E48–54.
- Hoofnagle, J. H., Serrano, J., Knoben, J. E., and Navarro, V. J. (2013). LiverTox: a website on drug-induced liver injury. *Hepatology*, 57(3):873–4.
- Horsmans, Y., Desager, J. P., and Harvengt, C. (1990). Biochemical changes and morphological alterations of the liver in guinea-pigs after administration of simvastatin (HMG CoA reductase-inhibitor). *Pharmacology & Toxicology*, 67(4):336–9.
- Howell, B. A., Yang, Y., Kumar, R., Woodhead, J. L., Harrill, A. H., Clewell, H. J., Andersen, M. E., Siler, S. Q., and Watkins, P. B. (2012). In vitro to in vivo extrapolation and species response comparisons for drug-induced liver injury (DILI) using DILIsym: a mechanistic, mathematical model of DILI. *Journal of Pharmacokinetics and Pharmacodynamics*, 39(5):527–541.
- Huang, J., Niu, C., Green, C. D., Yang, L., Mei, H., and Han, J.-D. J. (2013). Systematic prediction of pharmacodynamic drug-drug interactions through protein-protein-interaction network. *PLoS Computational Biology*, 9(3):e1002998.
- Huang, Z., Roy, P., and Waxman, D. J. (2000). Role of human liver microsomal CYP3A4 and CYP2B6 in catalyzing N-dechloroethylation of cyclophosphamide and ifosfamide. *Biochemical Pharmacology*, 59(99):961–972.
- Igarashi, Y., Nakatsu, N., Yamashita, T., Ono, A., Ohno, Y., Urushidani, T., and Yamada, H. (2015). Open TG-GATEs: a large-scale toxicogenomics database. *Nucleic Acids Research*, 43:D921–7.
- Iqbal, N., Ahmad, B., Janbaz, K. H., Gilani, A.-U. H., and Niazi, S. K. (1995). The effect of caffeine on the pharmacokinetics of acetaminophen in man. *Biopharmaceutics & Drug Disposition*, 16(6):481–487.
- Iskar, M., Zeller, G., Blattmann, P., Campillos, M., Kuhn, M., Kaminska, K. H., Runz, H., Gavin, A.-C., Pepperkok, R., van Noort, V., and Bork, P. (2013). Characterization of drug-induced transcriptional modules: towards drug repositioning and functional understanding. *Molecular Systems Biology*, 9(662):662.
- Jamei, M., Marciniak, S., Feng, K., Barnett, A., Tucker, G., and Rostami-Hodjegan, A. (2009). The Simcyp population-based ADME simulator. *Expert Opinion on Drug Metabolism & Toxicology*, 5(2):211–23.
- Jamis-Dow, C. A., Katki, A. G., Collins, J. M., and Klecker, R. W. (1997). Rifampin and rifabutin and their metabolism by human liver esterases. *Xenobiotica*, 27(10):1015–24.
- Jaw, S. and Jeffery, E. H. (1993). Interaction of caffeine with acetaminophen. 1. Correlation of the effect of caffeine on acetaminophen hepatotoxicity and acetaminophen bioactivation following treatment of mice with various cytochrome P450 inducing agents. *Biochemical Pharmacology*, 46(3):493–501.
- Jiang, X.-L., Zhao, P., Barrett, J. S., Lesko, L. J., and Schmidt, S. (2013). Application of physiologically based pharmacokinetic modeling to predict acetaminophen metabolism and pharmacokinetics in children. *CPT: Pharmacometrics & Systems Pharmacology*, 2(August):e80.
- Jones, H. M., Gardner, I. B., and Watson, K. J. (2009). Modelling and PBPK simulation in drug discovery. *The AAPS journal*, 11(1):155–166.

- Jones, H. M., Parrott, N., Jorga, K., and Lavé, T. (2006). A novel strategy for physiologically based predictions of human pharmacokinetics. *Clinical Pharmacokinetics*, 45(5):511–542.
- Judson, R., Houck, K., Martin, M., Knudsen, T., Thomas, R. S., Sipes, N., Shah, I., Wambaugh, J., and Crofton, K. (2014). In vitro and modelling approaches to risk assessment from the U.S. Environmental Protection Agency ToxCast programme. *Basic & Clinical Pharmacology & Toxicology*, 115(i):69–76.
- Judson, R. S., Kavlock, R. J., Setzer, R. W., Cohen Hubal, E. a., Martin, M. T., Knudsen, T. B., Houck, K. a., Thomas, R. S., Wetmore, B. a., and Dix, D. J. (2011). Estimating toxicity-related biological pathway altering doses for high-throughput chemical risk assessment. *Chemical Research in Toxicology*, 24:451–462.
- Juma, F. D., Rogers, H. J., and Trounce, J. R. (1979). Pharmacokinetics of cyclophosphamide and alkylating activity in man after intravenous and oral administration. *British Journal of Clinical Pharmacology*, 8(3):209–217.
- Juma, F. D., Rogers, H. J., and Trounce, J. R. (1981). Effect of renal insufficiency on the pharmacokinetics of cyclophosphamide and some of its metabolites. *European Journal of Clinical Pharmacology*, 19(6):443–451.
- Jusko, W. J. and Gretch, M. (1976). Plasma and tissue protein binding of drugs in pharmacokinetics. *Drug Metabolism Reviews*, 5(1):43–140.
- Kameyama, Y., Yamashita, K., Kobayashi, K., Hosokawa, M., and Chiba, K. (2005). Functional characterization of SLCO1B1 (OATP-C) variants, SLCO1B1*5, SLCO1B1*15 and SLCO1B1*15+C1007G, by using transient expression systems of HeLa and HEK293 cells. *Pharmacogenetics and Genomics*, 15(7):513–522.
- Kanehisa, M. and Goto, S. (2000). KEGG: kyoto encyclopedia of genes and genomes. *Nucleic Acids Research*, 28(1):27–30.
- Kaplan, G. B., Greenblatt, D. J., Ehrenberg, B. L., Goddard, J. E., Cotreau, M. M., Harmatz, J. S., and Shader, R. I. (1997). Dose-Dependent Pharmacokinetics and Psychomotor Effects of Caffeine in Humans. *The Journal of Clinical Pharmacology*, 37(8):693–703.
- Kaplowitz, N. (2004). Drug-induced liver injury. *Clinical Infectious Diseases*, 38(Suppl 2):S44–8.
- Kaplowitz, N. and Kuhlenkamp, J. (1978). Inhibition of hepatic metabolism of azathioprine in vivo. *Gastroenterology*, 74(1):90–2.
- Karran, P. (2006). Thiopurines, DNA damage, DNA repair and therapy-related cancer. *British Medical Bulletin*, 79-80:153–170.
- Kasim, N. a., Whitehouse, M., Ramachandran, C., Bermejo, M., Lennernäs, H., Hussain, A. S., Junginger, H. E., Stavchansky, S. a., Midha, K. K., Shah, V. P., and Amidon, G. L. (2004). Molecular properties of WHO essential drugs and provisional biopharmaceutical classification. *Molecular Pharmaceutics*, 1(1):85–96.
- Kastan, M. B. and Bartek, J. (2004). Cell-cycle checkpoints and cancer. *Nature*, 432(7015):316–23.
- Kiang, T. K. L., Ho, P. C., Anari, M. R., Tong, V., Abbott, F. S., and Chang, T. K. H. (2006). Contribution of CYP2C9, CYP2A6, and CYP2B6 to Valproic Acid Metabolism in Hepatic Microsomes from Individuals with the CYP2C9*1/*1 Genotype. *Toxicological Sciences*, 94(2):261–71.
- Kim, M. K., James, J., and Annunziata, C. M. (2015). Topotecan synergizes with CHEK1 (CHK1) inhibitor to induce apoptosis in ovarian cancer cells. *BMC Cancer*, 15(1):196.

- Kinzig-Schippers, M., Tomalik-Scharte, D., Jetter, A., Scheidel, B., Jakob, V., Rodamer, M., Cascorbi, I., Doroshyenko, O., Sörgel, F., and Fuhr, U. (2005). Should we use N-acetyltransferase type 2 genotyping to personalize isoniazid doses? *Antimicrobial Agents and Chemotherapy*, 49(5):1733–1738.
- Kola, I. and Landis, J. (2004). Can the pharmaceutical industry reduce attrition rates? *Nature Reviews Drug Discovery*, 3(8):711–5.
- Krauss, M., Schaller, S., Borchers, S., Findeisen, R., Lippert, J., and Kuepfer, L. (2012). Integrating Cellular Metabolism into a Multiscale Whole-Body Model. *PLoS Computational Biology*, 8(10):e1002750.
- Kroeger, M. (2006). How omics technologies can contribute to the '3R' principles by introducing new strategies in animal testing. *Trends in Biotechnology*, 24(8):343–6.
- Kuepfer, L. (2010). Towards whole-body systems physiology. *Molecular Systems Biology*, 6:409.
- Kuepfer, L., Lippert, J., and Eissing, T. (2012). Multiscale mechanistic modeling in pharmaceutical research and development. *Advances in Experimental Medicine and Biology*, 736:543–61.
- Kuepfer, L., Niederalt, C., Wendl, T., Schlender, J.-f., Willmann, S., Lippert, J., Block, M., Eissing, T., and Teutonico, D. (2016). Applied Concepts in PBPK modeling: How to build a PBPK/PD model. *CPT: Pharmacometrics & Systems Pharmacology*.
- Labeledzki, A., Buters, J., Jabrane, W., and Fuhr, U. (2002). Differences in caffeine and paraxanthine metabolism between human and murine CYP1A2. *Biochemical Pharmacology*, 63(12):2159–67.
- Latini, R., Tognoni, G., and Kates, R. E. (1984). Clinical pharmacokinetics of amiodarone. *Clinical Pharmacokinetics*, 9(2):136–56.
- Lee, C. A., Thummel, K. E., Kalhorn, T. F., Nelson, S. D., and Slattery, J. T. (1991). Inhibition and activation of acetaminophen reactive metabolite formation by caffeine. Roles of cytochromes P-450IA1 and IIIA2. *Drug Metabolism and Disposition*, 19(2):348–53.
- Lee, W. M. (1993). Acute Liver Failure. *New England Journal of Medicine*, 329(25):1862–1872.
- Lee, W. M. (1995). Drug-Induced Hepatotoxicity. *New England Journal of Medicine*, 333(17):1118–1127.
- Leemann, T., Transon, C., and Dayer, P. (1993). Cytochrome P450TB (CYP2C): a major monooxygenase catalyzing diclofenac 4'-hydroxylation in human liver. *Life Sciences*, 52(7):29–34.
- Legg, B., Gupta, S. K., and Rowland, M. (1988). A model to account for the variation in cyclosporin binding to plasma lipids in transplant patients. *Therapeutic Drug Monitoring*, 10(1):20–7.
- Lelo, A., Birkett, D. J., Robson, R. A., and Miners, J. O. (1986). Comparative pharmacokinetics of caffeine and its primary demethylated metabolites paraxanthine, theobromine and theophylline in man. *British Journal of Clinical Pharmacology*, 22(2):177–182.
- Levitt, D. G. (2002). PKQuest: a general physiologically based pharmacokinetic model. Introduction and application to propranolol. *BMC Clinical Pharmacology*, 2:5.
- Lewis, J. H., Ranard, R. C., Caruso, A., Jackson, L. K., Mullick, F., Ishak, K. G., Seeff, L. B., and Zimmerman, H. J. (1989). Amiodarone hepatotoxicity: prevalence and clinicopathologic correlations among 104 patients. *Hepatology*, 9(5):679–85.

- Lilja, J. J., Neuvonen, M., and Neuvonen, P. J. (2004). Effects of regular consumption of grapefruit juice on the pharmacokinetics of simvastatin. *British Journal of Clinical Pharmacology*, 58(1):56–60.
- Lippert, J., Brosch, M., Kampen, O. V., Meyer, M., Siegmund, H.-U., Schafmayer, C., Becker, T., Laffert, B., Görlitz, L., Schreiber, S., Neuvonen, P. J., Niemi, M., Hampe, J., Kuepfer, L., and von Kampen, O. (2013). A mechanistic, model-based approach to safety assessment in clinical development. *CPT: Pharmacometrics & Systems Pharmacology*, 1:e13.
- Löbrich, M. and Jeggo, P. A. (2007). The impact of a negligent G2/M checkpoint on genomic instability and cancer induction. *Nature Reviews Cancer*, 7(11):861–9.
- Louisse, J., de Jong, E., van de Sandt, J. J. M., Blaauboer, B. J., Woutersen, R. a., Piersma, A. H., Rietjens, I. M. C. M., and Verwei, M. (2010). The use of in vitro toxicity data and physiologically based kinetic modeling to predict dose-response curves for in vivo developmental toxicity of glycol ethers in rat and man. *Toxicological Sciences*, 118(2):470–484.
- Lucangioli, S. E., Kenndler, E., Carlucci, A., Tripodi, V. P., Scioscia, S. L., and Carducci, C. N. (2003). Relation between retention factors of immunosuppressive drugs in microemulsion electrokinetic chromatography with biosurfactants and octanol-water partition coefficients. *Journal of Pharmaceutical and Biomedical Analysis*, 33(5):871–8.
- Lund, L., Alvan, G., Berlin, A., and Alexanderson, B. (1974). Pharmacokinetics of single and multiple doses of phenytoin in man. *European Journal of Clinical Pharmacology*, 7(2):81–6.
- Maharaj, A. R., Barrett, J. S., and Edginton, A. N. (2013). A workflow example of PBPK modeling to support pediatric research and development: case study with lorazepam. *The AAPS journal*, 15(2):455–64.
- Mahoney, B. P., Raghunand, N., Baggett, B., and Gillies, R. J. (2003). Tumor acidity, ion trapping and chemotherapeutics. I. Acid pH affects the distribution of chemotherapeutic agents in vitro. *Biochemical Pharmacology*, 66(7):1207–18.
- Mazaleuskaya, L. L., Sangkuhl, K., Thorn, C. F., FitzGerald, G. A., Altman, R. B., and Klein, T. E. (2015). PharmGKB summary: pathways of acetaminophen metabolism at the therapeutic versus toxic doses. *Pharmacogenetics and Genomics*, 25(8):416–26.
- McDonald, G. B., Slattery, J. T., Bouvier, M. E., Ren, S., Batchelder, A. L., Kalhorn, T. F., Schoch, H. G., Anasetti, C., and Gooley, T. (2003). Cyclophosphamide metabolism, liver toxicity, and mortality following hematopoietic stem cell transplantation. *Blood*, 101(5):2043–2048.
- McNeely, S., Beckmann, R., and Bence Lin, A. K. (2014). CHEK again: Revisiting the development of CHK1 inhibitors for cancer therapy. *Pharmacology and Therapeutics*, 142(1):1–10.
- Medve, R. A., Wang, J., and Karim, R. (2001). Tramadol and acetaminophen tablets for dental pain. *Anesthesia Progress*, 48(3):79–81.
- Mendrick, D. L. (2011). Transcriptional profiling to identify biomarkers of disease and drug response. *Pharmacogenomics*, 12(2):235–49.
- Metsalu, T. and Vilo, J. (2015). ClustVis: a web tool for visualizing clustering of multivariate data using Principal Component Analysis and heatmap. *Nucleic Acids Research*, 43(W1):W566–570.
- Meyer, M., Schneckener, S., Ludewig, B., Kuepfer, L., and Lippert, J. (2012). Using expression data for quantification of active processes in physiologically based pharmacokinetic modeling. *Drug Metabolism and Disposition*,

- 40(5):892–901.
- Michaelis, L., Menten, M. L., Johnson, K. A., and Goody, R. S. (2011). The original Michaelis constant: translation of the 1913 Michaelis-Menten paper. *Biochemistry*, 50(39):8264–9.
- Michaelson, J. J., Trump, S., Rudzok, S., Gräbsch, C., Madureira, D. J., Dautel, F., Mai, J., Attinger, S., Schirmer, K., von Bergen, M., Lehmann, I., and Beyer, A. (2011). Transcriptional signatures of regulatory and toxic responses to benzo-[a]-pyrene exposure. *BMC Genomics*, 12:502.
- Miller, M. B. and Tang, Y. W. (2009). Basic concepts of microarrays and potential applications in clinical microbiology. *Clinical Microbiology Reviews*, 22(4):611–633.
- Mitchell, J. R., Thorgeirsson, U. P., Black, M., Timbrell, J. A., Snodgrass, W. R., Potter, W. Z., Jollow, H. R., and Keiser, H. R. (1975). Increased incidence of isoniazid hepatitis in rapid acetylators: possible relation to hydrazine metabolites. *Clinical Pharmacology and Therapeutics*, 18(1):70–9.
- Mitić-Zlatković, M. and Stefanović, V. (1999). Acute effects of acetaminophen on renal function and urinary excretion of some proteins and enzymes in patients with kidney disease. *Renal Failure*, 21(5):525–32.
- Muller, P. Y. and Milton, M. N. (2012). The determination and interpretation of the therapeutic index in drug development. *Nature Reviews Drug Discovery*, 11(10):751–61.
- Mutlib, A. E., Goosen, T. C., Bauman, J. N., Williams, J. A., Kulkarni, S., and Kostrubsky, S. (2006). Kinetics of acetaminophen glucuronidation by UDP-glucuronosyltransferases 1A1, 1A6, 1A9 and 2B15. Potential implications in acetaminophen-induced hepatotoxicity. *Chemical Research in Toxicology*, 19(5):701–709.
- Mutschler, E., Geisslinger, G., Kroemer, H. K., and Schäfer-Korting, M. (2001). *Mutschler Arzneimittelwirkungen: Lehrbuch der Pharmakologie und Toxikologie*. Wissenschaftliche Verlagsgesellschaft mbH Stuttgart.
- Nelson, E., Powell, J. R., Conrad, K., Likes, K., Byers, J., Baker, S., and Perrier, D. (1982). Phenobarbital pharmacokinetics and bioavailability in adults. *Journal of Clinical Pharmacology*, 22(2-3):141–8.
- Nelson, S. D. (1990). Molecular mechanisms of the hepatotoxicity caused by acetaminophen. *Seminars in Liver Disease*, 10(4):267–78.
- Newton, R., Broughton, L. J., Lind, M. J., Morrison, P. J., Rogers, H. J., and Bradbrook, I. D. (1981). Plasma and salivary pharmacokinetics of caffeine in man. *European Journal of Clinical Pharmacology*, 21(1):45–52.
- Nies, A. T. and Keppler, D. (2007). The apical conjugate efflux pump ABCC2 (MRP2). *Pflügers Archiv : European Journal of Physiology*, 453(5):643–59.
- Nigg, E. A. (1995). Cyclin-dependent protein kinases: key regulators of the eukaryotic cell cycle. *BioEssays*, 17(6):471–80.
- Nouchi, T., Lasker, J. M., and Lieber, C. S. (1986). Activation of acetaminophen oxidation in rat liver microsomes by caffeine. *Toxicology Letters*, 32(1-2):1–8.
- Obach, R. S., Lombardo, F., and Waters, N. J. a. a. a. (2008). Trend analysis of a database of intravenous pharmacokinetic parameters in humans for 670 drug compounds. *Drug Metabolism and Disposition*, 36(7):1385–405.
- O’Brien, P. J., Slaughter, M. R., Polley, S. R., and Kramer, K. (2002). Advantages of glutamate dehydrogenase as a blood biomarker of acute hepatic injury in rats. *Laboratory Animals*, 36(3):313–21.

- Odland, B., Hartvig, P., Lindström, B., Lönnerholm, G., Tufveson, G., and Grefberg, N. (1986). Serum azathioprine and 6-mercaptopurine levels and immunosuppressive activity after azathioprine in uremic patients. *International Journal of Immunopharmacology*, 8(1):1–11.
- Osol, A. and J.E. Hoover, e. a. e. (1976). Remington's pharmaceutical sciences. *Journal of Pharmaceutical Sciences*, 65(6):933.
- Palade, G. E., Simionescu, M., and Simionescu, N. (1979). Structural aspects of the permeability of the microvascular endothelium. *Acta Physiologica Scandinavica*, 463:11–32.
- Palmer, H., Graham, G., Williams, K., and Day, R. (2010). A risk-benefit assessment of paracetamol (acetaminophen) combined with caffeine. *Pain medicine*, 11(6):951–65.
- Park, J. W., Kerbel, R. S., Kelloff, G. J., Barrett, J. C., Chabner, B. A., Parkinson, D. R., Peck, J., Ruddon, R. W., Sigman, C. C., and Slamon, D. J. (2004). Rationale for biomarkers and surrogate end points in mechanism-driven oncology drug development. *Clinical Cancer Research*, 10(11):3885–3896.
- Pearson, T. A., Mensah, G. A., Alexander, R. W., Anderson, J. L., Cannon, R. O., Criqui, M., Fadl, Y. Y., Fortmann, S. P., Hong, Y., Myers, G. L., Rifai, N., Smith, S. C., Taubert, K., Tracy, R. P., Vinicor, F., Centers for Disease Control and Prevention, and American Heart Association (2003). Markers of inflammation and cardiovascular disease: application to clinical and public health practice: A statement for healthcare professionals from the Centers for Disease Control and Prevention and the American Heart Association. *Circulation*, 107(3):499–511.
- Periti, P., Mazzei, T., Mini, E., and Novelli, A. (1989). Clinical pharmacokinetic properties of the macrolide antibiotics. Effects of age and various pathophysiological states (Part I). *Clinical Pharmacokinetics*, 16(4):193–214.
- Persson, H. E., Sjöberg, G. K., Haines, J. A., and Pronczuk de Garbino, J. (1998). Poisoning severity score. Grading of acute poisoning. *Journal of Toxicology. Clinical Toxicology*, 36(3):205–213.
- Perucca, E., Gatti, G., Frigo, G. M., Crema, A., Calzetti, S., and Visintini, D. (1978). Disposition of sodium valproate in epileptic patients. *British Journal of Clinical Pharmacology*, 5(6):495–9.
- Perwitasari, D. A., Atthobari, J., and Wilffert, B. (2015). Pharmacogenetics of isoniazid-induced hepatotoxicity. *Drug Metabolism Reviews*, 47(2):222–8.
- Peterson, G. M., McLean, S., Aldous, S., Von Witt, R. J., and Millingen, K. S. (1982). Plasma protein binding of phenytoin in 100 epileptic patients. *British Journal of Clinical Pharmacology*, 14(2):298–300.
- Pfaffl, M. W. (2013). Transcriptional biomarkers. *Methods*, 59(1):1–2.
- Pillai, S., Behra, R., Nestler, H., Suter, M. J.-F., Sigg, L., and Schirmer, K. (2014). Linking toxicity and adaptive responses across the transcriptome, proteome, and phenotype of *Chlamydomonas reinhardtii* exposed to silver. *Proceedings of the National academy of Sciences of the United States of America*, 111(9):3490–5.
- Prescott, L. F. (1980). Kinetics and metabolism of paracetamol and phenacetin. *British Journal of Clinical Pharmacology*, 10(S2):291S–298S.
- Prueksaritanont, T., Chu, X., Gibson, C., Cui, D., Yee, K. L., Ballard, J., Cabalu, T., and Hochman, J. (2013). Drug-drug interaction studies: regulatory guidance and an industry perspective. *The American Association of Pharmaceutical Scientists Journal*, 15(3):629–45.

- Quackenbush, J. (2002). Microarray data normalization and transformation. *Nature Genetics*, 32(Suppl):496–501.
- Raińska, T., Juzwiak, S., Dutkiewicz, T., Krasowska, B., Olenderek, B., Rożewicka, L., Wójcicki, J., Samochowiec, L., and Juzyszyn, Z. (1992). Caffeine reduces the hepatotoxicity of paracetamol in mice. *The Journal of International Medical Research*, 20(4):331–342.
- Ramachandran, R. and Kakar, S. (2009). Histological patterns in drug-induced liver disease. *Journal of Clinical Pathology*, 62(6):481–492.
- Rashid, M. U. and Bateman, D. N. (1990). Effect of intravenous atropine on gastric emptying, paracetamol absorption, salivary flow and heart rate in young and fit elderly volunteers. *British Journal of Clinical Pharmacology*, 30(1):25–34.
- Rawlins, M. D., Henderson, D. B., and Hijab, A. R. (1977). Pharmacokinetics of paracetamol (acetaminophen) after intravenous and oral administration. *European Journal of Clinical Pharmacology*, 11(4):283–6.
- Renner, B., Clarke, G., Grattan, T., Beisel, A., Mueller, C., Werner, U., Kobal, G., and Brune, K. (2007). Caffeine accelerates absorption and enhances the analgesic effect of acetaminophen. *Journal of Clinical Pharmacology*, 47(6):715–726.
- Reynolds, F. and Knott, C. (1989). Pharmacokinetics in pregnancy and placental drug transfer. *Oxford Reviews of Reproductive Biology*, 11:389–449.
- Riches, Z., Bloomer, J. C., and Coughtrie, M. W. H. (2007). Comparison of 2-aminophenol and 4-nitrophenol as in vitro probe substrates for the major human hepatic sulfotransferase, SULT1A1, demonstrates improved selectivity with 2-aminophenol. *Biochemical Pharmacology*, 74(2):352–358.
- Riedmaier, I. and Pfaffl, M. W. (2013a). Transcriptional biomarkers - High throughput screening, quantitative verification, and bioinformatical validation methods. *Methods*, 59(1):3–9.
- Riedmaier, I. and Pfaffl, M. W. (2013b). Transcriptional biomarkers - High throughput screening, quantitative verification, and bioinformatical validation methods. *Methods*, 59(1):3–9.
- Riess, W. and W, R. (1968). The optimum dosage schedule for Rimactane. *A Symposium on Rimactane*, pages 36–42.
- Rippe, B. and Haraldsson, B. (1994). Transport of macromolecules across microvascular walls: the two-pore theory. *Physiological Reviews*, 74(1):163–219.
- Rodgers, T., Leahy, D., and Rowland, M. (2005). Physiologically based pharmacokinetic modeling 1: predicting the tissue distribution of moderate-to-strong bases. *Journal of Pharmaceutical Sciences*, 94(6):1259–76.
- Rodgers, T. and Rowland, M. (2006). Physiologically based pharmacokinetic modelling 2: predicting the tissue distribution of acids, very weak bases, neutrals and zwitterions. *Journal of Pharmaceutical Sciences*, 95(6):1238–57.
- Rollins, D. E. and Klaassen, C. D. (1979). Biliary Excretion of Drugs in Man. *Clinical Pharmacokinetics*, 4(5):368–379.
- Russmann, S., Jetter, A., and Kullak-Ublick, G. a. (2010). Pharmacogenetics of drug-induced liver injury. *Hepatology*, 52(2):748–761.
- Russmann, S., Kullak-Ublick, G. a., and Grattagliano, I. (2009). Current concepts of mechanisms in drug-induced hepatotoxicity. *Current Medicinal Chemistry*, 16(23):3041–3053.

- Saha, B. and Nandi, D. (2009). Farnesyltransferase inhibitors reduce Ras activation and ameliorate acetaminophen-induced liver injury in mice. *Hepatology*, 50(5):1547–57.
- Sahajwalla, C. G. and Ayres, J. W. (1991). Multiple-dose acetaminophen pharmacokinetics. *Journal of Pharmaceutical Sciences*, 80(9):855–60.
- Salminen, W. F., Yang, X., and Shi, Q. (2011). Using microRNA as Biomarkers of Drug-Induced Liver Injury. *Journal of Molecular Biomarkers & Diagnosis*, 02(5).
- Sánchez-Aguilera, a., García, J. F., Sánchez-Beato, M., and Piris, M. a. (2006). Hodgkin’s lymphoma cells express alternatively spliced forms of HDM2 with multiple effects on cell cycle control. *Oncogene*, 25(18):2565–2574.
- Sato, C. and Izumi, N. (1989). Mechanism of increased hepatotoxicity of acetaminophen by the simultaneous administration of caffeine in the rat. *The Journal of Pharmacology and Experimental Therapeutics*, 248(3):1243–7.
- Sato, C., Izumi, N., Nouchi, T., Hasumura, Y., and Takeuchi, J. (1985). Increased hepatotoxicity of acetaminophen by concomitant administration of caffeine in the rat. *Toxicology*, 34(2):95–101.
- Sawynok, J. and Yaksh, T. L. (1993). Caffeine as an analgesic adjuvant: a review of pharmacology and mechanisms of action. *Pharmacological Reviews*, 45(1):43–85.
- Schimmel, K. J. M., Richel, D. J., van den Brink, R. B. A., and Guchelaar, H. J. (2004). Cardiotoxicity of cytotoxic drugs. *Cancer Treatment Reviews*, 30(2):181–191.
- Schmitt, W. (2008). General approach for the calculation of tissue to plasma partition coefficients. *Toxicology in Vitro*, 22(2):457–467.
- Schuster, D., Laggner, C., and Langer, T. (2005). Why drugs fail—a study on side effects in new chemical entities. *Current Pharmaceutical Design*, 11(27):3545–3559.
- Scordo, M. G., Caputi, A. P., D’Arrigo, C., Fava, G., and Spina, E. (2004). Allele and genotype frequencies of CYP2C9, CYP2C19 and CYP2D6 in an Italian population. *Pharmacological Research*, 50(2):195–200.
- Shah, I. and Wambaugh, J. (2010). Virtual Tissues in Toxicology. *Journal of Toxicology and Environmental Health*, 13(2-4):314–328.
- Shapiro, R., Jordan, M. L., Scantlebury, V. P., Fung, J. J., Jensen, C., Vivas, C., McCauley, J., Irish, W. D., Mitchell, S., and Demetris, A. J. (1993). Randomized trial of FK 506/prednisone vs FK 506/azathioprine/prednisone after renal transplantation: preliminary report. *Transplantation Proceedings*, 25(1):669–72.
- Shet, M. S., McPhaul, M., Fisher, C. W., Stallings, N. R., and Estabrook, R. W. (1997). Metabolism of the antiandrogenic drug (Flutamide) by human CYP1A2. *Drug Metabolism and Disposition*, 25(11):1298–303.
- Shi, Q., Hong, H., Senior, J., and Tong, W. (2010). Biomarkers for drug-induced liver injury. *Expert Review of Gastroenterology & Hepatology*, 4(2):225–234.
- Shi, Y., Chen, J., Weng, C., Chen, R., Zheng, Y., Chen, Q., and Tang, H. (2003). Identification of the protein-protein contact site and interaction mode of human VDAC1 with Bcl-2 family proteins. *Biochemical and Biophysical Research Communications*, 305(4):989–96.
- Shinoda, S., Aoyama, T., Aoyama, Y., Tomioka, S., Matsumoto, Y., and Ohe, Y. (2007). Pharmacokinetics/pharmacodynamics of acetaminophen analgesia in Japanese patients with chronic pain. *Biological & Pharmaceutical Bulletin*, 30(1):157–61.

- Shivji, K. K., Kenny, M. K., and Wood, R. D. (1992). Proliferating cell nuclear antigen is required for DNA excision repair. *Cell*, 69(2):367–374.
- Skrbo, A., Begović, B., and Skrbo, S. (2004). Classification of drugs using the ATC system (Anatomic, Therapeutic, Chemical Classification) and the latest changes. *Medicinski Arhiv*, 58(1 Suppl 2):138–41.
- Smyth, G. K. (2004). Linear models and empirical bayes methods for assessing differential expression in microarray experiments. *Statistical Applications in Genetics and Molecular Biology*, 3:Article3.
- Song, S. H., Chang, H. E., Jun, S. H., Park, K. U., Lee, J. H., Lee, E.-M., Song, Y.-H., and Song, J. (2013). Relationship between CES2 genetic variations and rifampicin metabolism. *The Journal of Antimicrobial Chemotherapy*, 68(6):1281–4.
- Sousa, M., Pozniak, A., and Boffito, M. (2008). Pharmacokinetics and pharmacodynamics of drug interactions involving rifampicin, rifabutin and antimalarial drugs. *The Journal of Antimicrobial Chemotherapy*, 62(5):872–8.
- Spalding, C. T. and Buss, W. C. (1986). Toxic overdose of isoniazid, rifampicin and ethambutol. *European Journal of Clinical Pharmacology*, 30(3):381–2.
- Stegeman, H., Kaanders, J. H., Wheeler, D. L., van der Kogel, A. J., Verheijen, M. M., Waaijer, S. J., Iida, M., Grénman, R., Span, P. N., and Bussink, J. (2012). Activation of AKT by hypoxia: a potential target for hypoxic tumors of the head and neck. *BMC Cancer*, 12(1):463.
- Stolerman, I. P. (2010). *Encyclopedia of Psychopharmacology*. Springer Berlin Heidelberg, Berlin, Heidelberg.
- Swain, M. (2012). chemicalize.org chemicalize.org by ChemAxon Ltd. *Journal of Chemical Information and Modeling*, 52(2):613–615.
- Takikawa, H., Murata, Y., Horiike, N., Fukui, H., and Onji, M. (2009). Drug-induced liver injury in Japan: An analysis of 1676 cases between 1997 and 2006. *Hepatology Research*, 39(5):427–431.
- Tang-Liu, D. D., Williams, R. L., and Riegelman, S. (1983). Disposition of caffeine and its metabolites in man. *The Journal of Pharmacology and Experimental Therapeutics*, 224(1):180–185.
- Teklay, G., Shiferaw, N., Legesse, B., and Bekele, M. L. (2014). Drug-drug interactions and risk of bleeding among inpatients on warfarin therapy: a prospective observational study. *Thrombosis Journal*, 12(1):20.
- Tenenbein, M. S. M. and Tenenbein, M. S. M. (2005). Acute pancreatitis due to erythromycin overdose. *Pediatric Emergency Care*, 21(10):675–6.
- Thiel, C., Cordes, H., Aschmann, H. E., Fabbri, L., Eloise, A. H., Baier, V., Smit, I., Atkinson, F., Blank, L. M., and Kuepfer, L. (2017a). A comparative analysis of drug-induced hepatotoxicity in clinically relevant situations. *PLoS Computational Biology*.
- Thiel, C., Cordes, H., Baier, V., Blank, L. M., and Kuepfer, L. (2017b). Multiscale modeling reveals inhibitory and stimulatory effects of caffeine on acetaminophen-induced toxicity in humans. *CPT: Pharmacometrics & Systems Pharmacology*.
- Thiel, C., Cordes, H., Conde, I., Castell, J. V., Blank, L. M., and Kuepfer, L. (2016). Model-based contextualization of in vitro toxicity data quantitatively predicts in vivo drug response in patients. *Archives of Toxicology*, 91(2):865–883.

- Thiel, C., Schneckener, S., Krauss, M., Ghallab, A., Hofmann, U., Kanacher, T., Zellmer, S., Gebhardt, R., Hengstler, J. G., and Kuepfer, L. (2015). A systematic evaluation of the use of physiologically based pharmacokinetic modeling for cross-species extrapolation. *Journal of Pharmaceutical Sciences*, 104(1):191–206.
- Value, S. J. R. I. and Samy, W. M. (2012). Class II drugs; a dissolution / bioavailability challenge: Flutamide-loaded spray dried lactose for dissolution control. *International Journal of Drug Development & Research*, 4(2):195–204.
- Van Delft, J., Gaj, S., Lienhard, M., Albrecht, M. W., Kirpiy, A., Brauers, K., Claessen, S., Lizarraga, D., Lehrach, H., Herwig, R., and Kleinjans, J. (2012). Rna-seq provides new insights in the transcriptome responses induced by the carcinogen benzo[a]pyrene. *Toxicological Sciences*, 130(2):427–439.
- van Furth, R., Gassmann, A. E., and Diesselhoff den Dulk, M. (1975). The effect of azathioprine (Imuran®) on the cell cycle of promonocytes and the production of monocytes in the bone marrow. *Journal of Experimental Medicine*, 141(531):531–546.
- Van Os, E. C., Zins, B. J., Sandborn, W. J., Mays, D. C., Tremaine, W. J., Mahoney, D. W., Zinsmeister, a. R., and Lipsky, J. J. (1996). Azathioprine pharmacokinetics after intravenous, oral, delayed release oral and rectal foam administration. *Gut*, 39(1):63–68.
- Velpandian, T., Jasuja, R., Bhardwaj, R. K., Jaiswal, J., and Gupta, S. K. (2001). Piperine in food: interference in the pharmacokinetics of phenytoin. *European Journal of Drug Metabolism and Pharmacokinetics*, 26(4):241–247.
- Veronese, M. E., McLean, S., and Hendriks, R. (1988). Plasma protein binding of amiodarone in a patient population: measurement by erythrocyte partitioning and a novel glass-binding method. *British Journal of Clinical Pharmacology*, 26(6):721–31.
- Vickers, A. E., Meyer, E., Dannecker, R., Keller, B., Tynes, R. E., and Maurer, G. (1995). Human liver cytochrome P4503A biotransformation of the cyclosporin derivative SDZ IMM 125. *Drug Metabolism and Disposition*, 23(3):321–6.
- Von Hoff, D. D., Rozenzweig, M., Layard, M., Slavik, M., and Muggia, F. M. (1977). Daunomycin-induced cardiotoxicity in children and adults. A review of 110 cases. *The American Journal of Medicine*, 62:200–208.
- von Mach, M. a., Hermanns-Clausen, M., Koch, I., Hengstler, J. G., Lauterbach, M., Kaes, J., and Weilemann, L. S. (2005). Experiences of a poison center network with renal insufficiency in acetaminophen overdose: an analysis of 17 cases. *Clinical Toxicology*, 43(1):31–37.
- Vuilleumier, N., Rossier, M. F., Chiappe, A., Degoumois, F., Dayer, P., Mermillod, B., Nicod, L., Desmeules, J., and Hochstrasser, D. (2006). CYP2E1 genotype and isoniazid-induced hepatotoxicity in patients treated for latent tuberculosis. *European Journal of Clinical Pharmacology*, 62(6):423–429.
- Waldhauser, K. M., To, M., Ha, H.-r., Thomet, U., Konrad, D., Brecht, K., Follath, F., Kra, S., Török, M., Ha, H.-r., Thomet, U., Konrad, D., Brecht, K., Follath, F., and Krähenbühl, S. (2006). Hepatocellular toxicity and pharmacological effect of amiodarone and amiodarone derivatives. *The Journal of Pharmacology and Experimental Therapeutics*, 319(3):1413–23.
- Walubo, A., Barr, S., Abraham, A. M., and Coetsee, C. (2004). The role of cytochrome-P450 inhibitors in the prevention of hepatotoxicity after paracetamol overdose in rats. *Human & Experimental Toxicology*, 23(1):49–54.
- Wang, K., Zhou, and Qin (2013). Biomarkers of drug-induced liver injury. *Current Biomarker Findings*, 13(3):1–9.

- Wang, R. W., Newton, D. J., Scheri, T. D., and Lu, A. Y. (1997). Human cytochrome P450 3A4-catalyzed testosterone 6 beta-hydroxylation and erythromycin N-demethylation. Competition during catalysis. *Drug Metabolism and Disposition*, 25(4):502–507.
- Waring, M. J. (2010). Lipophilicity in drug discovery. *Expert Opinion on Drug Discovery*, 5(3):235–248.
- Waring, M. J., Arrowsmith, J., Leach, A. R., Leeson, P. D., Mandrell, S., Owen, R. M., Pairaudeau, G., Pennie, W. D., Pickett, S. D., Wang, J., Wallace, O., and Weir, A. (2015). An analysis of the attrition of drug candidates from four major pharmaceutical companies. *Nature Reviews Drug Discovery*, 14(7):475–86.
- Watanabe, A., Hobara, N., and Nagashima, H. (1978). Demonstration of enzymatic activity converting azathioprine to 6-mercaptopurine. *Acta Medica Okayama*, 32(3):173–179.
- Waters, M. D. and Fostel, J. M. (2004). Toxicogenomics and systems toxicology: Aims and perspectives. *Nature Reviews Genetics*, 5(12):936–48.
- Wetmore, B. a., Wambaugh, J. F., Ferguson, S. S., Li, L., Clewell, H. J., Judson, R. S., Freeman, K., Bao, W., Sochaski, M. a., Chu, T. M., Black, M. B., Healy, E., Allen, B., Andersen, M. E., Wolfinger, R. D., and Thomas, R. S. (2013). Relative impact of incorporating pharmacokinetics on predicting in vivo hazard and mode of action from high-throughput in vitro toxicity assays. *Toxicological Sciences*, 132(2):327–346.
- Willis, J., Kendall, M., Flinn, R., Thornbill, D., and Welling, P. (1979). The pharmacokinetics of diclofenac sodium following intravenous and oral administration. *European Journal of Clinical Pharmacology*, 16(6):405 – 410.
- Willmann, S., Lippert, J., and Schmitt, W. (2005). From physicochemistry to absorption and distribution: predictive mechanistic modelling and computational tools. *Expert Opinion on Drug Metabolism & Toxicology*, 1(1):159–68.
- Willmann, S., Lippert, J., Sevestre, M., Solodenko, J., Fois, F., and Schmitt, W. (2003). PK-Sim®: a physiologically based pharmacokinetic 'whole-body' model. *Biosilico*, 1(4):121–124.
- Willmann, S., Solodenko, J., Sevestre, M., Lippert, J., and Schmitt, W. (2004). A pharmacodynamic extension for the physiology-based pharmacokinetic whole-body model PK-Sim®. *European Journal of Pharmaceutical Sciences*, 23:S75–S75.
- Wilmes, A., Limonciel, A., Aschauer, L., Moenks, K., Bielow, C., Leonard, M. O., Hamon, J., Carpi, D., Ruzek, S., Handler, A., Schmal, O., Herrgen, K., Bellwon, P., Burek, C., Truisi, G. L., Hewitt, P., Di Consiglio, E., Testai, E., Blaauboer, B. J., Guillou, C., Huber, C. G., Lukas, A., Pfaller, W., Mueller, S. O., Bois, F. Y., Dekant, W., and Jennings, P. (2013). Application of integrated transcriptomic, proteomic and metabolomic profiling for the delineation of mechanisms of drug induced cell stress. *Journal of Proteomics*, 79:180–94.
- Winter, J. M., Yeo, C. J., and Brody, J. R. (2013). Diagnostic, prognostic, and predictive biomarkers in pancreatic cancer. *Journal of Surgical Oncology*, 107(1):15–22.
- Wishart, D. S., Knox, C., Guo, A. C., Shrivastava, S., Hassanali, M., Stothard, P., Chang, Z., and Woolsey, J. (2006). DrugBank: a comprehensive resource for in silico drug discovery and exploration. *Nucleic Acids Research*, 34(Database issue):D668–D672.
- Wishart, D. S., Tzur, D., Knox, C., Eisner, R., Guo, A. C., Young, N., Cheng, D., Jewell, K., Arndt, D., Sawhney, S., Fung, C., Nikolai, L., Lewis, M., Coutouly, M.-A., Forsythe, I., Tang, P., Shrivastava, S., Jeroncic, K., Stothard, P., Amegbey, G., Block, D., Hau, D. D., Wagner, J., Miniaci, J., Clements, M., Gebremedhin, M., Guo, N., Zhang, Y., Duggan, G. E., Macinnis, G. D., Weljie, A. M., Dowlatabadi, R., Bamforth, F., Clive, D., Greiner, R., Li, L., Marrie, T., Sykes, B. D., Vogel, H. J., and Querengesser, L. (2007). HMDB: the Human

- Metabolome Database. *Nucleic Acids Research*, 35(Database issue):D521–6.
- Woodhead, J. L., Howell, B. A., Yang, Y., Harrill, A. H., Clewell, H. J., Andersen, M. E., Siler, S. Q., and Watkins, P. B. (2012). An analysis of N-acetylcysteine treatment for acetaminophen overdose using a systems model of drug-induced liver injury. *The Journal of Pharmacology and Experimental Therapeutics*, 342(2):529–40.
- Wrighton, S. A. and Stevens, J. C. (1992). The human hepatic cytochromes P450 involved in drug metabolism. *Critical Reviews in Toxicology*, 22(1):1–21.
- Wu, Z., Irizarry, R. A., Gentleman, R., Martinez-Murillo, F., and Spencer, F. (2004). A Model-Based Background Adjustment for Oligonucleotide Expression Arrays. *Journal of the American Statistical Association*, 99(468):909–917.
- Yagi, Y., Fushida, S., Harada, S., Kinoshita, J., Makino, I., Oyama, K., Tajima, H., Fujita, H., Takamura, H., Ninomiya, I., Fujimura, T., Ohta, T., Yashiro, M., and Hirakawa, K. (2010). Effects of valproic acid on the cell cycle and apoptosis through acetylation of histone and tubulin in a scirrhous gastric cancer cell line. *Journal of Experimental & Clinical Cancer Research*, 29(1):149.
- Yu, L. X., Lipka, E., Crison, J. R., and Amidon, G. L. (1996). Transport approaches to the biopharmaceutical design of oral drug delivery systems: prediction of intestinal absorption. *Advanced Drug Delivery Reviews*, 19(3):359–76.
- Yukawa, E. and Mamiya, K. (2006). Effect of CYP2C19 genetic polymorphism on pharmacokinetics of phenytoin and phenobarbital in Japanese epileptic patients using Non-linear Mixed Effects Model approach. *Journal of Clinical Pharmacy and Therapeutics*, 31(3):275–82.
- Zakeri-Milani, P., Ghanbarzadeh, S., Lotfi poor, F., Milani, M., and Valizadeh, H. (2010). Pharmacokinetic Study of Two Macrolide Antibiotic Oral Suspensions Using an Optimized Bioassay Procedure. *Journal of Bioequivalence & Bioavailability*, 02(5):111–115.
- Zhang, J. D., Berntsen, N., Roth, A., and Ebeling, M. (2014). Data mining reveals a network of early-response genes as a consensus signature of drug-induced in vitro and in vivo toxicity. *The Pharmacogenomics Journal*, 14(3):208–16.
- Zhang, P., Mourad, R., Xiang, Y., Huang, K., Huang, T., Nephew, K., Liu, Y., and Li, L. (2012). A dynamic time order network for time-series gene expression data analysis. *BMC Systems Biology*, 6(Suppl 3):S9.
- Zhang, X., Jones, D. R., and Hall, S. D. (2009). Prediction of the effect of erythromycin, diltiazem, and their metabolites, alone and in combination, on CYP3A4 inhibition. *Drug Metabolism and Disposition*, 37(1):150–160.
- Zhivotovsky, B. and Kroemer, G. (2004). Apoptosis and genomic instability. *Nature Reviews Molecular Cell Biology*, 5(9):752–762.
- Zhou, D., Bui, K., Sostek, M., and Al-Huniti, N. (2016). Simulation and Prediction of the Drug-Drug Interaction Potential of Naloxegol by Physiologically Based Pharmacokinetic Modeling. *CPT: Pharmacometrics & Systems Pharmacology*, 5(5):250–7.
- Zins, B. J., Sandborn, W. J., McKinney, J. a., Mays, D. C., van Os, E. C., Tremaine, W. J., Mahoney, D. W., Zinsmeister, a. R., and Lipsky, J. J. (1997). A dose-ranging study of azathioprine pharmacokinetics after single-dose administration of a delayed-release oral formulation. *Journal of Clinical Pharmacology*, 37(1):38–46.

Part III

Appendix

General supplementary information to Part II

A.1 Toxicogenomics database

Time-series gene expression profiles from Open TG-GATEs [Igarashi et al., 2015] (ArrayExpress accession numbers: E-MTAB-797, E-MTAB-798, E-MTAB-799), a large-scale toxicogenomics database, were used to obtain quantitative drug response data measured in human and rat hepatocytes, as well as in rat livers. Human and rat hepatocytes were exposed to three different concentrations (low, middle, and high). In the original in vitro assay, the highest concentration was selected such that cell viability was decreased by 10-20 % [Igarashi et al., 2015]. The low and middle concentrations were then determined by diluting the highest concentration by five and twenty-five, respectively [Igarashi et al., 2015]. In the in vivo study, a minimum toxic dose identified in a 4-week toxicity study was set as highest dose, while the low and middle dose were one third and one tenth of the high dose, respectively [Igarashi et al., 2015]. Gene expression levels were measured after three exposure durations (2 h, 8 h, and 24 h) in the in vitro study and after four exposure durations (3 h, 6 h, 9 h, 24 h) in the in vivo study leading to nine and twelve different treatments, respectively.

In addition, time-dependent gene expression data of control samples were collected. Fold change values were calculated to indicate gene expression changes compared to the time-matched controls. Cell viability of human and rat hepatocytes was assessed by measuring the total DNA content. Cytotoxicity in each treatment was calculated by the difference of total DNA content between treated hepatocytes and their particular time-matched controls.

A.2 Software

All PBPK models were built by using the software PK-Sim® [Eissing et al., 2011; Willmann et al., 2003, 2004, 2005] (version 6.0, Bayer Technology Services, GmbH, Leverkusen, Germany) and MoBi® (version 3.4, Bayer Technology Services), which are freely available for academic use. Transcriptome analysis was performed in the statistical language R (version 3.1.0, 2014, R Core Team, <http://www.R-project.org>). PICD was implemented in MATLAB (version 8.3.0; The MathWorks, Inc., Natick, MA) by use of the MoBi® Toolbox for MATLAB (version 2.3; Bayer Technology Services GmbH).

B

Supplementary information to Chapter 7

B.1 Supplementary materials

B.1.1 Filtering of gene ontology terms

In gene ontology, genes and gene products are annotated with biological terms from three different sub-ontologies: (i) biological process (BP), (ii) cellular component (CC), and (iii) molecular function (MF) [Ashburner et al., 2000]. These GO terms and their relations are represented as a directed acyclic graph (DAG). In this graph, lower levels characterizing higher specialization. To analyze only significantly affected GO terms with a high degree of specialization, all enriched GO terms having a significant enriched descendant in the DAG were filtered out. An example of this filtering procedure is illustrated in Figure B.1.

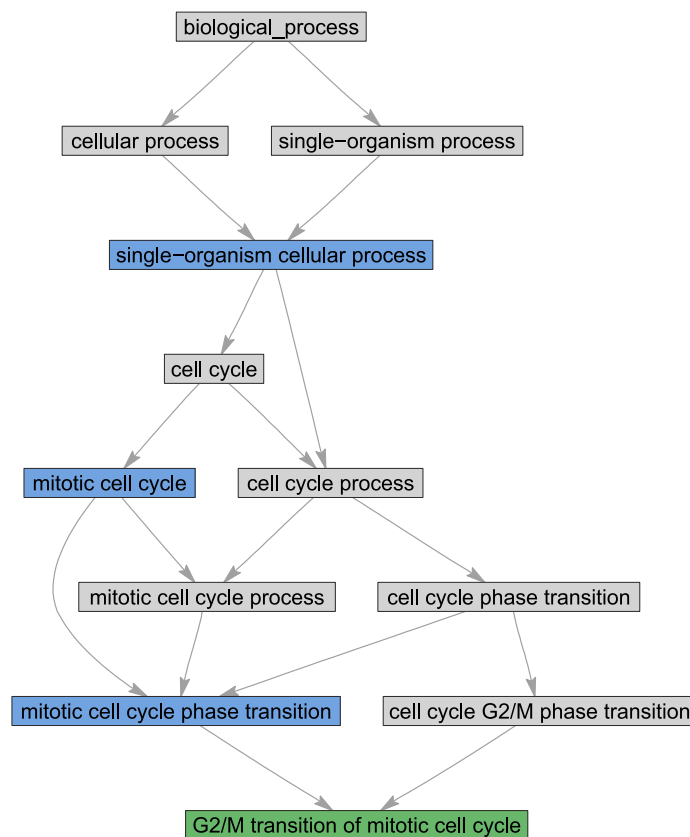


Figure B.1: Filtering gene ontology terms. The presented graph illustrates an exemplary subgraph of the complete GO graph. In total, four biological processes were identified as significantly enriched (blue and green nodes). After applying the filtering procedure, three terms were filtered out (blue nodes) while one remained for further analysis (green). Note that the green node represents the highest specialization.

B.2 Supplementary tables

B.2.1 Analysis of in vitro toxicity data

Table B.1: Enriched terms and pathways. Significantly overrepresented terms (GO) and pathways (KEGG, TOX) identified for human and rat hepatocytes, as well as correspondent p-values. The list of GO terms presents all terms except those removed by the filtering method.

Species	Category	Term ID	Term name	Treatment	P-value
Human	KEGG	hsa00240	Pyrimidine metabolism	Low - 24 h	0.0001855
Human	KEGG	hsa00982	Drug metabolism - cytochrome P450	Low - 24 h	0.00018996
Human	KEGG	hsa03030	DNA replication	Low - 24 h	1.10E-07
Human	KEGG	hsa04110	Cell cycle	Low - 24 h	1.25E-16
Human	KEGG	hsa04114	Oocyte meiosis	Low - 24 h	1.44E-05
Human	KEGG	hsa04115	p53 signaling pathway	Low - 24 h	4.98E-07
Human	KEGG	hsa00830	Retinol metabolism	Middle - 24 h	3.84E-05
Human	KEGG	hsa03030	DNA replication	Middle - 24 h	1.59E-12
Human	KEGG	hsa03420	Nucleotide excision repair	Middle - 24 h	5.47E-05
Human	KEGG	hsa03430	Mismatch repair	Middle - 24 h	4.99E-07
Human	KEGG	hsa03460	Fanconi anemia pathway	Middle - 24 h	2.99E-05
Human	KEGG	hsa04110	Cell cycle	Middle - 24 h	2.62E-17
Human	KEGG	hsa04115	p53 signaling pathway	Middle - 24 h	4.83E-07
Human	KEGG	hsa04141	Protein processing in endoplasmic reticulum	Middle - 24 h	1.41E-05
Human	KEGG	hsa05202	Transcriptional misregulation in cancer	Middle - 24 h	0.00011211
Human	KEGG	hsa04068	FoxO signaling pathway	High - 8 h	8.96E-07
Human	KEGG	hsa04110	Cell cycle	High - 8 h	1.87E-06
Human	KEGG	hsa04115	p53 signaling pathway	High - 8 h	3.66E-05
Human	KEGG	hsa00240	Pyrimidine metabolism	High - 24 h	0.00012092
Human	KEGG	hsa03030	DNA replication	High - 24 h	2.92E-12
Human	KEGG	hsa03430	Mismatch repair	High - 24 h	2.98E-05
Human	KEGG	hsa03460	Fanconi anemia pathway	High - 24 h	4.33E-05
Human	KEGG	hsa04110	Cell cycle	High - 24 h	2.43E-15
Human	KEGG	hsa04115	p53 signaling pathway	High - 24 h	3.20E-05
Human	KEGG	hsa04141	Protein processing in endoplasmic reticulum	High - 24 h	1.06E-08
Human	TOX	TOX:04	DNA Damage & Repair	Low - 24 h	4.86E-06
Human	TOX	TOX:08	Immunotoxicity	Low - 24 h	0.00026011
Human	TOX	TOX:02	Cholestasis	Middle - 8 h	0.0032688
Human	TOX	TOX:04	DNA Damage & Repair	Middle - 24 h	4.45E-09
Human	TOX	TOX:08	Immunotoxicity	Middle - 24 h	0.00087295
Human	TOX	TOX:11	Oxidative Stress & Antioxidant Response	Middle - 24 h	0.0016711
Human	TOX	TOX:07	Heat Shock Response	High - 8 h	8.55E-05
Human	TOX	TOX:04	DNA Damage & Repair	High - 24 h	5.10E-07
Human	TOX	TOX:05	ER Stress & Unfolded Protein Response	High - 24 h	0.00062041
Human	TOX	TOX:07	Heat Shock Response	High - 24 h	0.00031518
Human	TOX	TOX:08	Immunotoxicity	High - 24 h	0.0038211
Human	TOX	TOX:11	Oxidative Stress & Antioxidant Response	High - 24 h	0.0049039
Human	TOX	TOX:12	Phospholipidosis	High - 24 h	0.0014279
Human	GO (BP)	GO:0007091	metaphase/anaphase transition of mitotic cell cycle	Low - 24 h	1.16E-10
Human	GO (BP)	GO:0006271	DNA strand elongation involved in DNA replication	Low - 24 h	1.42E-09
Human	GO (BP)	GO:0034080	CENP-A containing nucleosome assembly	Low - 24 h	6.04E-08
Human	GO (BP)	GO:0051988	regulation of attachment of spindle microtubules to kinetochore	Low - 24 h	9.93E-08
Human	GO (BP)	GO:0006206	pyrimidine nucleobase metabolic process	Low - 24 h	1.80E-07
Human	GO (BP)	GO:0007076	mitotic chromosome condensation	Low - 24 h	7.54E-07
Human	GO (BP)	GO:0007094	mitotic spindle assembly checkpoint	Low - 24 h	8.99E-07
Human	GO (BP)	GO:0008608	attachment of spindle microtubules to kinetochore	Low - 24 h	1.20E-06

Continued on next page

Species	Category	Term ID	Term name	Treatment	P-value
Human	GO (BP)	GO:0000086	G2/M transition of mitotic cell cycle	Low - 24 h	1.48E-06
Human	GO (BP)	GO:0042493	response to drug	Low - 24 h	2.09E-06
Human	GO (BP)	GO:0045132	meiotic chromosome segregation	Low - 24 h	2.42E-06
Human	GO (BP)	GO:0006084	acetyl-CoA metabolic process	Low - 24 h	1.33E-05
Human	GO (BP)	GO:0007100	mitotic centrosome separation	Low - 24 h	2.14E-05
Human	GO (BP)	GO:0008283	cell proliferation	Low - 24 h	3.28E-05
Human	GO (BP)	GO:0055114	oxidation-reduction process	Low - 24 h	3.46E-05
Human	GO (BP)	GO:0006200	ATP catabolic process	Low - 24 h	3.64E-05
Human	GO (BP)	GO:1901606	alpha-amino acid catabolic process	Low - 24 h	4.91E-05
Human	GO (BP)	GO:0007131	reciprocal meiotic recombination	Low - 24 h	5.97E-05
Human	GO (BP)	GO:0009411	response to UV	Low - 24 h	7.00E-05
Human	GO (BP)	GO:0007018	microtubule-based movement	Low - 24 h	7.17E-05
Human	GO (BP)	GO:0015949	nucleobase-containing small molecule interconversion	Low - 24 h	8.60E-05
Human	GO (BP)	GO:0009636	response to toxic substance	Low - 24 h	9.46E-05
Human	GO (BP)	GO:0031570	DNA integrity checkpoint	Low - 24 h	0.00011555
Human	GO (BP)	GO:0090399	replicative senescence	Low - 24 h	0.00011972
Human	GO (BP)	GO:0000910	cytokinesis	Low - 24 h	0.00016247
Human	GO (BP)	GO:0006270	DNA replication initiation	Low - 24 h	0.00017279
Human	GO (BP)	GO:0009437	carnitine metabolic process	Low - 24 h	0.0001839
Human	GO (BP)	GO:0051382	kinetochore assembly	Low - 24 h	0.00026965
Human	GO (BP)	GO:0090068	positive regulation of cell cycle process	Low - 24 h	0.00031613
Human	GO (BP)	GO:0006366	transcription from RNA polymerase II promoter	Middle - 8 h	7.37E-07
Human	GO (BP)	GO:0031016	pancreas development	Middle - 8 h	4.88E-06
Human	GO (BP)	GO:0060412	ventricular septum morphogenesis	Middle - 8 h	1.59E-05
Human	GO (BP)	GO:0006271	DNA strand elongation involved in DNA replication	Middle - 24 h	4.43E-13
Human	GO (BP)	GO:0034080	CENP-A containing nucleosome assembly	Middle - 24 h	6.75E-12
Human	GO (BP)	GO:0007091	metaphase/anaphase transition of mitotic cell cycle	Middle - 24 h	5.31E-09
Human	GO (BP)	GO:0008283	cell proliferation	Middle - 24 h	2.30E-08
Human	GO (BP)	GO:0007076	mitotic chromosome condensation	Middle - 24 h	9.58E-08
Human	GO (BP)	GO:0006987	activation of signaling protein activity involved in unfolded protein response	Middle - 24 h	2.03E-07
Human	GO (BP)	GO:0000083	regulation of transcription involved in G1/S transition of mitotic cell cycle	Middle - 24 h	2.82E-07
Human	GO (BP)	GO:0006270	DNA replication initiation	Middle - 24 h	3.35E-07
Human	GO (BP)	GO:0008608	attachment of spindle microtubules to kinetochore	Middle - 24 h	8.49E-07
Human	GO (BP)	GO:0031100	organ regeneration	Middle - 24 h	9.09E-07
Human	GO (BP)	GO:0032201	telomere maintenance via semi-conservative replication	Middle - 24 h	3.24E-06
Human	GO (BP)	GO:0007094	mitotic spindle assembly checkpoint	Middle - 24 h	4.88E-06
Human	GO (BP)	GO:0051988	regulation of attachment of spindle microtubules to kinetochore	Middle - 24 h	5.33E-06
Human	GO (BP)	GO:0000722	telomere maintenance via recombination	Middle - 24 h	7.00E-06
Human	GO (BP)	GO:0007080	mitotic metaphase plate congression	Middle - 24 h	7.44E-06
Human	GO (BP)	GO:0000910	cytokinesis	Middle - 24 h	1.10E-05
Human	GO (BP)	GO:0070365	hepatocyte differentiation	Middle - 24 h	1.12E-05
Human	GO (BP)	GO:0051382	kinetochore assembly	Middle - 24 h	2.13E-05
Human	GO (BP)	GO:0045132	meiotic chromosome segregation	Middle - 24 h	2.20E-05
Human	GO (BP)	GO:0007019	microtubule depolymerization	Middle - 24 h	2.61E-05
Human	GO (BP)	GO:0014070	response to organic cyclic compound	Middle - 24 h	2.63E-05
Human	GO (BP)	GO:0006302	double-strand break repair	Middle - 24 h	4.12E-05
Human	GO (BP)	GO:0006206	pyrimidine nucleobase metabolic process	Middle - 24 h	4.63E-05
Human	GO (BP)	GO:0006297	nucleotide-excision repair, DNA gap filling	Middle - 24 h	4.77E-05
Human	GO (BP)	GO:0046394	carboxylic acid biosynthetic process	Middle - 24 h	4.80E-05
Human	GO (BP)	GO:0007584	response to nutrient	Middle - 24 h	6.01E-05
Human	GO (BP)	GO:0000086	G2/M transition of mitotic cell cycle	Middle - 24 h	6.59E-05
Human	GO (BP)	GO:0090307	spindle assembly involved in mitosis	Middle - 24 h	9.96E-05
Human	GO (BP)	GO:0006283	transcription-coupled nucleotide-excision repair	Middle - 24 h	0.0001042

Continued on next page

Species	Category	Term ID	Term name	Treatment	P-value
Human	GO (BP)	GO:0016572	histone phosphorylation	Middle - 24 h	0.00010875
Human	GO (BP)	GO:0006268	DNA unwinding involved in DNA replication	Middle - 24 h	0.00010983
Human	GO (BP)	GO:0009411	response to UV	Middle - 24 h	0.00013072
Human	GO (BP)	GO:0071281	cellular response to iron ion	Middle - 24 h	0.00013533
Human	GO (BP)	GO:1901606	alpha-amino acid catabolic process	Middle - 24 h	0.00013547
Human	GO (BP)	GO:0006084	acetyl-CoA metabolic process	Middle - 24 h	0.00014285
Human	GO (BP)	GO:0006200	ATP catabolic process	Middle - 24 h	0.00014961
Human	GO (BP)	GO:0071479	cellular response to ionizing radiation	Middle - 24 h	0.00015656
Human	GO (BP)	GO:0009200	deoxyribonucleoside triphosphate metabolic process	Middle - 24 h	0.00022348
Human	GO (BP)	GO:0015949	nucleobase-containing small molecule interconversion	Middle - 24 h	0.00022348
Human	GO (BP)	GO:0008630	intrinsic apoptotic signaling pathway in response to DNA damage	Middle - 24 h	0.00024137
Human	GO (BP)	GO:0043065	positive regulation of apoptotic process	Middle - 24 h	0.00029346
Human	GO (BP)	GO:0010332	response to gamma radiation	Middle - 24 h	0.00030114
Human	GO (BP)	GO:0007100	mitotic centrosome separation	Middle - 24 h	0.00030171
Human	GO (BP)	GO:0051255	spindle midzone assembly	Middle - 24 h	0.00030171
Human	GO (BP)	GO:0060236	regulation of mitotic spindle organization	Middle - 24 h	0.00030171
Human	GO (BP)	GO:0045765	regulation of angiogenesis	Middle - 24 h	0.00030212
Human	GO (BP)	GO:0040001	establishment of mitotic spindle localization	Middle - 24 h	0.00031938
Human	GO (BP)	GO:0070301	cellular response to hydrogen peroxide	Middle - 24 h	0.00036094
Human	GO (BP)	GO:0000725	recombinational repair	Middle - 24 h	0.000415
Human	GO (BP)	GO:0008283	cell proliferation	High - 8 h	1.78E-06
Human	GO (BP)	GO:0006366	transcription from RNA polymerase II promoter	High - 8 h	3.23E-06
Human	GO (BP)	GO:0033993	response to lipid	High - 8 h	7.54E-06
Human	GO (BP)	GO:0045736	negative regulation of cyclin-dependent protein serine/threonine kinase activity	High - 8 h	7.98E-06
Human	GO (BP)	GO:0014070	response to organic cyclic compound	High - 8 h	1.96E-05
Human	GO (BP)	GO:0009725	response to hormone	High - 8 h	7.34E-05
Human	GO (BP)	GO:0031016	pancreas development	High - 8 h	7.59E-05
Human	GO (BP)	GO:0045944	positive regulation of transcription from RNA polymerase II promoter	High - 8 h	7.98E-05
Human	GO (BP)	GO:0060412	ventricular septum morphogenesis	High - 8 h	9.00E-05
Human	GO (BP)	GO:0090009	primitive streak formation	High - 8 h	0.00010067
Human	GO (BP)	GO:0008285	negative regulation of cell proliferation	High - 8 h	0.00010913
Human	GO (BP)	GO:0048872	homeostasis of number of cells	High - 8 h	0.00012165
Human	GO (BP)	GO:0060537	muscle tissue development	High - 8 h	0.00019426
Human	GO (BP)	GO:0048661	positive regulation of smooth muscle cell proliferation	High - 8 h	0.00019805
Human	GO (BP)	GO:0070647	protein modification by small protein conjugation or removal	High - 8 h	0.0002139
Human	GO (BP)	GO:0055088	lipid homeostasis	High - 8 h	0.0002197
Human	GO (BP)	GO:0030518	intracellular steroid hormone receptor signaling pathway	High - 8 h	0.00026118
Human	GO (BP)	GO:0070848	response to growth factor	High - 8 h	0.00026479
Human	GO (BP)	GO:0006271	DNA strand elongation involved in DNA replication	High - 24 h	1.12E-12
Human	GO (BP)	GO:0034080	CENP-A containing nucleosome assembly	High - 24 h	1.12E-10
Human	GO (BP)	GO:0006987	activation of signaling protein activity involved in unfolded protein response	High - 24 h	2.42E-08
Human	GO (BP)	GO:0006270	DNA replication initiation	High - 24 h	3.57E-07
Human	GO (BP)	GO:0007076	mitotic chromosome condensation	High - 24 h	5.39E-07
Human	GO (BP)	GO:0007091	metaphase/anaphase transition of mitotic cell cycle	High - 24 h	7.41E-07
Human	GO (BP)	GO:0000086	G2/M transition of mitotic cell cycle	High - 24 h	1.86E-06
Human	GO (BP)	GO:0000083	regulation of transcription involved in G1/S transition of mitotic cell cycle	High - 24 h	2.21E-06
Human	GO (BP)	GO:0032201	telomere maintenance via semi-conservative replication	High - 24 h	2.21E-06
Human	GO (BP)	GO:1901606	alpha-amino acid catabolic process	High - 24 h	3.21E-06
Human	GO (BP)	GO:0000722	telomere maintenance via recombination	High - 24 h	5.25E-06

Continued on next page

Species	Category	Term ID	Term name	Treatment	P-value
Human	GO (BP)	GO:0008608	attachment of spindle microtubules to kinetochore	High - 24 h	5.45E-06
Human	GO (BP)	GO:0015949	nucleobase-containing small molecule interconversion	High - 24 h	7.90E-06
Human	GO (BP)	GO:0007584	response to nutrient	High - 24 h	1.09E-05
Human	GO (BP)	GO:0040001	establishment of mitotic spindle localization	High - 24 h	1.33E-05
Human	GO (BP)	GO:0042493	response to drug	High - 24 h	1.84E-05
Human	GO (BP)	GO:0051988	regulation of attachment of spindle microtubules to kinetochore	High - 24 h	1.94E-05
Human	GO (BP)	GO:0060236	regulation of mitotic spindle organization	High - 24 h	3.15E-05
Human	GO (BP)	GO:0007080	mitotic metaphase plate congression	High - 24 h	3.22E-05
Human	GO (BP)	GO:0007094	mitotic spindle assembly checkpoint	High - 24 h	4.01E-05
Human	GO (BP)	GO:0006206	pyrimidine nucleobase metabolic process	High - 24 h	4.33E-05
Human	GO (BP)	GO:0006200	ATP catabolic process	High - 24 h	4.50E-05
Human	GO (BP)	GO:0031100	organ regeneration	High - 24 h	5.62E-05
Human	GO (BP)	GO:0051382	kinetochore assembly	High - 24 h	7.56E-05
Human	GO (BP)	GO:0055114	oxidation-reduction process	High - 24 h	8.31E-05
Human	GO (BP)	GO:0000910	cytokinesis	High - 24 h	8.57E-05
Human	GO (BP)	GO:0008283	cell proliferation	High - 24 h	9.44E-05
Human	GO (BP)	GO:0045132	meiotic chromosome segregation	High - 24 h	0.00010895
Human	GO (BP)	GO:0007019	microtubule depolymerization	High - 24 h	0.00014913
Human	GO (BP)	GO:0046394	carboxylic acid biosynthetic process	High - 24 h	0.00015846
Human	GO (BP)	GO:0006297	nucleotide-excision repair, DNA gap filling	High - 24 h	0.00019643
Human	GO (BP)	GO:0006081	cellular aldehyde metabolic process	High - 24 h	0.00021462
Human	GO (BP)	GO:0071479	cellular response to ionizing radiation	High - 24 h	0.00021462
Human	GO (BP)	GO:0030433	ER-associated ubiquitin-dependent protein catabolic process	High - 24 h	0.00021546
Human	GO (BP)	GO:0090068	positive regulation of cell cycle process	High - 24 h	0.00030154
Human	GO (BP)	GO:0006268	DNA unwinding involved in DNA replication	High - 24 h	0.00031637
Human	GO (BP)	GO:0009157	deoxyribonucleoside monophosphate biosynthetic process	High - 24 h	0.00032348
Human	GO (BP)	GO:0009221	pyrimidine deoxyribonucleotide biosynthetic process	High - 24 h	0.00032348
Human	GO (BP)	GO:0071281	cellular response to iron ion	High - 24 h	0.00032348
Human	GO (BP)	GO:0090307	spindle assembly involved in mitosis	High - 24 h	0.00034088
Human	GO (BP)	GO:0042060	wound healing	High - 24 h	0.00034532
Human	GO (CC)	GO:0032993	protein-DNA complex	Low - 24 h	6.19E-17
Human	GO (CC)	GO:0000922	spindle pole	Low - 24 h	1.28E-12
Human	GO (CC)	GO:0005829	cytosol	Low - 24 h	7.53E-11
Human	GO (CC)	GO:0030496	midbody	Low - 24 h	1.31E-08
Human	GO (CC)	GO:0005654	nucleoplasm	Low - 24 h	8.27E-08
Human	GO (CC)	GO:0005876	spindle microtubule	Low - 24 h	2.18E-07
Human	GO (CC)	GO:0072686	mitotic spindle	Low - 24 h	2.68E-07
Human	GO (CC)	GO:0000778	condensed nuclear chromosome kinetochore	Low - 24 h	3.33E-07
Human	GO (CC)	GO:0005871	kinesin complex	Low - 24 h	6.06E-06
Human	GO (CC)	GO:0000796	condensin complex	Low - 24 h	8.61E-06
Human	GO (CC)	GO:0000940	condensed chromosome outer kinetochore	Low - 24 h	1.12E-05
Human	GO (CC)	GO:0051233	spindle midzone	Low - 24 h	1.74E-05
Human	GO (CC)	GO:0005813	centrosome	Low - 24 h	4.51E-05
Human	GO (CC)	GO:0042555	MCM complex	Low - 24 h	0.00011022
Human	GO (CC)	GO:0008278	cohesin complex	Low - 24 h	0.00016939
Human	GO (CC)	GO:0005730	nucleolus	Low - 24 h	0.00020934
Human	GO (CC)	GO:0035371	microtubule plus-end	Low - 24 h	0.00064107
Human	GO (CC)	GO:0045120	pronucleus	Low - 24 h	0.00083603
Human	GO (CC)	GO:0032993	protein-DNA complex	Middle - 24 h	1.76E-21
Human	GO (CC)	GO:0005654	nucleoplasm	Middle - 24 h	2.22E-12
Human	GO (CC)	GO:0000922	spindle pole	Middle - 24 h	1.17E-11
Human	GO (CC)	GO:0005829	cytosol	Middle - 24 h	5.35E-10
Human	GO (CC)	GO:0000796	condensin complex	Middle - 24 h	2.70E-08
Human	GO (CC)	GO:0030496	midbody	Middle - 24 h	1.53E-07

Continued on next page

Species	Category	Term ID	Term name	Treatment	P-value
Human	GO (CC)	GO:0000778	condensed nuclear chromosome kinetochore	Middle - 24 h	1.80E-07
Human	GO (CC)	GO:0005876	spindle microtubule	Middle - 24 h	2.98E-07
Human	GO (CC)	GO:0000940	condensed chromosome outer kinetochore	Middle - 24 h	9.16E-07
Human	GO (CC)	GO:0005663	DNA replication factor C complex	Middle - 24 h	2.84E-06
Human	GO (CC)	GO:0042555	MCM complex	Middle - 24 h	4.69E-06
Human	GO (CC)	GO:0072686	mitotic spindle	Middle - 24 h	9.32E-06
Human	GO (CC)	GO:0005871	kinesin complex	Middle - 24 h	4.48E-05
Human	GO (CC)	GO:0000785	chromatin	Middle - 24 h	0.00021058
Human	GO (CC)	GO:0005788	endoplasmic reticulum lumen	Middle - 24 h	0.0002234
Human	GO (CC)	GO:0005813	centrosome	Middle - 24 h	0.00051081
Human	GO (CC)	GO:0032300	mismatch repair complex	Middle - 24 h	0.00053004
Human	GO (CC)	GO:0000407	pre-autophagosomal structure	Middle - 24 h	0.00053852
Human	GO (CC)	GO:0051233	spindle midzone	Middle - 24 h	0.00071916
Human	GO (CC)	GO:0035371	microtubule plus-end	Middle - 24 h	0.00093564
Human	GO (CC)	GO:0005654	nucleoplasm	High - 8 h	1.40E-06
Human	GO (CC)	GO:0032993	protein-DNA complex	High - 24 h	5.80E-21
Human	GO (CC)	GO:0000922	spindle pole	High - 24 h	6.20E-11
Human	GO (CC)	GO:0005829	cytosol	High - 24 h	8.18E-10
Human	GO (CC)	GO:0000940	condensed chromosome outer kinetochore	High - 24 h	5.82E-09
Human	GO (CC)	GO:0005654	nucleoplasm	High - 24 h	2.02E-08
Human	GO (CC)	GO:0005876	spindle microtubule	High - 24 h	7.54E-08
Human	GO (CC)	GO:0000796	condensin complex	High - 24 h	1.02E-07
Human	GO (CC)	GO:0030496	midbody	High - 24 h	1.10E-07
Human	GO (CC)	GO:0000778	condensed nuclear chromosome kinetochore	High - 24 h	6.69E-07
Human	GO (CC)	GO:0070062	extracellular vesicular exosome	High - 24 h	6.20E-06
Human	GO (CC)	GO:0005813	centrosome	High - 24 h	7.40E-06
Human	GO (CC)	GO:0005663	DNA replication factor C complex	High - 24 h	8.43E-06
Human	GO (CC)	GO:0042555	MCM complex	High - 24 h	1.68E-05
Human	GO (CC)	GO:0005788	endoplasmic reticulum lumen	High - 24 h	0.00013482
Human	GO (CC)	GO:0005871	kinesin complex	High - 24 h	0.0003161
Human	GO (CC)	GO:0072686	mitotic spindle	High - 24 h	0.00035081
Human	GO (CC)	GO:0032155	cell division site part	High - 24 h	0.00051871
Human	GO (MF)	GO:0005524	ATP binding	Low - 24 h	2.76E-09
Human	GO (MF)	GO:0008017	microtubule binding	Low - 24 h	1.50E-06
Human	GO (MF)	GO:0003777	microtubule motor activity	Low - 24 h	8.25E-06
Human	GO (MF)	GO:0048037	cofactor binding	Low - 24 h	4.04E-05
Human	GO (MF)	GO:0016725	oxidoreductase activity, acting on CH or CH2 groups	Low - 24 h	0.00013223
Human	GO (MF)	GO:0008094	DNA-dependent ATPase activity	Low - 24 h	0.00015474
Human	GO (MF)	GO:0032405	MutLalpha complex binding	Low - 24 h	0.00023851
Human	GO (MF)	GO:0004861	cyclin-dependent protein serine/threonine kinase inhibitor activity	Middle - 8 h	6.21E-06
Human	GO (MF)	GO:0008017	microtubule binding	Middle - 24 h	4.36E-06
Human	GO (MF)	GO:0005524	ATP binding	Middle - 24 h	4.87E-06
Human	GO (MF)	GO:0008094	DNA-dependent ATPase activity	Middle - 24 h	1.88E-05
Human	GO (MF)	GO:0032405	MutLalpha complex binding	Middle - 24 h	4.62E-05
Human	GO (MF)	GO:0030983	mismatched DNA binding	Middle - 24 h	5.60E-05
Human	GO (MF)	GO:0016725	oxidoreductase activity, acting on CH or CH2 groups	Middle - 24 h	0.00010692
Human	GO (MF)	GO:0035174	histone serine kinase activity	Middle - 24 h	0.00013239
Human	GO (MF)	GO:0004861	cyclin-dependent protein serine/threonine kinase inhibitor activity	High - 8 h	6.18E-06
Human	GO (MF)	GO:0035257	nuclear hormone receptor binding	High - 8 h	8.27E-05
Human	GO (MF)	GO:0008017	microtubule binding	High - 24 h	8.41E-06
Human	GO (MF)	GO:0005524	ATP binding	High - 24 h	1.71E-05
Rat	KEGG	rno00051	Fructose and mannose metabolism - Rattus norvegicus (rat)	Middle - 24 h	7.38E-05
Rat	KEGG	rno00830	Retinol metabolism - Rattus norvegicus (rat)	Middle - 24 h	5.98E-05

Continued on next page

Species	Category	Term ID	Term name	Treatment	P-value
Rat	KEGG	rno04610	Complement and coagulation cascades - Rattus norvegicus (rat)	Middle - 24 h	2.46E-06
Rat	KEGG	rno00260	Glycine, serine and threonine metabolism - Rattus norvegicus (rat)	High - 24 h	1.34E-08
Rat	KEGG	rno04610	Complement and coagulation cascades - Rattus norvegicus (rat)	High - 24 h	2.30E-12
Rat	TOX	TOX:04	DNA Damage & Repair	High - 8 h	0.00083009
Rat	GO (BP)	GO:0055114	oxidation-reduction process	Middle - 24 h	5.40E-08
Rat	GO (BP)	GO:0006805	xenobiotic metabolic process	Middle - 24 h	6.05E-06
Rat	GO (BP)	GO:0017144	drug metabolic process	Middle - 24 h	1.01E-05
Rat	GO (BP)	GO:0010043	response to zinc ion	Middle - 24 h	1.39E-05
Rat	GO (BP)	GO:0006790	sulfur compound metabolic process	Middle - 24 h	7.12E-05
Rat	GO (BP)	GO:0001889	liver development	Middle - 24 h	8.44E-05
Rat	GO (BP)	GO:0010468	regulation of gene expression	High - 8 h	8.90E-06
Rat	GO (BP)	GO:0072395	signal transduction involved in cell cycle checkpoint	High - 8 h	2.23E-05
Rat	GO (BP)	GO:0030330	DNA damage response, signal transduction by p53 class mediator	High - 8 h	2.67E-05
Rat	GO (BP)	GO:2000112	regulation of cellular macromolecule biosynthetic process	High - 8 h	2.82E-05
Rat	GO (BP)	GO:0019219	regulation of nucleobase-containing compound metabolic process	High - 8 h	3.00E-05
Rat	GO (BP)	GO:0016070	RNA metabolic process	High - 8 h	4.43E-05
Rat	GO (BP)	GO:0010467	gene expression	High - 8 h	5.87E-05
Rat	GO (BP)	GO:0055114	oxidation-reduction process	High - 24 h	5.09E-13
Rat	GO (BP)	GO:0009071	serine family amino acid catabolic process	High - 24 h	5.31E-07
Rat	GO (BP)	GO:0032787	monocarboxylic acid metabolic process	High - 24 h	1.82E-06
Rat	GO (BP)	GO:0006958	complement activation, classical pathway	High - 24 h	3.06E-06
Rat	GO (BP)	GO:0006544	glycine metabolic process	High - 24 h	3.35E-06
Rat	GO (BP)	GO:1901653	cellular response to peptide	High - 24 h	1.43E-05
Rat	GO (BP)	GO:0001889	liver development	High - 24 h	2.10E-05
Rat	GO (BP)	GO:0006805	xenobiotic metabolic process	High - 24 h	2.43E-05
Rat	GO (BP)	GO:0006006	glucose metabolic process	High - 24 h	2.62E-05
Rat	GO (BP)	GO:0006695	cholesterol biosynthetic process	High - 24 h	3.76E-05
Rat	GO (BP)	GO:0006733	oxidoreduction coenzyme metabolic process	High - 24 h	4.55E-05
Rat	GO (BP)	GO:0042632	cholesterol homeostasis	High - 24 h	4.74E-05
Rat	GO (BP)	GO:0044724	single-organism carbohydrate catabolic process	High - 24 h	5.51E-05
Rat	GO (BP)	GO:0051289	protein homotetramerization	High - 24 h	6.92E-05
Rat	GO (BP)	GO:0006790	sulfur compound metabolic process	High - 24 h	8.35E-05
Rat	GO (BP)	GO:0009070	serine family amino acid biosynthetic process	High - 24 h	8.37E-05
Rat	GO (BP)	GO:0009074	aromatic amino acid family catabolic process	High - 24 h	8.37E-05
Rat	GO (BP)	GO:0072524	pyridine-containing compound metabolic process	High - 24 h	9.02E-05
Rat	GO (BP)	GO:0043434	response to peptide hormone	High - 24 h	9.23E-05
Rat	GO (BP)	GO:0010878	cholesterol storage	High - 24 h	9.44E-05
Rat	GO (CC)	GO:0005615	extracellular space	Middle - 24 h	8.86E-05
Rat	GO (CC)	GO:0005634	nucleus	High - 8 h	3.42E-06
Rat	GO (CC)	GO:0070062	extracellular vesicular exosome	High - 24 h	7.36E-07
Rat	GO (CC)	GO:0005615	extracellular space	High - 24 h	0.00010594
Rat	GO (MF)	GO:0005506	iron ion binding	Middle - 24 h	4.35E-07
Rat	GO (MF)	GO:0005543	phospholipid binding	Middle - 24 h	5.16E-05
Rat	GO (MF)	GO:0016712	oxidoreductase activity, acting on paired donors, ...	Middle - 24 h	5.45E-05
Rat	GO (MF)	GO:0030170	pyridoxal phosphate binding	High - 24 h	2.92E-05
Rat	GO (MF)	GO:0043546	molybdopterin cofactor binding	High - 24 h	2.95E-05

Table B.2: Deleted gene ontology terms. Gene ontology terms that have been deleted after applying the presented filtering method of GO terms (see more in B.1.1). SO, sub-ontologies; BP, biological processes; CC, cellular component; MF, molecular function

Species	SO	Term ID	Term name
Human	BP	GO:0000070	mitotic sister chromatid segregation
Human	BP	GO:0000075	cell cycle checkpoint
Human	BP	GO:0000079	regulation of cyclin-dependent protein ser/thr kinase activity
Human	BP	GO:0000082	G1/S transition of mitotic cell cycle
Human	BP	GO:0000226	microtubule cytoskeleton organization
Human	BP	GO:0000278	mitotic cell cycle
Human	BP	GO:0000280	nuclear division
Human	BP	GO:0000723	telomere maintenance
Human	BP	GO:0000819	sister chromatid segregation
Human	BP	GO:0001702	gastrulation with mouth forming second
Human	BP	GO:0001889	liver development
Human	BP	GO:0001932	regulation of protein phosphorylation
Human	BP	GO:0001933	negative regulation of protein phosphorylation
Human	BP	GO:0003281	ventricular septum development
Human	BP	GO:0006082	organic acid metabolic process
Human	BP	GO:0006259	DNA metabolic process
Human	BP	GO:0006260	DNA replication
Human	BP	GO:0006261	DNA-dependent DNA replication
Human	BP	GO:0006281	DNA repair
Human	BP	GO:0006310	DNA recombination
Human	BP	GO:0006312	mitotic recombination
Human	BP	GO:0006323	DNA packaging
Human	BP	GO:0006333	chromatin assembly or disassembly
Human	BP	GO:0006334	nucleosome assembly
Human	BP	GO:0006336	DNA replication-independent nucleosome assembly
Human	BP	GO:0006338	chromatin remodeling
Human	BP	GO:0006351	transcription, DNA-templated
Human	BP	GO:0006355	regulation of transcription, DNA-templated
Human	BP	GO:0006357	regulation of transcription from RNA polymerase II promoter
Human	BP	GO:0006461	protein complex assembly
Human	BP	GO:0006464	cellular protein modification process
Human	BP	GO:0006468	protein phosphorylation
Human	BP	GO:0006577	amino-acid betaine metabolic process
Human	BP	GO:0006793	phosphorus metabolic process
Human	BP	GO:0006796	phosphate-containing compound metabolic process
Human	BP	GO:0006807	nitrogen compound metabolic process
Human	BP	GO:0006915	apoptotic process
Human	BP	GO:0006950	response to stress
Human	BP	GO:0006974	cellular response to DNA damage stimulus
Human	BP	GO:0006984	ER-nucleus signaling pathway
Human	BP	GO:0006986	response to unfolded protein
Human	BP	GO:0006996	organelle organization
Human	BP	GO:0007010	cytoskeleton organization
Human	BP	GO:0007017	microtubule-based process
Human	BP	GO:0007049	cell cycle
Human	BP	GO:0007051	spindle organization
Human	BP	GO:0007052	mitotic spindle organization
Human	BP	GO:0007059	chromosome segregation
Human	BP	GO:0007067	mitotic nuclear division
Human	BP	GO:0007088	regulation of mitosis
Human	BP	GO:0007093	mitotic cell cycle checkpoint
Human	BP	GO:0007126	meiotic nuclear division

Continued on next page

Species	SO	Term ID	Term name
Human	BP	GO:0007127	meiosis I
Human	BP	GO:0007346	regulation of mitotic cell cycle
Human	BP	GO:0008152	metabolic process
Human	BP	GO:0008219	cell death
Human	BP	GO:0009056	catabolic process
Human	BP	GO:0009058	biosynthetic process
Human	BP	GO:0009059	macromolecule biosynthetic process
Human	BP	GO:0009063	cellular amino acid catabolic process
Human	BP	GO:0009112	nucleobase metabolic process
Human	BP	GO:0009123	nucleoside monophosphate metabolic process
Human	BP	GO:0009125	nucleoside monophosphate catabolic process
Human	BP	GO:0009128	purine nucleoside monophosphate catabolic process
Human	BP	GO:0009158	ribonucleoside monophosphate catabolic process
Human	BP	GO:0009169	purine ribonucleoside monophosphate catabolic process
Human	BP	GO:0009262	deoxyribonucleotide metabolic process
Human	BP	GO:0009263	deoxyribonucleotide biosynthetic process
Human	BP	GO:0009605	response to external stimulus
Human	BP	GO:0009719	response to endogenous stimulus
Human	BP	GO:0009889	regulation of biosynthetic process
Human	BP	GO:0009891	positive regulation of biosynthetic process
Human	BP	GO:0009892	negative regulation of metabolic process
Human	BP	GO:0009893	positive regulation of metabolic process
Human	BP	GO:0009987	cellular process
Human	BP	GO:0009991	response to extracellular stimulus
Human	BP	GO:0010033	response to organic substance
Human	BP	GO:0010035	response to inorganic substance
Human	BP	GO:0010212	response to ionizing radiation
Human	BP	GO:0010468	regulation of gene expression
Human	BP	GO:0010556	regulation of macromolecule biosynthetic process
Human	BP	GO:0010557	positive regulation of macromolecule biosynthetic process
Human	BP	GO:0010564	regulation of cell cycle process
Human	BP	GO:0010604	positive regulation of macromolecule metabolic process
Human	BP	GO:0010605	negative regulation of macromolecule metabolic process
Human	BP	GO:0010628	positive regulation of gene expression
Human	BP	GO:0010639	negative regulation of organelle organization
Human	BP	GO:0010833	telomere maintenance via telomere lengthening
Human	BP	GO:0010941	regulation of cell death
Human	BP	GO:0010942	positive regulation of cell death
Human	BP	GO:0010948	negative regulation of cell cycle process
Human	BP	GO:0012501	programmed cell death
Human	BP	GO:0016043	cellular component organization
Human	BP	GO:0016053	organic acid biosynthetic process
Human	BP	GO:0016054	organic acid catabolic process
Human	BP	GO:0016265	death
Human	BP	GO:0016310	phosphorylation
Human	BP	GO:0018130	heterocycle biosynthetic process
Human	BP	GO:0019222	regulation of metabolic process
Human	BP	GO:0019438	aromatic compound biosynthetic process
Human	BP	GO:0019538	protein metabolic process
Human	BP	GO:0019752	carboxylic acid metabolic process
Human	BP	GO:0022402	cell cycle process
Human	BP	GO:0022616	DNA strand elongation
Human	BP	GO:0030071	regulation of mitotic metaphase/anaphase transition
Human	BP	GO:0030261	chromosome condensation
Human	BP	GO:0030968	endoplasmic reticulum unfolded protein response
Human	BP	GO:0031055	chromatin remodeling at centromere
Human	BP	GO:0031109	microtubule polymerization or depolymerization

Continued on next page

Species	SO	Term ID	Term name
Human	BP	GO:0031145	anaphase-promoting complex-dependent...
Human	BP	GO:0031323	regulation of cellular metabolic process
Human	BP	GO:0031324	negative regulation of cellular metabolic process
Human	BP	GO:0031325	positive regulation of cellular metabolic process
Human	BP	GO:0031326	regulation of cellular biosynthetic process
Human	BP	GO:0031328	positive regulation of cellular biosynthetic process
Human	BP	GO:0031399	regulation of protein modification process
Human	BP	GO:0031497	chromatin assembly
Human	BP	GO:0031577	spindle checkpoint
Human	BP	GO:0031667	response to nutrient levels
Human	BP	GO:0032069	regulation of nuclease activity
Human	BP	GO:0032075	positive regulation of nuclease activity
Human	BP	GO:0032200	telomere organization
Human	BP	GO:0032268	regulation of cellular protein metabolic process
Human	BP	GO:0032269	negative regulation of cellular protein metabolic process
Human	BP	GO:0032774	RNA biosynthetic process
Human	BP	GO:0032787	monocarboxylic acid metabolic process
Human	BP	GO:0032886	regulation of microtubule-based process
Human	BP	GO:0033043	regulation of organelle organization
Human	BP	GO:0033260	nuclear cell cycle DNA replication
Human	BP	GO:0033554	cellular response to stress
Human	BP	GO:0034453	microtubule anchoring
Human	BP	GO:0034508	centromere complex assembly
Human	BP	GO:0034620	cellular response to unfolded protein
Human	BP	GO:0034641	cellular nitrogen compound metabolic process
Human	BP	GO:0034645	cellular macromolecule biosynthetic process
Human	BP	GO:0034654	nucleobase-containing compound biosynthetic process
Human	BP	GO:0034724	DNA replication-independent nucleosome organization
Human	BP	GO:0034728	nucleosome organization
Human	BP	GO:0034976	response to endoplasmic reticulum stress
Human	BP	GO:0035556	intracellular signal transduction
Human	BP	GO:0035825	reciprocal DNA recombination
Human	BP	GO:0035966	response to topologically incorrect protein
Human	BP	GO:0035967	cellular response to topologically incorrect protein
Human	BP	GO:0036211	protein modification process
Human	BP	GO:0042127	regulation of cell proliferation
Human	BP	GO:0042221	response to chemical
Human	BP	GO:0042325	regulation of phosphorylation
Human	BP	GO:0042326	negative regulation of phosphorylation
Human	BP	GO:0042542	response to hydrogen peroxide
Human	BP	GO:0042592	homeostatic process
Human	BP	GO:0042981	regulation of apoptotic process
Human	BP	GO:0043044	ATP-dependent chromatin remodeling
Human	BP	GO:0043067	regulation of programmed cell death
Human	BP	GO:0043068	positive regulation of programmed cell death
Human	BP	GO:0043086	negative regulation of catalytic activity
Human	BP	GO:0043170	macromolecule metabolic process
Human	BP	GO:0043412	macromolecule modification
Human	BP	GO:0043436	oxoacid metabolic process
Human	BP	GO:0043486	histone exchange
Human	BP	GO:0043549	regulation of kinase activity
Human	BP	GO:0043933	macromolecular complex subunit organization
Human	BP	GO:0044237	cellular metabolic process
Human	BP	GO:0044238	primary metabolic process
Human	BP	GO:0044248	cellular catabolic process
Human	BP	GO:0044249	cellular biosynthetic process
Human	BP	GO:0044260	cellular macromolecule metabolic process

Continued on next page

Species	SO	Term ID	Term name
Human	BP	GO:0044267	cellular protein metabolic process
Human	BP	GO:0044271	cellular nitrogen compound biosynthetic process
Human	BP	GO:0044281	small molecule metabolic process
Human	BP	GO:0044282	small molecule catabolic process
Human	BP	GO:0044283	small molecule biosynthetic process
Human	BP	GO:0044699	single-organism process
Human	BP	GO:0044710	single-organism metabolic process
Human	BP	GO:0044711	single-organism biosynthetic process
Human	BP	GO:0044712	single-organism catabolic process
Human	BP	GO:0044763	single-organism cellular process
Human	BP	GO:0044770	cell cycle phase transition
Human	BP	GO:0044772	mitotic cell cycle phase transition
Human	BP	GO:0044784	metaphase/anaphase transition of cell cycle
Human	BP	GO:0044786	cell cycle DNA replication
Human	BP	GO:0044839	cell cycle G2/M phase transition
Human	BP	GO:0044843	cell cycle G1/S phase transition
Human	BP	GO:0045185	maintenance of protein location
Human	BP	GO:0045786	negative regulation of cell cycle
Human	BP	GO:0045787	positive regulation of cell cycle
Human	BP	GO:0045839	negative regulation of mitosis
Human	BP	GO:0045841	negative regulation of mitotic metaphase/anaphase transition
Human	BP	GO:0045859	regulation of protein kinase activity
Human	BP	GO:0045893	positive regulation of transcription, DNA-templated
Human	BP	GO:0045935	positive regulation of nucleobase-containing compound met. process
Human	BP	GO:0046395	carboxylic acid catabolic process
Human	BP	GO:0046483	heterocycle metabolic process
Human	BP	GO:0048285	organelle fission
Human	BP	GO:0048518	positive regulation of biological process
Human	BP	GO:0048519	negative regulation of biological process
Human	BP	GO:0048522	positive regulation of cellular process
Human	BP	GO:0048523	negative regulation of cellular process
Human	BP	GO:0048660	regulation of smooth muscle cell proliferation
Human	BP	GO:0050000	chromosome localization
Human	BP	GO:0050789	regulation of biological process
Human	BP	GO:0050790	regulation of catalytic activity
Human	BP	GO:0050794	regulation of cellular process
Human	BP	GO:0050896	response to stimulus
Human	BP	GO:0051129	negative regulation of cellular component organization
Human	BP	GO:0051171	regulation of nitrogen compound metabolic process
Human	BP	GO:0051173	positive regulation of nitrogen compound metabolic process
Human	BP	GO:0051225	spindle assembly
Human	BP	GO:0051235	maintenance of location
Human	BP	GO:0051246	regulation of protein metabolic process
Human	BP	GO:0051248	negative regulation of protein metabolic process
Human	BP	GO:0051252	regulation of RNA metabolic process
Human	BP	GO:0051254	positive regulation of RNA metabolic process
Human	BP	GO:0051276	chromosome organization
Human	BP	GO:0051293	establishment of spindle localization
Human	BP	GO:0051299	centrosome separation
Human	BP	GO:0051301	cell division
Human	BP	GO:0051302	regulation of cell division
Human	BP	GO:0051303	establishment of chromosome localization
Human	BP	GO:0051310	metaphase plate congression
Human	BP	GO:0051321	meiotic cell cycle
Human	BP	GO:0051338	regulation of transferase activity
Human	BP	GO:0051383	kinetochore organization
Human	BP	GO:0051493	regulation of cytoskeleton organization

Continued on next page

Species	SO	Term ID	Term name
Human	BP	GO:0051640	organelle localization
Human	BP	GO:0051716	cellular response to stimulus
Human	BP	GO:0051726	regulation of cell cycle
Human	BP	GO:0051783	regulation of nuclear division
Human	BP	GO:0051784	negative regulation of nuclear division
Human	BP	GO:0051983	regulation of chromosome segregation
Human	BP	GO:0060255	regulation of macromolecule metabolic process
Human	BP	GO:0061008	hepaticobiliary system development
Human	BP	GO:0061641	CENP-A containing chromatin organization
Human	BP	GO:0065003	macromolecular complex assembly
Human	BP	GO:0065004	protein-DNA complex assembly
Human	BP	GO:0065007	biological regulation
Human	BP	GO:0065008	regulation of biological quality
Human	BP	GO:0065009	regulation of molecular function
Human	BP	GO:0070271	protein complex biogenesis
Human	BP	GO:0070507	regulation of microtubule cytoskeleton organization
Human	BP	GO:0070887	cellular response to chemical stimulus
Human	BP	GO:0071103	DNA conformation change
Human	BP	GO:0071173	spindle assembly checkpoint
Human	BP	GO:0071174	mitotic spindle checkpoint
Human	BP	GO:0071310	cellular response to organic substance
Human	BP	GO:0071704	organic substance metabolic process
Human	BP	GO:0071822	protein complex subunit organization
Human	BP	GO:0071824	protein-DNA complex subunit organization
Human	BP	GO:0071840	cellular component organization or biogenesis
Human	BP	GO:0071900	regulation of protein serine/threonine kinase activity
Human	BP	GO:0071901	negative regulation of protein serine/threonine kinase activity
Human	BP	GO:0072527	pyrimidine-containing compound metabolic process
Human	BP	GO:0080090	regulation of primary metabolic process
Human	BP	GO:0090224	regulation of spindle organization
Human	BP	GO:1901342	regulation of vasculature development
Human	BP	GO:1901360	organic cyclic compound metabolic process
Human	BP	GO:1901362	organic cyclic compound biosynthetic process
Human	BP	GO:1901564	organonitrogen compound metabolic process
Human	BP	GO:1901565	organonitrogen compound catabolic process
Human	BP	GO:1901575	organic substance catabolic process
Human	BP	GO:1901576	organic substance biosynthetic process
Human	BP	GO:1901605	alpha-amino acid metabolic process
Human	BP	GO:1901987	regulation of cell cycle phase transition
Human	BP	GO:1901988	negative regulation of cell cycle phase transition
Human	BP	GO:1901990	regulation of mitotic cell cycle phase transition
Human	BP	GO:1901991	negative regulation of mitotic cell cycle phase transition
Human	BP	GO:1902099	regulation of metaphase/anaphase transition of cell cycle
Human	BP	GO:1902100	negative regulation of metaphase/anaphase transition of cell cycle
Human	BP	GO:1902589	single-organism organelle organization
Human	BP	GO:1902680	positive regulation of RNA biosynthetic process
Human	BP	GO:1902850	microtubule cytoskeleton organization involved in mitosis
Human	BP	GO:1903046	meiotic cell cycle process
Human	BP	GO:1903047	mitotic cell cycle process
Human	BP	GO:2000112	regulation of cellular macromolecule biosynthetic process
Human	BP	GO:2001141	regulation of RNA biosynthetic process
Human	MF	GO:0000166	nucleotide binding
Human	MF	GO:0001882	nucleoside binding
Human	MF	GO:0001883	purine nucleoside binding
Human	MF	GO:0003690	double-stranded DNA binding
Human	MF	GO:0003824	catalytic activity
Human	MF	GO:0004860	protein kinase inhibitor activity

Continued on next page

Species	SO	Term ID	Term name
Human	MF	GO:0005515	protein binding
Human	MF	GO:0015631	tubulin binding
Human	MF	GO:0016491	oxidoreductase activity
Human	MF	GO:0016538	cyclin-dependent protein serine/threonine kinase regulator activity
Human	MF	GO:0016887	ATPase activity
Human	MF	GO:0017076	purine nucleotide binding
Human	MF	GO:0019207	kinase regulator activity
Human	MF	GO:0019210	kinase inhibitor activity
Human	MF	GO:0019887	protein kinase regulator activity
Human	MF	GO:0030291	protein serine/threonine kinase inhibitor activity
Human	MF	GO:0030554	adenyl nucleotide binding
Human	MF	GO:0032404	mismatch repair complex binding
Human	MF	GO:0032549	ribonucleoside binding
Human	MF	GO:0032550	purine ribonucleoside binding
Human	MF	GO:0032553	ribonucleotide binding
Human	MF	GO:0032555	purine ribonucleotide binding
Human	MF	GO:0032559	adenyl ribonucleotide binding
Human	MF	GO:0035173	histone kinase activity
Human	MF	GO:0035639	purine ribonucleoside triphosphate binding
Human	MF	GO:0036094	small molecule binding
Human	MF	GO:0043168	anion binding
Human	MF	GO:0043566	structure-specific DNA binding
Human	MF	GO:0097367	carbohydrate derivative binding
Human	MF	GO:1901265	nucleoside phosphate binding
Human	CC	GO:0000228	nuclear chromosome
Human	CC	GO:0000775	chromosome, centromeric region
Human	CC	GO:0000776	kinetochore
Human	CC	GO:0000777	condensed chromosome kinetochore
Human	CC	GO:0000779	condensed chromosome, centromeric region
Human	CC	GO:0000780	condensed nuclear chromosome, centromeric region
Human	CC	GO:0000793	condensed chromosome
Human	CC	GO:0000794	condensed nuclear chromosome
Human	CC	GO:0005622	intracellular
Human	CC	GO:0005623	cell
Human	CC	GO:0005634	nucleus
Human	CC	GO:0005657	replication fork
Human	CC	GO:0005694	chromosome
Human	CC	GO:0005737	cytoplasm
Human	CC	GO:0005783	endoplasmic reticulum
Human	CC	GO:0005815	microtubule organizing center
Human	CC	GO:0005819	spindle
Human	CC	GO:0005856	cytoskeleton
Human	CC	GO:0005874	microtubule
Human	CC	GO:0005875	microtubule associated complex
Human	CC	GO:0015630	microtubule cytoskeleton
Human	CC	GO:0031974	membrane-enclosed lumen
Human	CC	GO:0031981	nuclear lumen
Human	CC	GO:0031988	membrane-bounded vesicle
Human	CC	GO:0032153	cell division site
Human	CC	GO:0043226	organelle
Human	CC	GO:0043227	membrane-bounded organelle
Human	CC	GO:0043228	non-membrane-bounded organelle
Human	CC	GO:0043229	intracellular organelle
Human	CC	GO:0043230	extracellular organelle
Human	CC	GO:0043231	intracellular membrane-bounded organelle
Human	CC	GO:0043232	intracellular non-membrane-bounded organelle
Human	CC	GO:0043233	organelle lumen

Continued on next page

Species	SO	Term ID	Term name
Human	CC	GO:0044421	extracellular region part
Human	CC	GO:0044422	organelle part
Human	CC	GO:0044424	intracellular part
Human	CC	GO:0044427	chromosomal part
Human	CC	GO:0044428	nuclear part
Human	CC	GO:0044430	cytoskeletal part
Human	CC	GO:0044432	endoplasmic reticulum part
Human	CC	GO:0044444	cytoplasmic part
Human	CC	GO:0044446	intracellular organelle part
Human	CC	GO:0044454	nuclear chromosome part
Human	CC	GO:0044464	cell part
Human	CC	GO:0044815	DNA packaging complex
Human	CC	GO:0065010	extracellular membrane-bounded organelle
Human	CC	GO:0070013	intracellular organelle lumen
Human	CC	GO:1990391	DNA repair complex
Rat	BP	GO:0005996	monosaccharide metabolic process
Rat	BP	GO:0006066	alcohol metabolic process
Rat	BP	GO:0006082	organic acid metabolic process
Rat	BP	GO:0006520	cellular amino acid metabolic process
Rat	BP	GO:0006629	lipid metabolic process
Rat	BP	GO:0006694	steroid biosynthetic process
Rat	BP	GO:0006725	cellular aromatic compound metabolic process
Rat	BP	GO:0006732	coenzyme metabolic process
Rat	BP	GO:0006950	response to stress
Rat	BP	GO:0006956	complement activation
Rat	BP	GO:0008152	metabolic process
Rat	BP	GO:0008202	steroid metabolic process
Rat	BP	GO:0008203	cholesterol metabolic process
Rat	BP	GO:0008652	cellular amino acid biosynthetic process
Rat	BP	GO:0009056	catabolic process
Rat	BP	GO:0009063	cellular amino acid catabolic process
Rat	BP	GO:0009069	serine family amino acid metabolic process
Rat	BP	GO:0009410	response to xenobiotic stimulus
Rat	BP	GO:0009725	response to hormone
Rat	BP	GO:0009889	regulation of biosynthetic process
Rat	BP	GO:0010556	regulation of macromolecule biosynthetic process
Rat	BP	GO:0016052	carbohydrate catabolic process
Rat	BP	GO:0016053	organic acid biosynthetic process
Rat	BP	GO:0016054	organic acid catabolic process
Rat	BP	GO:0016125	sterol metabolic process
Rat	BP	GO:0016126	sterol biosynthetic process
Rat	BP	GO:0019222	regulation of metabolic process
Rat	BP	GO:0019318	hexose metabolic process
Rat	BP	GO:0019752	carboxylic acid metabolic process
Rat	BP	GO:0031323	regulation of cellular metabolic process
Rat	BP	GO:0033554	cellular response to stress
Rat	BP	GO:0043436	oxoacid metabolic process
Rat	BP	GO:0044237	cellular metabolic process
Rat	BP	GO:0044238	primary metabolic process
Rat	BP	GO:0044248	cellular catabolic process
Rat	BP	GO:0044281	small molecule metabolic process
Rat	BP	GO:0044282	small molecule catabolic process
Rat	BP	GO:0044283	small molecule biosynthetic process
Rat	BP	GO:0044710	single-organism metabolic process
Rat	BP	GO:0044711	single-organism biosynthetic process
Rat	BP	GO:0044712	single-organism catabolic process
Rat	BP	GO:0046394	carboxylic acid biosynthetic process

Continued on next page

Species	SO	Term ID	Term name
Rat	BP	GO:0046395	carboxylic acid catabolic process
Rat	BP	GO:0046483	heterocycle metabolic process
Rat	BP	GO:0050789	regulation of biological process
Rat	BP	GO:0050794	regulation of cellular process
Rat	BP	GO:0051171	regulation of nitrogen compound metabolic process
Rat	BP	GO:0051186	cofactor metabolic process
Rat	BP	GO:0055088	lipid homeostasis
Rat	BP	GO:0055092	sterol homeostasis
Rat	BP	GO:0061008	hepaticobiliary system development
Rat	BP	GO:0071466	cellular response to xenobiotic stimulus
Rat	BP	GO:0071704	organic substance metabolic process
Rat	BP	GO:0072331	signal transduction by p53 class mediator
Rat	BP	GO:0072376	protein activation cascade
Rat	BP	GO:0080090	regulation of primary metabolic process
Rat	BP	GO:1901360	organic cyclic compound metabolic process
Rat	BP	GO:1901564	organonitrogen compound metabolic process
Rat	BP	GO:1901575	organic substance catabolic process
Rat	BP	GO:1901605	alpha-amino acid metabolic process
Rat	BP	GO:1901606	alpha-amino acid catabolic process
Rat	BP	GO:1901615	organic hydroxy compound metabolic process
Rat	BP	GO:1901652	response to peptide
Rat	BP	GO:1901700	response to oxygen-containing compound
Rat	CC	GO:0005576	extracellular region
Rat	CC	GO:0005622	intracellular
Rat	CC	GO:0031982	vesicle
Rat	CC	GO:0031988	membrane-bounded vesicle
Rat	CC	GO:0043226	organelle
Rat	CC	GO:0043227	membrane-bounded organelle
Rat	CC	GO:0043230	extracellular organelle
Rat	CC	GO:0044421	extracellular region part
Rat	CC	GO:0044424	intracellular part
Rat	CC	GO:0065010	extracellular membrane-bounded organelle
Rat	MF	GO:0003824	catalytic activity
Rat	MF	GO:0004497	monooxygenase activity
Rat	MF	GO:0016491	oxidoreductase activity
Rat	MF	GO:0016705	oxidoreductase activity, acting on paired donors, ...
Rat	MF	GO:0043168	anion binding
Rat	MF	GO:0048037	cofactor binding
Rat	MF	GO:0050662	coenzyme binding

B.2.2 Assessment of predicted in vivo drug responses in rats

Table B.3: Correlation results for significantly regulated pathways and cellular processes in rats. Comparison between predicted drug response and in vivo measurements in rats for significantly regulated pathways and cellular processes. r, Pearson's correlation coefficient; p, p-value.

Term ID	Term name	r	p
rno00830	retinol metabolism - Rattus norvegicus (rat)	0.81	0.001
GO:0005506	iron ion binding	0.76	0.004
GO:0006805	xenobiotic metabolic process	0.76	0.004
GO:0030170	pyridoxal phosphate binding	0.71	0.01
GO:0070062	extracellular vesicular exosome	0.68	0.015
GO:0006790	sulfur compound metabolic process	0.67	0.018
GO:0043546	molybdopterin cofactor binding	0.65	0.023
GO:0001889	liver development	0.64	0.025
GO:0005634	nucleus	0.63	0.029
GO:0010467	gene expression	0.62	0.031
GO:0006695	cholesterol biosynthetic process	0.62	0.031
GO:0032787	monocarboxylic acid metabolic process	0.62	0.032
TOX:04	DNA Damage & Repair	0.62	0.032
GO:0055114	oxidation-reduction process	0.61	0.034
GO:0006006	glucose metabolic process	0.61	0.037
GO:0044724	single-organism carbohydrate catabolic process	0.60	0.041
GO:0016070	RNA metabolic process	0.59	0.041
GO:0051289	protein homotetramerization	0.58	0.049
rno04610	complement and coagulation cascades - Rattus norvegicus (rat)	0.56	0.058
GO:0043434	response to peptide hormone	0.55	0.063
GO:2000112	regulation of cellular macromolecule biosynthetic process	0.54	0.071
GO:0019219	regulation of nucleobase-containing compound metabolic process	0.54	0.073
GO:1901653	cellular response to peptide	0.53	0.076
GO:0010468	regulation of gene expression	0.52	0.082
GO:0016712	oxidoreductase activity, acting on paired donors, ...	0.51	0.088
GO:0042632	cholesterol homeostasis	0.43	0.164
rno00260	glycine, serine and threonine metabolism - Rattus norvegicus (rat)	0.42	0.171
GO:0005543	phospholipid binding	0.42	0.172
GO:0017144	drug metabolic process	0.39	0.211
GO:0009074	aromatic amino acid family catabolic process	0.39	0.214
GO:0010878	cholesterol storage	0.37	0.235
GO:0006733	oxidoreduction coenzyme metabolic process	0.36	0.254
GO:0072524	pyridine-containing compound metabolic process	0.34	0.286
GO:0006958	complement activation, classical pathway	0.33	0.295
GO:0030330	DNA damage response, signal transduction by p53 class mediator	0.33	0.296
GO:0005615	extracellular space	0.32	0.304
GO:0009070	serine family amino acid biosynthetic process	0.32	0.31
GO:0010043	response to zinc ion	0.29	0.356
GO:0072395	signal transduction involved in cell cycle checkpoint	-0.27	0.40
GO:0009071	serine family amino acid catabolic process	0.17	0.602
rno00051	fructose and mannose metabolism - Rattus norvegicus (rat)	-0.11	0.741
GO:0006544	glycine metabolic process	0.10	0.76

B.2.3 Genes and pathways

Table B.4: Toxicity-related biological pathways. Symbols as well as human and rat Entrez IDs for 370 genes showing high response to toxic compounds were grouped in thirteen different biological pathways. The genes and the functional gene grouping terms were taken from the Human Molecular Toxicology PathwayFinder RT² ProfilerTM PCR Array (SABiosciences, www.sabiosciences.com). Rat Entrez IDs were identified through the use of QIAGENs Ingenuity Pathway Analysis (IPA®), QIAGEN Redwood City, www.qiagen.com/ingenuity).

ID	Term name	Symbols	Entrez IDs (human)	Entrez IDs (rat)
TOX:01	Apoptosis	ABL1, AKT1, APAF1, BAD, BAK1, BAX, BCL2, BCL2L1, BCL2L11, BID, BIRC3, CASP1, CASP3, CASP7, CASP8, CASP9, CD40, CD40LG, CFLAR, FADD, FAS, FASLG, GADD45A, MCL1, TNF, TNFRSF10A, TNFRSF10B, TNFRSF1A, TNFSF10, TP53, XIAP	25, 207, 317, 572, 578, 581, 596, 598, 10018, 637, 330, 834, 836, 840, 841, 842, 958, 959, 8837, 8772, 355, 356, 1647, 4170, 7124, 8797, 8795, 7132, 8743, 7157, 331	311860, 24185, 78963, 64639, 116502, 24887, 24224, 24888, 64547, 64625, 78971, 25166, 25402, 64026, 64044, 58918, 171369, 84349, 117279, 266610, 246097, 25385, 25112, 60430, 24835, 364420, not found , 25625, 246775, 24842, 63879
TOX:02	Cholestasis	ABCB1, ABCB4, ABCC1, ABCC2, ABCC3, APOE, ATP8B1, CYP3A4, CYP7A1, DLAT, ESR1, HLA-DRB1, ICAM1, IL10, IL1B, IL2, IL6, JAG1, MPO, NR1H4, NUP210, OSTALPHA, OSTBETA, PDYN, RDX, SLC10A1, TGFB1, TNF	5243, 5244, 4363, 1244, 8714, 348, 5205, 1576, 1581, 1737, 2099, 3123, 3383, 3586, 3553, 3558, 3569, 182, 4353, 9971, 23225, 200931, 123264, 5173, 5962, 6554, 7040, 7124	170913, 24891, 24565, 25303, 140668, 25728, 291555, 266682, 25428, 81654, 24890, not found , 25464, 25325, 24494, 116562, 24498, 29146, not found , 60351, 58958, 29190, 315655, 24777, 303879, 300790, 59086, 24835
TOX:03	Cytochrome P450s & Phase I Drug Metabolism	CYP1A1, CYP1A2, CYP2B6, CYP2C19, CYP2C9, CYP2D6, CYP2E1, CYP3A4, ESD, FMO2, FMO3, FMO4, FMO5, MAOA, MAOB	1543, 1544, 1555, 1557, 1559, 1565, 1571, 1576, 2098, 2327, 2328, 2329, 2330, 4128, 4129	24296, 24297, 24300, 293989, 29277, 24303, 25086, 266682, 290401, 246245, 84493, 246247, 246248, 29253, 25750
TOX:04	DNA Damage & Repair	APEX1, ATM, ATR, BRCA1, BRCA2, CDKN1A, CHEK1, CHEK2, DDIT3, ERCC1, ERCC2, ERCC3, ERCC5, ERCC6, GADD45A, LIG4, MDM2, MGMT, MLH1, MSH2, OGG1, PARP1, PCNA, PRKDC, RAD51, TP53, XPA, XPC, XRCC1, XRCC5	328, 472, 545, 672, 675, 1026, 1111, 11200, 1649, 2067, 2068, 2071, 2073, 2074, 1647, 3981, 4193, 4255, 4292, 4436, 4968, 142, 5111, 5591, 5888, 7157, 7507, 7508, 7515, 7520	79116, 300711, 685055, 497672, 360254, 114851, 140583, 114212, 29467, 292673, 308415, 291703, 301382, 306274, 25112, 290907, 314856, 25332, 81685, 81709, 81528, 25591, 25737, 360748, 499870, 24842, 298074, 312560, 84495, 363247
TOX:05	ER Stress & Unfolded Protein Response	AMFR, ATF4, ATF6, BAX, DDIT3, DERL1, EDEM1, EDEM3, EIF2AK3, ERN2, ERO1L, ERO1LB, FBXO6, GADD45A, HERPUD1, HTRA2, HTRA4, MBTPS1, MBTPS2, NPLOC4, NUCB1, OS9, PFDN5, PPIA, SEC62, SEL1L, SELS, SERP1, SYVN1, UBE2G2, UBE2J2, UBXLN4, VCP, XBP1	267, 468, 22926, 581, 1649, 79139, 9695, 80267, 9451, 10595, 30001, 56605, 26270, 1647, 9709, 27429, 203100, 8720, 51360, 55666, 4924, 10956, 5204, 5478, 7095, 6400, 55829, 27230, 84447, 7327, 118424, 23190, 7415, 7495	361367, 79255, 304962, 24887, 29467, 362912, 297504, 289085, 29702, 365363, 171562, 364755, 192351, 25112, 85430, 297376, 306564, 89842, 302705, 140639, 84595, 362891, 300257, 25518, 294912, 314352, 80881, 361712, 294331, 298689, 304766, 116643, 286900, not found

Continued on next page

ID	Term name	Symbols	Entrez IDs (human)	Entrez IDs (rat)
TOX:06	Fatty Acid Metabolism	ACAA1, ACAA2, ACAD11, ACAD9, ACADL, ACADM, ACADS, ACADSB, ACADVL, ACAT1, ACAT2, ACOT1, ACOT12, ACOT2, ACOT6, ACOT7, ACOT8, ACOT9, ACOX1, ACOX2, ACOX3, CPT1A, CPT1B, CPT2, CRAT, CROT, ECHS1, EHHADH, GCDH, HADHA	30, 10449, 84129, 28976, 33, 34, 35, 36, 37, 38, 39, 641371, 134526, 10965, 641372, 11332, 10005, 23597, 51, 8309, 8310, 1374, 1375, 1376, 1384, 54677, 1892, 1962, 2639, 3030	24157, 170465, 315973, 294973, 25287, 24158, 64304, 25618, 25363, 25014, 308100, 314304, 170570, 192272, not found, 26759, 170588, 302640, 50681, 252898, 83522, 25757, 25756, 25413, 311849, 83842, 140547, 171142, 364975, 170670
TOX:07	Heat Shock Response	CRYAA, CRYAB, DNAJA1, DNAJA2, DNAJA3, DNAJB1, DNAJB6, DNAJC3, DNAJC5, DNAJC6, HSF1, HSF2, HSP90AA1, HSP90AB1, HSP90B1, HSPA1A, HSPA1B, HSPA1L, HSPA2, HSPA4, HSPA5, HSPA8, HSPA9, HSPB1, HSPB2, HSPB6, HSPB8, HSPD1, HSPE1, HSPH1, TCP1	1409, 1410, 3301, 10294, 9093, 3337, 10049, 5611, 80331, 9829, 3297, 3298, 3320, 3326, 7184, 3303, 3304, 3305, 3306, 3308, 3309, 3312, 3313, 3315, 3316, 126393, 26353, 3329, 3336, 10808, 6950	24273, 25420, 65028, 84026, 360481, 361384, 362293, 63880, 79130, 313409, 79245, 64441, 299331, 301252, 362862, 294254, 24472, 24963, 60460, 266759, 25617, 24468, 291671, 24471, 161476, 192245, 113906, 63868, 25462, 288444, 24818
TOX:08	Immunotoxicity	ADH1C, AHR, AHSG, ALB, APOA5, APOF, C3, C9, CASP3, CD19, CD4, CD44, CD80, CD86, CD8A, CTSE, CYP1A1, CYP3A4, CYP3A4, EP300, F2, FABP1, FAS, GPT, GSTA3, HPX, HRG, HSPA5, IFNA1, IFNG, IL10, IL13, IL1A, IL1B, IL2, IL4, IL5, IL6, ITGAX, KLF1, LYZ, LYZ, METAP2, MKI67, NFKB1, NR5A2, PON1, POU3F3, PTGS2, PTPRC, SOD1, TNF, TRIM10, UBQLN2	126, 196, 197, 213, 116519, 319, 718, 735, 836, 930, 920, 960, 941, 942, 925, 1510, 1543, 1576, 1576, 2033, 2147, 2168, 355, 2875, 2940, 3263, 3273, 3309, 3439, 3458, 3586, 3596, 3552, 3553, 3558, 3565, 3567, 3569, 3687, 10661, 4069, 4069, 10988, 4288, 4790, 2494, 5444, 5455, 5743, 5788, 6647, 7124, 10107, 29978	24172, 25690, 25373, 24186, 140638, 500761, 24232, 117512, 25402, 365367, 24932, 25406, 25408, 56822, 24930, 25424, 24296, 266682, 170915, 29251, 24360, 246097, 81670, 494500, 58917, not found, 25617, not found, 25712, 25325, 116553, 24493, 24494, 116562, 287287, 24497, 24498, 499271, 304666, 25211, 64370, 291234, 81736, 60349, 84024, 192109, 29527, 24699, 24786, 24835, 294210, 317396
TOX:09	Mitochondrial Energy Metabolism	ACLY, ACO1, ACO2, COX6B1, COX8A, CS, CYC1, DLD, DLST, FH, IDH1, IDH2, IDH3A, IDH3B, IDH3G, MDH1, MDH1B, MDH2, OGDH, SDHA, SDHB, SDHC, SDHD, SUCLA2, SUCLG1, SUCLG2, UCP1, UCP2, UCP3	47, 48, 50, 1340, 1351, 1431, 1537, 1738, 1743, 2271, 3417, 3418, 3419, 3420, 3421, 4190, 130752, 4191, 4967, 6389, 6390, 6391, 6392, 8803, 8802, 8801, 7350, 7351, 7352	24159, 50655, 79250, 688869, 171335, 170587, 300047, 298942, 299201, 24368, 24479, 361596, 114096, 94173, 25179, 24551, 316444, 81829, 360975, 157074, 298596, 289217, 363061, 361071, 114597, 362404, 24860, 54315, 25708

Continued on next page

ID	Term name	Symbols	Entrez IDs (human)	Entrez IDs (rat)
TOX:10	Necrosis	ATP6V1G2, BMF, CCDC103, CD300LD, CLEC18A, COMMD4, CYLD, DEFB1, DPYSL4, EIF5B, FOXI1, GALNT5, GRB2, HOXA3, HSPBAP1, JPH3, KCNIP1, MAG, NUDT13, OR10J3, PARP2, PVR, RAB25, S100A7A, SPATA2, SYCP2, TMEM57, TNFAIP8L1, TNFRSF1A, TXNL4B	534, 90427, 388389, 100131439, 348174, 54939, 1540, 1672, 10570, 9669, 2299, 11227, 2885, 3200, 79663, 57338, 30820, 4099, 25961, 441911, 10038, 5817, 57111, 338324, 9825, 10388, 55219, 126282, 7132, 54957	368044, 246142, 498006, 360655, not found , 363068, 312937, not found , 25417, 308306, 287185, 83627, 81504, 500125, 171460, 307916, 65023, 29409, 682978, 289240, 290027, not found , 310632, not found , 114210, 83820, 313618, 301131, 25625, 292008
TOX:11	Oxidative Stress & Antioxidant Response	AASS, CAT, CTSB, DHCR24, DUOX1, DUOX2, EPX, GPX1, GPX2, GPX3, GPX4, GPX5, GPX6, GPX7, IDH1, MPO, NQO1, NUDT1, NUDT15, PPP1R15B, PRDX1, PRDX2, PRDX6, SOD1, TPO, TXNIP, TXNRD2, UCP3	10157, 847, 1508, 1718, 53905, 50506, 8288, 2876, 2877, 2878, 2879, 2880, 257202, 2882, 3417, 4353, 1728, 4521, 55270, 84919, 5052, 7001, 9588, 6647, 7173, 10628, 10587, 7352	296925, 24248, 64529, 298298, 266807, 79107, 303414, 24404, 29326, 64317, 29328, 113919, 259233, 298376, 24479, not found , 24314, 117260, 290365, 304799, 117254, 29338, 94167, 24786, 54314, 117514, 50551, 25708
TOX:12	Phospholipidosis	ABCB1, ALDH1A1, ASAH1, ASNS, CES2, CTSB, EPHX1, FABP1, FXC1, GSTM4, HPN, INHBE, LSS, MANBA, MLX, MRPS18B, NR0B2, POR, S100A8, SC4MOL, SERPINA3, SLC2A3, SLC01A2, SMPD1, STBD1, TAGLN, UGT1A1, UGT2A1, UGT2B4, WIP1	5243, 216, 427, 440, 8824, 1508, 2052, 2168, 26515, 2948, 3249, 83729, 4047, 4126, 6945, 28973, 8431, 5447, 6279, 6307, 12, 6515, 6579, 6609, 8987, 6876, 54658, 10941, 7363, 55062	170913, 24188, 84431, 25612, 498940, 64529, 25315, 24360, 499689, 29135, 83711, 81681, 310864, 360631, 294230, 140910, 117274, 29441, 116547, 24795, 25551, 80900, 308909, 305234, 25123, 84384, 24861, 63867, 286989, 303630
TOX:13	Steatosis	ACACA, ADK, ALDH2, AQP4, CD36, COMT, CYP2E1, CYP7B1, DNM1, ENO1, FAS, FASN, GPD1, HAAO, HADHB, KHK, LMNA, LPL, LY6D, MAPK8, MTP, PCCA, PNPLA3, PPARA, RETN, SCD, SREBF1, SYT1, TFF3, VCP	31, 132, 217, 361, 948, 1312, 1571, 9420, 1759, 2023, 355, 2194, 2819, 23498, 3032, 3795, 4000, 4023, 8581, 5599, 4547, 5095, 80339, 5465, 56729, 6319, 6720, 6857, 7033, 7415	60581, 25368, 29539, 25293, 29184, 24267, 25086, 25429, 140694, 24333, 246097, 50671, 60666, 56823, 171155, 25659, 60374, 24539, 315075, 116554, 310900, 687008, 362972, 25747, 246250, 246074, 78968, 25716, 25563, 116643

Table B.5: Genes involved in the DNA damage & repair pathway. Symbols, Entrez gene name, type, as well as human and rat Entrez identifier for all genes involved in the DNA damage & repair pathway. Functional classifications were taken from QIAGENs Ingenuity Pathway Analysis (IPA®), QIAGEN Redwood City, www.qiagen.com/ingenuity).

Gene	Entrez gene name	Type	Entrez ID (human)	Entrez ID (rat)
APEX1	APEX nuclease (multifunctional DNA repair enzyme) 1	enzyme	328	79116
ATM	ATM serine/threonine kinase	kinase	472	300711
ATR	ATR serine/threonine kinase	kinase	545	685055
BRCA1	breast cancer 1, early onset	transcription regulator	672	497672
BRCA2	breast cancer 2, early onset	transcription regulator	675	360254
CDKN1A	cyclin-dependent kinase inhibitor 1A (p21, Cip1)	kinase	1026	114851
CHEK1	checkpoint kinase 1	kinase	1111	140583
CHEK2	checkpoint kinase 2	kinase	11200	114212
DDIT3	DNA-damage-inducible transcript 3	transcription regulator	1649	29467
ERCC1	excision repair cross-complementation group 1	enzyme	2067	292673
ERCC2	excision repair cross-complementation group 2	enzyme	2068	308415
ERCC3	excision repair cross-complementation group 3	enzyme	2071	291703
ERCC5	excision repair cross-complementation group 5	enzyme	2073	301382
ERCC6	excision repair cross-complementation group 6	transcription regulator	2074	306274
GADD45A	growth arrest and DNA-damage-inducible, alpha	other	1647	25112
LIG4	ligase IV, DNA, ATP-dependent	enzyme	3981	290907
MDM2	MDM2 proto-oncogene, E3 ubiquitin protein ligase	transcription regulator	4193	314856
MGMT	O-6-methylguanine-DNA methyltransferase	enzyme	4255	25332
MLH1	mutL homolog 1	enzyme	4292	81685
MSH2	mutS homolog 2	enzyme	4436	81709
OGG1	8-oxoguanine DNA glycosylase	enzyme	4968	81528
PARP1	poly (ADP-ribose) polymerase 1	enzyme	142	25591
PCNA	proliferating cell nuclear antigen	enzyme	5111	25737
PRKDC	protein kinase, DNA-activated, catalytic polypeptide	kinase	5591	360748
RAD51	RAD51 recombinase	enzyme	5888	499870
TP53	tumor protein p53	transcription regulator	7157	24842
XPA	xeroderma pigmentosum, complementation group A	other	7507	298074
XPC	xeroderma pigmentosum, complementation group C	other	7508	312560
XRCC1	X-ray repair complementing defective repair in Chinese hamster cells 1	other	7515	84495
XRCC5	X-ray repair complementing defective repair in Chinese hamster cells 5	enzyme	7520	363247

Table B.6: Interaction network. Interactions between genes involved in DNA damage and repair processes. The interactions were identified through the use of QIAGENs Ingenuity Pathway Analysis (IPA®; QIAGEN Redwood City, www.qiagen.com/ingenuity).

From Molecule Interaction(s)		To Molecule
ATM	activation	TP53
ATM	phosphorylation	CHEK1
ATM	phosphorylation	CHEK2
ATM	phosphorylation, protein-DNA interaction	TP53
ATR	phosphorylation	CHEK1
ATR	phosphorylation	TP53
BRCA1	protein-protein interactions	ATR
BRCA2	protein-protein interaction	BRCA1
CDKN1A	protein-protein interaction	PCNA
CHEK1	phosphorylation, protein-protein interaction	TP53
ERCC3	protein-protein interaction	ATM
MDM2	activation, expression, protein-DNA interaction, protein-protein interaction	CDKN1A
MDM2	activation, protein-protein interaction, ubiquitination	TP53
MDM2	expression	MDM2
MDM2	protein-protein interaction	ATM
MLH1	protein-protein interaction	BRCA1
PARP1	protein-DNA interaction	PARP1
PARP1	protein-protein interaction	ATM
PCNA	protein-protein interaction	APEX1
PCNA	protein-protein interaction	CDKN1A
PCNA	protein-protein interaction	GADD45A
PRKDC	phosphorylation	CHEK1
PRKDC	protein-protein interaction	LIG4
PRKDC	protein-protein interaction	MLH1
PRKDC	protein-protein interaction	PARP1
PRKDC	protein-protein interaction	XRCC5
RAD51	protein-protein interaction	ATM
RAD51	protein-protein interaction	BRCA1
RAD51	protein-protein interaction	BRCA2
TP53	activation, expression, protein-protein interaction	TP53
TP53	expression, protein-protein interaction, transcription	BRCA1
TP53	expression, protein-DNA interaction, transcription	CDKN1A
TP53	expression, protein-protein interaction	CHEK2
TP53	expression	GADD45A
TP53	expression, protein-DNA interaction, protein-protein interaction, transcription	MDM2
TP53	expression	XPC
TP53	protein-protein interaction	CHEK1
TP53	protein-protein interaction	RAD51
XPA	protein-protein interaction	PARP1
XPC	protein-protein interaction	ATM
XPC	protein-protein interaction	ERCC3
XRCC5	protein-protein interaction	BRCA1
XRCC5	protein-protein interaction	LIG4
XRCC5	protein-protein interaction	PARP1
XRCC5	protein-protein interaction	PRKDC

Table B.7: Genes related to jaundice. Symbol, Entrez gene name, type, human and rat Entrez identifier and assigned relation for all genes associated with jaundice. Functional classifications and assigned relations on jaundice were taken from QIAGENs Ingenuity Pathway Analysis (IPA®), QIAGEN Redwood City, www.qiagen.com/ingenuity).

Gene	Entrez gene name	Type	Relation	Entrez ID (human)	Entrez ID (rat)
ABCC2	ATP-binding cassette, sub-family C (CFTR/MRP), member 2	transporter	affect	1244	25303
ABCC3	ATP-binding cassette, sub-family C (CFTR/MRP), member 3	transporter	affect	8714	140668
ALPP	alkaline phosphatase, placental	phosphatase	affect	250	24197
BLVRA	biliverdin reductase A	enzyme	affect	644	116599
CAT	catalase	enzyme	affect	847	24248
CHUK	conserved helix-loop-helix ubiquitous kinase	kinase	decrease	1147	309361
FAH	fumarylacetoacetate hydrolase (fumarylacetoacetase)	enzyme	decrease	2184	29383
IKBKB	inhibitor of kappa light polypeptide gene enhancer in B-cells, kinase beta	kinase	decrease	3551	84351
IL18	interleukin 18	cytokine	affect	3606	29197
JAG1	jagged 1	growth factor	decrease	182	29146
LAMA4	laminin, alpha 4	enzyme	decrease	3910	309816
NOTCH2	notch 2	transcription regulator	affect	4853	29492
NR1H4	nuclear receptor subfamily 1, group H, member 4	ligand-dependent nuclear receptor	decrease	9971	60351
ONECUT1	one cut homeobox 1	transcription regulator	decrease	3175	25231
UGT1A6	UDP glucuronosyltransferase 1 family, polypeptide A6	enzyme	affect	54578	113992

C

Supplementary information to Chapter 8

C.1 Supplementary tables

C.1.1 Key cellular processes

Table C.1: Toxicity lists. Seventy-four toxicity lists representing key cellular processes were taken from QIAGENs Ingenuity Pathway Analysis (IPA®), QIAGEN Redwood City, www.qiagen.com/ingenuity.

Toxicity list id	Toxicity list name
TOX_LIST:01	Anti-apoptosis
TOX_LIST:02	Aryl hydrocarbon receptor signaling
TOX_LIST:03	Biogenesis of mitochondria
TOX_LIST:04	CAR/RXR activation
TOX_LIST:05	Cardiac fibrosis
TOX_LIST:06	Cardiac hypertrophy
TOX_LIST:07	Cardiac necrosis/cell death
TOX_LIST:08	Cell cycle G1/S checkpoint regulation
TOX_LIST:09	Cell cycle G2/M DNA damage checkpoint regulation
TOX_LIST:10	Cholesterol biosynthesis
TOX_LIST:11	Cytochrome p450 - substrate is a eicosanoid
TOX_LIST:12	Cytochrome p450 - substrate is a fatty acid
TOX_LIST:13	Cytochrome p450 - substrate is a sterol
TOX_LIST:14	Cytochrome p450 - substrate is a vitamin
TOX_LIST:15	Cytochrome p450 - substrate is a xenobiotic
TOX_LIST:16	Decreases depolarization of mitochondria and mitochondria membrane
TOX_LIST:17	Decreases permeability transition of mitochondria and mitochondrial membrane
TOX_LIST:18	Decreases respiration of mitochondria
TOX_LIST:19	Decreases transmembrane potential of mitochondria and mitochondrial membrane
TOX_LIST:20	Fatty acid metabolism
TOX_LIST:21	FXR/RXR activation
TOX_LIST:22	Genes associated with chronic allograft nephropathy
TOX_LIST:23	Genes upregulated in response to proteinuria-induced oxidative stress in renal proximal tubule cells
TOX_LIST:24	Glutathione depletion - CYP induction and reactive metabolites
TOX_LIST:25	Glutathione depletion - hepatocellular hypertrophy
TOX_LIST:26	Glutathione depletion - phase II reactions
TOX_LIST:27	Hepatic cholestasis
TOX_LIST:28	Hepatic fibrosis
TOX_LIST:29	Hepatic stellate cell activation
TOX_LIST:30	Hormone receptor regulated cholesterol metabolism
TOX_LIST:31	Hypoxia-inducible factor signaling
TOX_LIST:32	Increases bradycardia
TOX_LIST:33	Increases cardiac dilation
TOX_LIST:34	Increases cardiac dysfunction

Continued on next page

Toxicity list id	Toxicity list name
TOX_LIST:35	Increases cardiac proliferation
TOX_LIST:36	Increases damage of mitochondria
TOX_LIST:37	Increases depolarization of mitochondria and mitochondrial membrane
TOX_LIST:38	Increases glomerular injury
TOX_LIST:39	Increases heart failure
TOX_LIST:40	Increases liver damage
TOX_LIST:41	Increases liver hepatitis
TOX_LIST:42	Increases liver hyperplasia/hyperproliferation
TOX_LIST:43	Increases liver steatosis
TOX_LIST:44	Increases permeability transition of mitochondria and mitochondrial membrane
TOX_LIST:45	Increases renal damage
TOX_LIST:46	Increases renal nephritis
TOX_LIST:47	Increases renal proliferation
TOX_LIST:48	Increases transmembrane potential of mitochondria and mitochondrial membrane
TOX_LIST:49	Liver necrosis/cell death
TOX_LIST:50	Liver proliferation
TOX_LIST:51	LPS/IL-1 mediated inhibition of RXR function
TOX_LIST:52	LXR/RXR activation
TOX_LIST:53	Mechanism of gene regulation by peroxisome proliferations via PPAR α
TOX_LIST:54	Mitochondrial dysfunction
TOX_LIST:55	Negative acute phase response proteins
TOX_LIST:56	NF- κ -B signaling
TOX_LIST:57	Nongenotoxic hepatocarcinogenicity biomarker panel
TOX_LIST:58	NRF-2 mediated oxidative stress response
TOX_LIST:59	Oxidative stress
TOX_LIST:60	p53 signaling
TOX_LIST:61	Positive acute phase response proteins
TOX_LIST:62	PPAR α /RXR α activation
TOX_LIST:63	Primary glomerulonephritis biomarker panel
TOX_LIST:64	Pro-apoptosis
TOX_LIST:65	PXR/RXR activation
TOX_LIST:66	RAR activation
TOX_LIST:67	Renal glomerulus panel
TOX_LIST:68	Renal necrosis/cell death
TOX_LIST:69	Renal safety biomarker panel
TOX_LIST:70	Swelling of mitochondria
TOX_LIST:71	TGF- β signaling
TOX_LIST:72	TR/RXR activation
TOX_LIST:73	VDR/RXR activation
TOX_LIST:74	Xenobiotic metabolism signaling

C.1.2 Analysis of in vitro toxicity data

Table C.2: Over-representation analysis for humans. Significantly overrepresented key cellular processes identified in human hepatocytes.

Drug	Toxicity list id	Toxicity list name	P-value
PB	TOX LIST:02	aryl hydrocarbon receptor signaling	0.000286168
PB	TOX LIST:15	cytochrome P450 - substrate is a xenobiotic	4.21183E-06
PB	TOX LIST:20	fatty acid metabolism	0.000134661
PB	TOX LIST:51	LPS\IL-1 mediated inhibition of RXR function	4.29637E-06
PB	TOX LIST:58	NRF-2 mediated oxidative stress response	0.000566976
PB	TOX LIST:65	PXR\RXR activation	1.13176E-07
PB	TOX LIST:74	xenobiotic metabolism signaling	0.001179793
PB	TOX LIST:04	CAR\RXR activation	2.03831E-10
PB	TOX LIST:25	glutathione depletion - hepatocellular hypertrophy	0.000154936
PB	TOX LIST:60	p53 signaling	0.000292447
PB	TOX LIST:06	cardiac hypertrophy	0.00112723
PB	TOX LIST:27	hepatic cholestasis	0.001045264
PB	TOX LIST:29	hepatic stellate cell activation	0.00089887
PB	TOX LIST:40	increases liver damage	0.007387102
PB	TOX LIST:07	cardiac necrosis\cell death	0.003574689
PB	TOX LIST:09	cell cycle G2\M DNA damage checkpoint regulation	3.61986E-06
PB	TOX LIST:10	cholesterol biosynthesis	3.92886E-07
PB	TOX LIST:17	decreases permeability transition of mitochondria and mitochondrial membrane	0.002345284
PB	TOX LIST:28	hepatic fibrosis	1.44239E-06
PB	TOX LIST:41	increases liver hepatitis	0.000212934
PB	TOX LIST:49	liver necrosis\cell death	6.58612E-06
PB	TOX LIST:50	liver proliferation	0.001166366
PB	TOX LIST:52	LXR\RXR activation	0.002309053
PB	TOX LIST:68	renal necrosis\cell death	0.00173289
PB	TOX LIST:53	mechanism of gene regulation by peroxisome proliferations via PPAR- α	5.78641E-05
PB	TOX LIST:63	primary glomerulonephritis biomarker panel	5.82104E-05
PB	TOX LIST:01	anti-apoptosis	9.63174E-05
PB	TOX LIST:08	cell cycle G1\S checkpoint regulation	2.65453E-05
PB	TOX LIST:21	FXR\RXR activation	0.000736987
PB	TOX LIST:42	increases liver hyperplasia\hyperproliferation	4.69256E-05
PB	TOX LIST:43	increases liver steatosis	0.001289049
PB	TOX LIST:48	increases transmembrane potential of mitochondria and mitochondrial membrane	0.003463157
PB	TOX LIST:56	NF- κ B signaling	0.001579079
PB	TOX LIST:62	PPAR- α \RXR- α activation	0.00028559
PB	TOX LIST:66	RAR activation	0.000342818
PB	TOX LIST:71	TGF- β signaling	0.00125109
DFN	TOX LIST:02	aryl hydrocarbon receptor signaling	0.003570267
DFN	TOX LIST:15	cytochrome P450 - substrate is a xenobiotic	5.45039E-05
DFN	TOX LIST:20	fatty acid metabolism	0.001702188
DFN	TOX LIST:51	LPS\IL-1 mediated inhibition of RXR function	0.007666879
DFN	TOX LIST:58	NRF-2 mediated oxidative stress response	0.000247212
DFN	TOX LIST:65	PXR\RXR activation	0.000721469
DFN	TOX LIST:49	liver necrosis\cell death	8.95752E-05
DFN	TOX LIST:50	liver proliferation	3.6434E-05
DFN	TOX LIST:56	NF- κ B signaling	0.000650062
DFN	TOX LIST:60	p53 signaling	0.000871197
DFN	TOX LIST:68	renal necrosis\cell death	8.33236E-05
DFN	TOX LIST:04	CAR\RXR activation	0.000153619
DFN	TOX LIST:09	cell cycle G2\M DNA damage checkpoint regulation	2.21769E-06
DFN	TOX LIST:21	FXR\RXR activation	2.50151E-06
DFN	TOX LIST:28	hepatic fibrosis	0.000650805

Continued on next page

Drug	Toxicity list id	Toxicity list name	P-value
DFN	TOX LIST:42	increases liver hyperplasia\hyperproliferation	0.000425274
DFN	TOX LIST:43	increases liver steatosis	0.000894571
DFN	TOX LIST:63	primary glomerulonephritis biomarker panel	0.001033791
DFN	TOX LIST:74	xenobiotic metabolism signaling	0.000777912
SST	TOX LIST:02	aryl hydrocarbon receptor signaling	0.002158192
SST	TOX LIST:04	CAR\RXR activation	0.001086992
SST	TOX LIST:10	cholesterol biosynthesis	0.00000000023
SST	TOX LIST:22	genes associated with chronic allograft nephropathy	0.000706534
SST	TOX LIST:28	hepatic fibrosis	3.10667E-05
SST	TOX LIST:29	hepatic stellate cell activation	3.84406E-05
SST	TOX LIST:51	LPS\IL-1 mediated inhibition of RXR function	0.006496297
SST	TOX LIST:52	LXR\RXR activation	6.51901E-05
SST	TOX LIST:58	NRF-2 mediated oxidative stress response	0.00565058
SST	TOX LIST:65	PXR\RXR activation	0.005872694
SST	TOX LIST:68	renal necrosis\cell death	0.001717696
SST	TOX LIST:72	TR\RXR activation	0.000562696
SST	TOX LIST:20	fatty acid metabolism	0.000181992
SST	TOX LIST:15	cytochrome P450 - substrate is a xenobiotic	1.4645E-07
SST	TOX LIST:74	xenobiotic metabolism signaling	0.000152437
SST	TOX LIST:01	anti-apoptosis	0.003487097
SST	TOX LIST:06	cardiac hypertrophy	4.18165E-05
SST	TOX LIST:07	cardiac necrosis\cell death	5.00383E-05
SST	TOX LIST:08	cell cycle G1\S checkpoint regulation	0.000277696
SST	TOX LIST:19	decreases transmembrane potential of mitochondria and mitochondrial membrane	0.001463913
SST	TOX LIST:21	FXR\RXR activation	2.89378E-08
SST	TOX LIST:38	increases glomerular injury	0.000121035
SST	TOX LIST:40	increases liver damage	0.000845616
SST	TOX LIST:41	increases liver hepatitis	0.00183715
SST	TOX LIST:42	increases liver hyperplasia\hyperproliferation	5.25337E-05
SST	TOX LIST:43	increases liver steatosis	3.14252E-07
SST	TOX LIST:45	increases renal damage	2.80394E-05
SST	TOX LIST:49	liver necrosis\cell death	3.6093E-10
SST	TOX LIST:50	liver proliferation	1.281E-09
SST	TOX LIST:55	negative acute phase response proteins	0.00206382
SST	TOX LIST:57	nongenotoxic hepatocarcinogenicity biomarker panel	6.0414E-05
SST	TOX LIST:60	p53 signaling	0.000151463
SST	TOX LIST:61	positive acute phase response proteins	0.000275759
SST	TOX LIST:63	primary glomerulonephritis biomarker panel	0.000395235
SST	TOX LIST:71	TGF- β signaling	0.003796414
SST	TOX LIST:73	VDR\RXR activation	0.00486591
CPA	TOX LIST:02	aryl hydrocarbon receptor signaling	1.79755E-05
CPA	TOX LIST:04	CAR\RXR activation	0.000417648
CPA	TOX LIST:15	cytochrome P450 - substrate is a xenobiotic	0.000175892
CPA	TOX LIST:20	fatty acid metabolism	0.000174505
CPA	TOX LIST:51	LPS\IL-1 mediated inhibition of RXR function	8.35344E-05
CPA	TOX LIST:65	PXR\RXR activation	0.002293931
CPA	TOX LIST:74	xenobiotic metabolism signaling	0.000283309
CPA	TOX LIST:06	cardiac hypertrophy	0.000347866
CPA	TOX LIST:07	cardiac necrosis\cell death	0.000722765
CPA	TOX LIST:25	glutathione depletion - hepatocellular hypertrophy	4.07495E-05
CPA	TOX LIST:58	NRF-2 mediated oxidative stress response	2.69825E-08
CPA	TOX LIST:09	cell cycle G2\M DNA damage checkpoint regulation	0.000121068
CPA	TOX LIST:41	increases liver hepatitis	0.001750199
CPA	TOX LIST:68	renal necrosis\cell death	0.000975332
PHE	TOX LIST:02	aryl hydrocarbon receptor signaling	4.57886E-08
PHE	TOX LIST:04	CAR\RXR activation	4.8743E-07
PHE	TOX LIST:07	cardiac necrosis\cell death	0.003203868

Continued on next page

Drug	Toxicity list id	Toxicity list name	P-value
PHE	TOX LIST:08	cell cycle G1\S checkpoint regulation	0.000495112
PHE	TOX LIST:09	cell cycle G2\M DNA damage checkpoint regulation	0.006371064
PHE	TOX LIST:15	cytochrome P450 - substrate is a xenobiotic	4.69872E-10
PHE	TOX LIST:20	fatty acid metabolism	3.61051E-06
PHE	TOX LIST:51	LPS\IL-1 mediated inhibition of RXR function	1.08274E-05
PHE	TOX LIST:57	nongenotoxic hepatocarcinogenicity biomarker panel	0.001237985
PHE	TOX LIST:58	NRF-2 mediated oxidative stress response	8.11613E-06
PHE	TOX LIST:60	p53 signaling	1.53856E-07
PHE	TOX LIST:65	PXR\RXR activation	8.69931E-09
PHE	TOX LIST:74	xenobiotic metabolism signaling	6.45806E-05
ERY	n/a	no significantly regulated toxicity lists found	n/a
AZA	TOX LIST:02	aryl hydrocarbon receptor signaling	9.76033E-05
AZA	TOX LIST:09	cell cycle G2\M DNA damage checkpoint regulation	5.23367E-11
AZA	TOX LIST:42	increases liver hyperplasia\hyperproliferation	0.000225791
AZA	TOX LIST:55	negative acute phase response proteins	1.96588E-05
AZA	TOX LIST:30	hormone receptor regulated cholesterol metabolism	6.54465E-05
AZA	TOX LIST:73	VDR\RXR activation	0.000165847
AZA	TOX LIST:07	cardiac necrosis\cell death	0.000249004
AZA	TOX LIST:17	decreases permeability transition of mitochondria and mitochondrial membrane	0.001879006
AZA	TOX LIST:20	fatty acid metabolism	0.00045852
AZA	TOX LIST:47	increases renal proliferation	0.00169862
AZA	TOX LIST:48	increases transmembrane potential of mitochondria and mitochondrial membrane	0.002191292
AZA	TOX LIST:50	liver proliferation	0.000165778
AZA	TOX LIST:58	NRF-2 mediated oxidative stress response	4.16903E-07
AZA	TOX LIST:60	p53 signaling	5.31218E-05
AZA	TOX LIST:63	primary glomerulonephritis biomarker panel	8.40816E-05
AZA	TOX LIST:68	renal necrosis\cell death	2.31996E-05
AZA	TOX LIST:06	cardiac hypertrophy	3.67241E-05
AZA	TOX LIST:08	cell cycle G1\S checkpoint regulation	0.000723685
AZA	TOX LIST:16	decreases depolarization of mitochondria and mitochondria membrane	0.002078835
AZA	TOX LIST:49	liver necrosis\cell death	5.28818E-05
AZA	TOX LIST:21	FXR\RXR activation	0.000188516
AZA	TOX LIST:25	glutathione depletion - hepatocellular hypertrophy	0.000158909
AZA	TOX LIST:28	hepatic fibrosis	0.0013554
AZA	TOX LIST:40	increases liver damage	0.000275681
AZA	TOX LIST:41	increases liver hepatitis	0.000143131
AZA	TOX LIST:51	LPS\IL-1 mediated inhibition of RXR function	2.65025E-06
AZA	TOX LIST:52	LXR\RXR activation	0.003133804
AZA	TOX LIST:74	xenobiotic metabolism signaling	0.000464689
RIF	TOX LIST:02	aryl hydrocarbon receptor signaling	6.5054E-06
RIF	TOX LIST:15	cytochrome P450 - substrate is a xenobiotic	1.06983E-08
RIF	TOX LIST:20	fatty acid metabolism	2.09037E-06
RIF	TOX LIST:51	LPS\IL-1 mediated inhibition of RXR function	1.62398E-07
RIF	TOX LIST:58	NRF-2 mediated oxidative stress response	1.81876E-05
RIF	TOX LIST:65	PXR\RXR activation	1.24827E-09
RIF	TOX LIST:74	xenobiotic metabolism signaling	5.46648E-05
RIF	TOX LIST:04	CAR\RXR activation	1.27787E-13
RIF	TOX LIST:25	glutathione depletion - hepatocellular hypertrophy	7.6281E-05
RIF	TOX LIST:27	hepatic cholestasis	0.005731506
RIF	TOX LIST:62	PPAR α \RXR- α activation	0.006563244
RIF	TOX LIST:72	TR\RXR activation	0.001002065
RIF	TOX LIST:07	cardiac necrosis\cell death	0.003414468
RIF	TOX LIST:21	FXR\RXR activation	9.66854E-06
RIF	TOX LIST:73	VDR\RXR activation	0.003807258
RIF	TOX LIST:42	increases liver hyperplasia\hyperproliferation	0.001002886
RIF	TOX LIST:52	LXR\RXR activation	0.002217754
RIF	TOX LIST:10	cholesterol biosynthesis	0.002057857

Continued on next page

Drug	Toxicity list id	Toxicity list name	P-value
RIF	TOX LIST:29	hepatic stellate cell activation	0.002443519
RIF	TOX LIST:41	increases liver hepatitis	0.001423704
RIF	TOX LIST:43	increases liver steatosis	0.001509416
RIF	TOX LIST:49	liver necrosis\cell death	0.000303362
RIF	TOX LIST:50	liver proliferation	0.002526186
CSA	TOX LIST:09	cell cycle G2\M DNA damage checkpoint regulation	0.000327036
CSA	TOX LIST:42	increases liver hyperplasia\hyperproliferation	0.000107058
CSA	TOX LIST:08	cell cycle G1\S checkpoint regulation	0.000651512
CSA	TOX LIST:02	aryl hydrocarbon receptor signaling	2.60308E-05
CSA	TOX LIST:10	cholesterol biosynthesis	0.000998012
CSA	TOX LIST:20	fatty acid metabolism	0.000331327
CSA	TOX LIST:60	p53 signaling	1.04965E-05
AD	TOX LIST:74	xenobiotic metabolism signaling	0.002894527
FT	TOX LIST:20	fatty acid metabolism	0.000334559
FT	TOX LIST:02	aryl hydrocarbon receptor signaling	0.001766036
FT	TOX LIST:05	cardiac fibrosis	0.004474226
FT	TOX LIST:06	cardiac hypertrophy	2.2194E-05
FT	TOX LIST:07	cardiac necrosis\cell death	0.004618513
FT	TOX LIST:09	cell cycle G2\M DNA damage checkpoint regulation	0.003436649
FT	TOX LIST:28	hepatic fibrosis	0.003194366
FT	TOX LIST:40	increases liver damage	0.000468898
FT	TOX LIST:41	increases liver hepatitis	0.004081569
FT	TOX LIST:49	liver necrosis\cell death	0.001176328
FT	TOX LIST:50	liver proliferation	0.000385249
FT	TOX LIST:53	mechanism of gene regulation by peroxisome proliferations via PPAR α	0.002848445
FT	TOX LIST:60	p53 signaling	0.003440257
FT	TOX LIST:63	primary glomerulonephritis biomarker panel	0.002087952
FT	TOX LIST:68	renal necrosis\cell death	0.000182067
FT	TOX LIST:73	VDR\RXR activation	0.001358634
FT	TOX LIST:08	cell cycle G1\S checkpoint regulation	0.001032048
FT	TOX LIST:15	cytochrome P450 - substrate is a xenobiotic	0.00122226
FT	TOX LIST:21	FXR\RXR activation	0.00032928
FT	TOX LIST:51	LPS\IL-1 mediated inhibition of RXR function	0.001529601
FT	TOX LIST:65	PXR\RXR activation	4.63479E-05
FT	TOX LIST:04	CAR\RXR activation	0.000722632
FT	TOX LIST:10	cholesterol biosynthesis	2.51466E-12
FT	TOX LIST:30	hormone receptor regulated cholesterol metabolism	0.002244183
FT	TOX LIST:42	increases liver hyperplasia\hyperproliferation	1.73366E-05
FT	TOX LIST:43	increases liver steatosis	0.000939497
FT	TOX LIST:52	LXR\RXR activation	4.39136E-05
FT	TOX LIST:55	negative acute phase response proteins	0.002244183
FT	TOX LIST:58	NRF-2 mediated oxidative stress response	0.00036787
FT	TOX LIST:74	xenobiotic metabolism signaling	0.0032974
HPL	TOX LIST:02	aryl hydrocarbon receptor signaling	0.000763659
HPL	TOX LIST:04	CAR\RXR activation	0.000535199
HPL	TOX LIST:15	cytochrome P450 - substrate is a xenobiotic	1.37601E-06
HPL	TOX LIST:20	fatty acid metabolism	0.000253544
HPL	TOX LIST:43	increases liver steatosis	0.004506756
HPL	TOX LIST:45	increases renal damage	0.003837486
HPL	TOX LIST:51	LPS\IL-1 mediated inhibition of RXR function	0.002362033
HPL	TOX LIST:58	NRF-2 mediated oxidative stress response	0.002046113
HPL	TOX LIST:65	PXR\RXR activation	1.18772E-06
HPL	TOX LIST:74	xenobiotic metabolism signaling	0.000462583
HPL	TOX LIST:73	VDR\RXR activation	0.002621724
INH	TOX LIST:02	aryl hydrocarbon receptor signaling	0.00254057
INH	TOX LIST:15	cytochrome P450 - substrate is a xenobiotic	3.84713E-05
INH	TOX LIST:20	fatty acid metabolism	0.001207754

Continued on next page

Drug	Toxicity list id	Toxicity list name	P-value
INH	TOX LIST:58	NRF-2 mediated oxidative stress response	0.004967207
INH	TOX LIST:74	xenobiotic metabolism signaling	0.001040834
INH	TOX LIST:06	cardiac hypertrophy	7.83973E-05
INH	TOX LIST:10	cholesterol biosynthesis	0.000702744
INH	TOX LIST:42	increases liver hyperplasia\hyperproliferation	0.003145396
INH	TOX LIST:50	liver proliferation	0.000656753
INH	TOX LIST:51	LPS\IL-1 mediated inhibition of RXR function	0.000497412
INH	TOX LIST:65	PXR\RXR activation	0.000609704
INH	TOX LIST:72	TR\RXR activation	0.002847026
INH	TOX LIST:73	VDR\RXR activation	0.001652946
INH	TOX LIST:30	hormone receptor regulated cholesterol metabolism	0.001673703
INH	TOX LIST:47	increases renal proliferation	0.000395823
INH	TOX LIST:49	liver necrosis\cell death	3.54931E-05
INH	TOX LIST:53	mechanism of gene regulation by peroxisome proliferations via PPAR α	0.000846634
INH	TOX LIST:68	renal necrosis\cell death	0.000360454
INH	TOX LIST:04	CAR\RXR activation	2.51429E-06
INH	TOX LIST:09	cell cycle G2\M DNA damage checkpoint regulation	0.000363938
INH	TOX LIST:21	FXR\RXR activation	0.000597562
INH	TOX LIST:43	increases liver steatosis	0.003078586
INH	TOX LIST:52	LXR\RXR activation	0.001077018
INH	TOX LIST:60	p53 signaling	0.000107343
APAP	TOX LIST:74	xenobiotic metabolism signaling	0.002894527
APAP	TOX LIST:02	aryl hydrocarbon receptor signaling	0.005388967
APAP	TOX LIST:21	FXR\RXR activation	0.003636574
APAP	TOX LIST:40	increases liver damage	0.000141098
APAP	TOX LIST:49	liver necrosis\cell death	0.004272223
APAP	TOX LIST:50	liver proliferation	0.000212794
APAP	TOX LIST:53	mechanism of gene regulation by peroxisome proliferations via PPAR α	4.1877E-06
APAP	TOX LIST:59	oxidative stress	0.007167245
APAP	TOX LIST:63	primary glomerulonephritis biomarker panel	0.000356947
APAP	TOX LIST:66	RAR activation	0.00010946
APAP	TOX LIST:68	renal necrosis\cell death	2.46648E-05
APAP	TOX LIST:71	TGF- β signaling	0.001592685
APAP	TOX LIST:06	cardiac hypertrophy	0.000161493
APAP	TOX LIST:07	cardiac necrosis\cell death	0.000414748
APAP	TOX LIST:28	hepatic fibrosis	2.11396E-05
APAP	TOX LIST:30	hormone receptor regulated cholesterol metabolism	0.000404951
APAP	TOX LIST:35	increases cardiac proliferation	0.001920824
APAP	TOX LIST:51	LPS\IL-1 mediated inhibition of RXR function	0.000784304
APAP	TOX LIST:73	VDR\RXR activation	0.000780962
APAP	TOX LIST:09	cell cycle G2\M DNA damage checkpoint regulation	0.000511807
APAP	TOX LIST:42	increases liver hyperplasia\hyperproliferation	1.73444E-05
APAP	TOX LIST:39	increases heart failure	0.002328136
APAP	TOX LIST:08	cell cycle G1\S checkpoint regulation	5.21546E-07
APAP	TOX LIST:65	PXR\RXR activation	0.001339052
APAP	TOX LIST:04	CAR\RXR activation	8.11397E-08
APAP	TOX LIST:15	cytochrome P450 - substrate is a xenobiotic	4.21655E-05
APAP	TOX LIST:20	fatty acid metabolism	3.80436E-07
APAP	TOX LIST:24	glutathione depletion - CYP induction and reactive metabolites	0.002733687
APAP	TOX LIST:43	increases liver steatosis	0.00022404
APAP	TOX LIST:55	negative acute phase response proteins	0.002926586
APAP	TOX LIST:57	nongenotoxic hepatocarcinogenicity biomarker panel	7.33508E-05
APAP	TOX LIST:58	NRF-2 mediated oxidative stress response	3.00566E-05
APAP	TOX LIST:60	p53 signaling	0.000458014
APAP	TOX LIST:62	PPAR α \RXR α activation	0.001671642
VPA	TOX LIST:28	hepatic fibrosis	0.006570028
VPA	TOX LIST:73	VDR\RXR activation	0.004170474

Continued on next page

Drug	Toxicity list id	Toxicity list name	P-value
VPA	TOX LIST:06	cardiac hypertrophy	0.000524214
VPA	TOX LIST:15	cytochrome P450 - substrate is a xenobiotic	0.000152072
VPA	TOX LIST:20	fatty acid metabolism	0.000309822
VPA	TOX LIST:49	liver necrosis\cell death	0.000203697
VPA	TOX LIST:50	liver proliferation	0.002127803
VPA	TOX LIST:65	PXR\RXR activation	0.00057639
VPA	TOX LIST:72	TR\RXR activation	0.000204537
VPA	TOX LIST:74	xenobiotic metabolism signaling	0.000373053
VPA	TOX LIST:08	cell cycle G1\S checkpoint regulation	0.002797395
VPA	TOX LIST:42	increases liver hyperplasia\hyperproliferation	0.005549688
VPA	TOX LIST:43	increases liver steatosis	0.004170474
VPA	TOX LIST:53	mechanism of gene regulation by peroxisome proliferations via PPAR α	0.006178077
VPA	TOX LIST:63	primary glomerulonephritis biomarker panel	8.46564E-05
VPA	TOX LIST:68	renal necrosis\cell death	0.000264508
VPA	TOX LIST:02	aryl hydrocarbon receptor signaling	0.002099075
VPA	TOX LIST:07	cardiac necrosis\cell death	3.31273E-05
VPA	TOX LIST:09	cell cycle G2\M DNA damage checkpoint regulation	0.000734029
VPA	TOX LIST:21	FXR\RXR activation	4.39565E-05
VPA	TOX LIST:29	hepatic stellate cell activation	0.001912755
VPA	TOX LIST:51	LPS\IL-1 mediated inhibition of RXR function	2.48093E-06
VPA	TOX LIST:57	nongenotoxic hepatocarcinogenicity biomarker panel	0.000546665
VPA	TOX LIST:05	cardiac fibrosis	0.004323402
VPA	TOX LIST:35	increases cardiac proliferation	0.002793691
VPA	TOX LIST:38	increases glomerular injury	0.002619294
VPA	TOX LIST:04	CAR\RXR activation	2.43965E-05
VPA	TOX LIST:19	decreases transmembrane potential of mitochondria and mitochondrial membrane	0.000410859
VPA	TOX LIST:25	glutathione depletion - hepatocellular hypertrophy	1.03793E-05
VPA	TOX LIST:58	NRF-2 mediated oxidative stress response	7.46266E-05

Table C.3: Over-representation analysis for rats. Significantly overrepresented key cellular processes identified in rat hepatocytes.

Drug	Toxicity list id	Toxicity list name	P-value
PB	TOX LIST:02	aryl hydrocarbon receptor signaling	4.2615E-09
PB	TOX LIST:04	CAR\RXR activation	1.8291E-07
PB	TOX LIST:15	cytochrome p450 - substrate is a xenobiotic	4.4302E-05
PB	TOX LIST:20	fatty acid metabolism	4.2611E-10
PB	TOX LIST:21	FXR\RXR activation	1.2968E-07
PB	TOX LIST:24	glutathione depletion - CYP induction and reactive metabolites	0.00053764
PB	TOX LIST:26	glutathione depletion - phase II reactions	9.033E-05
PB	TOX LIST:29	hepatic stellate cell activation	0.00260527
PB	TOX LIST:40	increases liver damage	0.00036196
PB	TOX LIST:49	liver necrosis\cell death	1.1807E-10
PB	TOX LIST:50	liver proliferation	2.3521E-07
PB	TOX LIST:51	LPS\IL-1 mediated inhibition of RXR function	7.625E-13
PB	TOX LIST:52	LXR\RXR activation	0.00038186
PB	TOX LIST:54	mitochondrial dysfunction	0.00055979
PB	TOX LIST:58	NRF-2 mediated oxidative stress response	3.2146E-11
PB	TOX LIST:59	oxidative stress	0.00257413
PB	TOX LIST:65	PXR\RXR activation	7.4423E-06
PB	TOX LIST:68	renal necrosis\cell death	5.2251E-08
PB	TOX LIST:74	xenobiotic metabolism signaling	2.5224E-10
PB	TOX LIST:10	cholesterol biosynthesis	0.00241297
PB	TOX LIST:28	hepatic fibrosis	2.7189E-07
PB	TOX LIST:06	cardiac hypertrophy	0.00021492
PB	TOX LIST:27	hepatic cholestasis	0.00076461
PB	TOX LIST:60	p53 signaling	0.00021721
PB	TOX LIST:05	cardiac fibrosis	0.00019824
PB	TOX LIST:25	glutathione depletion - hepatocellular hypertrophy	0.00235479
PB	TOX LIST:53	mechanism of gene regulation by peroxisome proliferations via PPAR α	0.00090444
PB	TOX LIST:62	PPAR α \RXR α activation	0.00193518
PB	TOX LIST:07	cardiac necrosis\cell death	0.00230541
PB	TOX LIST:56	NF- κ B signaling	0.00290596
PB	TOX LIST:43	increases liver steatosis	2.8958E-05
PB	TOX LIST:19	decreases transmembrane potential of mitochondria and mitochondrial membrane	0.00021965
DFN	TOX LIST:05	cardiac fibrosis	1.6091E-05
DFN	TOX LIST:06	cardiac hypertrophy	1.1666E-05
DFN	TOX LIST:20	fatty acid metabolism	0.00011856
DFN	TOX LIST:34	increases cardiac dysfunction	2.3364E-05
DFN	TOX LIST:43	increases liver steatosis	0.00049036
DFN	TOX LIST:50	liver proliferation	0.00061792
DFN	TOX LIST:51	LPS\IL-1 mediated inhibition of RXR function	5.615E-06
DFN	TOX LIST:52	LXR\RXR activation	0.00136809
DFN	TOX LIST:53	mechanism of gene regulation by peroxisome proliferations via PPAR α	7.9885E-05
DFN	TOX LIST:65	PXR\RXR activation	0.00303806
DFN	TOX LIST:74	xenobiotic metabolism signaling	0.00023965
DFN	TOX LIST:04	CAR\RXR activation	0.00076046
DFN	TOX LIST:49	liver necrosis\cell death	3.3108E-06
DFN	TOX LIST:60	p53 signaling	0.00068869
DFN	TOX LIST:68	renal necrosis\cell death	2.3336E-05
DFN	TOX LIST:21	FXR\RXR activation	0.00033025
DFN	TOX LIST:28	hepatic fibrosis	0.00043534
DFN	TOX LIST:58	NRF-2 mediated oxidative stress response	3.589E-06
DFN	TOX LIST:61	positive acute phase response proteins	1.0545E-06
SST	TOX LIST:10	cholesterol biosynthesis	0.0000000034
SST	TOX LIST:52	LXR\RXR activation	0.00051233

Continued on next page

Drug	Toxicity list id	Toxicity list name	P-value
SST	TOX LIST:20	fatty acid metabolism	0.0001126
SST	TOX LIST:34	increases cardiac dysfunction	0.00056436
SST	TOX LIST:50	liver proliferation	0.00065468
SST	TOX LIST:51	LPS\IL-1 mediated inhibition of RXR function	0.00175732
SST	TOX LIST:65	PXR\RXR activation	0.00050272
SST	TOX LIST:12	cytochrome P450 - substrate is a fatty acid	0.00083796
SST	TOX LIST:06	cardiac hypertrophy	0.00061671
SST	TOX LIST:27	hepatic cholestasis	0.00189216
SST	TOX LIST:43	increases liver steatosis	0.0010397
SST	TOX LIST:49	liver necrosis\cell death	0.00014332
SST	TOX LIST:53	mechanism of gene regulation by peroxisome proliferations via PPAR α	1.0525E-05
SST	TOX LIST:02	aryl hydrocarbon receptor signaling	4.0525E-06
SST	TOX LIST:04	CAR\RXR activation	7.5614E-05
SST	TOX LIST:05	cardiac fibrosis	0.00194693
SST	TOX LIST:15	cytochrome P450 - substrate is a xenobiotic	0.00046529
SST	TOX LIST:21	FXR\RXR activation	3.8966E-06
SST	TOX LIST:25	glutathione depletion - hepatocellular hypertrophy	0.00015136
SST	TOX LIST:28	hepatic fibrosis	5.7916E-08
SST	TOX LIST:29	hepatic stellate cell activation	0.00124841
SST	TOX LIST:42	increases liver hyperplasia\hyperproliferation	4.1432E-05
SST	TOX LIST:58	NRF-2 mediated oxidative stress response	0.00331944
SST	TOX LIST:74	xenobiotic metabolism signaling	0.00021136
CPA	TOX LIST:04	CAR\RXR activation	0.00011727
CPA	TOX LIST:05	cardiac fibrosis	0.00059279
CPA	TOX LIST:74	xenobiotic metabolism signaling	0.00060935
CPA	TOX LIST:02	aryl hydrocarbon receptor signaling	2.5807E-05
CPA	TOX LIST:06	cardiac hypertrophy	1.4431E-07
CPA	TOX LIST:22	genes associated with chronic allograft nephropathy	1.7806E-06
CPA	TOX LIST:28	hepatic fibrosis	7.5438E-10
CPA	TOX LIST:29	hepatic stellate cell activation	0.00083334
CPA	TOX LIST:34	increases cardiac dysfunction	0.00159167
CPA	TOX LIST:35	increases cardiac proliferation	0.00101216
CPA	TOX LIST:40	increases liver damage	4.3945E-05
CPA	TOX LIST:52	LXR\RXR activation	0.00151092
CPA	TOX LIST:68	renal necrosis\cell death	5.5469E-06
PHE	n/a	no significantly regulated toxicity lists found	n/a
ERY	TOX LIST:02	aryl hydrocarbon receptor signaling	0.00273674
ERY	TOX LIST:21	FXR\RXR activation	0.00189852
ERY	TOX LIST:27	hepatic cholestasis	0.00300305
ERY	TOX LIST:28	hepatic fibrosis	1.6283E-05
ERY	TOX LIST:40	increases liver damage	0.00115096
ERY	TOX LIST:47	increases renal proliferation	0.00186229
ERY	TOX LIST:50	liver proliferation	0.00636631
ERY	TOX LIST:51	LPS\IL-1 mediated inhibition of RXR function	0.00555133
ERY	TOX LIST:52	LXR\RXR activation	0.00139051
ERY	TOX LIST:53	mechanism of gene regulation by peroxisome proliferations via PPAR α	0.0011797
ERY	TOX LIST:56	NF- κ B signaling	0.00342457
ERY	TOX LIST:05	cardiac fibrosis	0.00583389
AZA	TOX LIST:15	cytochrome P450 - substrate is a xenobiotic	0.00018965
AZA	TOX LIST:20	fatty acid metabolism	8.6937E-05
AZA	TOX LIST:51	LPS\IL-1 mediated inhibition of RXR function	0.00135229
AZA	TOX LIST:58	NRF-2 mediated oxidative stress response	0.00022444
AZA	TOX LIST:74	xenobiotic metabolism signaling	9.0003E-05
AZA	TOX LIST:06	cardiac hypertrophy	0.00025556
AZA	TOX LIST:07	cardiac necrosis\cell death	0.00131371
AZA	TOX LIST:10	cholesterol biosynthesis	0.00023487
AZA	TOX LIST:49	liver necrosis\cell death	5.2564E-05

Continued on next page

Drug	Toxicity list id	Toxicity list name	P-value
AZA	TOX LIST:60	p53 signaling	8.5364E-05
AZA	TOX LIST:02	aryl hydrocarbon receptor signaling	0.00011467
AZA	TOX LIST:21	FXR\RXR activation	1.7358E-08
AZA	TOX LIST:50	liver proliferation	5.4922E-07
AZA	TOX LIST:52	LXR\RXR activation	1.0366E-05
RIF	TOX LIST:51	LPS\IL-1 mediated inhibition of RXR function	0.0043543
RIF	TOX LIST:10	cholesterol biosynthesis	1.3985E-07
RIF	TOX LIST:60	p53 signaling	0.0009869
RIF	TOX LIST:04	CAR\RXR activation	0.00026508
RIF	TOX LIST:15	cytochrome P450 - substrate is a xenobiotic	0.00072246
RIF	TOX LIST:20	fatty acid metabolism	0.00016777
RIF	TOX LIST:21	FXR\RXR activation	1.6155E-05
RIF	TOX LIST:25	glutathione depletion - hepatocellular hypertrophy	5.9775E-05
RIF	TOX LIST:52	LXR\RXR activation	0.00062664
RIF	TOX LIST:58	NRF-2 mediated oxidative stress response	9.9115E-07
RIF	TOX LIST:74	xenobiotic metabolism signaling	0.0016744
CSA	TOX LIST:68	renal necrosis\cell death	6.2159E-06
CSA	TOX LIST:04	CAR\RXR activation	0.00112241
CSA	TOX LIST:51	LPS\IL-1 mediated inhibition of RXR function	7.1257E-05
CSA	TOX LIST:52	LXR\RXR activation	2.6804E-05
CSA	TOX LIST:19	decreases transmembrane potential of mitochondria and mitochondrial membrane	0.00051233
CSA	TOX LIST:49	liver necrosis\cell death	0.00033517
CSA	TOX LIST:58	NRF-2 mediated oxidative stress response	2.7852E-05
CSA	TOX LIST:10	cholesterol biosynthesis	1.8383E-08
CSA	TOX LIST:20	fatty acid metabolism	1.5842E-06
CSA	TOX LIST:21	FXR\RXR activation	8.8545E-08
CSA	TOX LIST:65	PXR\RXR activation	0.000805
CSA	TOX LIST:72	TR\RXR activation	0.00112369
CSA	TOX LIST:74	xenobiotic metabolism signaling	0.00042041
AD	TOX LIST:50	liver proliferation	0.00272582
FT	n/a	no significantly regulated toxicity lists found	n/a
HPL	TOX LIST:04	CAR\RXR activation	2.9299E-05
HPL	TOX LIST:10	cholesterol biosynthesis	4.9711E-08
HPL	TOX LIST:16	decreases depolarization of mitochondria and mitochondria membrane	4.6219E-05
HPL	TOX LIST:21	FXR\RXR activation	0.00070613
HPL	TOX LIST:25	glutathione depletion - hepatocellular hypertrophy	0.00024376
HPL	TOX LIST:51	LPS\IL-1 mediated inhibition of RXR function	8.0142E-05
HPL	TOX LIST:74	xenobiotic metabolism signaling	0.00096773
INH	TOX LIST:02	aryl hydrocarbon receptor signaling	0.00037389
INH	TOX LIST:09	cell cycle G2\M DNA damage checkpoint regulation	0.00101895
INH	TOX LIST:15	cytochrome P450 - substrate is a xenobiotic	0.00106862
INH	TOX LIST:58	NRF-2 mediated oxidative stress response	0.00020876
INH	TOX LIST:49	liver necrosis\cell death	0.00105308
INH	TOX LIST:65	PXR\RXR activation	0.0010867
INH	TOX LIST:38	increases glomerular injury	0.00193362
INH	TOX LIST:50	liver proliferation	0.00092468
INH	TOX LIST:52	LXR\RXR activation	0.00181214
INH	TOX LIST:74	xenobiotic metabolism signaling	5.7056E-05
INH	TOX LIST:04	CAR\RXR activation	1.2689E-05
INH	TOX LIST:25	glutathione depletion - hepatocellular hypertrophy	0.00015272
INH	TOX LIST:26	glutathione depletion - phase II reactions	0.00056137
INH	TOX LIST:28	hepatic fibrosis	0.00081699
INH	TOX LIST:51	LPS\IL-1 mediated inhibition of RXR function	1.199E-05
INH	TOX LIST:68	renal necrosis\cell death	2.8774E-06
INH	TOX LIST:73	VDR\RXR activation	0.00216595
INH	TOX LIST:08	cell cycle G1\S checkpoint regulation	0.00125641
INH	TOX LIST:20	fatty acid metabolism	9.068E-06

Continued on next page

Drug	Toxicity list id	Toxicity list name	P-value
INH	TOX LIST:59	oxidative stress	8.7184E-05
APAP	TOX LIST:02	aryl hydrocarbon receptor signaling	3.2809E-07
APAP	TOX LIST:04	CAR\RXR activation	6.3888E-06
APAP	TOX LIST:07	cardiac necrosis\cell death	6.8194E-05
APAP	TOX LIST:15	cytochrome P450 - substrate is a xenobiotic	0.00034625
APAP	TOX LIST:20	fatty acid metabolism	0.00000004
APAP	TOX LIST:21	FXR\RXR activation	1.8381E-07
APAP	TOX LIST:26	glutathione depletion - phase II reactions	0.00304329
APAP	TOX LIST:28	hepatic fibrosis	0.00045026
APAP	TOX LIST:29	hepatic stellate cell activation	0.00141773
APAP	TOX LIST:40	increases liver damage	0.00011008
APAP	TOX LIST:43	increases liver steatosis	7.746E-05
APAP	TOX LIST:49	liver necrosis\cell death	7.4515E-09
APAP	TOX LIST:50	liver proliferation	1.3624E-05
APAP	TOX LIST:51	LPS\IL-1 mediated inhibition of RXR function	2.5283E-11
APAP	TOX LIST:52	LXR\RXR activation	0.00066371
APAP	TOX LIST:53	mechanism of gene regulation by peroxisome proliferations via PPAR α	0.00087848
APAP	TOX LIST:57	nongenotoxic hepatocarcinogenicity biomarker panel	1.0974E-05
APAP	TOX LIST:58	NRF-2 mediated oxidative stress response	3.0864E-14
APAP	TOX LIST:62	PPAR α \RXR α activation	0.00209672
APAP	TOX LIST:65	PXR\RXR activation	0.00010498
APAP	TOX LIST:68	renal necrosis\cell death	7.0319E-07
APAP	TOX LIST:74	xenobiotic metabolism signaling	5.3931E-11
APAP	TOX LIST:06	cardiac hypertrophy	0.0029842
APAP	TOX LIST:24	glutathione depletion - CYP induction and reactive metabolites	0.00271573
APAP	TOX LIST:48	increases transmembrane potential of mitochondria and mitochondrial membrane	0.00031675
APAP	TOX LIST:66	RAR activation	0.0019025
APAP	TOX LIST:27	hepatic cholestasis	0.00029173
VPA	TOX LIST:06	cardiac hypertrophy	0.00042555
VPA	TOX LIST:40	increases liver damage	0.00095899
VPA	TOX LIST:49	liver necrosis\cell death	0.00022092
VPA	TOX LIST:68	renal necrosis\cell death	0.00151297
VPA	TOX LIST:20	fatty acid metabolism	0.00031809
VPA	TOX LIST:50	liver proliferation	0.00028604
VPA	TOX LIST:02	aryl hydrocarbon receptor signaling	0.00169091
VPA	TOX LIST:04	CAR\RXR activation	8.1655E-10
VPA	TOX LIST:12	cytochrome P450 - substrate is a fatty acid	0.00226088
VPA	TOX LIST:21	FXR\RXR activation	5.7828E-10
VPA	TOX LIST:25	glutathione depletion - hepatocellular hypertrophy	0.00085227
VPA	TOX LIST:27	hepatic cholestasis	0.00081141
VPA	TOX LIST:43	increases liver steatosis	0.00062511
VPA	TOX LIST:51	LPS\IL-1 mediated inhibition of RXR function	0.00000027
VPA	TOX LIST:58	NRF-2 mediated oxidative stress response	2.3561E-07
VPA	TOX LIST:65	PXR\RXR activation	2.2572E-06
VPA	TOX LIST:74	xenobiotic metabolism signaling	2.8949E-09
VPA	TOX LIST:53	mechanism of gene regulation by peroxisome proliferations via PPAR α	0.0002067
VPA	TOX LIST:10	cholesterol biosynthesis	4.7194E-09
VPA	TOX LIST:15	cytochrome P450 - substrate is a xenobiotic	0.00237911
VPA	TOX LIST:26	glutathione depletion - phase II reactions	0.00233137
VPA	TOX LIST:60	p53 signaling	4.6739E-05

C.1.3 Physiologically-based pharmacokinetic model development

Table C.4: Intestinal permeabilities. Intestinal permeability values for all drugs and their metabolites. Some intestinal permeability values originally provided by the modeling software (Initial intestinal permeability) were slightly adjusted (Intestinal permeability used in model) to best describe the experimental data for oral administration.

ID	Drug/Metabolite	Initial intestinal permeability [cm/min]	Intestinal permeability used in model [cm/min]
1	APAP	5.33E-06	2.95E-05
1	APAPC	6.01E-07	6.01E-07
1	APAPG	8.06E-09	8.06E-09
1	APAPS	1.11E-07	1.11E-07
1	NAPQI	3.32E-06	3.32E-06
2	AD	8.64E-04	2.30E-04
3	6-MP	1.71E-04	1.71E-04
3	AZA	2.04E-07	9.04E-04
4	CPA	3.08E-06	5.08E-05
5	CSA	1.67E-06	4.80E-04
6	DFN	3.13E-03	6.00E-03
7	ERY	2.33E-06	2.33E-06
7	ERY-PED	6.81E-06	6.50E-04
8	2-hydroxy FT	3.65E-05	3.65E-05
8	FT	4.64E-04	1.85E-04
9	HPL	2.69E-04	4.69E-04
10	Acetyl-INH	1.46E-07	1.46E-07
10	INH	8.24E-07	2.00E-05
11	PB	4.81E-05	7.00E-05
12	PHE	4.51E-05	9.00E-05
13	RIF	1.03E-06	1.12E-04
14	SST	1.22E-03	5.90E-04
14	SST-acid	4.20E-04	6.90E-05
15	Hydroxyl-VPA	5.03E-05	5.03E-05
15	VPA	6.21E-04	6.21E-04
15	VPA- β -glucuronide	6.00E-07	6.00E-07

Table C.5: Calculation methods for partition coefficients and cellular permeabilities. Different calculation methods used in the established PBPK models to calculate intracellular to plasma partition coefficients as well as permeabilities between interstitial and cellular space. The calculation methods are provided in the modeling software.

ID	Drug/Metabolite	Partition coefficients	Cellular permeabilities
1	APAP	Schmitt	Charge dependent Schmitt
1	APAPC	Schmitt	Charge dependent Schmitt
1	APAPG	Schmitt	Charge dependent Schmitt
1	APAPS	Schmitt	Charge dependent Schmitt
1	NAPQI	Schmitt	Charge dependent Schmitt
2	AD	Schmitt	PK-Sim Standard
3	6-MP	Schmitt	PK-Sim Standard
3	AZA	PK-Sim Standard	PK-Sim Standard
4	CPA	Schmitt	PK-Sim Standard
5	CSA	PK-Sim Standard	PK-Sim Standard
6	DFN	Schmitt	PK-Sim Standard
7	ERY	PK-Sim Standard	PK-Sim Standard
7	ERY-PED	PK-Sim Standard	PK-Sim Standard
8	2-hydroxy-FT	Rodgers and Rowland	PK-Sim Standard
8	FT	Rodgers and Rowland	PK-Sim Standard
9	HPL	Schmitt	PK-Sim Standard
10	Acetyl-INH	Schmitt	Charge dependent Schmitt
10	INH	Schmitt	Charge dependent Schmitt
11	PB	PK-Sim Standard	PK-Sim Standard
12	PHE	Rodgers and Rowland	PK-Sim Standard
13	RIF	Schmitt	PK-Sim Standard
14	SST	PK-Sim Standard	PK-Sim Standard
14	SST-acid	PK-Sim Standard	PK-Sim Standard
15	Hydroxyl-VPA	Schmitt	PK-Sim Standard
15	VPA	Schmitt	PK-Sim Standard
15	VPA- β -glucuronide	Schmitt	PK-Sim Standard

Table C.6: Bioavailability values. Bioavailability values after 24 h calculated by use of the modeling software PK-Sim® [Willmann et al., 2003]

Drug	Bioavailability [%]
APAP	92
AD	59
AZA	18
CPA	98
CSA	18
DFN	79
ERY	80
FT	84
HPL	93
INH	94
PB	98
PHE	76
RIF	94
SST	44
VPA	99

C.1.4 Prediction of molecular biomarkers and potential drug interactions

Table C.7: Molecular biomarkers. Individual molecular biomarkers identified for the high-responsive- and low-responsive drugs.

Group	Drug	Gene	Location	Type	Entrez ID	TP
high-responsive	PB	CYP3A5	Cytoplasm	enzyme	1577	8h
high-responsive	PB	CYP3A7	Cytoplasm	enzyme	1551	8h
high-responsive	PB	ALAS1	Cytoplasm	enzyme	211	24h
high-responsive	PB	CYP2B6	Cytoplasm	enzyme	1555	24h
high-responsive	PB	CYP2C8	Cytoplasm	enzyme	1558	24h
high-responsive	PB	CYP3A4	Cytoplasm	enzyme	1576	24h
high-responsive	PB	CYP3A5	Cytoplasm	enzyme	1577	24h
high-responsive	PB	CYP3A7	Cytoplasm	enzyme	1551	24h
high-responsive	PB	CYP1A1	Cytoplasm	enzyme	1543	8h
high-responsive	PB	CYP4X1	Cytoplasm	enzyme	260293	24h
high-responsive	PB	SULT1E1	Cytoplasm	enzyme	6783	24h
high-responsive	CPA	CYP3A4	Cytoplasm	enzyme	1576	24h
high-responsive	CPA	CYP3A7	Cytoplasm	enzyme	1551	24h
high-responsive	AZA	CYP4X1	Cytoplasm	enzyme	260293	24h
high-responsive	AZA	BORA	Cytoplasm	other	79866	24h
high-responsive	AZA	CCNB1	Cytoplasm	kinase	891	24h
high-responsive	AZA	PLK1	Nucleus	kinase	5347	24h
high-responsive	RIF	CYP3A4	Cytoplasm	enzyme	1576	8h
high-responsive	RIF	CYP3A5	Cytoplasm	enzyme	1577	8h
high-responsive	RIF	CYP3A7	Cytoplasm	enzyme	1551	8h
high-responsive	RIF	ALAS1	Cytoplasm	enzyme	211	24h
high-responsive	RIF	CYP2B6	Cytoplasm	enzyme	1555	24h
high-responsive	RIF	CYP2C19	Cytoplasm	enzyme	1557	24h
high-responsive	RIF	CYP2C8	Cytoplasm	enzyme	1558	24h
high-responsive	RIF	CYP2C9	Cytoplasm	enzyme	1559	24h
high-responsive	RIF	CYP3A4	Cytoplasm	enzyme	1576	24h
high-responsive	RIF	CYP3A5	Cytoplasm	enzyme	1577	24h
high-responsive	RIF	CYP3A7	Cytoplasm	enzyme	1551	24h
high-responsive	RIF	CYP3A43	Cytoplasm	enzyme	64816	24h
high-responsive	RIF	AKR1D1	Cytoplasm	enzyme	6718	24h
high-responsive	RIF	GAL3ST1	Cytoplasm	enzyme	9514	24h
high-responsive	RIF	POR	Cytoplasm	enzyme	5447	24h
high-responsive	HPL	CYP3A4	Cytoplasm	enzyme	1576	24h
high-responsive	HPL	CYP3A7	Cytoplasm	enzyme	1551	24h
high-responsive	INH	CYP1A2	Cytoplasm	enzyme	1544	8h
high-responsive	INH	CYP1A2	Cytoplasm	enzyme	1544	24h
high-responsive	INH	CYP1A1	Cytoplasm	enzyme	1543	8h
high-responsive	INH	CYP1A1	Cytoplasm	enzyme	1543	24h
high-responsive	APAP	NR1I2	Nucleus	ligand-dependent nuclear receptor	8856	8h
high-responsive	APAP	PPARGC1A	Nucleus	transcription regulator	10891	8h
high-responsive	APAP	CYP1A1	Cytoplasm	enzyme	1543	8h
high-responsive	APAP	SULT1B1	Cytoplasm	enzyme	27284	24h
high-responsive	APAP	SULT1E1	Cytoplasm	enzyme	6783	24h
high-responsive	APAP	UGT2B17	Cytoplasm	enzyme	7367	24h
high-responsive	APAP	EGR1	Nucleus	transcription regulator	1958	2h
high-responsive	APAP	IER3	Cytoplasm	other	8870	2h
high-responsive	APAP	CCNE2	Nucleus	other	9134	24h
high-responsive	APAP	PCK1	Cytoplasm	kinase	5105	8h
high-responsive	APAP	SULT1B1	Cytoplasm	enzyme	27284	8h
high-responsive	VPA	PPARGC1A	Nucleus	transcription regulator	10891	8h
high-responsive	VPA	ABCB11	Plasma Membrane	transporter	8647	24h

Continued on next page

Group	Drug	Gene	Location	Type	Entrez ID	TP
high-responsive	VPA	CYP1A2	Cytoplasm	enzyme	1544	24h
high-responsive	VPA	CYP2B6	Cytoplasm	enzyme	1555	24h
high-responsive	VPA	CYP3A4	Cytoplasm	enzyme	1576	24h
high-responsive	VPA	CYP3A7	Cytoplasm	enzyme	1551	24h
high-responsive	VPA	HMGCS2	Cytoplasm	enzyme	3158	24h
high-responsive	VPA	NR1I3	Nucleus	ligand-dependent nuclear receptor	9970	24h
high-responsive	VPA	PPARGC1A	Nucleus	transcription regulator	10891	24h
high-responsive	VPA	SULT2A1	Cytoplasm	enzyme	6822	24h
high-responsive	VPA	CYP1A1	Cytoplasm	enzyme	1543	24h
high-responsive	VPA	ACSL1	Cytoplasm	enzyme	2180	24h
high-responsive	VPA	ADH1A	Cytoplasm	enzyme	124	24h
high-responsive	VPA	ADH1C	Cytoplasm	enzyme	126	24h
high-responsive	VPA	ADH4	Cytoplasm	enzyme	127	24h
high-responsive	VPA	ADHFE1	Cytoplasm	enzyme	137872	24h
high-responsive	VPA	AKR1D1	Cytoplasm	enzyme	6718	24h
high-responsive	VPA	CYP4A11	Cytoplasm	enzyme	1579	24h
high-responsive	VPA	CYP4F12	Cytoplasm	enzyme	66002	24h
high-responsive	VPA	CYP4X1	Cytoplasm	enzyme	260293	24h
high-responsive	VPA	SLC27A1	Plasma Membrane	transporter	376497	24h
high-responsive	VPA	SRD5A2	Cytoplasm	enzyme	6716	24h
high-responsive	VPA	EPHX2	Cytoplasm	enzyme	2053	24h
high-responsive	VPA	FMO1	Cytoplasm	enzyme	2326	24h
high-responsive	VPA	KEAP1	Cytoplasm	transcription regulator	9817	24h
high-responsive	VPA	MAP2K6	Cytoplasm	kinase	5608	24h
high-responsive	VPA	PPM1J	Other	phosphatase	333926	24h
high-responsive	VPA	SULT1E1	Cytoplasm	enzyme	6783	24h
high-responsive	VPA	UGT2B15	Cytoplasm	enzyme	7366	24h
high-responsive	VPA	IER3	Cytoplasm	other	8870	24h
high-responsive	VPA	CYP2U1	Cytoplasm	enzyme	113612	24h
high-responsive	VPA	SLC10A1	Plasma Membrane	transporter	6554	24h
high-responsive	VPA	CCNA2	Nucleus	other	890	24h
high-responsive	VPA	TGFB3	Extracellular Space	growth factor	7043	24h
high-responsive	VPA	PLK1	Nucleus	kinase	5347	24h
high-responsive	VPA	FOSL1	Nucleus	transcription regulator	8061	24h
high-responsive	VPA	PMF1/PMF1-BGLAP	Nucleus	transcription regulator	11243	24h
low-responsive	PHE	CYP1A1	Cytoplasm	enzyme	1543	8h
low-responsive	PHE	CYP3A4	Cytoplasm	enzyme	1576	24h
low-responsive	PHE	CYP3A5	Cytoplasm	enzyme	1577	24h
low-responsive	PHE	CYP3A7	Cytoplasm	enzyme	1551	24h
low-responsive	PHE	CYP4A11	Cytoplasm	enzyme	1579	24h
low-responsive	PHE	CYP4X1	Cytoplasm	enzyme	260293	24h
low-responsive	PHE	IGFBP1	Extracellular Space	other	3484	8h
low-responsive	PHE	HMGCS2	Cytoplasm	enzyme	3158	24h
low-responsive	PHE	BAX	Cytoplasm	transporter	581	24h
low-responsive	PHE	PCK1	Cytoplasm	kinase	5105	8h
low-responsive	PHE	PCK1	Cytoplasm	kinase	5105	24h
low-responsive	CSA	MAP3K8	Cytoplasm	kinase	1326	24h
low-responsive	CSA	IL1RN	Extracellular Space	cytokine	3557	24h

Table C.8: Drug-drug interactions. Drug-drug interactions predicted for the high-responsive drugs (RIF, CPA, PB, INH, HPL, AZA, APAP, and VPA).

Drug A	Drug B	Gene	drugs are inducer/ inhibitor/ substrate of CYP enzyme	Reference	Type	Entrez ID	TP	Toxic change drug A	Toxic change drug B	Absolute difference
APAP	VPA	PPARGC1A	-	-	transcription regulator	10891	8h	1.35	1.01	0.34
APAP	VPA	SULT1E1	-	-	enzyme	6783	24h	1.40	2.11	0.71
AZA	VPA	PLK1	-	-	kinase	5347	24h	1.42	1.45	0.03
AZA	VPA	CYP4X1	no	DrugBank	enzyme	260293	24h	1.05	1.79	0.74
CPA	VPA	CYP3A7	no	DrugBank	enzyme	1551	24h	2.12	3.74	1.62
CPA	RIF	CYP3A4	yes	DrugBank	enzyme	1576	24h	1.67	6.25	4.58
CPA	HPL	CYP3A4	yes	DrugBank	enzyme	1576	24h	1.67	2.11	0.44
CPA	VPA	CYP3A4	yes	DrugBank	enzyme	1576	24h	1.67	4.42	2.75
CPA	RIF	CYP3A7	yes	DrugBank	enzyme	1551	24h	2.12	4.76	2.64
CPA	HPL	CYP3A7	yes	DrugBank	enzyme	1551	24h	2.12	2.11	0.01
HPL	VPA	CYP3A7	no	DrugBank	enzyme	1551	24h	2.11	3.74	1.63
HPL	VPA	CYP3A4	yes	DrugBank	enzyme	1576	24h	2.11	4.42	2.31
INH	APAP	CYP1A1	no	DrugBank	enzyme	1543	8h	2.37	2.12	0.25
INH	VPA	CYP1A1	no	DrugBank	enzyme	1543	24h	3.65	4.19	0.54
INH	VPA	CYP1A2	yes	DrugBank	enzyme	1544	24h	2.05	2.50	0.45
PB	RIF	ALAS1	-	-	enzyme	211	24h	1.24	1.54	0.30
PB	APAP	SULT1E1	-	-	enzyme	6783	24h	1.11	1.40	0.29
PB	VPA	SULT1E1	-	-	enzyme	6783	24h	1.11	2.11	1.00
PB	INH	CYP1A1	no	DrugBank	enzyme	1543	8h	1.04	2.37	1.33
PB	VPA	CYP3A7	no	DrugBank	enzyme	1551	24h	5.40	3.74	1.66
PB	AZA	CYP4X1	no	DrugBank	enzyme	260293	24h	1.36	1.05	0.31
PB	VPA	CYP4X1	no	DrugBank	enzyme	260293	24h	1.36	1.79	0.43
PB	APAP	CYP1A1	yes	DrugBank	enzyme	1543	8h	1.04	2.12	1.08
PB	RIF	CYP2B6	yes	DrugBank	enzyme	1555	24h	1.18	2.00	0.82
PB	VPA	CYP2B6	yes	DrugBank	enzyme	1555	24h	1.18	1.48	0.3
PB	RIF	CYP2C8	yes	DrugBank	enzyme	1558	24h	1.74	1.62	0.12
PB	CPA	CYP3A4	yes	DrugBank	enzyme	1576	24h	6.11	1.67	4.44
PB	RIF	CYP3A4	yes	DrugBank	enzyme	1576	24h	6.11	6.25	0.14
PB	HPL	CYP3A4	yes	DrugBank	enzyme	1576	24h	6.11	2.11	4.00
PB	VPA	CYP3A4	yes	DrugBank	enzyme	1576	24h	6.11	4.42	1.69
PB	RIF	CYP3A5	yes	DrugBank	enzyme	1577	24h	1.73	1.78	0.05
PB	RIF	CYP3A5	yes	DrugBank	enzyme	1577	8h	1.40	1.52	0.12
PB	CPA	CYP3A7	yes	DrugBank	enzyme	1551	24h	5.40	2.12	3.28
PB	RIF	CYP3A7	yes	DrugBank	enzyme	1551	8h	1.58	2.11	0.53
PB	RIF	CYP3A7	yes	DrugBank	enzyme	1551	24h	5.40	4.76	0.64
PB	HPL	CYP3A7	yes	DrugBank	enzyme	1551	24h	5.40	2.11	3.29
RIF	VPA	AKR1D1	-	-	enzyme	1576	24h	6.25	4.42	1.83
RIF	VPA	CYP3A7	no	DrugBank	enzyme	1551	24h	4.76	3.74	1.02
RIF	VPA	CYP2B6	yes	DrugBank	enzyme	1555	24h	2.00	1.48	0.52
RIF	HPL	CYP3A4	yes	DrugBank	enzyme	1576	24h	6.25	2.11	4.14
RIF	VPA	CYP3A4	yes	DrugBank	enzyme	6718	24h	1.35	3.20	1.85
RIF	HPL	CYP3A7	yes	DrugBank	enzyme	1551	24h	4.76	2.11	2.65

D

Supplementary information to Chapter 9

D.1 Supplementary tables

D.1.1 Physiologically-based pharmacokinetic model development and validation

Table D.1: Relative expression values of relevant enzymes and transporters. Relative expression values for the vascular system, as well as all organs and tissues used to estimate relative abundance of relevant ADME enzymes and transporters, which are involved in metabolism and elimination processes of APAP and CAF.

	ABCB1	ABCG2	CYP1A2	CYP2E1	GSTT1	SULT1A1	UGT1A9
Plasma	0	0	0	0	0.02	0.14	0
Vascular Endothelium	0	0	0	0	0	0	0
Blood Cells	0	0	0	0	0.02	0.14	0
Bone	0.09	0.21	0	0	8.18E-03	0.05	0
Brain	0.31	0.46	0	6.97E-04	0.09	0.06	0
Fat	0	0	0	0	0	0	0
Gonads	0.19	0.27	2.96E-04	1.11E-03	0.04	0.1	1.62E-04
Heart	0.17	0.11	0	0	0.33	0.09	0
Kidney	0.66	0.09	4.40E-06	4.24E-04	0.06	0.06	1
Liver	0.28	0.28	1	1	0.21	1	0.1
Lung	0.14	0.22	2.49E-05	6.38E-04	0.06	0.13	0
Muscle	0.06	0.03	0	0	1	0.07	0
Pancreas	0.1	5.43E-03	0	0	9.49E-03	0.04	0
Skin	0.11	0	0	0	0	0	0
Spleen	0.21	0.06	0	0	0.06	0.12	0
Duodenum	1	1	0	8.12E-03	0.15	0.3	4.13E-03
Jejunum	1	1	0	8.12E-03	0.15	0.3	4.13E-03
Ileum	1	1	0	8.12E-03	0.15	0.3	4.13E-03
Cecum	0	0	0	0	0	0	0
Colon	0.45	0.16	0	0	0.14	0.22	7.95E-03
Rectum	0	0	0	0	0	0	0
Stomach	0.14	0.04	0	0	0.07	0.05	1.73E-03
Small Intestine	1	1	0	8.12E-03	0.15	0.3	4.13E-03
Large Intestine	0.45	0.16	0	0	0.14	0.22	7.95E-03

Table D.2: Comparison between observed and predicted pharmacokinetic parameters. Comparison between observed vs. predicted pharmacokinetic parameters for the area under the curve (AUC) and the maximal concentration (Cmax) calculated during PBPK model development and validation. Information about the different studies can be found in Table 9.4

Study ID	Drug/Metabolite	Observed AUC(0-t) [$\mu\text{mol}/\text{min}/\text{l}$]	Predicted AUC(0-t) [$\mu\text{mol}/\text{min}/\text{l}$]	Observed Cmax [$\mu\text{mol}/\text{l}$]	Predicted Cmax [$\mu\text{mol}/\text{l}$]
1	CAF	15352.03	18138.13	45.45	63.65
2	CAF	16454.46	16948.87	42.55	44.99
3	CAF	8801.67	8561.24	34.36	32.94
3	PX	3281.31	3064.54	8.3	7.44
3	TB	932.19	854.68	2.43	2.1
3	TP	333.45	327.64	0.97	0.95
4	CAF	20022.62	17521.79	84.74	66.65
4	PX	5910.42	6006.03	15.41	14.67
4	TB	1468.9	1646.02	3.75	4.09
4	TP	582.09	664.45	1.61	1.94
5	CAF	12575.88	15209.84	23.53	27.4
5	PX	8055.72	8032.27	8.62	7.8
5	TB	727.93	2348.92	1.64	2.22
5	TP	255.32	389.53	0.8	0.98
6	CAF	38045.37	26026.6	59.42	50.46
6	PX	22721.04	13927.44	18.36	15.31
6	TB	2008.78	4540.18	1.59	4.31
6	TP	2434.37	3137.84	1.58	2.07
7	CAF	3136.22	2822.1	6.41	5.79
8	CAF	18331.09	17405.76	34.67	35.15
9	CAF	38934.18	29637.11	66.48	59.05
10	CAF	48814.04	45627.33	83.73	89.42
11	APAP	20525.83	15740.6	114.33	94.66
11	APAPG	8039.71	5894.59	30.6	19.51
11	APAPS	4206.66	3004.43	15.55	13.44
11	APAPC	2106.23	1744.3	7.73	6.18
12	APAP	26802.18	23210.7	122.72	142.35
12	APAPG	12478.09	10453.6	38.58	28
12	APAPS	8145.02	6386.79	26.84	26.42
13	APAP	4856.58	6896.4	27.42	40.66
14	APAP	13396.63	14059.81	88.1	84.48
15	APAP	26806.68	28897.79	131.9	176.04
16	APAP	17493.32	16807.26	97.74	101.09
17	APAP	8674.87	20003.71	106.85	114.8
18	APAP	4459.37	8709.99	22.95	46.3
19	APAP	6290.79	10400.37	27.25	53.63

D.1.2 System biology models of acetaminophen

Table D.3: Other system biology models for APAP and their application.

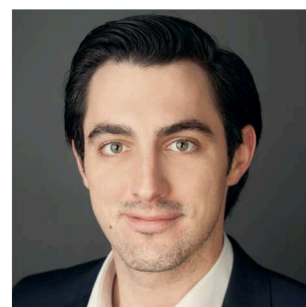
	Our study	[Krauss et al., 2012]	[Jiang et al., 2013]	[Ben-Shachar et al., 2012]	[Woodhead et al., 2012]	[Howell et al., 2012]
Modeling Software	PK-Sim®	PK-Sim®	SimCYP®	Own mathematical model with 21 differential equations	DILISym®	DILISym®
Clinical PK profiles used for model development & validation	PO data (500 mg, 1000 mg, 2000 mg, 20 mg/kg) (human)	PO data (1000 mg) (human)	IV data (5 mg/kg, 20 mg/kg) (adults), PO data (975 mg, 1000 mg) (adults), IV data (12.5 mg/kg, 15 mg/kg, 20 mg/kg) (children)	PO data (20 mg/kg) (human)	Amongst others: IV data (300 mg/kg) (rat), PO data (300 mg/kg) (rat) (other data used to calibrate (sub-)models e.g., human urinary excretion of APAP and metabolites, ALT or GSH levels)	Amongst others: IV data (300 mg/kg) (rat), PO data (300 mg/kg) (rat) (other data used to calibrate (sub-)models e.g., human urinary excretion of APAP and metabolites, ALT or GSH levels)
Implementation of APAP metabolism & active transport	APAP metabolism: APAPG: UGT1A9, APAPS: SULT1A1, NAPQI: CYP2E1, APAPC: GSTT1; Active transport: APAP: ABCB1, APAPG: ABCG2, APAPS: ABCG2;	Specific liver clearance: processes for APAP, APAPG, APAPS, APAPC NAPQI: CYP2C9, C19, D6, E1, CYP3A4	APAP metabolism: APAPG: UGT1A9, A2, UGT2B15, APAPS: SULTs, NAPQI: CYP1A2, CYP2C9, C19, D6, E1, CYP3A4 APAPC: GST	APAP metabolism: APAPG: UGT1A1, A6, A9 UGT2B15, APAPS: SULTs, NAPQI: CYP1A2, CYP2E1, CYP3A4, APAPC: GST	Active clearance processes for APAP, APAPG, APAPS, NAPQI	Active clearance processes for APAP, APAPG, APAPS, NAPQI
Modeling application & results	-Integration of coupled PBPK models of APAP and CAF with in vitro response data; -Investigation of the stimulatory and inhibitory effects of CAF on APAP induced toxicity in humans for co-administration of both drugs	-Integration of genome-scale network reconstruction of human hepatocyte into PBPK model of APAP; -Studying APAP-induced toxication at systems level by addressing downstream effects of drug administration on metabolic functionality at cellular scale	-Application of developed PBPK model of APAP for subgroup extrapolations between adults and children by accounting for maturational changes from birth; -PK profiles of neonates, children and adolescents successfully predicted following intravenously and orally administered APAP	-Creation of a mathematical model of APAP and connection to glutathione metabolism to represent APAP pharmacokinetics in humans; -Study extent of liver damage induced by APAP overdose or chronic treatment; Development of different N-acetyl cysteine (NAC) dosing strategies	-Investigation of optimal NAC treatment after a single APAP overdose for a mean patient and a sample population	-Simulation of temporal profiles of viable liver mass, ALT and GSH levels for different species induced by oral administration of APAP; -Comparison of APAP-induced hepatotoxicity between mice, rats, and humans

E

Curriculum vitae

Christoph Thiel

Date of birth	26/09/1986
Place of birth	Saarbrücken
Marital status	Single
Citizenship	German
Address	Elsaßstraße 54 50677 Cologne Germany



Education

09/1997 - 07/2006	Robert-Schuman-Gymnasium Saarlouis Abitur (grade: 2.1) - Biology, Latin, and Sports as major
09/1994 - 07/1997	Grundschule Ensdorf

Civilian service

09/2006 - 04/2007	Assisted transport (Red Cross)
-------------------	--------------------------------

Study and further education

10/2010 - 10/2013	Master of Science in Bioinformatics, Saarland University (grade: 1.6)
03/2013 - 10/2013	Master Thesis, Bayer Technology Services, Leverkusen, Title: 'A Knowledge-Driven Approach for Cross-Species Extrapolation in Pharmaceutical Development' (grade: 1.3)
09/2007 - 09/2010	Bachelor of Science in Bioinformatics, Saarland University (grade: 2.4)
06/2010 - 09/2010	Bachelor Thesis, Center for Bioinformatics, Saarbrücken, Title: 'Prediction of Hot Spots at Protein-Protein Interfaces' (grade: 1.3)

Work experience

07/2017 - 10/2017	Postdoctoral researcher, Institute of Applied Microbiology (iAMB), RWTH Aachen University, Aachen
12/2013 - 06/2017	Doctoral researcher, Institute of Applied Microbiology (iAMB), RWTH Aachen University, Aachen

02/2011 - 02/2013	Research assistant, Fraunhofer Institute for Biomedical Engineering (IBMT), Sankt Ingbert
01/2011 - 02/2011	Intern, Institute for Biochemistry, University of Cologne, Cologne
10/2010 - 12/2010	Research assistant, Synexa Life Sciences, Cape Town
12/2009 - 05/2010	Research assistant, Fraunhofer Institute for Biomedical Engineering (IBMT), Sankt Ingbert
08/2009 - 10/2009	Intern, Institute of Bioinformatics and Systems Biology (IBIS), Helmholtz Center Munich, Munich

Professional training

08/06/2015 - 12/06/2015	Organ/System toxicology, University of Constance, Constance
21/05/2014 - 23/05/2014	Molecular networks in toxicogenomics, Max Planck Institute for Molecular Genetics (MPIMG), Berlin
08/04/2014 - 10/04/2014	Functional interpretation of toxicogenomic data, European Molecular Biology Laboratory's European Bioinformatics Institute (EMBL-EBI), Hinxton
10/03/2014 - 14/03/2014	Toxicogenomics and systems toxicology, Leiden/Amsterdam Center for Drug Research (LACDR), Leiden

Skills & Interests

Language skills	German (native speaker), English (very good knowledge), French (basic knowledge), Latin (Latin proficiency certificate)
Programming skills	Java, C#, C++, Matlab, R, Python, SQL
Professional interests	<ul style="list-style-type: none">– Physiologically-based pharmacokinetic modeling– Clinical pharmacokinetics– Systems pharmacology– Bioinformatics– Computational toxicology– Toxicogenomics
Further interests	Volleyball, swimming, cooking, traveling, skiing

Awards

2016	Primary recipient of the 2016 Ebert Price - the oldest pharmacy award in existence in the United States (http://www.pharmacist.com/ebert-prize). <i>American Pharmacist Association (APhA)</i> , 2016, Baltimore, USA
------	---

Publications (peer-reviewed)

2017	Kuepfer, L., Clayton, O., Thiel, C., Cordes, H., Nudischer, R., Blank, L. M., Baier, V., Heymans, S., Caiment, F., Roth, A., Fluri, D. A., Kelm, J. M., Castell, J., Selevsek, N., Schlapbach, R., Keun, H., Hynes, J., Sarkans, U., Gmuender, H., Herwig, R., Niederer, S., Schuchhardt, J., Segall, M., Kleinjans, J., (2017). A model-based assay design to reproduce in vivo patterns of acute drug-induced toxicity. <i>Archives of Toxicology</i> ; 1-3
------	---

- Thiel, C., Hofmann, U., Ghallab, A., Gebhardt, R., Hengstler, J.G., Kuepfer, L. (2017). Towards knowledge-driven cross-species extrapolation. *Drug Discovery Today: Disease Models*
- Thiel, C., Cordes, H., Baier, V., Blank, L. M., and Kuepfer, L. (2017). Multiscale modeling reveals inhibitory and stimulatory effects of caffeine on acetaminophen-induced toxicity in humans. *CPT Pharmacometrics & Systems Pharmacology*; 6(2); 136-146
- Thiel, C., Cordes, H., Fabbri, L., Aschmann, H. E., Baier, V., Smit, I., Atkinson, F., Blank, L. M., and Kuepfer, L. (2017). A comparative analysis of drug-induced hepatotoxicity in clinically relevant situations. *PLoS Computational Biology*; 13(2); e1005280
- 2016 Thiel, C., Cordes, H., Conde, I., Castell, J. V., Blank, L. M., Kuepfer, L. (2016). Model-based contextualization of in vitro toxicity data quantitatively predicts in vivo drug response in patients. *Archives of Toxicology*; 91(2); 865–883
- Cordes, H., Thiel, C., Aschmann, H. E., Baier, V., Blank, L. M., Kuepfer, L. (2016). A Physiologically based pharmacokinetic model of isoniazid and its application in individualizing tuberculosis chemotherapy. *Antimicrobial Agents and Chemotherapy*; 60; 6134-6145
- 2015 Thiel, C., Schneckener, S., Krauss, M., Ghallab, A., Hofmann, U., Kanacher, T., Zellmer, S., Gebhardt, R., Hengstler, J., Kuepfer, L. (2015). A systematic evaluation of the use of physiologically based pharmacokinetic modeling for cross-species extrapolation. *Journal of Pharmaceutical Sciences*; 104(1); 191-206
- 2013 Walter, P., Metzger, J., Thiel, C., Helms, V. (2013). Predicting where small molecules bind at protein-protein interfaces. *PLoS One*; 8(3); e58583

Publications (non-peer-reviewed)

- 2016 Hofmann, U., Thiel, C., Ghallab, A., Gebhardt, R., Hengstler, J. G., Kuepfer, L. (2016). Von der Maus zum Menschen: Computermodelle in der klinischen Translation. *Systembiologie.de*; 16(11); 28-31
- 2014 Cordes, H., Thiel, C., Blank, L., Kuepfer, L. (2014). Modellierung metabolischer Netzwerke im menschlichen Körper. *BIOspektrum*; 20(1); 39-41
- 2012 Hewener, H., Thiel, C., Kubale, R., Tretbar, S. H. (2012). Entwicklung neuer Ultraschallverfahren - Eine Software für die Verarbeitung von Ultraschallsignalen. *Ultraschall in der Medizin*; 33 - A1102

